


Winter 2014

Photoproduction of π^0 on Hydrogen With CLAS From 1.1 GeV - 5.45 GeV Using $e^+e^- \rightarrow \gamma$ Decay

Michael C. Kunkel
Old Dominion University

Follow this and additional works at: https://digitalcommons.odu.edu/physics_etds

 Part of the [Elementary Particles and Fields and String Theory Commons](#), and the [Nuclear Commons](#)

Recommended Citation

Kunkel, Michael C.. "Photoproduction of π^0 on Hydrogen With CLAS From 1.1 GeV - 5.45 GeV Using $e^+e^- \rightarrow \gamma$ Decay" (2014). Doctor of Philosophy (PhD), dissertation, Physics, Old Dominion University, DOI: 10.25777/yxgj-3c96
https://digitalcommons.odu.edu/physics_etds/54

This Dissertation is brought to you for free and open access by the Physics at ODU Digital Commons. It has been accepted for inclusion in Physics Theses & Dissertations by an authorized administrator of ODU Digital Commons. For more information, please contact digitalcommons@odu.edu.

**PHOTOPRODUCTION OF π^0 ON HYDROGEN WITH
CLAS FROM 1.1 GEV - 5.45 GEV USING $e^+e^-\gamma$ DECAY**

by

Michael C. Kunkel
M.S. May 2008, Old Dominion University

A Dissertation Submitted to the Faculty of
Old Dominion University in Partial Fulfillment of the
Requirements for the Degree of

DOCTOR OF PHILOSOPHY

PHYSICS

OLD DOMINION UNIVERSITY
December 2014

Approved by:

Moskov Amaryan, (Director)

Ian Balitsky (Member)

Alex Godunov (Member)

Chester Grosch (Member)

Lawrence Weinstein (Member)

ABSTRACT

PHOTOPRODUCTION OF π^0 ON HYDROGEN WITH CLAS FROM 1.1 GEV - 5.45 GEV USING $e^+e^-\gamma$ DECAY

Michael C. Kunkel
Old Dominion University, 2014
Director: Dr. Moskov Amaryan

Photoproduction of the π^0 meson was studied using the CLAS detector at the Thomas Jefferson National Accelerator Facility using tagged incident photon energies spanning the range $E_\gamma = 1.1 \text{ GeV} - 5.45 \text{ GeV}$. The measurement is performed on a liquid hydrogen target in the reaction $\gamma p \rightarrow p e^+ e^- (\gamma)$. The final state of the reaction is the sum of two subprocesses for π^0 decay, the Dalitz decay mode of $\pi^0 \rightarrow e^+ e^- \gamma$ and conversion mode where one photon from $\pi^0 \rightarrow \gamma\gamma$ decay is converted into a $e^+ e^-$ pair. This specific final state reaction avoided limitations caused by single prompt track triggering, while the span of incident photon energies allowed for measurements of π^0 photoproduction to a domain never systematically measured before.

We report the measurement of the π^0 differential cross sections $\frac{d\sigma}{d\Omega}$ and $\frac{d\sigma}{dt}$. The angular distributions agree well with the SAID parametrization for incident beam energies below 3 GeV. As a result with this new data, the $\chi^2/p.d.f.$ of the global fit in the SAID parametrization improved to 3.1 from 3.7. For incident beam energies greater than 3 GeV a comparison of a model based on Generalized Parton Distributions (GPD) with experimental data shows significant discrepancy, requiring further model developments to describe the data.

Copyright, 2015, by Michael C. Kunkel, All Rights Reserved.

ACKNOWLEDGEMENTS

For most of my life, I have been a person with little to say about those that have been part of my inspiration, motivation and education. Since I am a creature of habit, please excuse my forgetfulness and thoughtlessness.

Lets start with United States Marine Corps!

My greatest accomplishment was proving to myself that I was born a Marine. It has been an honor to know and serve amongst the likes of all my hard-working, hard-hitting, adrenaline junky Teufel Hunden. Stay thirsty my friends and Semper Fi.

To the Embry-Riddle Aeronautical University Prescott Campus Physics department of 2007;

Dr. Darrel Smith, Dr. Nicholas A. Devereux and Dr. Phillip Anz-Meador, I send you my everlasting gratitude for showing to me that my mind is that of a physicist, displaying overwhelming support on my education and showing patience in teaching. To my colleagues at **JLAB** ;

Dr. Dennis Weygand, Dr. Michael Paolone, and Dr. Johann Goetz, the patience you have shown me is unprecedented. You have taught me the tools I needed to *debug debug debug*, perform outstanding analyses and even though we agreed on nothing but science, we are still able to be great colleagues.

To the Old Dominion University Physics department;

Dr. Lawrence Weinstein, thank you for showing support throughout my studies and being a rock of knowledge.

Dr. Anatoly Radyuskin, you are always a source of well placed meaningful knowledge along a sense of humor. I thank you for all of our conversations and laughs.

Dr. Moskov Amaryan, there are no words that I can muster to properly convey what I would like to write about the time you were my advisor. A few underrated words would be *lucky, indebted, kindness, patience*, and not to mention *frustrating*. However, I believe the greatest thing you have taught me comes from one of your many analogies in which you stated, "Michael, have patience, you cannot change ones rest frame."

To My family;

Dr. Ash Tandoğan my loving wife. I was smitten the first day I met you and I have

been smitten with you everyday afterward. You are a great source of my happiness. I look forward to all the hard work and dedication we will input into our lives with the reward of companionship and love. Thank you for your support and honesty you have given throughout this endeavor we both have undertaken.

Michael-Çınar Kunkel and future sons and daughters. When there is something you want to achieve in life, you must first understand the terrain to achievement, be willing to take necessary detours, be steadfast in your commitments, be intelligent with your falls, never be afraid to fail, and never settle for anything less than sixth gear pinned wide open. These guidelines might appear to be a lengthy list of nonsense, but throughout my life I have held onto these as if they were virtues. I have won, I have lost, I have smiled and I have pouted but I climbed my pinnacles, if only to gaze onto other crags. Whichever paths you choose, remember that “Baba might not know, but Baba knows.”

DEDICATION

This dissertation is dedicated to my fellow Belleau Woodsman,
brother

SSGT Christopher Michael Zimmerman USMC

04/01/1978 - 09/20/2006 KIA Afghanistan.

I can imagine a life in which you and I would discuss the meaning of me receiving a doctorate in physics. This conversation probably ends with me saying to you "True, I am an assclown but now I am thee assclown." to which you would jovially reply with "Still an assclown though. Now pass me the tap".

Semper Fidelis

TABLE OF CONTENTS

	Page
LIST OF TABLES	x
LIST OF FIGURES	xviii
 Chapter	
1. INTRODUCTION AND MOTIVATION	1
1.1 HADRONS	2
1.2 π^0 PRODUCTION	4
1.3 π^0 DECAYS	12
 2. THE CLAS DETECTOR AT THOMAS JEFFERSON NATIONAL ACCEL- ERATOR FACILITY	22
2.1 CONTINUOUS ELECTRON BEAM ACCELERATOR FACILITY ..	24
2.2 BEAM POSITIONING	27
2.3 PHOTON TAGGER	30
2.4 CEBAF LARGE ACCEPTANCE SPECTROMETER (CLAS)	32
2.5 START COUNTER	36
2.6 SUPERCONDUCTING TOROIDAL MAGNET	37
2.7 DRIFT CHAMBERS	39
2.8 CHERENKOV RADIATION AND DETECTORS	42
2.9 TIME-OF-FLIGHT DETECTORS	46
2.10 ELECTROMAGNETIC CALORIMETERS	49
 3. THE <i>G12</i> EXPERIMENT	55
3.1 <i>G12</i> DATA ACQUISITION AND TRIGGERING	56
3.2 <i>G12</i> RUN SUMMARY	62
3.3 RAW DATA RECONSTRUCTION	65
3.4 PARTICLE IDENTIFICATION	68
 4. PARTICLE RECONSTRUCTION AND ANALYSIS	71
4.1 DATA REDUCTION AND EVENT SELECTION	71
4.2 <i>G12</i> CORRECTIONS	75
4.3 FIDUCIAL CUTS	87
4.4 SIMULATION	98
4.5 PLUTO++ EVENT GENERATOR	101
4.6 KINEMATIC FITTING	102
4.7 PARTICLE VERTEX TIMING CUTS	128
4.8 Z VERTEX CUTS	129
4.9 SIMULATION KINEMATIC VARIABLES VERIFICATION	132
4.10 LEPTON TRIGGER EFFICIENCY FOR π^0 CANDIDATES	140

4.11	TARGET DENSITY	140
4.12	PHOTON NORMALIZATION	142
4.13	NORMALIZATION	143
5.	RESULTS	159
5.1	CROSS-SECTION	159
5.2	ACCEPTANCE	160
5.3	STATISTICAL UNCERTAINTIES	161
5.4	SYSTEMATIC UNCERTAINTY	164
5.5	COMPARISON TO WORLD DATA AND SAID FITS	173
5.6	CONCLUSIONS	188
	BIBLIOGRAPHY	190
	APPENDICES	194

LIST OF TABLES

Table	Page
1. Types of mesons	2
2. Branching Ratios of the π^0 Decay	4
3. CEBAF Operating Specifications	25
4. Number of Photo-electrons per Unit Length in Cherenkov Detection	44
5. $g12$ Running Parameters	55
6. Trigger Configuration 1	60
7. Trigger Configuration 2	60
8. Trigger Configuration for Single-sector Runs	61
9. Trigger Configuration (Tagger)	61
10. EC and CC Trigger Thresholds	61
11. Production Run List	62
12. Single-prong Run List	63
13. $g12$ Special Run List	64
14. $g12$ Production Run List Excluded From Current Analysis	72
15. Skim requirements	73
16. TOF Cut Parameters	90
17. EC UVW Cut Parameters	95
18. EC UVW Good Fiducial Parameters	95
19. Examples of Constraint Fits	102
20. Target Density Constants	141
21. Number of Events Used in Efficiency Study	144
22. Binning Used in Efficiency Study	147

23. Cross-section Constants	160
24. Generated Quantities	161
25. Branching Ratios of π^0	166
26. Variance of Data Cut Systematics	167
27. Run Groups Used to Determine Photon Flux Systematic Error	168
28. Systematics	172

LIST OF FIGURES

Figure	Page
1. Nonet of Pseudoscalar Mesons	3
2. Diagram for photoproduction of the π^0 meson	5
3. The handbag-type diagram for photoproduction of mesons	11
4. The soft physics contribution to the cross-section for photoproduction of π^0	12
5. Feynman diagram of $P_p(\pi^0)$ two photon decay and Dalitz decay	13
6. Probability of pair production, $\gamma \rightarrow e^+e^-$, as a function of distance in liquid hydrogen	16
7. Aerial view of Jefferson Laboratory (JLAB) facing east	23
8. The Continuous Electron Beam Accelerator Facility (CEBAF) at Jefferson Laboratory (JLAB)	23
9. Accelerating Cavity Diagram	26
10. A CEBAF superconducting niobium cavity pair	26
11. Beamline and components of CLAS	28
12. A typical <i>harp</i> scan done just prior to run 56426	29
13. Beamline and components after CLAS	29
14. Scale drawing of the photon tagger system	31
15. Scale drawing of the E -counters (blue) and the T -counters (green) showing examples of recoiled electrons (red lines) entering from the upper left	32
16. Schematic of the CLAS detector with subsystems identified	33
17. A cross section view of the CLAS detector showing an event with three tracks emanating from the target	34
18. The coils of the CLAS toroidal magnet prior to installation of the rest of the detector	34

19.	Blueprint schematic of the conical Kapton target cell used for $g12$	35
20.	The 40 cm long conical Kapton target cell used for $g12$	35
21.	Schematic of the start counter (ST) with the 40 cm long target cell (purple) at the center	36
22.	Cross-section view of the start counter illustrating the labeled components and its angular coverage when at the center of CLAS	37
23.	The CLAS Superconducting Toroidal Magnet and its placement in relation to Region-1 and Region-3	38
24.	Schematic cross-sectional view of the CLAS detector, perpendicular to the beam line	38
25.	Momentum and angular resolution for protons as determined from the measured angle of the scattered electron for data collected and Monte-Carlo simulation	40
26.	A cross section view of the CLAS detector showing an event with three tracks emanating from the target	41
27.	Illustration of Cherenkov Radiation	42
28.	Illustration of Cherenkov Angle	43
29.	Schematic of one CC showing the 18 symmetrical, mirrored segments of the CLAS CC	46
30.	Diagram of one sector of the time-of-flight (TOF) paddles	48
31.	Photon and Electron processes in Pb	50
32.	A simple Electromagnetic shower in a calorimeter	51
33.	A real Electromagnetic shower in a calorimeter	52
34.	Separated view of one sector of the forward electromagnetic calorimeter (EC) showing the three planes (u , v , w) of scintillator-lead pairs which make up one of the 13 logical layers	54
35.	Trigger logic for one of the six sectors of CLAS	57
36.	Trigger logic for any of the six sectors of CLAS along with MOR asynchronous logic trigger input	58

37.	Flow chart of the reconstruction process from raw data to identified tracks with momentum	66
38.	Flow chart of the hit-based tracking part of the reconstruction	67
39.	Flow chart of the time-based tracking part of the reconstruction	68
40.	β vs. mometum(p) \times charge(q) for run 56855	70
41.	Probability of single and multiple photons within the CEBAF timing window of 2.004 ns	74
42.	Probability of multiple photons within the CEBAF timing window of 2.004 ns	75
43.	Plot of <i>g12</i> run number vs. undetected proton mass with and without the “energy-loss” applied	78
44.	Plot of <i>g12</i> run number vs. undetected neutron mass with and without the “energy-loss” applied	78
45.	Plot of $\pi^+\pi^-$ mass for runs 56515 and 57130	79
46.	Tagger magnet current according to EPICS	80
47.	Tagger magnet current according to accelerator group via EPICS	81
48.	Electron beam current delivered to hall B(red) and hall C (green) according to the accelerator group during <i>g12</i>	81
49.	Tagger dump beam spot y-position according to EPICS	82
50.	Plot depicting magnetic field strength vs. magnet current showing the process of hysteresis	82
51.	Beam correction factor for run 56515	84
52.	Plot of proton mass for runs 56515 after beam correction was applied	85
53.	Plot of neutron mass for runs 56515 after beam correction was applied	85
54.	Plot of the correction factor x as a function of run number	86
55.	Plot of missing neutron mass vs. run number using various corrections	86
56.	Positive charged tracks in CLAS DC prior to fiducial cuts being applied, and after being applied	88

57.	Negative charged tracks in CLAS DC prior to fiducial cuts being applied, and after being applied	89
58.	θ vs. ϕ of π^+ data	91
59.	Inefficiency cut for π^+ and proton data	92
60.	Inefficient EC u, v, w strips vs. ϕ for sector 5 in CLAS e^- data	93
61.	Number of hit vs. inefficient EC u, v, w strips for sector 5 for e^- data	94
62.	EC u, v, w strips vs. ϕ for sector 5 with fiducial cuts and inefficient paddle knockouts applied to e^- data	96
63.	Number of hits vs. EC u, v, w strips for sector 5 with fiducial cuts and inefficient paddle knockouts applied to e^- data	97
64.	Number of events vs. Pull distribution for the (4-C) kinematic fit for $\gamma p \rightarrow pe^+e^-$ for $g12$ data with a 1% Confidence Level cut applied, and a Gaussian fit to each	105
65.	Number of events vs. Pull distribution for the (4-C) kinematic fit for $\gamma p \rightarrow pe^+e^-$ for $g12$ simulation with a 1% Confidence Level cut applied, and a Gaussian fit to each	106
66.	Number of events vs. Confidence Level for $g12$ (top) data and $g12$ simulation (bottom) for a (4-C) fit using $\gamma p \rightarrow pe^+e^-$	107
67.	Number of events vs. Pull distribution for the (4-C) kinematic fit for $\gamma p \rightarrow p\pi^+\pi^-$ for $g12$ data with a 1% Confidence Level cut applied, and a Gaussian fit to each	108
68.	Number of events vs. Pull distribution for the (4-C) kinematic fit for $\gamma p \rightarrow p\pi^+\pi^-$ for $g12$ simulation with a 1% Confidence Level cut applied, and a Gaussian fit to each	109
69.	Number of events vs. Confidence Level for $g12$ (top) data and $g12$ simulation (bottom) for a (4-C) fit using $\gamma p \rightarrow p\pi^+\pi^-$	110
70.	Number of data events plotted vs. Pull distribution for the 1-C(red), 4-C(black), 2-C(blue) for $g12$ data	112
71.	Number of data events plotted vs. Pull distribution for the 1-C(red), 4-C(black), 2-C(blue) for $g12$ simulation	113
72.	Number of data events plotted vs. missing mass $M_x(\gamma p \rightarrow pX)$ for uncut data and $E_\gamma < 3.6$ GeV	115

73.	Number of data events plotted vs. missing mass $M_x(\gamma p \rightarrow pX)$ for uncut data and $E_\gamma > 3.6$ GeV	116
74.	Number of MC events plotted vs. missing mass $M_x(\gamma p \rightarrow pX)$ for uncut data and $E_\gamma < 3.6$ GeV	117
75.	Number of MC events plotted vs. missing mass $M_x(\gamma p \rightarrow pX)$ for uncut data and $E_\gamma > 3.6$ GeV	118
76.	Number of events vs. Pull distributions after a 1% cut placed on the 1-C (top plots) and 4-C fit (middle plots) for data and MC	120
77.	Number of data events plotted vs. missing mass $M_x(\gamma p \rightarrow pX)$	121
78.	$M_x^2(\gamma p \rightarrow pX)$ vs. $M_E(\gamma p \rightarrow pe^+e^-X)$	123
79.	Number of data events plotted vs. missing mass $M_x(\gamma p \rightarrow pX)$ after the 1-C, 4-C and 75 MeV missing energy cut	124
80.	Number of data events plotted vs. missing mass $M_x(\gamma p \rightarrow pX)$ after the 1-C, 4-C, 2-C and 75 MeV missing energy cut	126
81.	Number of MC events plotted vs. missing mass $M_x(\gamma p \rightarrow pX)$ after the 1-C, 4-C, 2-C and 75 MeV missing energy cut	127
82.	Number of events vs. $t_{pho} + t_{prop} - (t_{TOF} - l_{TOF}/(c\beta))$ for MC and data for proton, e^- , and e^+	129
83.	Number of data events plotted vs. z -vertex	130
84.	Proton θ vs. z -vertex	131
85.	Number of data events plotted vs. missing mass $M_x(\gamma p \rightarrow pX)$ for $\gamma p \rightarrow pe^+e^-(\gamma)$ events after all cuts and corrections.	132
86.	Total Number of π^0 and $\pi^+\pi^-$ Events Expected Between E_γ 1.1 GeV-2.8 GeV	133
87.	$M_x^2(\gamma p \rightarrow pX)$ vs. $M_E^2(\gamma p \rightarrow pe^+e^-X)$ for simulation systematic check ...	134
88.	Number of events vs. beam momentum for simulation systematic check ..	135
89.	Number of events vs. proton momentum (top), proton θ (middle) and proton ϕ kinematics for MC (black) events and data (red) when generating MC via differential cross-sections	136

90.	Number of events vs. positron momentum (top), positron θ (middle) and positron ϕ kinematics for MC (black) events and data (red) when generating MC via differential cross-sections	137
91.	Number of events vs. electron momentum (top), electron θ (middle) and electron ϕ kinematics for MC (black) events and data (red) when generating MC via differential cross-sections	138
92.	Number of events vs. e^+e^- mass distribution for all MC (black) events and data (red)	139
93.	Normalized Lepton Trigger “Bit 6” for π^0 candidates	140
94.	Target density for $g12$	142
95.	Photon flux for analysis	143
96.	Number of events vs. the pull distribution for the reactions used in the normalization study for data	145
97.	Number of events vs. the pull distribution for the reactions used in the normalization study for MC	146
98.	$\theta \cos \phi$ vs. $\theta \sin \phi$ plot showing the efficiency of detecting the proton with z-vertex $-90 < z < -85$ cm and momentum $0.75 < p < 1$ GeV from a 2 charged track reaction using CLAS detection for $g12$	148
99.	$\theta \cos \phi$ vs. $\theta \sin \phi$ plot showing the efficiency of reconstructing the proton with z-vertex $-90 < z < -85$ cm and momentum $0.75 < p < 1$ GeV from a 2 charged track reaction using CLAS Monte-Carlo for $g12$	149
100.	$\theta \cos \phi$ vs. $\theta \sin \phi$ plot showing the over-efficiency of simulating the proton with z-vertex $-90 < z < -85$ cm and momentum $0.75 < p < 1$ GeV from a 2 charged track reaction	150
101.	$\theta \cos \phi$ vs. $\theta \sin \phi$ plot showing the efficiency of detecting the π^+ with z-vertex $-90 < z < -85$ cm and momentum $0.75 < p < 1$ GeV from a 2 charged track reaction using CLAS detection for $g12$	151
102.	$\theta \cos \phi$ vs. $\theta \sin \phi$ plot showing the efficiency of reconstructing the π^+ with z-vertex $-90 < z < -85$ cm and momentum $0.75 < p < 1$ GeV from a 2 charged track reaction using CLAS Monte-Carlo for $g12$	152
103.	$\theta \cos \phi$ vs. $\theta \sin \phi$ plot showing the over-efficiency of simulating the π^+ with z-vertex $-90 < z < -85$ cm and momentum $0.75 < p < 1$ GeV from a 2 charged track reaction	153

104. $\theta \cos \phi$ vs. $\theta \sin \phi$ plot showing the efficiency of detecting the π^- with z-vertex $-90 < z < -85$ cm and momentum $0.75 < p < 1$ GeV from a 2 charged track reaction using CLAS detection for $g12$	154
105. $\theta \cos \phi$ vs. $\theta \sin \phi$ plot showing the efficiency of reconstructing the π^- with z-vertex $-90 < z < -85$ cm and momentum $0.75 < p < 1$ GeV from a 2 charged track reaction using CLAS Monte-Carlo for $g12$	155
106. $\theta \cos \phi$ vs. $\theta \sin \phi$ plot showing the over-efficiency of simulating the π^- with z-vertex $-90 < z < -85$ cm and momentum $0.75 < p < 1$ GeV from a 2 charged track reaction	156
107. $\frac{d\sigma}{d\Omega}$ vs. $\cos \theta$ plot showing the $g12$ π^0 differential cross-section when the $g11$ global normalization is used (blue) and when the $g12$ dynamic normalization is used (red) for various bins of beam energy inside lepton trigger acceptance	157
108. $\frac{d\sigma}{d\Omega}$ vs. $\cos \theta$ plot showing the $g12$ π^0 differential cross-section when the $g11$ global normalization is used (blue) and when the $g12$ dynamic normalization is used (red) for various bins of beam energy above MORB threshold	158
109. The uncertainty plotted vs. the total number of detected events and reconstructed events from MC, for small values of Υ	164
110. Probability of Photon Conversion vs. $\cos \theta$ for various values of E_γ	165
111. Plot showing the contribution of the data cut systematic error and the incoming beam dependence of the error	167
112. Plot showing the contribution of the flux systematic error and the incoming beam dependence of the error	169
113. The sector systematic uncertainty as a function of the incoming photon energy	170
114. Comparison of sector systematic uncertainty to $g11$ measurement	171
115. The contribution of all systematic uncertainties	173
116. The π^0 proton photoproduction cross section, $(d\sigma/d\Omega)$, at $E_\gamma = 1.275 - 2.225$ GeV versus $\cos \theta$ where θ is the pion center-of-mass production angle	174
117. The π^0 proton photoproduction cross section at $E_\gamma = 2.275 - 3.375$ GeV versus cosine of the pion center-of-mass production angle	175
118. The π^0 proton photoproduction cross section at $E_\gamma = 3.425 - 4.425$ GeV versus cosine of the pion center-of-mass production angle	176

119.	The π^0 proton photoproduction cross section at $E_\gamma = 4.475 - 5.425$ GeV versus cosine of the pion center-of-mass production angle	177
120.	Fixed angle excitation functions of the π^0 photoproduction cross section, $(d\sigma/d\Omega)$, off the proton at $\theta = 31 - 75^\circ$ versus center-of-mass total energy W	178
121.	Fixed angle excitation functions of the π^0 photoproduction cross section, $(d\sigma/d\Omega)$, off the proton at $\theta = 76 - 140^\circ$ versus center-of-mass total energy W	179
122.	π^0 photoproduction cross section, $(d\sigma/dt)$, off the proton at $E_\gamma = 1275 - 2225$ MeV versus momentum transfer t	180
123.	π^0 photoproduction cross section, $(d\sigma/dt)$, off the proton at $E_\gamma = 2275 - 3375$ MeV versus momentum transfer t	181
124.	π^0 photoproduction cross section, $(d\sigma/dt)$, off the proton at $E_\gamma = 3425 - 4425$ MeV versus momentum transfer t	182
125.	π^0 photoproduction cross section, $(d\sigma/dt)$, off the proton at $E_\gamma = 4475 - 5425$ MeV versus momentum transfer t	183
126.	CGLN amplitude at $\theta = 60^\circ$	185
127.	Energy dependence of the χ^2/dp comparison to previous SAID fits	186
128.	Comparison of the π^0 differential cross section photoproduction data to GDP handbag model	188

CHAPTER 1

INTRODUCTION AND MOTIVATION

The goal of this analysis is to provide insight into the mechanisms, baryon resonances and productions channels involved in π^0 production for incident beam energies already explored as well as for incident beam energies in which there exists only a sparse and in some cases no amount of data. Nucleons are composite particles, meaning they are made up of smaller constituents. To gain insight into the structure of the nucleon, physics employ baryon spectroscopy to explore for baryon resonances. Experimental, theoretical and phenomenological methods have been developed to refine and expand the known resonance masses, widths, and electromagnetic couplings [58]. Precise measurements of the cross-section and polarization asymmetries are important to extract photo-decay amplitudes and production mechanisms. Recently there has been improvement in Wide Angle Compton Scattering predictions using a General Parton Distribution (GPD) handbag model. This framework has also been recently adopted into π^0 production [1] to describe the production as single quark excitation in photon-quark scattering.

In this analysis, we report on an experiment that was performed with the Cebaf Large Angle Spectrometer (CLAS) setup at the Thomas Jefferson National Accelerator Facility (TJNAF). The experiment used a tagged photon beam produced via bremsstrahlung from a 5.715 GeV electron beam delivered from the CEBAF accelerator. The photon beam struck a liquid hydrogen target. The reaction of interest is photoproduction of neutral pions on a hydrogen target, $\gamma p \rightarrow p\pi^0$, with subsequent Dalitz decay $\pi^0 \rightarrow e^+e^-\gamma$ or standard decay plus photon conversion conversion mode $\pi^0 \rightarrow \gamma\gamma \rightarrow e^+e^-\gamma$. Neither the Dalitz decay mode of π^0 with very small branching ratio of $\sim 1.2\%$, nor the conversion mode from the main decay mode $\pi^0 \rightarrow \gamma\gamma$ with branching ratio $\sim 98.8\%$ is preferred. The conversion rate of γ to e^+e^- is substantial enough that the Dalitz and the conversion process share the total statistical sample. The cross-section measurement is performed for the reaction $\gamma p \rightarrow pe^+e^-(\gamma)$ using a tagged photon beam spanning the energy interval $E_\gamma = 1.142 \text{ GeV} - 5.425 \text{ GeV}$. In the final state of the reaction the photon is missing, pe^+e^- are detected and π^0 is identified in the missing mass of the proton.

Using e^+e^- decay products of π^0 , contrary to $\gamma\gamma$ decay of π^0 , along with detection of the proton allowed the experiment to run with high current. This was achieved by requiring a trigger configuration comprised of multiple charged tracks along with Cherenkov and Electromagnetic Calorimeter detection for photon beam energies $1.142 \text{ GeV} < E_\gamma < 3.6 \text{ GeV}$. For photon beam energies greater than 3.6 GeV a trigger configuration comprised of just multiple charged tracks was utilized.

1.1 HADRONS

In the quark model, a hadron is a colorless particle formed of quarks and anti-quarks that are bound together by the strong force. Hadrons are organized and classified according to their quark content. The standard model permits multiple valence quark configurations for hadrons, however to date only two configurations have been verified, baryons and mesons. Baryons are hadrons with three quarks with suitable colors, while hadrons with two valence quarks, a quark and an anti-quark with color and “anti-color”, are called mesons. Since baryons have an odd number of valence quarks, they are spin $\frac{1}{2}$ particles and thus are fermions, however mesons are spin 0 or 1 particles are bosons. As in any quantum-mechanical bound system, the valence quarks have a discrete energy level spectrum due to the various modes of the di-quark excitations, vibrations, orientations and vibrations which give rise to the quantum numbers J^{PC} . Here $J = L + S$ is defined as the total angular momentum containing orbital angular momentum L and spin S , while $P = (-1)^{L+1}$ and $C = (-1)^{L+S}$ are defined as parity and charge conjugation. Each type of meson can be categorized by their spin configuration and are shown in Tab. 1.

TABLE 1. Types of mesons

Type	J	P	L	S	J^P
Pseudoscalar	0	-	0	0	0^-
Scalar	0	+	1	1	0^+
Vector	1	-	0	1	1^-
Axial Vector	1	+	1	0	1^+
Tensor	2	+	1	1	2^+

1.1.1 LIGHT PSEUDOSCALAR MESONS

The following analysis will concentrate on the lightest neutral pseudoscalar meson, π^0 , which is member of the family of $P_p(\pi^0, \eta, \eta')(J^P = 0^-)$ mesons that are subject to U(3) flavor symmetry. The nonet, the resulting nine states that can be decomposed into a singlet and an octet state, of the pseudoscalar mesons are seen in Fig. 1, where strangeness increases upward on the page and charge increases toward the right side of the page. It should be noted that the η and η' are not exact octet (η_8) and singlet

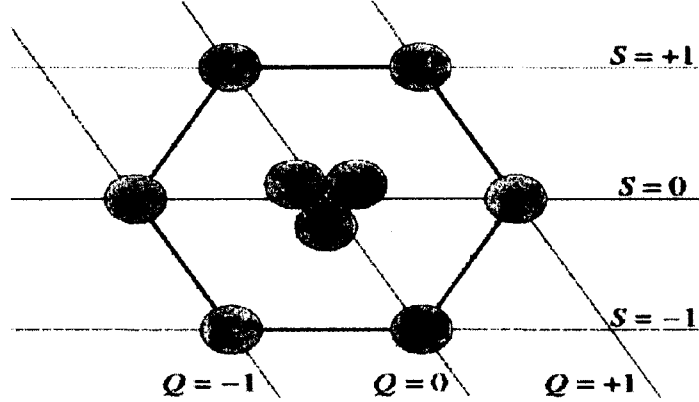


FIG. 1. Nonet of Pseudoscalar Mesons [2].

(η_0) states, as they are linear combinations of η_8 and η_0 according to:

$$\begin{pmatrix} \eta \\ \eta' \end{pmatrix} = \begin{pmatrix} -\sin \theta_{mix} & \cos \theta_{mix} \\ \cos \theta_{mix} & \sin \theta_{mix} \end{pmatrix} \cdot \begin{pmatrix} \eta_0 \\ \eta_8 \end{pmatrix} \quad (1)$$

where $\theta_{mix} = -18.6^\circ$ [3] and η_8 and η_0 have quark content of:

$$\eta_0 \rightarrow \sqrt{\frac{1}{6}}(u\bar{u} + d\bar{d} + s\bar{s})$$

$$\eta_8 \rightarrow \sqrt{\frac{2}{3}}(u\bar{u} + d\bar{d} - 2s\bar{s})$$

The physical masses of η and η' are $m_\eta = 547.51 \pm 0.18$ MeV [4], $m_{\eta'} = 957.78 \pm$

TABLE 2. Branching ratios of the π^0 decay. [4]

Mode	Branching ratio
$\pi^0 \rightarrow 2\gamma$	$(98.823 \pm 0.034) \cdot 10^{-2}$
$\pi^0 \rightarrow e^+e^-\gamma$	$(1.174 \pm 0.035) \cdot 10^{-2}$
$\pi^0 \rightarrow \gamma$ positronium	$(1.82 \pm 0.29) \cdot 10^{-9}$
$\pi^0 \rightarrow e^+e^+e^-e^-$	$(3.34 \pm 0.16) \cdot 10^{-5}$
$\pi^0 \rightarrow e^+e^-$	$(6.46 \pm 0.33) \cdot 10^{-8}$
$\pi^0 \rightarrow 4\gamma$	$< 2 \cdot 10^{-8}$
$\pi^0 \rightarrow \nu\bar{\nu}$	$< 2.7 \cdot 10^{-7}$
$\pi^0 \rightarrow \nu_e\bar{\nu}_e$	$< 1.7 \cdot 10^{-6}$
$\pi^0 \rightarrow \nu_\mu\bar{\nu}_\mu$	$< 1.6 \cdot 10^{-6}$
$\pi^0 \rightarrow \nu_\tau\bar{\nu}_\tau$	$< 2.1 \cdot 10^{-6}$
$\pi^0 \rightarrow \gamma\nu\bar{\nu}$	$< 6 \cdot 10^{-4}$

0.14 MeV [4], and the widths are $\Gamma_\eta = 1.30 \pm 0.07$ keV and $\Gamma_{\eta'} = 0.203 \pm 0.016$ MeV. The lightest of the mesons π^0 has a quark content of:

$$\pi^0 = \frac{1}{\sqrt{2}}(u\bar{u} - d\bar{d})$$

and mass of $m_{\pi^0} = 134.9766 \pm 0.0006$ MeV [4]. The decay modes for π^0 are given in Table 2.

1.2 π^0 PRODUCTION

The present analysis uses two approaches to describe the behavior of the π^0 cross-section. One approach is for incident photon beam energies less than 2.8 GeV where the missing resonance search is most valid and the data can be described well by coupling of the π^0 electromagnetic wave functions. The second approach attempts to describe the behavior of the π^0 by using General Parton Distribution models, GPD for incident photon beam energies greater than 2.8 GeV.

1.2.1 LOW ENERGY π^0 PRODUCTION

For incoming photon beam energies less than 2.8 GeV, the production of the π^0 meson, with 4-momenta q , in photon-proton reactions, with 4-momenta k and p_i

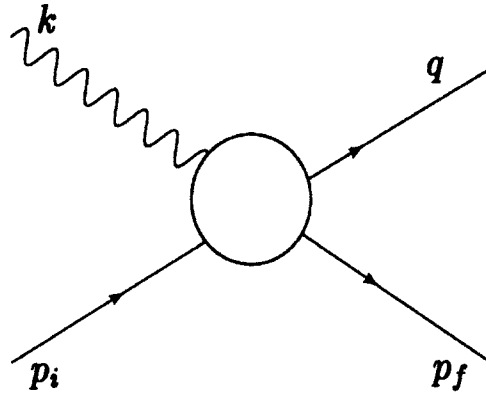


FIG. 2. Diagram for photoproduction of the π^0 meson. k and p_i are the incident photon beam and target proton 4-momenta respectively, q and p_f represent the produced π^0 meson and scattered proton 4-momenta respectively.

respectively and p_f being the 4-momenta of the scattered proton (see Fig. 2), can be described in terms of the three Lorentz invariant Mandelstam variables, s , t and u , where

$$\begin{aligned} s &= (k + p_i)^2 = (q + p_f)^2 \\ t &= (p_i - p_f)^2 = (k - q)^2 \\ u &= (k - p_f)^2 = (p_i - q)^2 . \end{aligned} \quad (2)$$

The sum of the Mandelstam variables linearly combine to give the sum of masses of the particles involved:

$$s + t + u = \sum_i^4 m_i^2 \quad (3)$$

and the definition of Lorentz-invariant mass:

$$p_i \cdot p_i = E_i^2 - \mathbf{p}_i \cdot \mathbf{p}_i = m_i^2 . \quad (4)$$

Using energy-momentum conservation:

$$k + p_i = q + p_f \quad (5)$$

it is seen that only three of the four momenta are independent. Conventionally the use of k and q and a combined 4-momenta of the nuclei

$$P = \frac{1}{2}(p_i + p_f) \quad (6)$$

are used as the independent kinematic variables. The three Mandelstam variables can be express in terms of the other two, therefore the scattering process is described by functions of only two of the Mandelstam variables. Conventionally they are chosen to be s and t , which in the center-of-mass frame (C.M.) of the initial and final state equal the invariant mass squared of the system and the momentum transfer in the production process respectively.

1.2.2 ISOSPIN REPRESENTATION

The scattering matrix \mathcal{M} for single pion photoproduction process is written as:

$$\begin{aligned} \mathcal{M} = (\epsilon_\mu k_\nu - \epsilon_\nu k_\mu) & \left[\frac{1}{2} i \gamma_5 \gamma_\mu \gamma_\nu A_1(s, t) + 2i \gamma_5 P_\mu (q - \frac{1}{2}k)_\nu A_2(s, t) \right. \\ & \left. + \gamma_5 \gamma_\mu q_\nu A_3(s, t) + \gamma_5 \gamma_\mu (2P_\nu - iM\gamma_\nu) A_4(s, t) \right] , \end{aligned} \quad (7)$$

where M is the nucleon mass, ϵ is the photon polarization and $A_i(s, t)$ are the invariant functions of the Mandelstam invariants s and t . The amplitude $A_i(s, t)$ refers to the emission of a pion of isospin index α , and is given by the well-known formula:

$$A_i(s, t) = A_i^{(0)} \tau_\alpha + A_i^{(+)} \delta_{\alpha 0} + \frac{1}{2} A_i^{(-)} [\tau_\alpha, \tau_0] , \quad (8)$$

where τ_α are the nucleon isospin transition operators, where the sign of α indicates the opposite sign of the pion isospin, this is by convention. Eq. 8 assumes that the photon interaction with hadrons occurs through isoscalar and isovector parts, so that $A_i^{(0)}$ is the isoscalar amplitude that corresponds to a zero net isospin transition resulting from the electromagnetic field. The amplitudes $A_i^{(+)}$ and $A_i^{(-)}$ are the isovector amplitudes and can be combined as $A_i^{(+)} + 2A_i^{(-)}$ and $A_i^{(+)} - A_i^{(-)}$ so that

the pion nucleon final state has definite isospin $\frac{1}{2}$ and $\frac{3}{2}$ respectively [10] by use of

$$\begin{aligned} A^S &= -(3)^{\frac{1}{2}} A^{(0)} \\ A^{V1} &= \left(\frac{1}{3}\right)^{\frac{1}{2}} A_i^{(+)} + 2A_i^{(-)} \\ A^{V2} &= \left(\frac{2}{3}\right)^{\frac{1}{2}} A_i^{(+)} - A_i^{(-)}, \end{aligned} \quad (9)$$

where A^S , A^{V1} and A^{V2} are the isoscalar amplitude, isovector amplitude of isospin $\frac{1}{2}$ and isovector amplitude of isospin $\frac{3}{2}$ respectively. The four possible pion nucleon amplitudes $A_i(s, t)$ of the initial and final state particles in the pion photoproduction process are in terms of the isoscalar and isovector are:

$$A_1(\gamma p \rightarrow n\pi^+) = -\sqrt{\frac{1}{3}} A^{V3} + \sqrt{\frac{2}{3}} (A^{V1} - A^S), \quad (10)$$

$$A_2(\gamma p \rightarrow p\pi^0) = \sqrt{\frac{2}{3}} A^{V3} + \sqrt{\frac{1}{3}} (A^{V1} - A^S), \quad (11)$$

$$A_3(\gamma n \rightarrow p\pi^-) = \sqrt{\frac{1}{3}} A^{V3} - \sqrt{\frac{2}{3}} (A^{V1} + A^S), \quad (12)$$

$$A_4(\gamma n \rightarrow n\pi^0) = \sqrt{\frac{2}{3}} A^{V3} + \sqrt{\frac{1}{3}} (A^{V1} + A^S). \quad (13)$$

Since the combination $\sqrt{\frac{2}{3}}(A^{V1} \mp A^S)$ gives the coupling of photons to positive and neutral isospin- $\frac{1}{2}$ states, respectively, [10], defined explicitly

$$A^p = +\sqrt{\frac{2}{3}}(A^{V1} - A^S), \quad (14)$$

$$A^n = -\sqrt{\frac{2}{3}}(A^{V1} + A^S). \quad (15)$$

1.2.3 STRUCTURE FUNCTIONS

To obtain the scattering matrix elements in terms of experimental quantities, it is preferred and easier to work in the C.M. system and reduce the \mathcal{M} to a form \mathcal{F}

by equating the invariant form of the scattering matrix elements in each frame, i.e.:

$$\bar{u}(p_2)\mathcal{M}u(p_1) \equiv \frac{4\pi W}{M}\chi_f^\dagger\mathcal{F}\chi_i, \quad (16)$$

where $\bar{u}(p_2)$ and $u(p_1)$ are final and initial state Dirac spinors respectively and χ_f and χ_i are final and initial state Pauli spinors. The differential cross-section for single pion production is:

$$\frac{d\sigma}{d\Omega} = \frac{q}{k}|\langle f|\mathcal{F}|i\rangle|^2, \quad (17)$$

The expression to express Dirac spinors in terms of Pauli spinors is written as:

$$\begin{aligned} \mathcal{F} = & i\vec{\sigma} \cdot \vec{\epsilon}\mathcal{F}_1 + \frac{1}{qk}(\vec{\sigma} \cdot \vec{q})\vec{\sigma} \cdot (\vec{k} \times \vec{\epsilon})\mathcal{F}_2 \\ & + \frac{i}{qk}(\vec{\sigma} \cdot \vec{k})(\vec{q} \cdot \vec{\epsilon})\mathcal{F}_3 + \frac{i}{q^2}(\vec{\sigma} \cdot \vec{q})(\vec{q} \cdot \vec{\epsilon})\mathcal{F}_4, \end{aligned} \quad (18)$$

where \vec{k} and \vec{q} are the C.M. 3-momenta and $\vec{\epsilon}$ is the polarization of the photon. The relationship between A_i and \mathcal{F} is found using the relations:

$$\mathcal{F}_1 = \frac{W-M}{8\pi W}(D_1D_2)^{\frac{1}{2}} \left[A_1 + (W-M)A_4 - \frac{k_0q_0 - \vec{k} \cdot \vec{q}}{W-M}(A_3 - A_4) \right] \quad (19)$$

$$\mathcal{F}_2 = qk \frac{W-M}{8\pi W} \left(\frac{D_2}{D_1} \right)^{\frac{1}{2}} \left[-A_1 + (W+M)A_4 + \frac{k_0q_0 - \vec{k} \cdot \vec{q}}{W+M}(A_3 - A_4) \right] \quad (20)$$

$$\mathcal{F}_3 = qk \frac{W-M}{8\pi W} (D_1D_2)^{\frac{1}{2}} q [(W-M)A_2 + A_3 - A_4] \quad (21)$$

$$\mathcal{F}_4 = q^2 \frac{W-M}{8\pi W} \left(\frac{D_2}{D_1} \right)^{\frac{1}{2}} q [-(W+M)A_2 + A_3 - A_4] \quad (22)$$

where

$$D_1 = (M^2 + \vec{k}^2)^{\frac{1}{2}} + M \quad (23)$$

$$D_2 = (M^2 + \vec{q}^2)^{\frac{1}{2}} + M. \quad (24)$$

$\mathcal{F}_i(s, t)$ are known as structure functions, alternatively known by Chew, Goldberger, Low and Nambu (CGLN) amplitudes. These amplitudes describe photoproduction as a function of s and t , and therefore in terms of momentum transfer. To represent the process in terms of angular momentum transitions, expansion of the structure

functions as partial waves in derivatives of Legendre polynomials, $P'_l(\cos \theta)$, results in the four multipole series:

$$\mathcal{F}_\infty = \sum_{l=0}^{\infty} [lM_{l+} + E_{l+}]P'_{l+1}(\cos \theta) + [(l+1)M_{l-} + E_{l-}]P'_{l-1}(\cos \theta) \quad (25)$$

$$\mathcal{F}_\epsilon = \sum_{l=1}^{\infty} [(l+1)M_{l+} + lM_{l-}]P'_l(\cos \theta) \quad (26)$$

$$\mathcal{F}_\exists = \sum_{l=1}^{\infty} [E_{l+} - M_{l+}]P''_{l+1}(\cos \theta) + [E_{l-} + M_{l-}]P''_{l-1}(\cos \theta) \quad (27)$$

$$\mathcal{F}_\Delta = \sum_{l=1}^{\infty} [M_{l+} - E_{l+} - M_{l-} - E_{l-}]P''_l(\cos \theta) \quad (28)$$

The energy-dependent amplitudes $M_{l\pm}$ and $E_{l\pm}$ refer to transitions initiated by magnetic and electric radiation, respectively, leading to final states of orbital angular momentum l and total angular momentum $j = l \pm \frac{1}{2}$.

The energy-dependent amplitudes $M_{l\pm}$ and $E_{l\pm}$ cannot be extracted directly from measurements, however using models on measured differential cross-sections and polarizations aide in the determination of the amplitudes. Constraining the production amplitudes aides in the determination of resonances. One such model that is used in this thesis is the SAID parameterization model discussed in Sec 1.2.4.

1.2.4 SAID

SAID [11] is a repository of experimental data and an interactive analysis facility, allowing to compare and extract data and partial wave solutions (PWA) for a variety of photoproduction, electro-production and pion production reactions. It was created by R. A. Arndt and L. D. Roper for the use of verifying model calculations against measured/fitted data, compare model calculations against SAID predictions for unmeasured observables, experimental planning, and simulations and event generators.

SAID is based upon the theoretical framework given in 1.2.2. SAID generates resonance couplings, in terms of angular momentum and isospin quantum numbers, that are extracted from a fit-based determination of multipoles using both an energy-dependent and an energy-independent parametrization. The photoproduction amplitude is assumed to be in the form of a Breit-Wigner and a background term in

the form of [6];

$$A = A_l(1 + iT_\pi) = A_r \left(\frac{k_0 q_0}{kq} \right)^{\frac{1}{2}} \frac{W_0 \sqrt{\Gamma \Gamma_\gamma}}{W_0^2 - W^2 - iW_0 \Gamma}, \quad (29)$$

in which A_l is the background parameter, W_0 , Γ and Γ_γ are functions of the full width Γ_0 and A_R being the resonant parameter in the form of;

$$A_r = \frac{\mu}{q} \left(\frac{k}{q} \right)^i \sum_{n=0}^N p_n \left(\frac{E_\pi}{\mu} \right)^n \quad (30)$$

where k_0 and q_0 are the pion and photon momenta at the resonance energy, μ is the pion mass, E_π is the pion kinetic energy in the lab frame and p_n is a free parameter. The background term is expanded as a set of Legendre polynomial terms with associated free parameters along with a sum of a pseudoscalar Born partial waves, which are determined by fitting the data. Multipoles can then be extracted by a fit of A close to the resonance position.

1.2.5 SUMMARY

A full set of differential cross-sections and polarization observables is required for the determination of multipoles. These can be related to the invariant amplitudes as functions of W and $\cos \theta$. For the separation of the different isospin contributions, both the proton and the neutron pion-photoproduction measurements are needed. An understanding of the invariant amplitudes, and subsequent CGLN structure functions, can provide information on the multipole transitions taking place. This allows to get direct information about the quantum numbers of the produced resonant states and constrain their position, widths and couplings. The work of this thesis is devoted to measuring of the differential cross-sections for better fit determinations and possible resonance searches using the SAID parameterizations.

1.2.6 HIGH ENERGY π^0 PRODUCTION

The production of the π^0 meson in photon-proton reactions, for incoming photon beam energies greater than 2.8 GeV, is considered to be a hard exclusive reaction. One approach to study the π^0 production, in photon-proton reactions, is use the handbag model. In the handbag approach, the reaction is factorized into two parts.

The first part is when one quark from the incoming and one from the outgoing nucleon participate in the hard sub-process, small blob in Fig. 3. This hard sub-process is achieved when the incident photon excites a quark, since quarks are bound quantum particles, the excited quark produces a jet of quarks that form the meson and then de-excites back into the nucleon. This is calculable using pQCD. The second part, the soft part seen as the large blob in Fig. 3, consists of all the other quarks that are spectators and can be described in terms of GPDs [12–15]. The hard exclusive meson (M) photo-production process factorizes into, $\gamma q \rightarrow Mq$, this is depicted in Fig. 3. The handbag mechanism is applicable when the Mandelstam variables, s , t , u , are large as compared to a hadronic scale of order 1 GeV. In Ref. [1] a model, derived from the handbag approach, has been applied to predict angular dependence of scaled photoproduction cross section of π^0 and is illustrated in Fig. 4. In the analysis presented, this model will be investigated using the data obtained in CLAS.

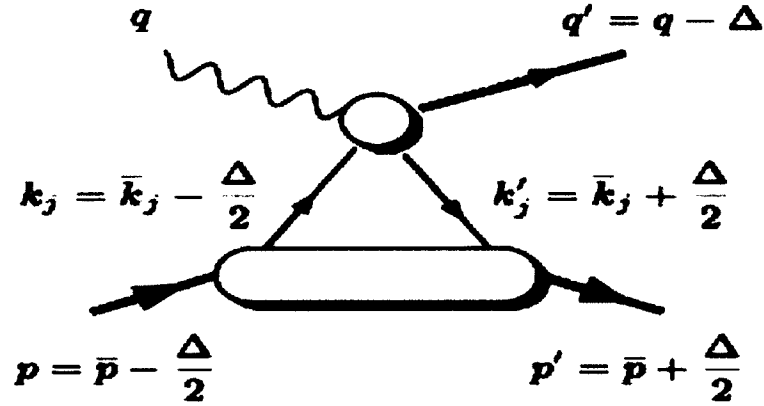


FIG. 3. The handbag-type diagram for photoproduction of mesons. The large blob represents a sum over all spectator configuration. k_j and k'_j denote the momenta of the active partons. The small blob stands for meson photoproduction off partons.

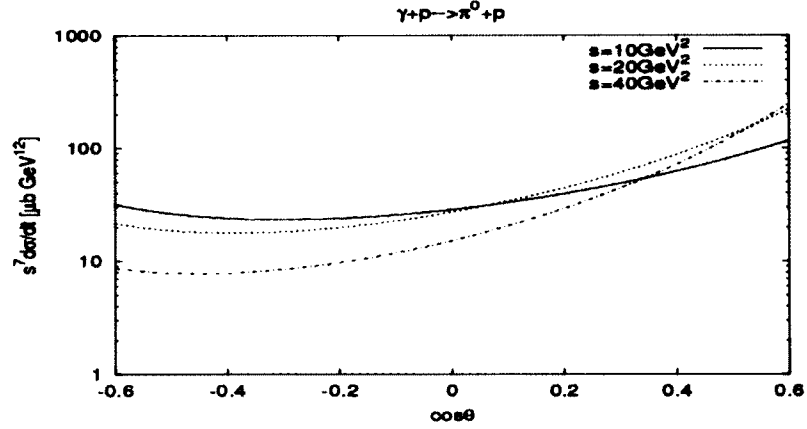


FIG. 4. The soft physics contribution to the cross-section for photoproduction of π^0 scaled by s^7 versus $\cos \theta$, where θ is the scattering angle in the γp c.m. system [1].

1.3 π^0 DECAYS

The main decays studied for this analysis are when a pseudoscalar meson, $P_p(\pi^0, \eta, \eta')$, decays via 2 photons $\gamma\gamma$ or a photon γ and a dilepton (l^+l^-) pair, which are the two most prevalent decays of π^0 as shown in Table 2. Figure 5 illustrates the Feynman diagrams for the “Two photon decay” and the “Dalitz decay”.

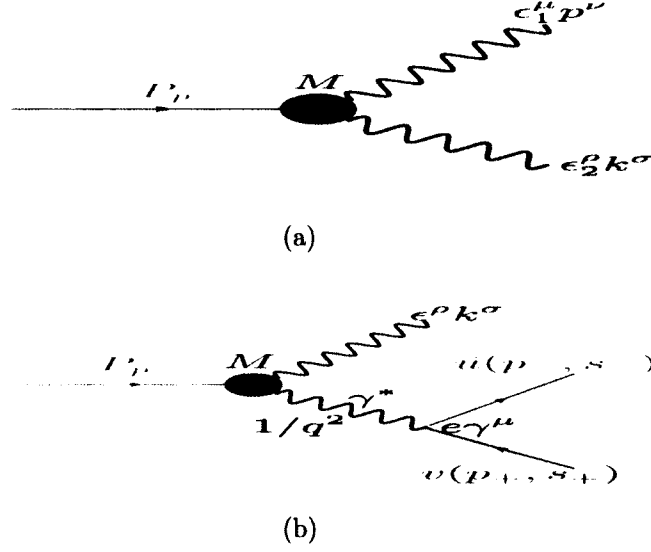


FIG. 5. Feynman diagram of $P_p(\pi^0)$ two photon decay (a), ϵ_1 and ϵ_2 are the polarizations, p and k are 4-momenta of the photons. Feynman diagram of $P_p(\pi^0)$ Dalitz decay (b), the variable s_\pm are the spin helicities of the outgoing leptons l^\pm with 4-momenta p_\pm and ϵ is the polarization of the outgoing photon with 4-momenta k . In both diagrams \mathcal{M} is the form factor.

1.3.1 TWO PHOTON DECAY

As shown in Fig. 5a, the two photon decay can be expressed in terms of the respective momentum, $P_p(\pi^0) \rightarrow \gamma(\epsilon_1, p)\gamma(\epsilon_2, k)$, where ϵ_1 and ϵ_2 are the polarizations of the photons with 4-momenta p and k . Dropping the nomenclature (π^0) in $P_p(\pi^0)$, the four momentum of the decaying meson is $P_p = p + k$. Using the Feynman rules as given in [16] and [17], which are Lorentz and gauge invariant and also parity conserving, the amplitude can be solved to be:

$$\mathcal{M}(P_P \rightarrow \gamma(\epsilon_1, p)\gamma(\epsilon_2, k)) = M_P(p^2 = 0, k^2 = 0)\epsilon_{\mu\nu\rho\sigma}\epsilon_1^\mu p^\nu \epsilon_2^\rho k^\sigma \quad (31)$$

where $\epsilon_{\mu\nu\rho\sigma}$ is the antisymmetric metric tensor. The form factor, $M_P(p^2 = 0, k^2 = 0)$, contains information of the decaying meson and since the decay products are on-shell

photons, which are massless, M_P is a constant given as;

$$M_P = \begin{cases} \frac{\alpha}{\pi f_\pi} & \text{if } P = \pi^0; \\ \frac{\alpha}{\pi f_\pi} \frac{1}{\sqrt{3}} \left(\frac{f_\pi}{f_8} \cos \theta_{mix} - 2\sqrt{2} \frac{f_\pi}{f_0} \sin \theta_{mix} \right) & \text{if } P = \eta; \\ \frac{\alpha}{\pi f_\pi} \frac{1}{\sqrt{3}} \left(\frac{f_\pi}{f_8} \sin \theta_{mix} + 2\sqrt{2} \frac{f_\pi}{f_0} \cos \theta_{mix} \right) & \text{if } P = \eta' \end{cases} \quad (32)$$

where $\alpha = e^2/4\pi \approx 1/137$ is the fine structure constant, $f_\pi \approx 92.4 \text{ MeV}$ is the physical value of the pion-decay constant and $f_0 \approx 1.04 f_\pi$ and $f_8 \approx 1.3 f_\pi$ are the singlet and octet Pseudo-Goldstone meson decay constants.

Squared Matrix Element

The squared matrix element of the decay $P_P \rightarrow \gamma(\epsilon_1, p)\gamma(\epsilon_2, k)$ is given by

$$|\mathcal{M}(P_P \rightarrow \gamma(\epsilon_1, p)\gamma(\epsilon_2, k))|^2 = |M_P|^2 \epsilon_{\mu\nu\rho\sigma} \epsilon_{\mu'\nu'\rho'\sigma'} \epsilon_1^\mu p^\nu \epsilon_2^\rho k^\sigma \epsilon_1^{\mu'} p^{\nu'} \epsilon_2^{\rho'} k^{\sigma'} \quad (33)$$

which can be simplified to;

$$|\mathcal{M}(P_P \rightarrow \gamma(p)\gamma(k))|^2 = |M_P|^2 \epsilon_{\mu\nu\rho\sigma} \epsilon^{\mu\nu}{}_{\rho'\sigma'} p^\rho p^{\rho'} k^\sigma k^{\sigma'} \quad (34)$$

by assuming that the polarizations of the photons remain unobserved, as they are in CLAS. Therefore the photon polarization vectors can be summed using Eq. 5.75 from [16] which reads as;

$$\sum_{\text{polarizations}} \epsilon_\mu \epsilon_{\mu'} \rightarrow -g_{\mu\mu'} \quad (35)$$

As indicated in [16], the right arrow indicates that this is not an actual equality, but the solution is valid as long as both sides are dotted into Eq. 33. The antisymmetric tensor, $\epsilon_{\mu\nu\rho\sigma} \epsilon^{\mu\nu}{}_{\rho'\sigma'}$ is simplified using Eq. A.30 of [16];

$$\epsilon_{\mu\nu\rho\sigma} \epsilon^{\mu\nu}{}_{\rho'\sigma'} = -2(g_{\rho\rho'} g_{\sigma\sigma'} - g_{\rho\sigma'} g_{\rho'\sigma}) \quad (36)$$

$$(37)$$

Applying Eq. 36 to Eq. 34 results in;

$$|\mathcal{M}(P_P \rightarrow \gamma(p)\gamma(k))|^2 = |M_P|^2 (-2)(p^2 k^2 - (p \cdot k)^2) . \quad (38)$$

Substituting

$$(p + k)^2 = p^2 + k^2 + 2(p \cdot k) , \quad (39)$$

and applying $p^2 = k^2 = 0$, since both photons are massless because they are on-shell, we can derive the final expression of the squared amplitude of the decay $P_P \rightarrow \gamma(\epsilon_1, p)\gamma(\epsilon_2, k)$ as;

$$|\mathcal{M}(P_P \rightarrow \gamma(p)\gamma(k))|^2 = |M_P|^2 \frac{1}{2}(p + k)^4 = \frac{1}{2} |M_P|^2 m_P^4 \quad (40)$$

where m_P^4 is the mass of the π^0 derived from the 4-momenta conservation equation $(p + k)^4 = m_P^4$

Decay rate

The decay rate of a two-body decay is explained in Equation 46.17 of [4] as

$$d\Gamma = \frac{1}{32\pi^2} A |\mathcal{M}|^2 \frac{|\mathbf{p}_1|}{m_p^2} d\Omega , \quad (41)$$

where $d\Omega$ is the solid angle of particle 1 and A is the symmetry factor which appears because of the Bose symmetry of the two outgoing photons. Substituting the square matrix element from Eq. 40 into Eq. 41 and integrating over the solid angle yields;

$$\Gamma_{P \rightarrow \gamma\gamma} = \frac{1}{32\pi^2} \frac{1}{2} |\mathcal{M}(P_P \rightarrow \gamma(p)\gamma(k))|^2 \frac{|\mathbf{p}|}{m_P^2} 4\pi = \frac{1}{32\pi} |M_P|^2 m_P^2 |\mathbf{p}| \quad (42)$$

Finally, in the center-of-mass (C.M.) frame of the decaying meson, $\mathbf{p} = \mathbf{E}_\gamma^{\text{C.M.}} = \frac{m_P}{2}$, we find the final expression of the decay rate of $P_P \rightarrow \gamma(\epsilon_1, p)\gamma(\epsilon_2, k)$ as;

$$\Gamma_{P \rightarrow \gamma\gamma} = \frac{1}{64\pi} |M_P|^2 m_P^3 . \quad (43)$$

Using the value for π^0 found in Eq. 32, the value of Eq. 43 calculates to be 7.73 eV theoretically, while the experimental value for the π^0 has been measured to be $7.7 \pm$

0.6 eV [4].

Photon Conversion to e^+e^- Pairs

When a photon travels through matter at energies greater than 100 MeV, it can convert into an electron-positron pair. The process of pair production, $\gamma Z \rightarrow Ze^+e^-$, occurs when a photon with $E_0 > 2m_e c^2$ converts into an electron and a positron. The cross section for this process can be written as;

$$\sigma_{\gamma \rightarrow e^+e^-} = \frac{A}{N_A \rho \lambda_\gamma}, \quad \lambda_\gamma = \frac{9}{7} X_0 \quad (44)$$

where λ is the interaction length, or mean free path, ρ is the density of the material, N_A is Avogadro's number and A is the atomic mass of the material. The probability of pair production to occur is solely based on X_0 , the radiation length of the medium and this probability can be expressed as;

$$\frac{dP}{dx} = \frac{1}{\lambda_\gamma} \exp\left(\frac{-x}{\lambda_\gamma}\right). \quad (45)$$

The probability of pair production when a photon, from the $\pi^0 \rightarrow \gamma\gamma$ decay, travels through liquid hydrogen, ℓH_2 , as shown in Fig. 6. This type of subprocess mimics the

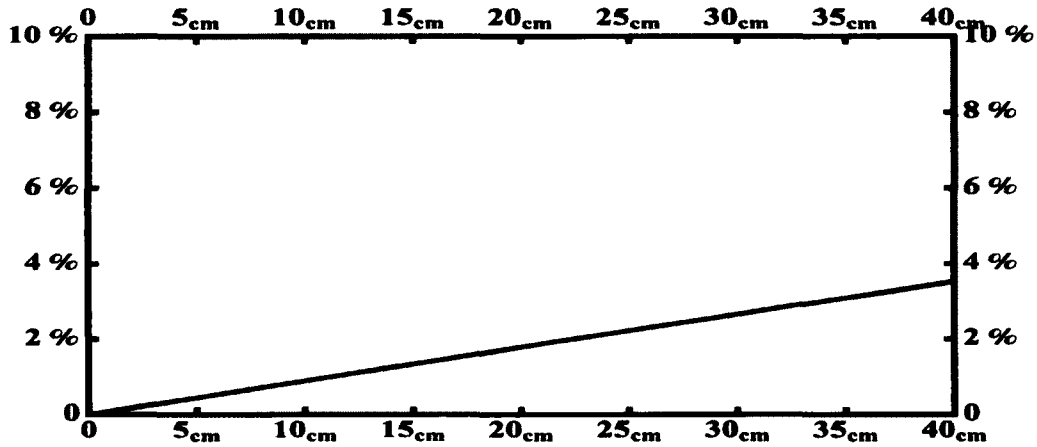


FIG. 6. Probability of pair production, $\gamma \rightarrow e^+e^-$, as a function of distance in liquid hydrogen.

Dalitz decay $\pi^0 \rightarrow e^+e^-\gamma$, described in Sec. 1.3.2. Since there are 2 photons with equal probability of conversion, the total probability is double that shown in Fig. 6.

1.3.2 DALITZ DECAY

When a pseudoscalar meson decays via a photon γ and a dilepton (l^+l^-) pair, it is known as a Dalitz decay or a so-called single off-shell decay. The Dalitz decay is related to the two photon decay. However, in the Dalitz decay, one of the photons is off-shell (γ^*) and decays into a dilepton pair. Since the Dalitz decay is related to the two photon decay, the form factor of the Dalitz decay, for $P(\pi^0, \eta, \eta')$, will be similar to the form factor of the two photon decay of $P(\pi^0, \eta, \eta')$, except there will be an effective mass dependence for the Dalitz decay. Figure 5b depicts the Feymann diagram of the Dalitz decay.

The amplitude for the decay $P_P \rightarrow \gamma^*(p)\gamma(k) \rightarrow l^+(p_+)l^-(p_-)\gamma(k)$ is given by the following expression:

$$\mathcal{M}(P \rightarrow l^+(p_+, s_+)l^-(p_-, s_-)\gamma) = M_P(p^2, k^2 = 0)\varepsilon_{\mu\nu\rho\sigma}\frac{1}{q^2}e\bar{u}(p_-, s_-)\gamma^\mu v(p_+, s_+)q^\nu \epsilon^\rho k^\sigma. \quad (46)$$

Comparing the amplitudes of Eq. 46 and Eq. 31 it is seen that the polarization of the off-shell photon turned into the current $e\bar{u}(p_-, s_-)\gamma^\mu v(p_+, s_+)$ of the lepton pair. The parameters s_\pm are the spin helicities of the outgoing leptons l^\pm and as in Eq. 33, ϵ is the polarization of the outgoing photon.

Squared Matrix Element

$$\begin{aligned} & |\mathcal{M}(P \rightarrow l^+(p_+, s_+)l^-(p_-, s_-)\gamma)|^2 = \\ & \frac{e^2}{q^4} |M|^2 \varepsilon_{\mu\nu\rho\sigma}\varepsilon_{\mu'\nu'\rho'\sigma'}\bar{u}(p_-, s_-)\gamma^\mu v(p_+, s_+)\bar{v}(p_+, s_+)\gamma^{\mu'} u(p_-, s_-)q^\nu \epsilon^\rho k^\sigma q^{\nu'} \epsilon^{\rho'} k^{\sigma'}. \quad (47) \end{aligned}$$

using an equation found between equation 5.3 and 5.4 found in [16]

$$\begin{aligned} & \sum_{s_-, s_+} \bar{u}(p_-, s_-)\gamma^\mu v(p_+, s_+)\bar{v}(p_+, s_+)\gamma^{\mu'} u(p_-, s_-) = Tr \left[(\not{p}_- + m)\gamma^\mu (\not{p}_+ - m)\gamma^{\mu'} \right] \\ & = 2q^2 \left[-(g_{\mu\mu'} - \frac{p_\mu p_{\mu'}}{q^2}) - \frac{(p_+ - p_-)_\mu (p_+ - p_-)_{\mu'}}{q^2} \right] \quad (48) \end{aligned}$$

where the identity $q = p_+ + p_-$ was used. Substituting Eq. 48 into Eq. 47

$$|\mathcal{M}|^2 = \frac{2e^2 |M_P|^2}{q^2} \varepsilon_{\mu\nu\rho\sigma} \varepsilon_{\mu'\nu'\rho'\sigma'} \left[-g^{\mu\mu'} - \frac{(p_+ - p_-)^\mu (p_+ - p_-)^{\mu'}}{q^2} \right] (-g^{\nu\nu'}) q^\rho k^\sigma q^{\rho'} k^{\sigma'} \quad (49)$$

Substituting $k = P - q$ and $p_- = q - p_+$ into Eq. 49

$$|\mathcal{M}|^2 = \frac{2e^2 |M_P|^2}{q^2} \varepsilon_{\mu\nu\rho\sigma} \varepsilon_{\mu'\nu'\rho'\sigma'} \left[-g^{\mu\mu'} - \frac{(2p_+ - q)^\mu (2p_+ - q)^{\mu'}}{q^2} \right] \times (-g^{\nu\nu'}) (q^\rho P^\sigma - q^\rho q^\sigma) (q^{\rho'} P^{\sigma'} - q^{\rho'} q^{\sigma'}) \quad (50)$$

Applying properties of $-g^{\mu\mu'}$ and $-g^{\nu\nu'}$ onto Eq. 50

$$|\mathcal{M}|^2 = \frac{2e^2 |M_P|^2}{q^2} \left[\varepsilon_{\mu\nu\rho\sigma} \varepsilon^{\mu\nu\rho'\sigma'} q^\rho P^\sigma q^{\rho'} P^{\sigma'} + \frac{4}{q^2} \varepsilon_{\mu\nu\rho\sigma} \varepsilon^{\mu\nu\rho'\sigma'} p_+^\nu p_+^{\nu'} q^\rho q^{\rho'} P^\sigma P^{\sigma'} \right] \quad (51)$$

Switching to the rest frame of the pseudoscalar meson, P_p , the 4-momenta is transformed to $P^\sigma = m_p \delta^{\sigma 0}$. The squared amplitude of Eq. 51 reads;

$$|\mathcal{M}|^2 = \frac{2e^2 |M_P|^2}{q^2} m_p^2 \left[\varepsilon_{\mu\nu\rho\sigma} \varepsilon^{\mu\nu\rho'\sigma'} q^\rho q^{\rho'} - \frac{4}{q^2} \varepsilon_{\mu\nu\rho\sigma} \varepsilon^{\mu\nu\rho'\sigma'} p_+^\nu p_+^{\nu'} q^\rho q^{\rho'} \right] \quad (52)$$

The sign change is due to $g^{\sigma\sigma'} = -\delta^{\sigma\sigma'}$. Using the antisymmetric tensor properties $\varepsilon_{\mu\nu\rho\sigma} \varepsilon^{\mu\nu\rho'\sigma'} = 2\delta_{\rho\rho'}$ and $\varepsilon_{\mu\nu\rho\sigma} \varepsilon^{\mu\nu\rho'\sigma'} = \delta_{\nu\nu'} \delta_{\rho\rho'} - \delta_{\nu\rho'} \delta_{\rho\nu'} = (\hat{e}_\nu \times \hat{e}_\rho) \cdot (\hat{e}_{\nu'} \times \hat{e}_{\rho'})$, Eq. 52 is reduced to

$$|\mathcal{M}|^2 = \frac{2e^2 |M_P|^2}{q^2} m_p^2 \left[2|\mathbf{q}|^2 - \frac{4}{q^2} |\mathbf{q}|^2 |\mathbf{p}_+|^2 \sin^2(\theta_{p_+q}) \right] \quad (53)$$

Decay rate

The decay rate of a three-body decay is given in Equation 46.19 of [4] as

$$d\Gamma = \frac{1}{(2\pi)^5} \frac{1}{16m_p^2} |\mathcal{M}|^2 |\mathbf{p}_1^*| |\mathbf{p}_3| d\Omega_1^* d\Omega_3 dm_{12}, \quad (54)$$

where $(|\mathbf{p}_1^*|, \Omega_1^*)$ is the momentum of particle 1 in the rest frame of 1 and 2, and Ω_3 is the angle of particle 3 in the rest frame of the decaying particle m_p [4]. Relating Eq. 54 to the variables in Eq. 53, where $(|\mathbf{p}_1^*|, \Omega_1^*) = (|\mathbf{p}_+|, \Omega_{p_+q})$, $m_{12} = q$ and

$(|\mathbf{p}_3|, \Omega_3) = (|\mathbf{p}_k|, \Omega_k)$, reads;

$$d\Gamma = \frac{1}{(2\pi)^5} \frac{1}{16m_p^2} |\mathcal{M}|^2 |\mathbf{p}_+| |\mathbf{p}_k| d\Omega_+ d\Omega_k dq, \quad (55)$$

In the rest frame of the decaying particle m_p , the 3-momenta $|\mathbf{p}_k| = |\mathbf{q}|$ and the solid angle $\Omega_k = \Omega_q$. Substituting the square matrix element from Eq. 53 into Eq. 55 yields;

$$d\Gamma = \frac{1}{(2\pi)^5} \frac{1}{16m_p^2} \frac{2e^2 |M_P|^2}{q^2} m_p^2 \left[2|\mathbf{q}|^2 - \frac{4}{q^2} |\mathbf{q}|^2 |\mathbf{p}_+|^2 \sin^2(\theta_{p+q}) \right] |\mathbf{p}_+| |\mathbf{q}| d\Omega_{p+q} d\Omega_q dq. \quad (56)$$

The variables $|\mathbf{q}|$ and $|\mathbf{p}_+|$ can be redefined, by means of Eq. 46.20b and Eq. 46.20a of [4], as

$$|\mathbf{q}| = \frac{m_p^2 - q^2}{2m_p} \quad (57)$$

$$|\mathbf{p}_+| = \frac{\sqrt{q^2 - 4m_l^2}}{2} = \frac{q\sqrt{1 - \frac{4m_l^2}{q^2}}}{2} = \frac{q\mathcal{K}}{2}, \quad (58)$$

where $\mathcal{K} = \sqrt{1 - \frac{4m_l^2}{q^2}}$. Replacing the variables calculated in Eq. 57 and Eq. 58 into Eq. 56 and collecting terms yields;

$$d\Gamma = \frac{1}{(2\pi)^5} \frac{1}{16m_p^2} |M_P|^2 \left[\frac{2e^2 m_p^2}{8} \left(\frac{m_p^2 - q^2}{2m_p} \right)^3 \right] (2 - \mathcal{K}^2 \sin^2(\theta_{p+q})) \frac{\mathcal{K}}{4q^2} dq^2 d\Omega_{p+q} d\Omega_q, \quad (59)$$

where the identity $qdq = \frac{dq^2}{2}$. Performing the integration of $\Omega_{p+q} d\Omega_q$ and replacing $e^2 = 4\pi\alpha$ transforms Eq. 59 into;

$$d\Gamma = \frac{1}{(2\pi)^3} \frac{1}{32} \frac{4\pi\alpha}{3} |M_P|^2 \left[\frac{m_p^6 \left(1 - \frac{q^2}{m_p^2}\right)^3}{m_p^3} \right] (3 - \mathcal{K}^2) \frac{\mathcal{K}}{q^2} dq^2, \quad (60)$$

which can be simplified further to;

$$d\Gamma = \left(\frac{1}{64\pi} |M_P|^2 m_P^3 \right) \frac{2\alpha}{3\pi} \frac{1}{q^2} \left(1 - \frac{q^2}{m_p^2} \right)^3 \left(1 + \frac{2m_l^2}{q^2} \right) \left(1 - \frac{4m_l^2}{q^2} \right)^{\frac{1}{2}} dq^2 . \quad (61)$$

The form factor $M_P(p^2, k^2 = 0)$ can be written as follows:

$$M_P \rightarrow M_P \times |F(q^2)| , \quad (62)$$

where M_p is the decay constant of two photons mentioned in Sec. 1.3.1 and $|F(q^2)|$ is called the transition form factor, which defines the electromagnetic space structure of the meson.

It can be seen that the first set of variables in parenthesis in Eq. 63 is Eq. 43, therefore;

$$\frac{d\Gamma}{\Gamma_{\gamma\gamma} dq^2} = \frac{2\alpha}{3\pi} \frac{1}{q^2} \left(1 - \frac{q^2}{m_p^2} \right)^3 \left(1 + \frac{2m_l^2}{q^2} \right) \left(1 - \frac{4m_l^2}{q^2} \right)^{\frac{1}{2}} |F(q^2)|^2 , \quad (63)$$

which is the Kroll-Wada equation founded in [18].

The value of $|F(q^2)|$ can be directly measured by comparison of the differential cross section with that of Q.E.D. pointlike differential cross section i.e.

$$\frac{d\sigma}{dq^2} = \left[\frac{d\sigma}{dq^2} \right]_{\text{pointlike}} |F(q^2)|^2 ,$$

or by performing a line shape analysis on the l^+l^- invariant system using assumptions on the structure of $|F(q^2)|$. One such assumption for $|F(q^2)|$ is the dipole approximation in which

$$F(q^2) = \left[1 - \frac{q^2}{\Lambda^2} \right]^{-1}$$

1.3.3 SUMMARY

The two photon decay and the Dalitz decay have different branching ratios. This difference is attributed to the factor of α along with a q^2 dependence calculated in the Dalitz decay. However, due to the probability of a photon converting into an

electron-positron pair in ℓH_2 , the total amount of e^+e^- pairs produced via photon conversion is about the same as via Dalitz decay.

CHAPTER 2

THE CLAS DETECTOR AT THOMAS JEFFERSON NATIONAL ACCELERATOR FACILITY

The Thomas Jefferson National Accelerator Facility (TJNAF, Fig. 7), also known as Jefferson Laboratory (JLAB) is located in Newport News, Virginia. It is one of 17 national laboratories funded by the U.S. Department of Energy and is home to three experimental halls, A, B, C, and the Continuous Electron Beam Accelerator Facility,[19] (CEBAF, Fig. 8).

JLAB's stated mission is "to provide forefront scientific facilities, opportunities and leadership essential for discovering the fundamental structure of nuclear matter; to partner in industry to apply its advanced technology; and to serve the nation and its communities through education and public outreach." [20] In addition to its science mission, the lab provides programs designed to help educate the next generation in science and technology, and to engage the public.

The analysis performed in this work utilizes experimental data collected with the CEBAF Large Acceptance Spectrometer (CLAS) in hall B, using CEBAF. The experiment *g12* collected over 126 TB of raw data in 44 days of beam time from April to June 2008, making *g12* the world's largest multi-particle dataset in the energy range $1.77 \text{ GeV} < \sqrt{s} < 3.33 \text{ GeV}$. This chapter is dedicated to the explanation of CEBAF, CLAS and other subsystems used during the *g12* run period.



FIG. 7. Aerial view of Jefferson Laboratory (JLAB) facing east. Image Source: [21]

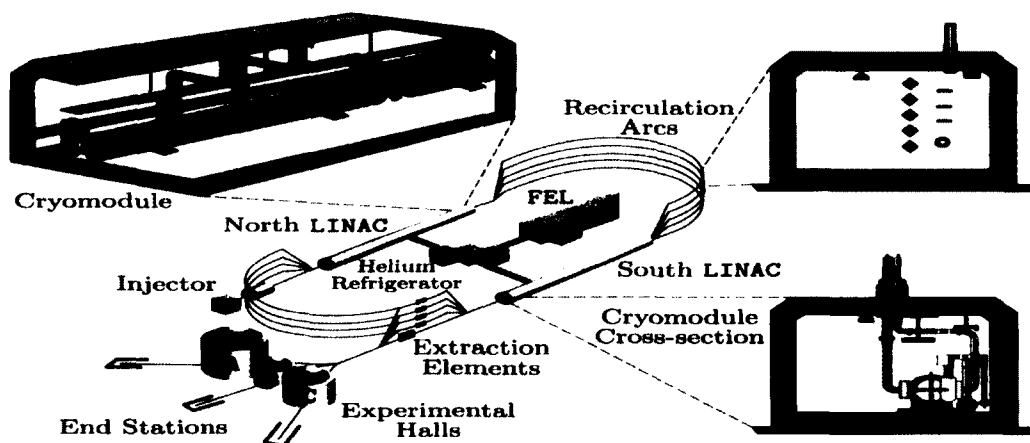


FIG. 8. The Continuous Electron Beam Accelerator Facility (CEBAF) at Jefferson Laboratory (JLAB) showing cross-sections of the linear accelerator (LINAC) halls and the recirculation arcs. Also depicted are the Free Electron Laser (FEL) and the helium refrigerator and distribution facility. Image Source:[19]

2.1 CONTINUOUS ELECTRON BEAM ACCELERATOR FACILITY

CEBAF utilizes superconducting radio-frequency (**SRF**) cavities to accelerate electrons and provide a continuous wave beam with 75% polarization to the three halls simultaneously. A list of some specifications for **CEBAF** can be found in Table 3.

To achieve the running conditions described in Table 3 **CEBAF** uses a GaAs photocathode laser driven injector system to produce a highly polarized electron beam. The laser pulses create three electron bunches that are bunched together in 2 ns groups, about 90 μm in length. Each bunch is 499 MHz at the source at 100 keV, spaced apart by 120° of **RF** phase. Together the electron bunches form a 1497 MHz beam that then enters two $1/4$ **SRF** cavities which accelerate the electrons to $\sim 1\%$ of the total machine energy before it is injected into the **CEBAF**'s main accelerator.

When the electron bunches enter the **Nb SRF** cavity, they undergo an acceleration gradient provided by **RF** standing wave established inside of the cavity. The standing waves are kept in phase with the electron bunches resulting in a continuous positive electric force on each bunch as it passed through a cavity, see Fig. 9

The main accelerator, Fig. 8, consists of a pair of linear accelerators (**LINACs**). Each **LINAC** contains 168 **SRF Nb** cavities that are submerged in liquid Helium and cooled to 2.08 K, the temperature by which **Nb** becomes superconducting. In total there are twenty cryogenic modules, each containing eight superconducting niobium cavities as depicted. in Fig. 10.

The beam, once inside the **LINAC** can be passed up to five times. The **LINACs** are connected by two sets of 180° magnetic-dipole bending arcs (see Fig. 8) with a radius of 80 meters. The beam is sent through both accelerators and is then recirculated up to four more times. Each **LINAC** is capable of accelerating the beam by up to 600 MeV giving approximately 1.2 GeV per pass. Each hall can choose to extract the beam after any number of passes, however the fifth (final) pass can be sent to all three halls simultaneously. It should be noted that although each hall can receive the fifth pass, no two halls can run with the same lower energy [22]. At the time of the *g12* experiment, the accelerator was capable of delivering a maximum electron beam energy of 5.714 GeV.

TABLE 3. Operating specifications of CEBAF at JLAB.[19]

E_{min}	0.6 GeV
E_{max}	6.0 GeV
I_{max}	200 μ A
Polarization	> 75%
Geometric emittance	< 10^9 m rad
Momentum Spread	10^{-5}
Average currents (Halls A and C)	1-150 μ A
Average currents (Hall B)	1-100nA
Bunch charge	< pC
Repetition rat	499 MHz/hall
Beam size (rms transverse)	$\sim 80 \mu$ m
Bunch length (rms)	300 fs, 90 μ m
Energy spread	2.5×10^5
Beam power	< MW
Beam loss	< μ A
Number of passes	5
Number of accelerating cavities	338
Fundamental mode frequency	1947 MHz
Accelerating cavity effective length	0.5m
Cells/cavity	5
Average Q_0	4.0×10^9
Implemented Q_{ext}	5.6×10^6
Cavity impedance (r/Q)	980 Ω
Average cavity accelerating gradient	7.5 MV/m
RF power	< 3.5 kW/cavity
Amplitude control	1.00×10^{-4} rms
Phase control	0.1 $^\circ$ rms
Cavity operating temperature	2.08 K
Heat load @ 2 K	< 9 W/cavity
Liquefier 2 k cooling power	5kW
Liquefier operating power	5MW

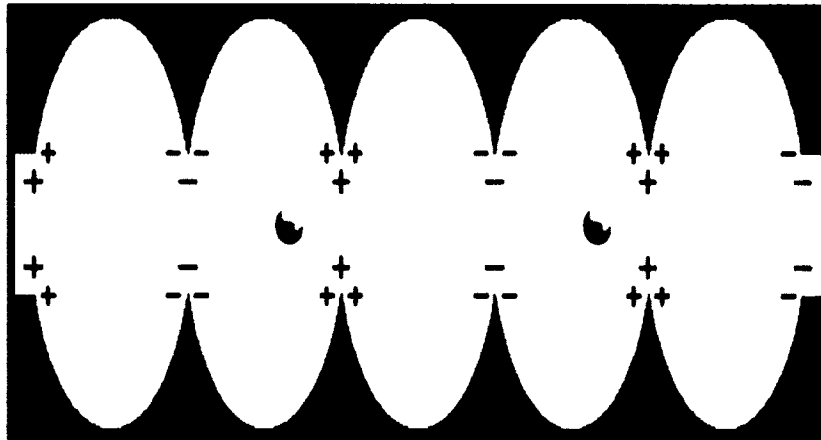


FIG. 9. Accelerating Cavity Diagram. Electron clusters experience a continuous acceleration due to a standing electromagnetic wave indicated by the positive and negative signs along the inner wall.

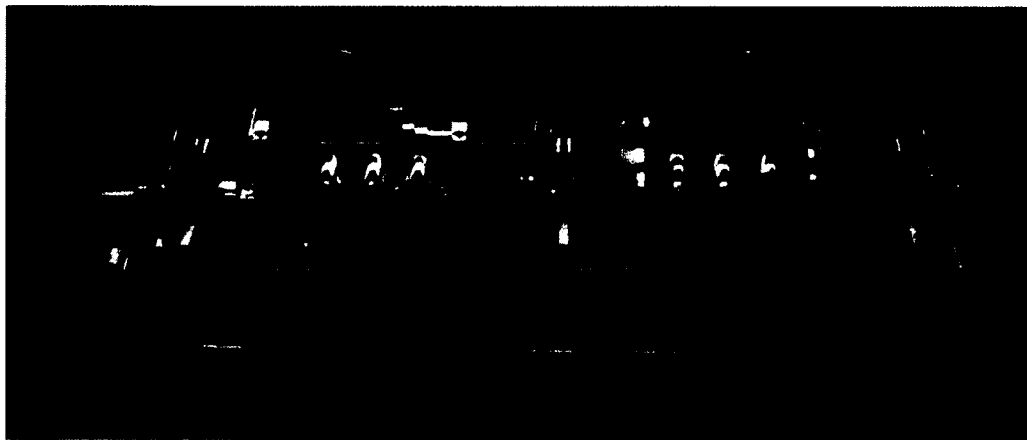


FIG. 10. A CEBAF superconducting niobium cavity pair. Image Source: [19]

2.2 BEAM POSITIONING

There are several beam monitoring stations in Hall B before and after the CLAS detector (Fig. 11) to scan the important details of the electron beam prior to conversion into a photon beam and the details of the photon beam before and after entering the target. Such quantities for the electron beam include position, intensity, dispersion, and current, and for the photon beam include position, dispersion and flux. Most of these monitoring stations are used by the accelerator group. There are two types of devices to measure the electron beam position. The first type is represented by two beam position monitors (BPMs) placed before the tagger. The position monitors use three radiofrequency cavities to measure the transverse location of the electron beam and its intensity. This information is used as feedback for the steering mechanism. The position monitors are noninvasive and measure at a rate of 1 Hz. The second type of device used to measure the beam position is the Harp Beam Profile Monitor, which also measures the electron beam dispersion. The harp devices consist of fine wires (20 and 50 μm W and 100 μm Fe) that can be passed through the beam at specific orientations and collect scattered electrons with a photomultiplier tube. This procedure measures the horizontal (x) and vertical (y) profile of the electron beam and is performed after any downtime or change in the beam. The accelerator group adjusts the beam position such that more than 99% of the electron beam goes through the radiator. Since this process is invasive, it was only done when the drift-chambers and DAQ were turned off. A harp scan measurement for $g12$ is shown in Fig. 12. The width of the beam was contained within a 200 μm diameter.

The Total Absorption Shower Counter located downstream of CLAS, measures the photon flux (see Fig. 13). The TASC, consists of four lead glass blocks of ~ 17 radiation lengths, each coupled to a photo-multiplier tube (PMT). The TASC is approximately 100% efficient at detecting photons at beam currents less than 100 pA[25, 26]. Since $g12$ ran with 65 nA current, special low current, 50 pA, normalization runs(see Table 13) were taken several times throughout $g12$. The ratio of electrons detected in the photon tagger (see Sec. 2.3) to that of photons detected in the TASC gives the tagging ratio used to calibrate the tagger and measure the flux throughout the entire $g12$ run period.

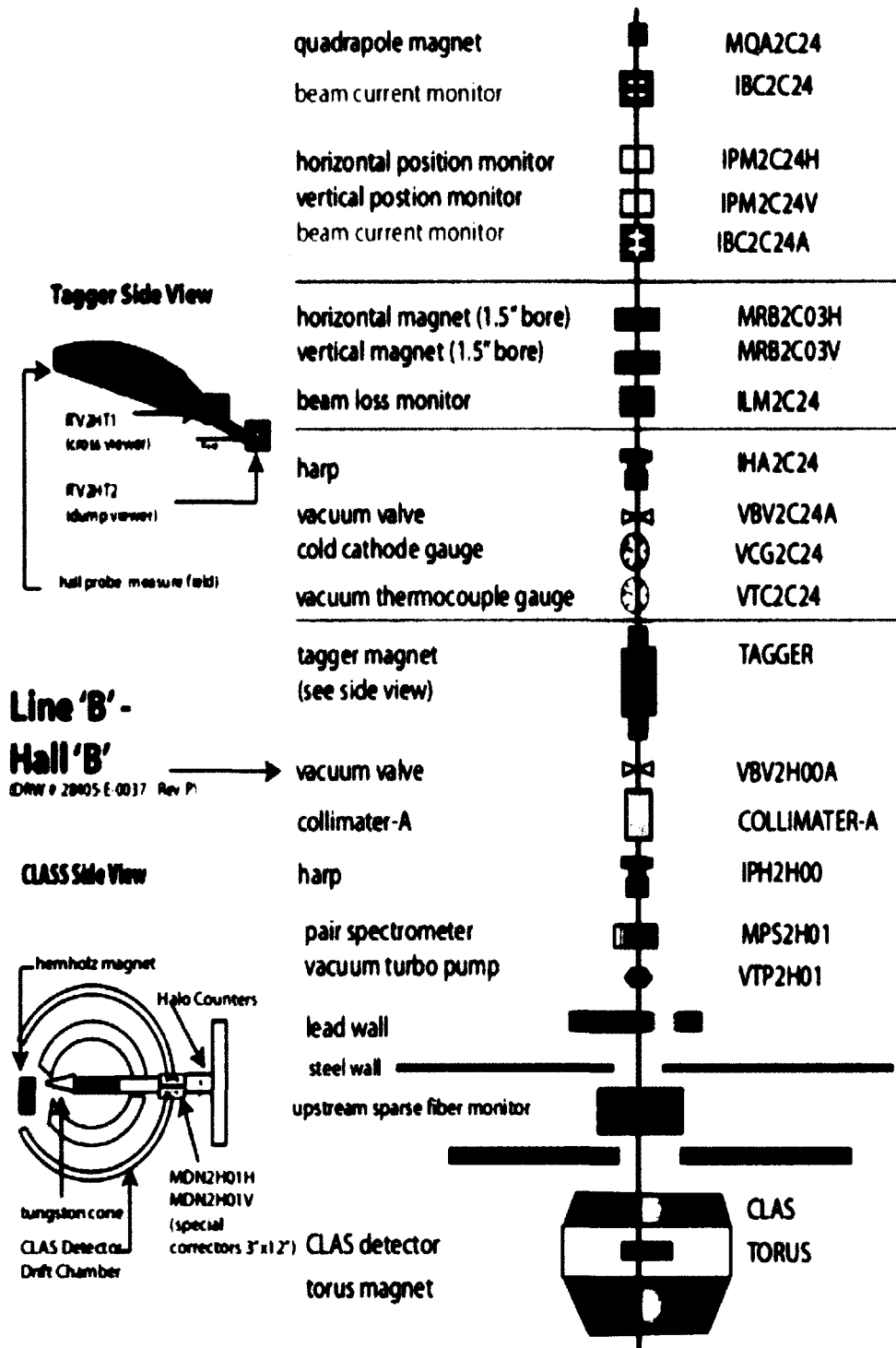


FIG. 11. Beamline and components of CLAS. Image Source [21]

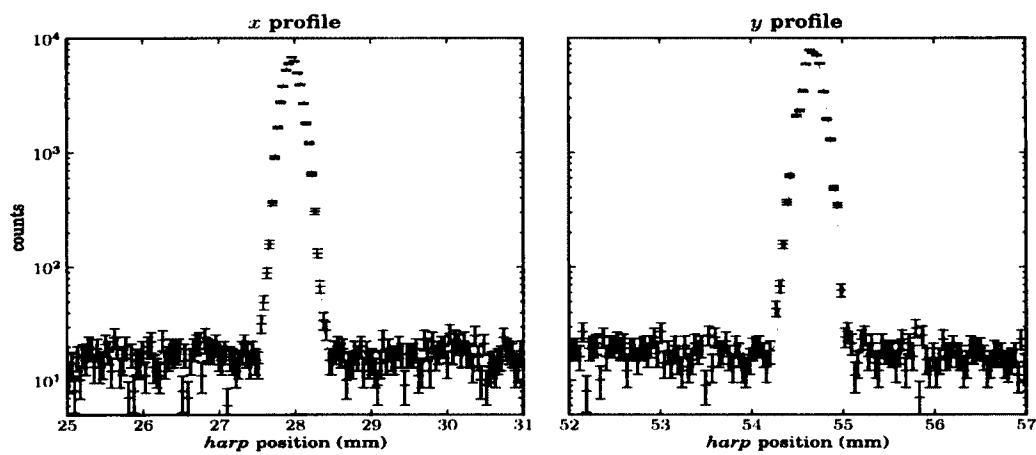


FIG. 12. A typical *harp* scan done just prior to run 56426. Shown are the x and y profiles of the electron beam just before the tagger. The dashed orange line is a Gaussian fit to the data: $\sigma_x = 0.115$ mm and $\sigma_y = 0.105$ mm. Image Source: [24]

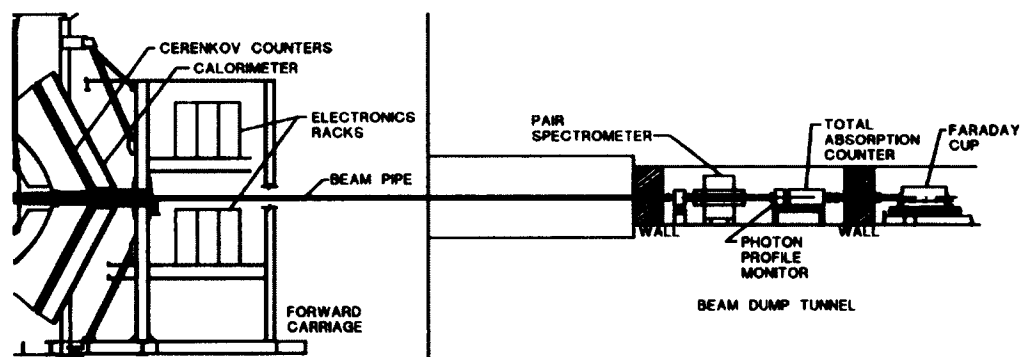


FIG. 13. Beamline components in $g12$ after CLAS

2.3 PHOTON TAGGER

The electron beam delivered to hall B from CEBAF can be sent directly to a target or the electron beam can produce a *real photon* beam by means of bremsstrahlung radiation by passing the electron beam through a radiator. Typical radiators have high atomic number to help reduce contamination of photons produced by electron-electron scattering. The *g12* experiment used a gold (Au) foil of 10^{-4} radiation length. This choice has a double purpose, to maximize the probability of the electron-nucleus interaction given that the bremsstrahlung cross section is proportional to Z^2 , and to minimize the number of interaction centers such that each electron interacts once, producing only one photon. After the electron beam passes through the radiator, the beam becomes a mixture of photons and electrons that did not interact with the radiator and recoil electrons. The mixed beam then travels into a dipole magnetic field which sweeps the electrons out of the electron-photon beam. The electrons present in the electron-photon beam are directed toward two hodoscope planes, each made of an overlapping array of scintillators to detect the energy-degraded electrons.

The first scintillator plane, referred to as the E-plane (Figs. 14, and 15), is used to determine the momentum of the recoiling electrons. The E-plane provides photon energy resolution on the order of 0.1% of the incident electron beam energy. It consists of 384 paddles that are 20 cm long, 4 mm thick and from 6 to 18 mm wide. The paddles are arranged in an overlapping fashion, thus increasing the number of logical paddles to 767. The trajectory of an electron or any charged particle in the magnetic field is governed by the equation

$$p = qrB \text{ (if } \vec{p} \perp \vec{B} \text{)} \quad (64)$$

where p is the particle's momentum, q is the particle's charge, r is the particle's radius of curvature and B is the magnetic field the particle passes through. By determining which paddle an electron hit we know the radius of curvature and we can calculate the momentum of the electron. The momentum of the electron can then be used to obtain the energy of the photon by means of the conservation relation

$$E_\gamma = E_0 - E_e \quad (65)$$

where E_0 is the energy of the incident electron given by CEBAF, E_e is the energy of

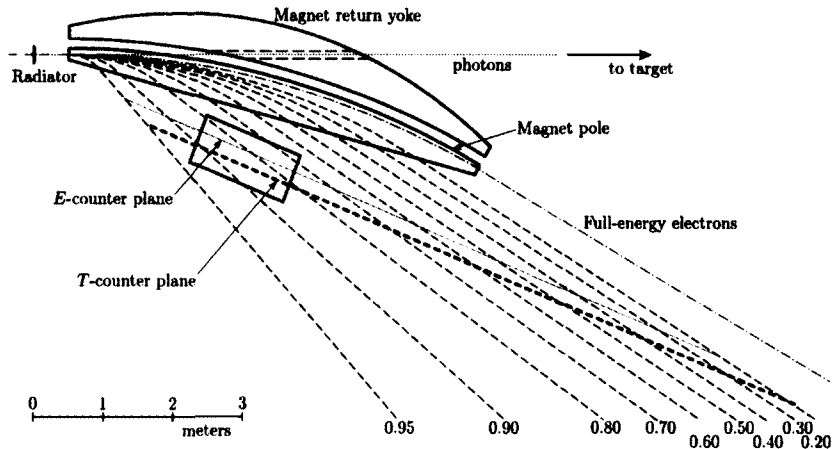


FIG. 14. Scale drawing of the photon tagger system. The rectangular area around the E and T -counter planes outlines the expanded view shown in Fig. 15.

the recoil electron and E_γ is the energy of the emitted photon.

The second scintillator plane, referred to as the T-plane, is used to make accurate timing measurements of the recoiling electrons. This plane comprises of 61 paddles that are each 2 cm thick. The added thickness of these paddles allow for a timing resolution of 110 ps.

The tagger can tag photons of energies from 20 to 95% of the incident electron beam energy. For $g12$ this corresponds to a photon energy range of 1.142 - 5.425 GeV. Due to the high current of the electron beam delivered to $g12$ from CEBAF there were usually more than one “hit” in the tagger for each event. Normally, the one associated with the photon that caused the event could be obtained by a timing coincidence with the tracks, although there are cases when this photon is ambiguous as discussed in Sec. 4.1.3.

The photons that pass through the radiator then pass through a 6.2 mm diameter collimator. Collimation is used to trim the beam halo prior to arriving at the CLAS cryotarget. In the $g12$ experiment the beam entering the cryotarget was 1.5 cm in radius. The collimator was positioned 537 cm upstream of the cryotarget which had a radius of 2 cm. A sweeping magnet were placed after the collimator to remove any charged particles created by interactions of photons with the collimator.

More detailed information on the Hall B tagging system and DAQ of the tagger system can be found in [25].

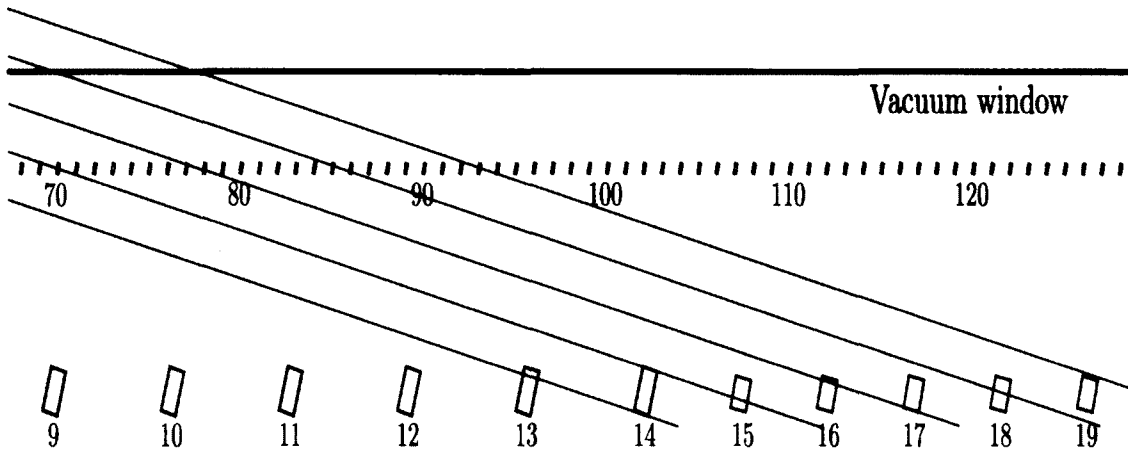


FIG. 15. Scale drawing of the E -counters (blue) and the T -counters (green) showing examples of recoiled electrons (red lines) entering from the upper left.

2.4 CEBAF LARGE ACCEPTANCE SPECTROMETER (CLAS)

The CLAS detector, shown in Figs. 16, 17, is assembled of four types of detectors, five detectors total, that are arranged in an onion like pattern (around the beam line) covering $\sim 3\pi$ with a diameter of 8 m. Each layer is segmented such that there are six segments around ϕ (angle about the beam line), called sectors, each with a polar coverage, θ (angle from beam line), of approximately $\frac{3}{4}\pi$ radians. Each sector consists of a scintillator start counter (ST) Sec. 2.5, three layers of drift chambers (DC) Sec. 2.7, a layer of scintillator “time-of-flight” counters (TOF) Sec. 2.9, a gas Cherenkov counter (CC) Sec. 2.8 and an electromagnetic calorimeter (EC) Sec. 2.10. There is a toroidal magnetic field generated by six superconducting coils that divide the sectors. The direction of the toroidal field is azimuthal, ϕ (angle about the beam line), such that the charged particles conserve their azimuthal angle along their trajectory, except near the coils. The magnetic field geometry guides the particles which allows for a simplified reconstruction algorithm to determine the particles’ momenta, see Eq. 64. This section will discuss the subsystems in more detail.

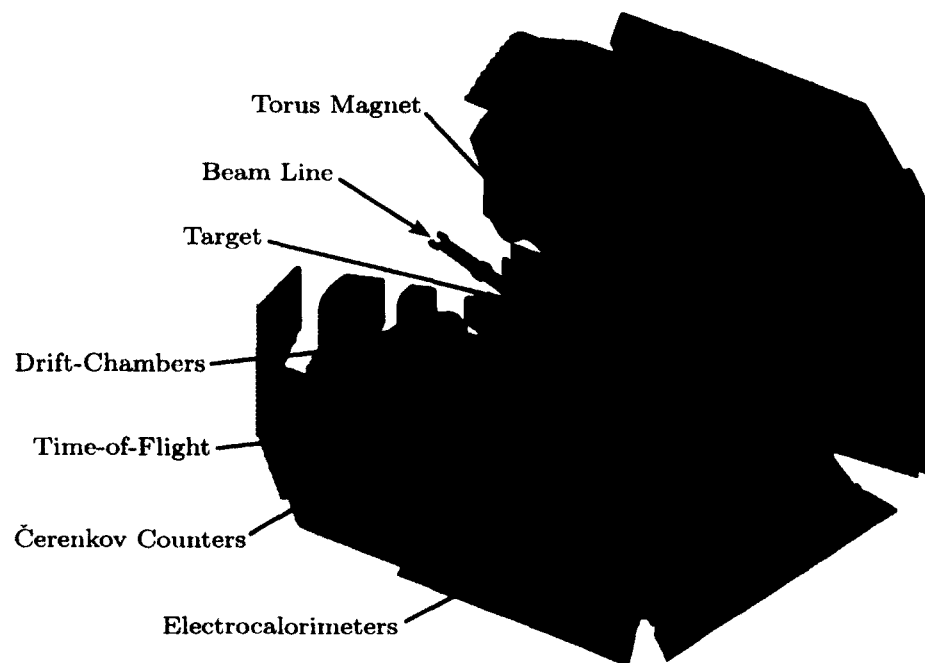


FIG. 16. Schematic of the CLAS detector[27] with subsystems identified. This view is looking upstream and the beam enters from the upper left. The detector is approximately 8 meters in diameter.

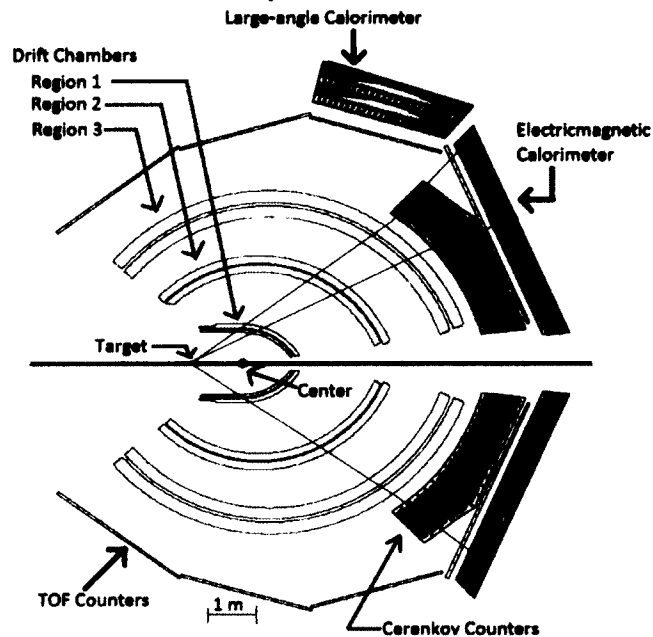


FIG. 17. A cross section view of the CLAS detector showing an event with three tracks emanating from the target. The two tracks leaving hit patterns CC and EC are leptons while the track on the bottom panel is a proton



FIG. 18. The coils of the CLAS toroidal magnet prior to installation of the rest of the detector. Image Source [28]

2.4.1 HYDROGEN CRYOTARGET

The target used by *g12* was conical as shown in Fig. 19. The target walls were constructed of $0.127\ \mu\text{m}$ thick Kapton. It is 40 cm in length and 2 cm in radius. The incident photon beam had a radius of 1.5 cm. The target cell design shown in Figs. 19 and 20 had been used in several experiments and is capable of containing a number of different materials, such as helium, deuterium and hydrogen. For *g12* the target was filled with liquid hydrogen (ℓH_2). The temperature and pressure of the target was continuously measured and recorded. In Sec 4.11, these measurements will be used to calculate the density of the liquid Hydrogen to determine the target thickness. The target was not polarized.

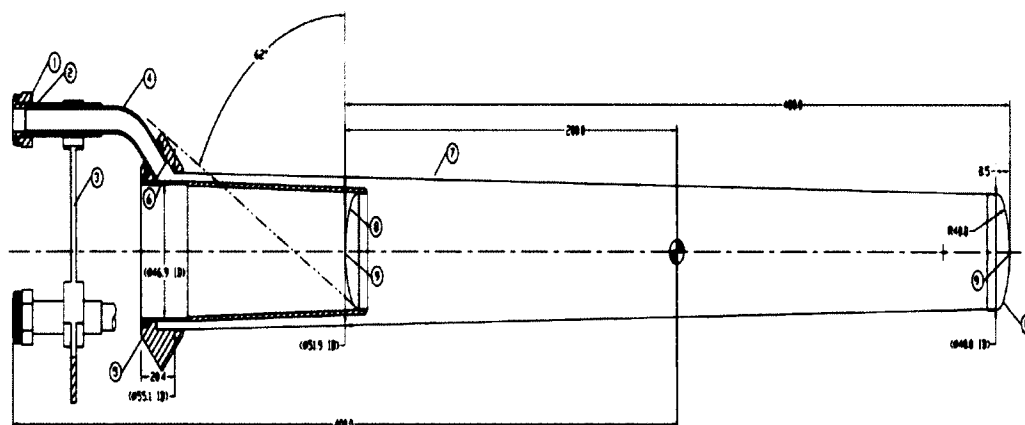


FIG. 19. Blueprint schematic of the conical Kapton target cell used for *g12*.

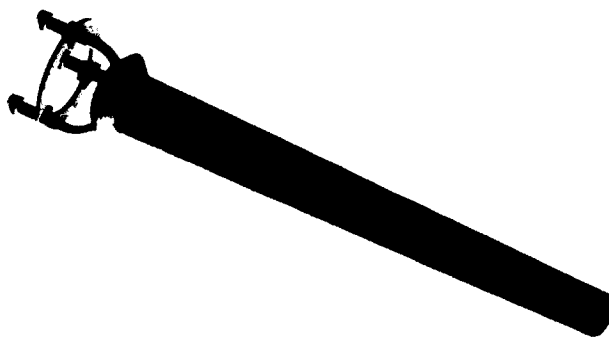


FIG. 20. The 40 cm long conical Kapton target cell used for *g12*.

The target was located 90 cm upstream of CLAS the center, see Fig. 17. This increased the forward angle acceptance from 8° to 6° . However, this also decreased the large angle acceptance from approximately 140° to 100° in the lab frame.

2.5 START COUNTER

The start counter, Figs. 21 and 22, is a PMT-instrumented scintillator detector that surrounds the CLAS cryotarget hermetically. It consists of 24 scintillation paddles divided into six sectors matching that of CLAS. Each sector of the start counter is constructed of four independently-instrumented scintillator strips. Timing resolution of the start counter is ~ 350 ps. The start counter information was used the *g12* triggers 3.1.1. More information on the CLAS start counter can be found in [29].



FIG. 21. Schematic of the start counter (ST) with the 40 cm long target cell (purple) at the center. The beam enters from the upper left of the figure.

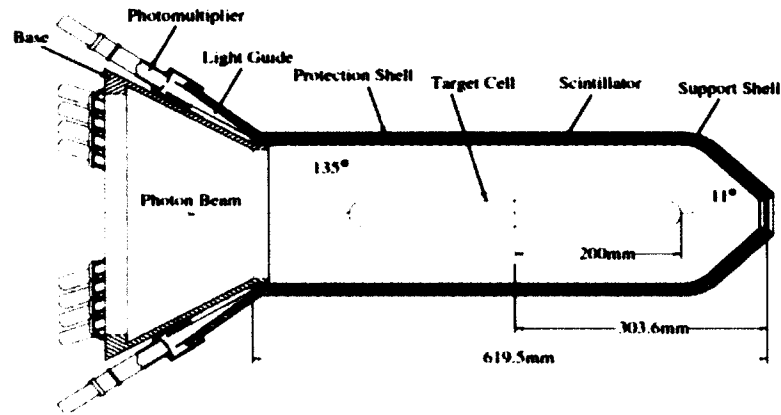


FIG. 22. Cross-section view of the start counter illustrating the labeled components and its angular coverage when at the center of CLAS.

2.6 SUPERCONDUCTING TOROIDAL MAGNET

The essence of CLAS is the use of a toroidal magnetic field generated by six superconducting coils consisting of 4 layers of 54 windings of aluminum-stabilized niobium titanium NbTi/Cu superconductor [27]. The coils are separated in the azimuthal direction, ϕ , by 60° and are located between Region-1 and Region-3 of the DC, see Fig 23. The placement of the coils is such that the magnetic field is encompassed by the volume of the DC, see Fig. 23. The direction of the toroidal field points along ϕ , except near the coils, such that the charged particles conserve their azimuthal angle along their trajectory, see Fig 24. The maximum current the magnet can support is 3861 A, resulting in a maximum field strength of 35 kG. During the *g12* experiment, the magnets operated at a current of 1930 A corresponding to a maximum field of about 20 kG. The field was oriented such that positive charged particles bent away from the beam-line, while negative charged particles bent toward the beam-line. Running at higher currents provides better momentum resolution but decreases the detector's acceptance for negative particles. Knowing the strength and direction of the magnetic field and the trajectory of a particle using the DC, the particle momentum can be determined by use of Eq. 64.

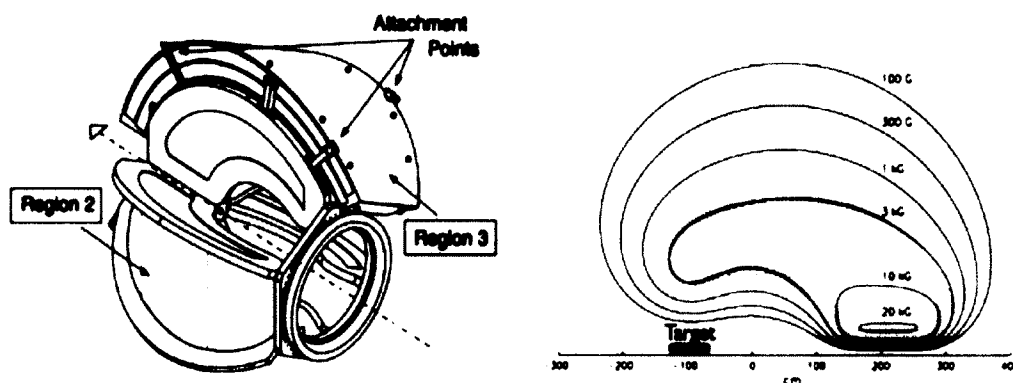


FIG. 23. The CLAS Superconducting Toroidal Magnet and its placement in relation to Region-1 and Region-3 (left). Cross-section of the CLAS Superconducting Toroidal Magnet at half current (1930 A). Region-2 of the DC is located inside the region of the coils shown as the kidney shaped loop at about 3 kG (right).

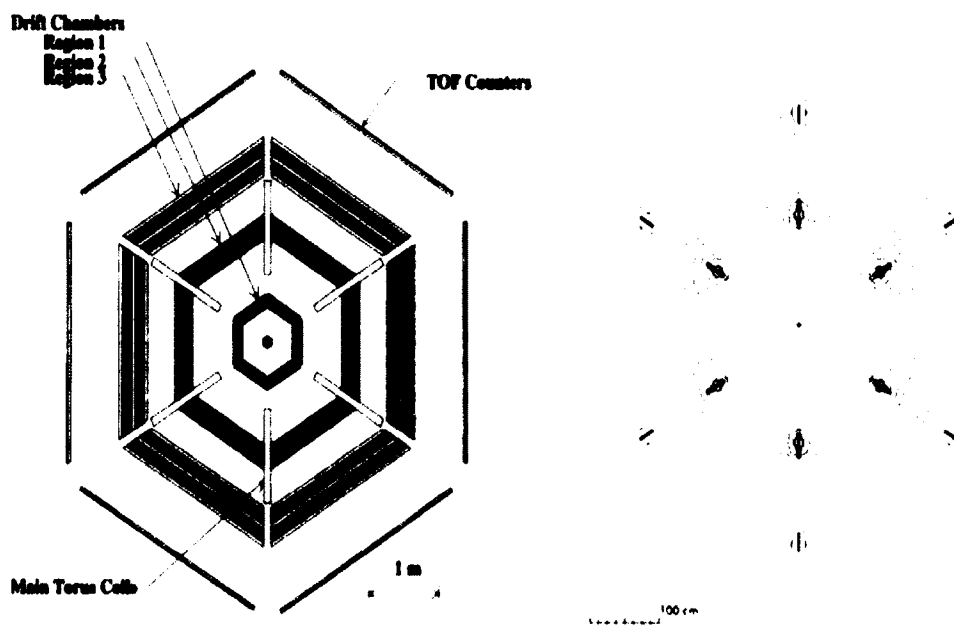


FIG. 24. Schematic cross-sectional view of the CLAS detector, perpendicular to the beam line (left). The magnetic field distribution corresponding to the view in the left figure. The field is purely azimuthal. The six torus coils are shown in grey, the field is in the counter-clockwise direction, the field strength is concentrated in the region between the coils (right).

2.7 DRIFT CHAMBERS

The CLAS drift chambers DC (Figs. 16, 24, 26) track charged particles above 200 MeV/c with polar angle resolution of 2-4 mrad and momentum resolution of 0.5 - 1%, depending on momentum, see Fig 25. Typical coverage of the DC is $8^\circ < \theta < 142^\circ$, when the target is at CLAS center. For the *g12* experiment the coverage of the DC was modified to $6^\circ < \theta < 100^\circ$ due to the placement of the target, see Sec 2.4.1 for reasons explained in [30], [31], [32].

The DC are divided into six sectors each containing three radial layers (Fig. 26), referred to as “Regions”, for a total of 18 separate drift chambers. Each DC region covers the same polar angular range and consist of two superlayers which each contain six layers of hexagonal wire cells which house evenly spaced 20 μm gold-plated tungsten sense wires (center of hexagon) each surrounded by six 140 μm gold-plated aluminum alloy field wires (vertices of hexagon). In the first superlayer, the wires are strung approximately parallel to the direction of the magnetic field (axial wires), while the second superlayer has wires tilted at a 6° angle with respect to the axial wires (stereo wires). A high voltage system maintains the sense wires at positive potential, while the field wires are maintained at a negative potential 50% lower than the positive value. The difference of potentials creates an avalanche of the electrons induced by the ionizing particle. The hexagonal shape of the cell mimics a circular geometry cell in which the drift time to drift distance is independent of entrance angle.

The inner region is denoted as Region 1. Its first superlayer has only 4 layers due to space constraints. Region 1 is nearly free from magnetic field, see Fig 23. Region 2 is situated between the magnetic coils which is subject to the highest magnetic field which is used to determine the particle’s curvature, needed to determine the particle’s momenta, see Eq. 64. Region 3 purpose is to provide global track reconstruction in connection with other CLAS detectors since Region 3 is located outside the volume of magnetic field. Each DC is filled with a gas mixture of 90% argon and 10% carbon-dioxide. This choice of gas provides high drift velocity (0.04 m/ μsec) and fast collection time which improves momentum resolution. For more information on the design of the CLAS DC system, see [33] and for more information on the calibration process of the CLAS DC system, see [34].

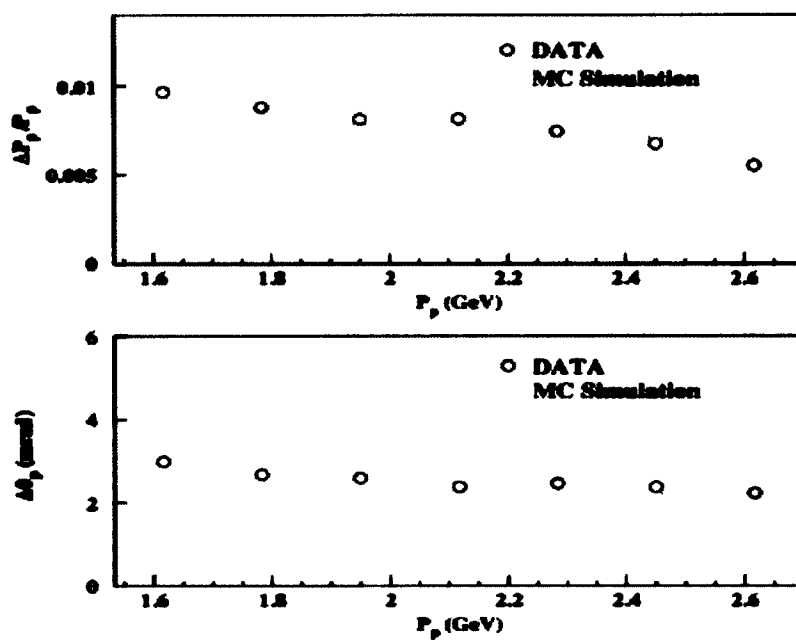


FIG. 25. Momentum and angular resolution for protons as determined from the measured angle of the scattered electron for data collected and Monte-Carlo simulation. Image Source [27]

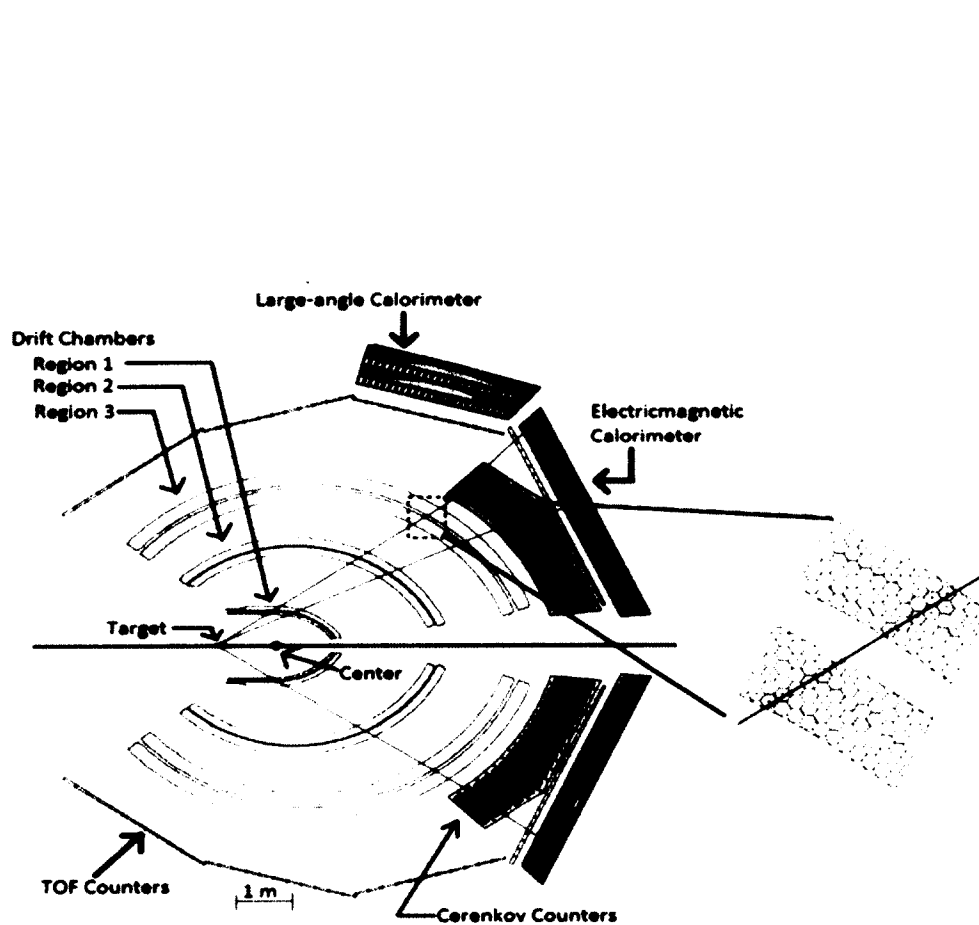


FIG. 26. A cross section view of the CLAS detector showing an event with three tracks emanating from the target. The two tracks leaving hit patterns CC and EC are leptons while the track on the bottom panel is a proton. The inlet shows hexagonal cells of drift chambers with a typical track indicated by shaded areas for the cut-out in Region-3.

2.8 CHERENKOV RADIATION AND DETECTORS

When a charged particle traverses through a medium with a velocity less than the speed of light for that medium ($v < c/n$) the dipoles of the molecules in the medium are symmetrically arranged such that the integrated dipole field along the particles path vanishes. However, when the particles speed is greater than that of the speed of light for that medium the dipoles of the molecules arrange themselves such that they are asymmetric along the particles path and thus creates a dipole field, see Fig 27.

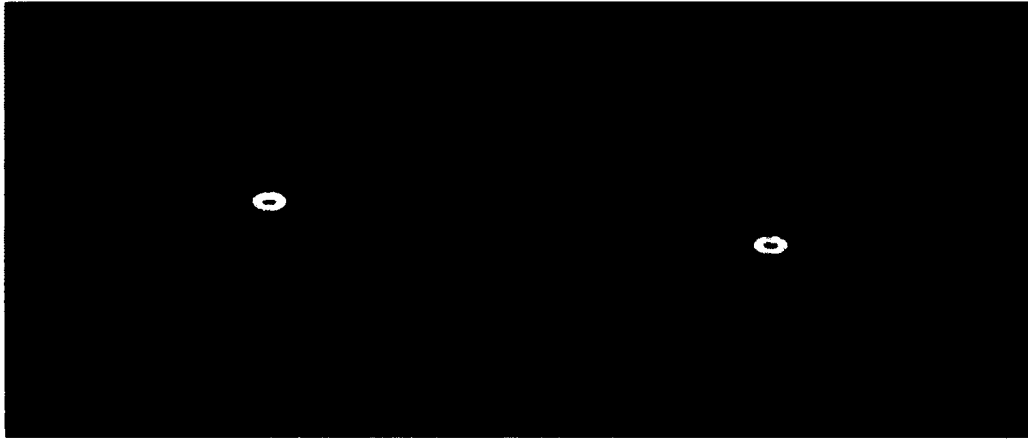


FIG. 27. Illustration of Cherenkov Radiation. Negative charged particle traveling through a medium with $v < c/n$ showing dipoles symmetrically arranged around particles path (left). Negative charged particle traveling through a medium with $v > c/n$ showing dipoles asymmetrically arranged around particles path given rise to dipole field(right). Image Source: [35]

The generated dipole field radiates the energy contained in this disturbance producing a coherent shockwave, this is known as Cherenkov radiation. An analogy of this phenomena is the sonic boom created in air from an object traveling faster than the speed of sound. Just as the sound wave of a sonic boom travels slower than the traveling object, so does the light emitted from the dipole field. This reduction in velocity creates the wave front of a continuous light spectrum, see Fig 28.

Inspecting Fig 28, when the particle has traveled the distance $RP = vt = t\beta c$, the photon has traveled $(c/n)t$, therefore

$$\cos \theta_c = \frac{(c/n)t}{t\beta c} = \frac{1}{n\beta} \quad (66)$$

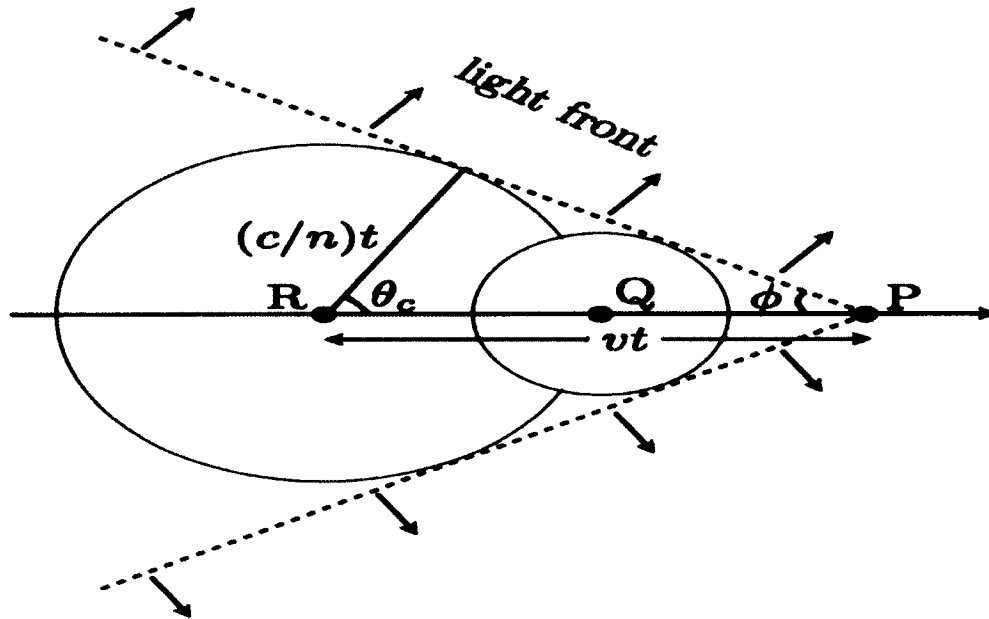


FIG. 28. Illustration of Cherenkov Angle. When the particle has traveled the distance $RP = vt \rightarrow \beta ct$, the photon (light front) has traveled $(c/n)t$.

and the threshold of Cherenkov radiation is

$$\beta_{th} > \frac{1}{n}. \quad (67)$$

Adding in quantum effects

$$\cos\theta_c = \frac{1}{n\beta} + \frac{\Lambda n^2 - 1}{\lambda 2n^2} \quad (68)$$

where

$$\Lambda = \frac{\sqrt{1 - \beta^2}}{\beta} \lambda_0, \quad (69)$$

λ = wavelength of light in medium, and λ_0 is the Compton wavelength 0.024 Å. For practical cases, and using CLAS, the 2nd order term is negligible ($n=1.00153$). To illustrate that quantum effects are negligible, an electron traveling at threshold in CLAS CC,

$$\beta_{th} > \frac{1}{n} > 0.998472, \quad (70)$$

$$\frac{\Lambda n^2 - 1}{\lambda 2n^2} = 1.07874 \cdot 10^{-9} \quad (71)$$

In CLAS, the Cherenkov counter (CC) is used to detect electrons and positrons while rejecting pions for momenta less than 2.5 GeV. The gas used in the CC for *g12* is perfluorobutane (C₄F₁₀) with an index of refraction of 1.00153. The threshold energy for producing Cherenkov radiation in C₄F₁₀ is

$$E_{th} = \gamma_{th} m_0 \text{ (Units of } c) \quad (72)$$

$$\gamma_{th} = \frac{n}{\sqrt{n^2 - 1}} = 18.09 \quad (73)$$

therefore the threshold energy of e^\pm is 9.23 MeV while the threshold energy of π^\pm is 2.52 GeV. The number of photons emitted per unit length at threshold for electrons or positrons is;

$$\frac{dN}{dx} = 2\pi z^2 \alpha \frac{\sin^2 \theta_c}{\lambda^2} d\lambda = 0.241246 \frac{d\lambda}{\lambda^2} \quad (74)$$

where α is the fine structure constant, $z = 1$ for electrons and positrons, and λ is the wavelength at which the photon is emitted. Table 4 lists the number of photons/cm for various wavelengths of light for the midpoint of β_{th} and a maximum velocity $\beta = 1$. Table 4 also lists the mirror reflectivity for that wavelength.

TABLE 4. Number of γ 's per unit length gas C₄F₁₀

Wavelength nm	$\frac{dN}{dx}$ photons/cm		Mirror reflectivity [36]
	$\beta = \frac{1}{2}(1 + \beta_{th})$	$\beta = 1$	
400-700 (visible)	0.75	1.5	90%
300-400 (near UV)	0.6	1.2	85 - 90 %
190-300 (near UV)	1.4	2.7	20 - 85%

The CC subsystem is physically located in the space between Region 3 of the DC subsystem and the TOF in the forward region covering polar angles 8° to 45° in each sector when the target is at CLAS center. For *g12* since the target was placed 90 cm upstream, the polar coverage was approximately from 6° to 35° in the lab frame. The CLAS CC's were fabricated as 6 independent identical sectors, with each sector divided into 18 regions of θ , and each θ segment divided into 2 modules. Light from

Cherenkov radiation is focused in ϕ thus preserving information on the lepton polar angle θ . The optical element of CC module comprises an assembly of one elliptical and one hyperbolic mirror providing primary light focusing into a “Winston” light collection cone, a cylindrical mirror used to compensate for imperfections in the focusing, and a photomultiplier used to count the number of photons in the light cone, see Fig 29a. More information on the CLAS Cherenkov detector can be found in [36]

The use of the CC was not included in the original proposals, however a significant drop in price on C_4F_{10} just prior to the start of *g12* allowed the gas to be added at the last minute. The price drop was due to the recent availability of another, much cheaper gas that was demonstrated to have the same general properties as C_4F_{10} and when *g12* contacted the original supplier of the C_4F_{10} for a price match, they committed.

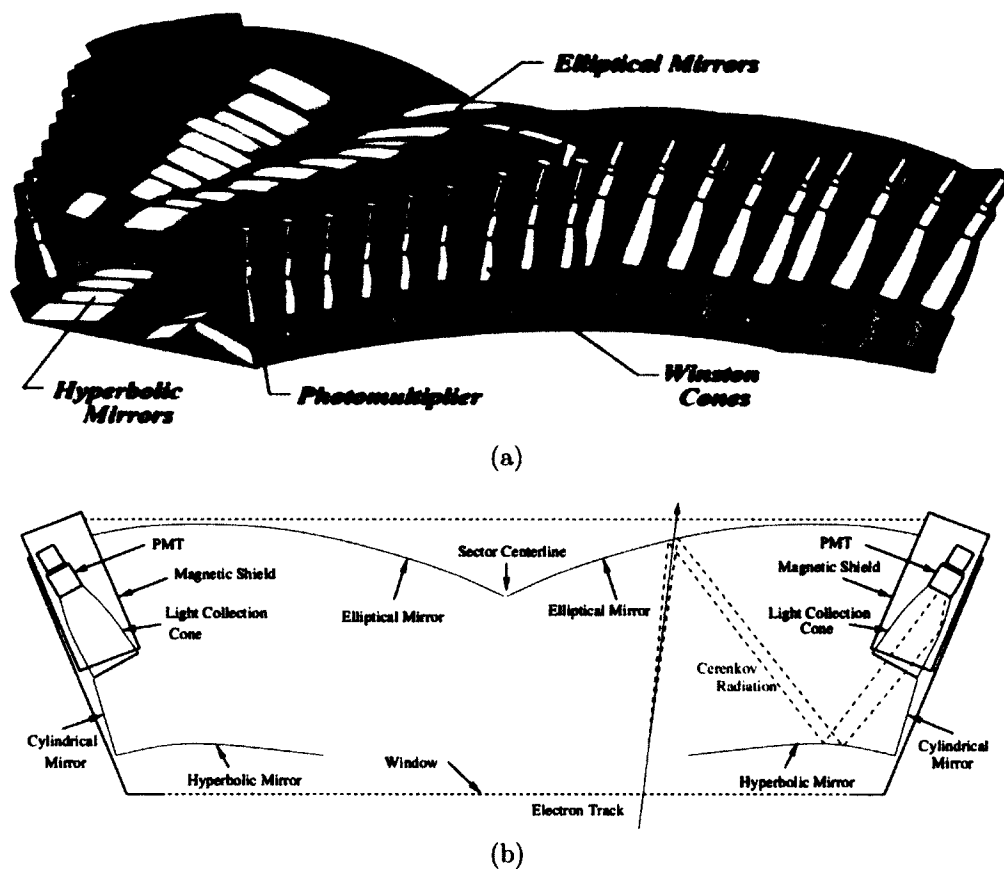


FIG. 29. Schematic of one CC showing the 18 symmetrical, mirrored segments of the CLAS CC (a). Diagram of one segment of the Cherenkov counters with an electron entering from the bottom (b).

2.9 TIME-OF-FLIGHT DETECTORS

The CLAS time-of-flight TOF subsystem provides precise timing measurements of charged particles that transverse the CLAS detector to help determine the particle masses. The TOF subsystem was also used in the $g12$ level 1 trigger (see Sec. 3.1.1) to identify track candidates. The TOF is constructed of organic plastic scintillant (Bicron BC-408). Scintillation is a process undergone by material when radiation traverses a medium.

The TOF subsystem is located between the CC and EC subsystems approximately 4 m from CLAS center, 5 m from the $g12$ target. Each sector 57 scintillator paddles divided into two subgroups. The first subgroup subtends angles of 8.6° to 45.9°

and consists of 23 scintillating paddles that are 15 cm in width. Each paddle is instrumented with two 2-in diameter PMT's, see Fig 30. The first group was optimized for timing resolution while being cost-effective and covering a large area. The second group consists of 34 paddles that are 22 cm wide, covering polar angles from 45.9° to 142°. Each paddle in this range is instrumented with two 3-in diameter PMT's. All paddle bars are 5.08 cm thick for 100% detection of minimum-ionizing tracks and a timing resolution of 150–200 ps. TOF information is used to reconstruct a particle's mass by measuring the difference between the event RF corrected start time and the time measured by the TOF, t_{stsc} . The RF corrected start time is the radio-frequency time (RF) from the accelerator beam aligned with the event start time. Using this time, t_{stsc} , the length of trajectory to the TOF, l_{stsc} , and the speed of light c , the particles' velocity can be calculated as

$$\beta = l_{sc}/(t_c \cdot c) \quad (75)$$

The particle's mass can be reconstructed from the measured velocity and momentum:

$$m = p\sqrt{(1 - \beta^2)}/\beta \quad (76)$$

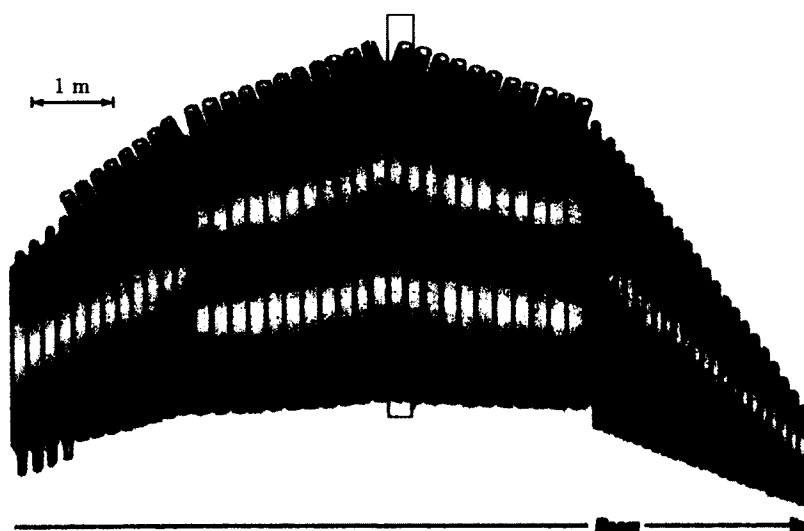


FIG. 30. Diagram of one sector of the time-of-flight (TOF) paddles. There are 57 scintillator paddles covering the entire acceptance region of the drift-chambers for each sector. PMT's are outlined in red while a scintillator paddle is outlined in yellow. Image Source: [38]

2.10 ELECTROMAGNETIC CALORIMETERS

The calorimetric method implies total absorption of the particle energy in a bulk of material followed by the measurement of the deposited energy. The process usually involves several layers of absorbers and detectors. Depending on the energies and species of particles there are different types of calorimeters. For instance, a 10 GeV muon will require 9 m of Fe or 8 m of Pb to absorb all the energy of the muon. However, a 10 GeV electron will only require 0.2 m of Pb to absorb all the energy. The Electromagnetic Calorimeter was built and used for detection of neutral particles as well as discrimination between electrons and pions.

2.10.1 ELECTROMAGNETIC CALORIMETER

At energies greater than 100 MeV, electrons lose their energy predominantly by bremsstrahlung while photons lose their energy by electron-positron pair production. The process of bremsstrahlung is electromagnetic radiation produced by the deceleration of an electron when deflected by an atomic nucleus i.e. $eZ \rightarrow Ze\gamma$. Its cross-section is proportional to Z^2 of the material the electron propagates through. The radiation loss of electrons with initial energy E_0 can be described as

$$-\left(\frac{dE}{dx}\right)_{rad} = \frac{E}{X_0} \quad (77)$$

$$E(x) = E_0 e^{-\frac{x}{X_0}} \quad (78)$$

where X_0 is the radiation length of the material the electron travels through. The process of pair production, $\gamma Z \rightarrow Ze^+e^-$ was discussed in Sec. 1.3.1.

To explain how an Electromagnetic Calorimeter works, assume the absorber for the calorimeter is lead(Pb), Fig 31a , 31b depicts the processes for photons and electrons in Pb. Lets start with a high energy electron E_0 , after $1X_0$, $1e^-$ and 1γ are produced each with $\frac{E_0}{2}$, after $2X_0$, $2e^-$, $1e^+$ and 1γ are produced each with $\frac{E_0}{4}$. Therefore after tX_0 , there is a total of

$$N(t) = 2^t \quad (79)$$

are produced each with

$$E(t) = E_0 2^{-t}. \quad (80)$$

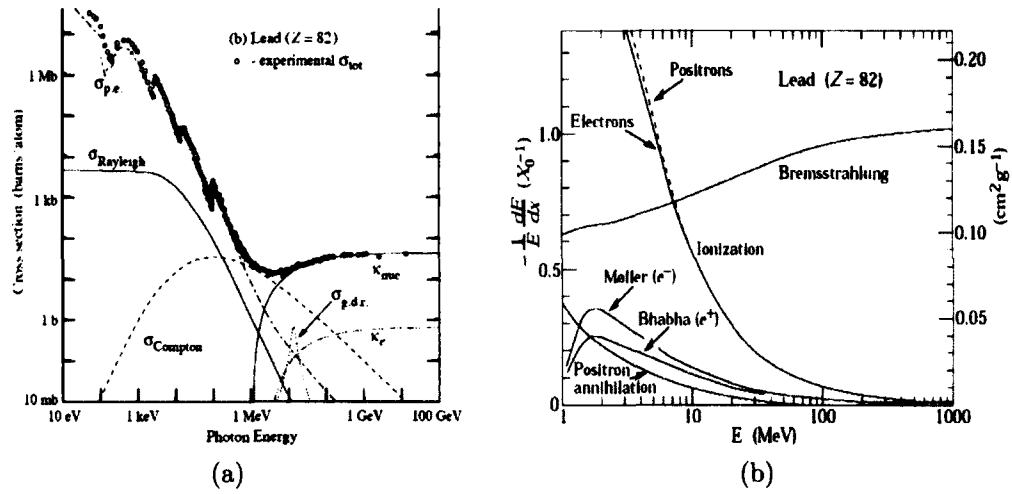


FIG. 31. Photon and Electron processes in **Pb** (a) and (b) respectively. Images Source: [37]

The multiplication of the shower particles continue as long as

$$\frac{E_0}{N} > E_c, \quad (81)$$

where E_c is the critical energy for showers to propagate,

$$E_c = E_0 2^{-t_{max}} \quad (82)$$

$$N_{max} = \frac{E_0}{E_c} \quad (83)$$

When a particle falls below critical energy, absorption processes (ionization, Compton and photoelectric) start to dominate the processes for photons and electrons. This leads to

$$t_{max} = \frac{\ln(\frac{E_0}{E_c})}{\ln 2}. \quad (84)$$

At the shower maximum e^\pm will stop within $1X_0$ however, photons at critical energy will penetrate further. To absorb 95% of photons produced in the shower maximum, an additional $7-9X_0$ is necessary. The semi-empirical value for $e^\pm E_c$ in Pb is,

$$E_c \approx \frac{610 \text{ MeV}}{Z - 1.24} = 7 \text{ MeV} \quad (85)$$

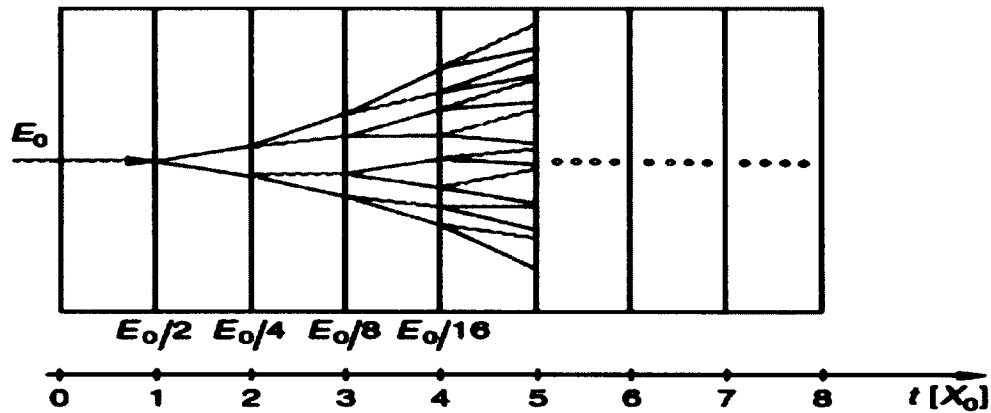


FIG. 32. A simple Electromagnetic shower in a calorimeter Image Source: [37]

which results in $t_{max} \approx 9.7X_0$ for electrons at 6 GeV.

The process shown in Fig 32 is a very crude and simple model of an actual shower shown in Fig 33, but the simple model correctly describes the important features of Electromagnetic Calorimeters

- The total calorimeter thickness should be more than 10-15 X_0 in order to absorb almost all of the energy of an incident photon
- The position of the shower maximum increases with energy, therefore the thickness of the calorimeter should increase as the logarithm of the energy.
- If there is energy leakage, it is caused by photons escaping the calorimeter at the sides or at the back.

2.10.2 THE CLAS ELECTROMAGNETIC CALORIMETER

The CLAS electromagnetic calorimeter (EC)[40], shown in Fig. 16 was designed with the following criteria;

- e/γ energy resolution $\sigma/E \leq 0.13/\sqrt{E(\text{GeV})}$
- Position resolution $\delta r \approx 2\text{cm}$ at 1GeV
- π/e rejection greater than 99% at $E \geq 1$ GeV

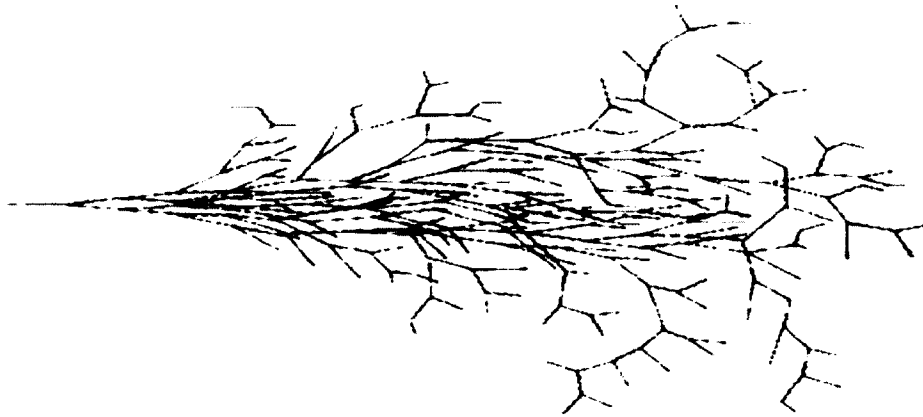


FIG. 33. A real Electromagnetic shower in a calorimeter Image Source: [37]

- Fast (< 100 ns) total energy sum for the event trigger
- Mass resolution for 2-photon decays $\delta m/m \leq 0.15$
- Neutron detection efficiency $> 50\%$ for $E > 0.5$ GeV
- Time-of-flight resolution ≈ 1 ns

The EC consists of alternating layers of Pb (absorber) and scintillator (detector). The lead to scintillator ratio of 0.2, i.e. 40 cm of scintillator, 8 cm of lead ($16 X_0$), was chosen so one third of the showering particle's energy is deposited into the scintillator. There are six triangular EC modules, one per sector, each a sandwich constructed of 39 layers. A layer is considered to be 10 mm thick BC412 scintillator followed by 2.2 mm lead. Each scintillator is made of 36 strips parallel to one side and are turned 120° from each other for each u , v and w view, 13 layers per view. The CLAS EC is subdivided into two stacks, inner and outer. The inner stack comprises of 8 layers while the outer stack comprises 5 logical layers. Each module contains $36(\text{strips}) \times 3(\text{views}) \times 2(\text{stacks})$ therefore 216 PMT's were needed per module, 1296 PMT's total for CLAS EC, and 8424 scintillator strips.

Using the three layers in each logical layer to provide pixel-like information, the transverse shower development for a given particle can be determined. All final-state photons were identified in the EC if no charged tracks have been associated with an

energy deposit and also the velocity, β , of the particle exceeds $0.9c$. Particles with $\beta < 0.9c$ are neutron candidates.

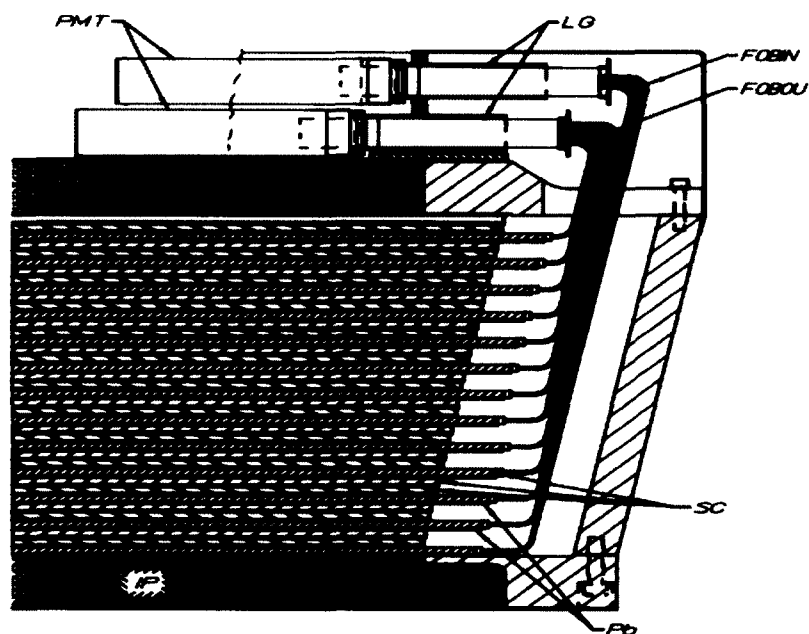
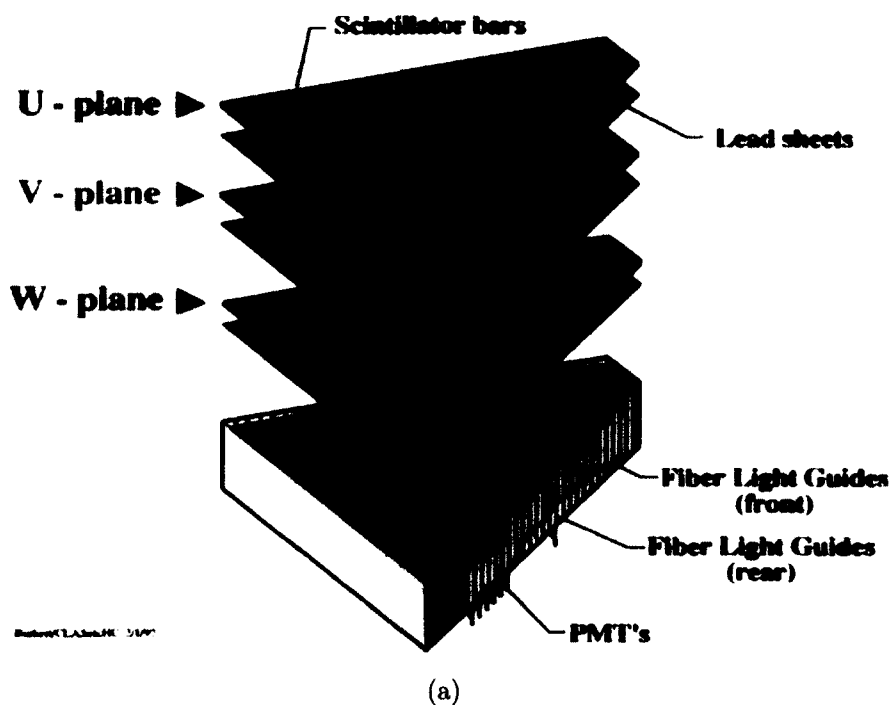


FIG. 34. Separated view of one sector of the forward electromagnetic calorimeter (EC) showing the three planes (u , v , w) of scintillator-lead pairs which make up one of the 13 logical layers (a). Side view of one plane of the forward electromagnetic calorimeter (EC) showing the the 13 logical layers, placement of the PMT's and light guides (b). Image Source: (a) [40] , (b) [40] respectively.

CHAPTER 3

THE *g12* EXPERIMENT

The *g12* experiment ran during March - June 2008 with a total of 44 days of good beam time. It collected over 128 TB of raw data that consisted of $26 \cdot 10^9$ events, with an integrated luminosity of 68 pb^{-1} . A detailed explanation of the CLAS data reconstruction and explanation of the DAQ for *g12* can be found in [41]. This chapter will briefly overview aspects of the *g12* running conditions and data retrieval found in [41]. Table 5 lists the general running conditions of *g12*.

TABLE 5. Running conditions for *g12*

Electron Beam Energy	5.714 GeV
Electron Beam Current	60-65 nA (production) & 24 nA(single-prong)
Electron Beam Polarization	Circular
Radiator Material/Density	Au / $646 \mu\text{g}/\text{cm}^2$
Radiator Thickness	$10^{-4} \chi_0$
Radius of Photon collimator	6.4 mm
Photon Beam Energy Range	1.142-5.425 GeV
Target Shell Material	Kapton
Target Length/Diameter	40 cm/4 cm
Target Inside Material	ℓH_2
Target Position	-90 cm from CLAS center
Target Polarization	None
Torus Magnetic Current	$\frac{1}{2} B_{max} = 1930 \text{ A}$

3.1 *g12* DATA ACQUISITION AND TRIGGERING

As described in previous sections, CLAS is a detector comprised of several subsystems. Each subsystem in CLAS has its own electronics package to monitor its components and collect signals. Discriminators determine whether a signal each each channel a subsystem exceeds a given threshold. In the case of the DC the signal is supplied from the sense wire. For the ST, CC, TOF, EC subsystems, the signal is supplied by converting the current supplied by an anode of a PMT or cluster of PMT's into a voltage. Each subsystem has a preset voltage threshold. The discriminator compares the signal output of a subsystem to the preset threshold. Signals that exceed the preset threshold are digitized by two types of hardware, Time-to-digital converters (TDCs) and Analog-to-digital converters (ADCs). TDCs report the time at which a signal arrives, while ADCs report a number corresponding to the integral of the signal.

The presence of a signal in a single subsystem does not constitute a physics event. There are a number of unwanted sources that could produce unwanted signals, such as cosmic radiation, electronic noise, Fano noise etc. It is the job of the trigger to determine which sets of signals constituted a physics event. The trigger is a list of signals from various subsystems required for an event to be written out to disk. An item in the trigger list is known as a trigger "bit". The *g12* rungroup used a field-programmable gate array (FPGA) as the trigger supervisor. The FPGA allowed for 12 independent trigger configurations to be employed at one time during the running of *g12* as well as the ability to change the trigger configuration during running. The detector subsystems used in the first-level (L1) triggering system of *g12* are the TAGR, ST, CC, TOF, and EC. The TOF and ST are used to identify charged tracks, at the trigger level, by using coincidence of any one TOF hit in a given sector with any one ST hit in the same sector. Also, a coincidence between the EC and CC was included as a lepton trigger. Fig. 35 depicts the L1 trigger configuration for the subsystems mentioned except for the TAGR subsystem. During the *g12* experiment, the interval for a trigger coincidence was 100 ns. All subsystems of CLAS except for the DC can acquire signals in a few nanoseconds.

When a first-level trigger requirement is satisfied, a second-level (L2) trigger requirement is sometimes necessary to verify the L1 trigger. A L2 trigger is usually a software routine unlike the L1 trigger which is based on hardware. The L2 trigger is typically employed for measurements from the DC and is slower than the L1 trigger

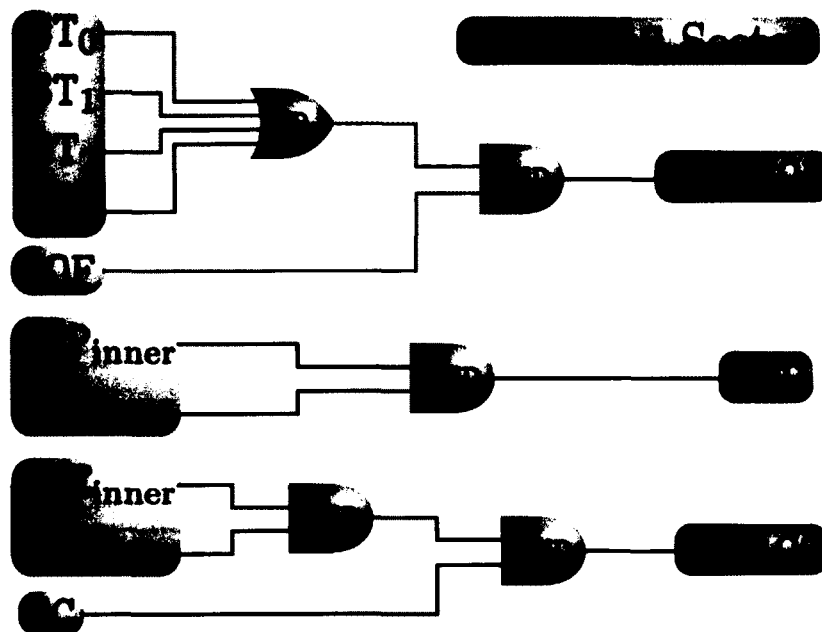


FIG. 35. Trigger logic for one of the six sectors of CLAS. The $ST \times TOF$ signal is a coincidence between any of the four start counter TDC signals (numbered from 0 to 3) and any of the 57 TOF TDC signals. The ECE_{inner} and ECE_{total} are the electron-threshold EC signals for the energy deposited in the *inner* layer and in *all* layers. These are combined with a CC signal to produce the $EC \times CC$ trigger for this sector. The ECP trigger signal is the photon-threshold EC signal. These trigger signals are discussed further in Sec. 3.1.1.

because it is software based. The software routine does coarse track reconstruction on the DC hits to confirm that the L1 coincidence was caused by particles traveling through CLAS rather than unwanted noise.

When a trigger configuration is completely satisfied, the data acquisition system (DAQ) collected the signals and wrote them to magnetic tape for future offline analysis. At the time *g12* was run, the DAQ was capable of running at 8 kHz.

3.1.1 *g12* TRIGGER CONFIGURATION

The trigger configuration used in the *g12* running period are listed in Tables 6, 7 and 8. All but one “bit” required a (ST·TOF) to be present along with other requirements. The (ST·TOF) configuration required a track to have coincidence in one sector between any one of the four start counter paddles of that sector, and any

one of the 57 time-of-flight paddles in the same sector. Any configuration listed in the Tables 6, 7 and 8 with the suffix “ $\times N$ ” after a parenthesis grouped configuration requires that given configuration to have “ N ” coincidences in different sectors. To illustrate this the configuration (ST·TOF) requires one coincidence in the same sector, while (ST·TOF) $\times 2$ requires two coincidences of (ST·TOF) in two different sectors and (ST·TOF) $\times 3$ requires three coincidences of (ST·TOF) in three different sectors. The hardware and configuration did not allow triggering of two tracks in the same sector because there were only six signals coming from the TOF, one for each sector.

Another component that can be included into a trigger “bit” is “Master-OR,” (MOR). This component is a signal with the photon tagger. These are defined in Table 9 and is illustrated with the other components of a “bit” in Fig. 36.

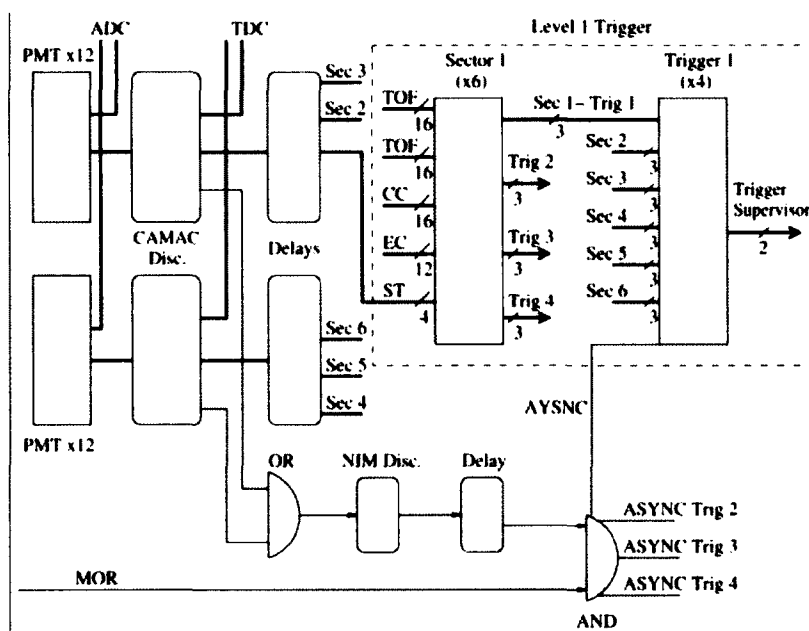


FIG. 36. Trigger logic for any of the six sectors of CLAS along with MOR asynchronous logic trigger input.

Lepton Triggering and Neutral Triggering

In *g12*, since the CC was filled with gas, it was possible to include the CC as a component of the trigger. There were three trigger “bits” used for lepton identification in *g12* as listed in Table 7. Each “bit” used a (EC·CC) configuration to identify leptons. The (EC·CC) configuration required a coincidence between the electromagnetic

calorimeter and the Cherenkov subsystems. This coincidence was established by using the voltage sum of the CC for a sector and the voltage sum of the EC for the same sector and comparing each sum to a preset threshold described in Table 10. The EC voltage sum threshold comparison is done on both the EC_{inner} and EC_{total} which are the EC voltage signals for the energy deposited in the inner layer and in all layers. The labels of photon or electron specified in Table 10 are not actual photons or electrons, but were considered a first-order approximation for detection. The particle identification is done at the analysis level. The method for determining the (EC-CC) does not allow for multiple lepton triggering in the same sector. Determining multiple leptons in the same sector is done at the analysis level.

The “bit 6” trigger configuration, (ST·TOF)·(EC·CC) requires a ST and TOF coincidence previously described in 3.1.1 along with a coincidence between the electromagnetic calorimeter and the Cherenkov subsystems described above. The (ST·TOF) configuration of “bit 6” did not have to be in the same sector as the (EC·CC) configuration of “bit 6”. The “bit 11” trigger configuration, (EC·CC)×2 requires two coincidences between the electromagnetic calorimeter and the Cherenkov subsystems described above, in two different sectors.

The “bit 5” trigger configuration was also established as a lepton trigger. It required EC hits in two sectors. The “bit 5” trigger configuration was also established to analyze physics involving two or more neutral particles accompanied with a charged track, such as exclusive π^0 production in which the π^0 decays via 2 photons. The method for “bit 5” voltage sum comparison is identical to the EC voltage sum of “bit 6” and “bit 11”

It should be noted that none of the lepton triggers required a MOR signal, allowing for physics involving leptons to be measured starting from $g12$'s lowest tagger detection value of 1.142 GeV.

TABLE 6. Trigger configuration for $g12$ runs from 56363 to 56594 and 56608 to 56647. $(\text{ST}\cdot\text{TOF})_i$ indicates a trigger-level track defined as a coincidence between a start counter and time-of-flight hit in the i^{th} sector. MORA and MORB represent coincidences with tagger hits within a certain energy range as specified in Table 9.

$g12$ runs 56363–56594, 56608–56647			
bit	definition	L2 multiplicity	prescale
1	$\text{MORA}\cdot(\text{ST}\cdot\text{TOF})_1\cdot(\text{ST}\cdot\text{TOF})_{i\neq 1}$	–	1
2	$\text{MORA}\cdot(\text{ST}\cdot\text{TOF})_2\cdot(\text{ST}\cdot\text{TOF})_{i\neq 2}$	–	1
3	$\text{MORA}\cdot(\text{ST}\cdot\text{TOF})_3\cdot(\text{ST}\cdot\text{TOF})_{i\neq 3}$	–	1
4	$\text{MORA}\cdot(\text{ST}\cdot\text{TOF})_4\cdot(\text{ST}\cdot\text{TOF})_{i\neq 4}$	–	1
5	$\text{MORA}\cdot(\text{ST}\cdot\text{TOF})_5\cdot(\text{ST}\cdot\text{TOF})_{i\neq 5}$	–	1
6	$\text{MORA}\cdot(\text{ST}\cdot\text{TOF})_6\cdot(\text{ST}\cdot\text{TOF})_{i\neq 6}$	–	1
7	ST·TOF	–	1
8	$\text{MORA}\cdot(\text{ST}\cdot\text{TOF})\times 2$	–	1
11 ^a	$\text{MORB}\cdot(\text{ST}\cdot\text{TOF})\times 2$	–	1
12	$(\text{ST}\cdot\text{TOF})\times 3$	–	1

^abit 11 and MORB were included in the trigger starting with run 56519.

TABLE 7. Trigger configuration for $g12$ runs from 56595 to 56607 and 56648 to 57323.

$g12$ runs 56595–56607, 56648–57323			
bit	definition	L2 multiplicity ^a	prescale
1	$\text{MORA}\cdot(\text{ST}\cdot\text{TOF})$	1	1000/300 ^b
2	$\text{MORA}\cdot(\text{ST}\cdot\text{TOF})\times 2$	2/– ^c	1
3	$\text{MORB}\cdot(\text{ST}\cdot\text{TOF})\times 2$	2	1
4	ST·TOF	1	1000/300
5	$(\text{ST}\cdot\text{TOF})\cdot\text{EC}\times 2$	1	1
6	$(\text{ST}\cdot\text{TOF})\cdot(\text{EC}\cdot\text{CC})$	2	1
7	$\text{MORA}\cdot(\text{ST}\cdot\text{TOF})\cdot(\text{EC}\cdot\text{CC})$	–	1
8	$\text{MORA}\cdot(\text{ST}\cdot\text{TOF})\times 2$	–	1
11	$(\text{EC}\cdot\text{CC})\times 2$	–	1
12	$(\text{ST}\cdot\text{TOF})\times 3$	–	1

^aLevel 2 triggering was turned off on all bits for runs 56605, 56607 and 56647.

^bPrescaling for bits 1 and 4 were 1000 for runs prior to 56668 at which point they both were changed to 300.

^cLevel 2 triggering of bit 2 was set to 2 for runs prior to 56665 at which point it was turned off.

TABLE 8. Trigger configuration for the single-prong runs of $g12$. Trigger bits 7–12 were not used for these runs.

bit	definition	L2 multiplicity	prescale
1	$\text{MORA} \cdot (\text{ST} \cdot \text{TOF})_1$	sector 1	1
2	$\text{MORA} \cdot (\text{ST} \cdot \text{TOF})_2$	sector 2	1
3	$\text{MORA} \cdot (\text{ST} \cdot \text{TOF})_3$	sector 3	1
4	$\text{MORA} \cdot (\text{ST} \cdot \text{TOF})_4$	sector 4	1
5	$\text{MORA} \cdot (\text{ST} \cdot \text{TOF})_5$	sector 5	1
6	$\text{MORA} \cdot (\text{ST} \cdot \text{TOF})_6$	sector 6	1

TABLE 9. Master-OR definitions for $g12$. The TDC counters were used in the trigger and since each of these corresponds to several energy paddles, the energies given here are approximate. T -counter number 1 corresponds to the highest energy photon of approximately 5.4 GeV. Both MORA and MORB are referenced in terms of the trigger logic in Tables 6, 7 and 8. The single-prong runs are listed in Table 12.

run range	MORA		MORB	
	T -counters	energy (GeV)	T -counters	energy (GeV)
56363–56400	1–47	1.7–5.4	–	–
56401–56518	1–25	3.6–5.4	–	–
56519–57323	1–19	4.4–5.4	20–25	3.6–4.4
<i>single-sector</i>	1–31	3.0–5.4	–	–

TABLE 10. Threshold values for the electromagnetic calorimeter (EC) and Cherenkov counter (CC) during the $g12$ running period. EC thresholds are shown as *inner/total*, and CC thresholds are shown as *left/right*.

EC		CC
<i>“photon”</i>	<i>“electron”</i>	
50/100 mV	60/80 mV	20/20 mV
150/300 MeV	180/240 MeV	~0.4 photo-electrons

3.2 *g12* RUN SUMMARY

The *g12* experiment was divided into 626 production runs, 37 single-prong runs, 13 special calibration runs and numerous diagnostic runs which were not recorded. Each run consisted of approximately 50 million triggered events. Table 11 contains a list of the runs that had at least 1M triggers and were reconstructed successfully, along with the beam current for these runs. If a run did not have at least 1M triggered events or if the run was corrupt, the run was discarded.

TABLE 11. List of successfully reconstructed production runs and their beam currents in nA.

runs current (nA)	runs current (nA)	runs current (nA)	runs current (nA)
56363	20	56505-56506	40
56365	30	56508-56510	60
56369	30	56513-56517	60
56384	5	56519	60
56386	20	56521-56542	60
56400-56401	50	56545-56550	60
56403	70	56555-56556	60
56404	60	56561-56564	60
56405	50	56573-56583	60
56406	40	56586-56593	60
56408	80	56605	60
56410	90	56608-56612	60
56420-56422	5	56614-56618	60
56435	5	56620-56628	60
56436	15	56630-56636	60
56441	35	56638-56644	60
56442	30	56646	60
56443	20	56653-56656	60
56445-56450	60	56660-56661	60
56453-56459	60	56665-56670	60
56460-56462	70	56673-56675	60
56465	70	56679-56681	60
56467-56472	70	56683	60
56478-56483	70	56685-56696	60
56485-56487	70	56700-56708	60
56489-56490	70	56710-56724	60
56499	70	56726-56744	60
56501	60	56748-56750	60
56503	57	56751-56768	65
56504	56	56770-56772	65
		56774-56778	65
		56780-56784	65
		56787-56788	65
		56791-56794	65
		56798-56802	65
		56805-56815	65
		56821-56827	65
		56831-56834	65
		56838-56839	65
		56841-56845	65
		56849	65
		56853-56862	65
		56864	65
		56865-56866	60
		56870	65
		56874-56875	60
		56877	60
		56879	60
		56897-56898	60
		56899	65
		56900-56908	60
		56914-56919	60
		56921-56922	60
		56923	65
		56924	70
		56925	80
		56926-56930	60
		56932	60
		56935-56940	60
		56948-56956	60
		56958	60
		56960-56975	60
		56977-56980	60
		56992-56994	60
		56996-57006	60
		57008-57017	60
		57021-57023	60
		57025-57027	60
		57030-57032	60
		57036-57039	60
		57062-57069	60
		57071-57073	60
		57075-57080	60
		57095-57097	60
		57100-57103	60
		57106-57108	60
		57114-57128	60
		57130-57152	60
		57159-57168	60
		57170-57185	60
		57189-57229	60
		57233-57236	60
		57249-57253	60
		57255-57258	60
		57260-57268	60
		57270-57288	60
		57290-57291	60
		57293-57312	60
		57314-57317	60

TABLE 12. A list of the single-prong runs using the trigger configuration described in Table 8.

run	current (nA)	run	current (nA)
56476	24	56910	35
56502	24	56911	30
56520	24	56912	25
56544	24	56913	24
56559	24	56933-56934	24
56585	24	56981-56983	24
56619	24	56985	15
56637	24	56986	15
56663-56664	24	56989	24
56697	24	57028	24
56725	24	57061	24
56747	24	57094	24
56769	24	57129	24
56804	24	57155-57156	24
56835	24	57237-57238	24
56869	5		

The single-prong data runs were incorporated into the *g12* running upon approval of proposal [32]. This data was obtained using a trigger requirement of a single track hit in a sector of CLAS. In order to properly trigger a single hit in the DC a lower current of 24 nA was used. This portion of the data has yet to be examined for any physics purpose, however the data had been preliminarily reconstructed by the author of this document. It was determined that timing calibrations must be redone for this specific data set. The amount of data that can be analyzed in these 37 runs is approximately equal to 60 % the amount of data in the higher current production runs. See Table 12.

Listed in Table 13 are several special calibration runs. These runs consist of normalization, zero-field, and empty-target data runs. The normalization runs were used to calibrate the tagger for the measurement of the total photon flux and consistency of the left and right TDC signals of the tagger. The zero-field data was taken with the main torus magnet off. This was done to account for the position and orientation of the drift-chambers in the reconstruction. The empty target runs were used to investigate the contributions of the

target wall to the data sample.

TABLE 13. List of special calibration runs done during the *g12* experiment.

run	current (nA)	description
56397	0.05	normalization
56475	10	zero-field
56511	0.05	normalization
56512	0.05	normalization
56584	0.05	normalization
56682	0.05	normalization
56790	0.05	normalization
56931	0.05	normalization
56947	0.05	normalization
57169	0.05	normalization
57239	24	empty-target, single-sector
57241	80	empty-target, production
57248	0.05	normalization

3.3 RAW DATA RECONSTRUCTION

The process of reconstructing tracks and their subsequent particle identification from raw data is referred to as “cooking” and was done by the program `a1c` for *g12*. “Cooking” is when the information recorded from the various detector subsystems is converted into a form suitable for physics analysis. During cooking, each detector subsystem was calibrated. The “cooking” of the *g12* dataset was performed by John Theodore Goetz and is fully documented in [41] and [24].

The “cooking” process performed by `a1c` is outlined in Fig. 37. Initial calibrations are done for each subsystem in each sector the process begins with “hit-based” tracking in the DC. “Hit-based” tracking requires only the positions of wires registering a hit in a given sector. Adjacent hits in each superlayer are assembled into clusters, and then these clusters are linked in each region to produce track segments. Refer to Fig. 26 for an illustration of a track segment. Track segments are linked over the three regions to produce full hit-based trajectories. See Fig 38 for a pictorial description of “hit-based” tracking. There was an overall failure of events that should have passed “hit-based” tracking but failed. This will be discussed fully in Sec. 4.4.1.

After “hit-based” tracking is performed, “time-based” tracking is performed on the hits obtained from “hit-based” track to the appropriate TOF panel. This is done to eliminate noise hits or whole clusters that are not associated with physical tracks. If a hit from “hit-based” tracking is found to match a TOF panel, the time measurement from the TOF panel is used to set an upper limit to the time of the drift-chamber hits. With this upper limit known, the DC hits associated with the track are checked individually, where each hit is required to be in increasing time order as the track moves away from the target, any hits or whole clusters not satisfying this requirement are removed. After the removal of the initial bad hits, the track is refit using the remaining hits and the process of removing bad hits is repeated up to two more times to further refine momentum measurements, as well as the measurement of the event vertex, which is determined by the distance of closest approach of the track to the beamline. When the processes of “time-based” tracking is finished, all other subsystem information is then added to the tracks properties list. See Fig 39 for a pictorial description of “time-based” tracking.

During the initial stages of “time-based” tracking, a ST signal must be present. This will be discussed in Sec. 4.4.1. If the track failed due to this error, it usually passed “time-based” on the second or third pass of the “time-based” tracking if another particle passed “time-based” during the initial pass. The average inefficiency for three track events for data was $< 0.01\%$

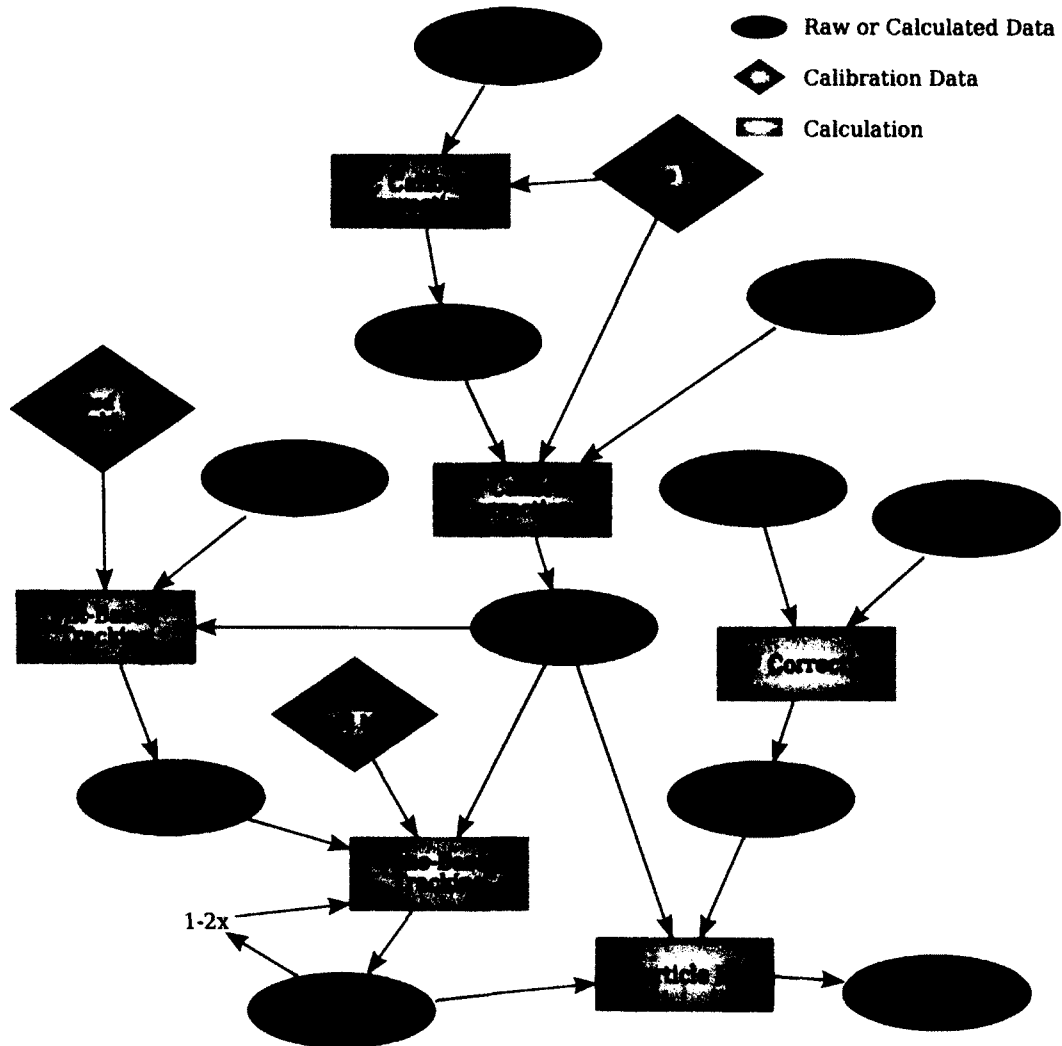


FIG. 37. Flow chart of the reconstruction process from raw data to identified tracks with momentum. "Subsystems" refers to the ST, CC, TOF and the EC detectors. Percentages shown indicate the relative time taken to do the calculations.

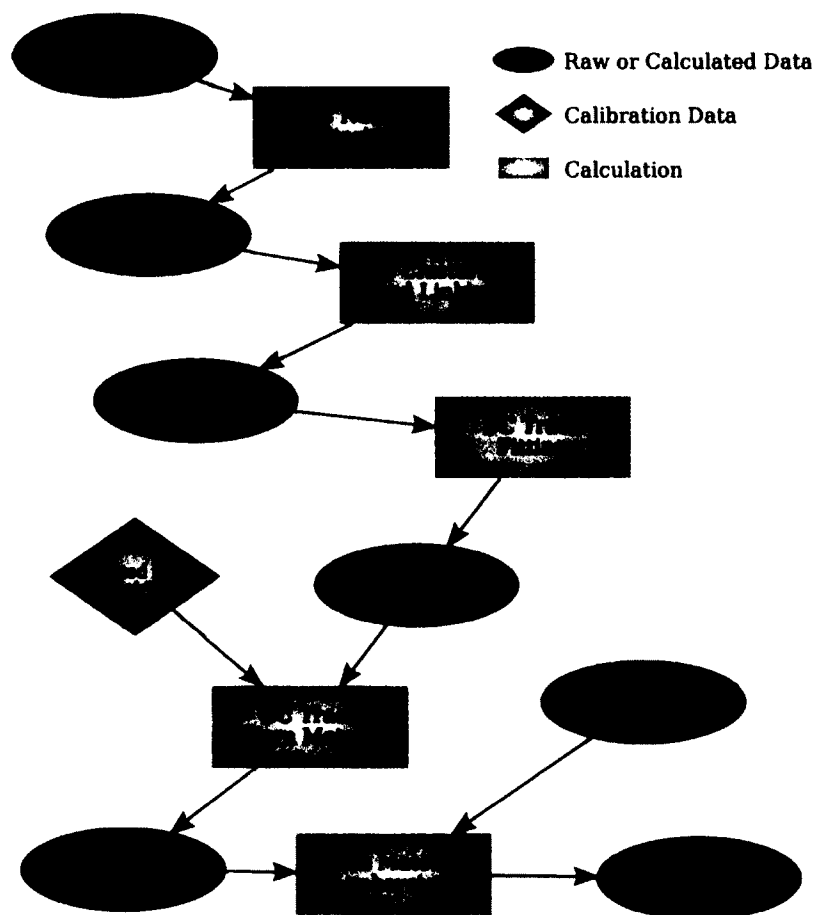


FIG. 38. Flow chart of the hit-based tracking part of the reconstruction shown in Fig.37. "Subsystems" refers to the ST, CC, TOF and the EC detectors. Percentages shown indicate the relative time taken to do the calculations with respect to the full reconstruction.

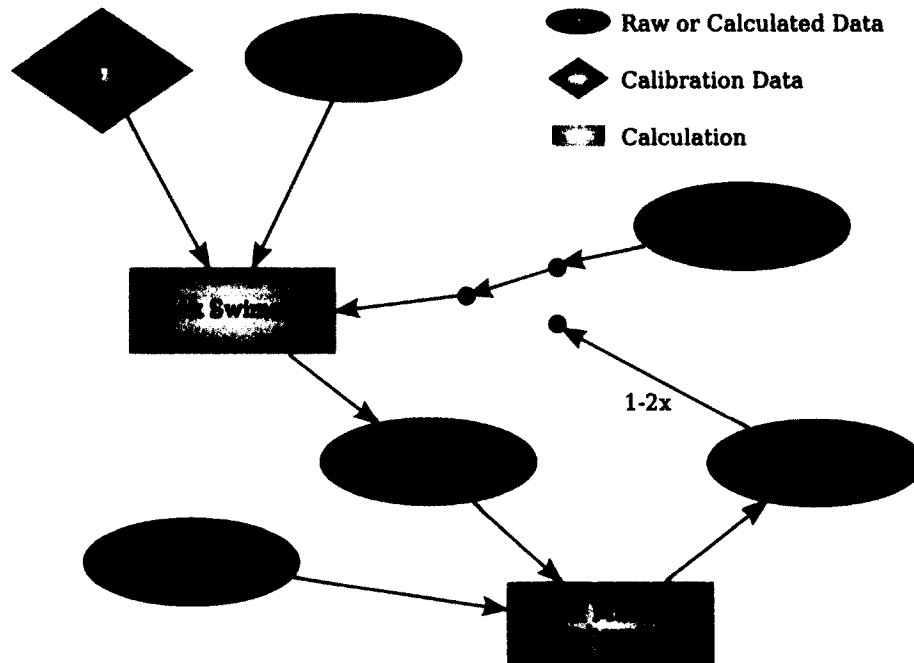


FIG. 39. Flow chart of the time-based tracking part of the reconstruction shown in Fig.37. “Subsystems” refers to the ST, CC, TOF and the EC detectors. The switch indicates that hit-based tracks are input into the swimming calculation, after which the time-based tracks are used creating a feedback loop. Percentages shown indicate the relative time taken to do the calculations with respect to the full reconstruction.

The process of “cooking” was performed for Monte-Carlo data for the purpose of verifying the simulation package and the presence of this error and the “hit-based” inefficiency is discussed in Sec. 4.4.1.

3.4 PARTICLE IDENTIFICATION

The final procedure is to assign the track a particle mass (m). In Sec. 2.9 Eqs. 75 and 76 explain how the mass of a particle is determined. Fig. 40 depicts a 2-dimensional plot of the quantities used to determine the particle mass. Once the mass has been determined,

particle identification PID is determined by the following criteria;

$$\text{PID} = \begin{cases} \pi^\pm, & \text{if } m < 0.3 \text{ GeV and } q^\pm \\ K^\pm, & \text{if } 0.35 < m < 0.35 \text{ GeV and } q^\pm \\ p^\pm, & \text{if } 0.8 < m < 1.2 \text{ GeV and } q^\pm \\ d, & \text{if } 1.75 < m < 2.2 \text{ GeV} \end{cases} \quad (86)$$

The events which had particles falling within the undefined regions of the cuts listed in Eq. 86 were deemed ambiguous events and were given the PID of “*unknown*”. For the analysis of this work, “*unknown*” were used and is described in Sec. 4

Since tracking began after the particle had already traversed through the target and ST, the measured momentum determination was decreased by the “energy-loss” the particle underwent before entering the Region 1 DC. These effects were taken into account as part of the “energy-loss” correction during the analysis phase as discussed in Sec. 4.2.1. Once particle identification is completed on the reconstruction level, all relevant information about the particle is collected into the event of occurrence and this information is written in BOS format. There are multiple methods for analyzing BOS format, the chapter 4 will discuss the method used in this analysis.

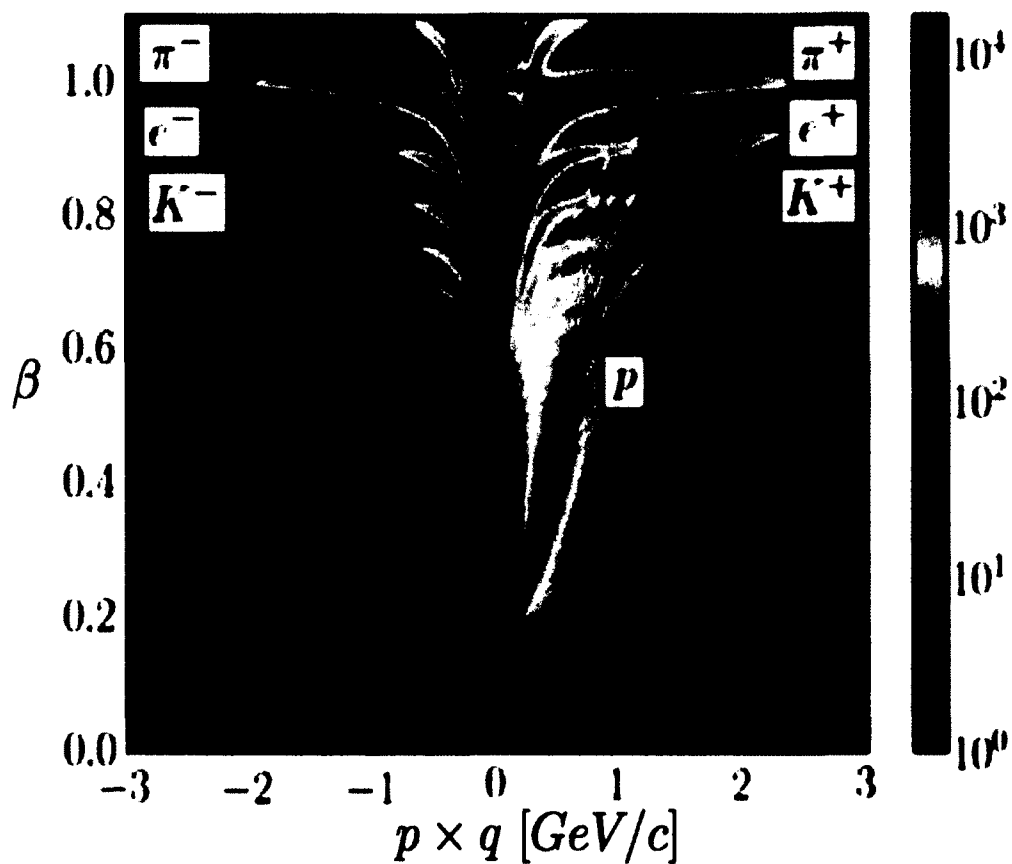


FIG. 40. β vs. momentum(p) \times charge(q) for run 56855. This plot is a graphical representation of how particle ID assignments are made in CLAS reconstruction. The “ribs” seen represent tracks that were “out-of-time” with a incident photon. Image Source: [42]

CHAPTER 4

PARTICLE RECONSTRUCTION AND ANALYSIS

This chapter will explore the methods and techniques used for particle reconstruction and analysis. There were 2 packages of algorithms used to perform particle identification, while only one was used for the analysis part. The algorithms used for particle identification were codes compiled in the “*clas6-trunk*” under the package CLASEVENT. CLASEVENT is a C++, class-based package written primarily by Dennis Weygand for the purpose of analyzing the output of the reconstruction program that was discussed in Sec. 3.3. For this analysis, CLASEVENT was utilized to skim the reconstructed data and output the data into ROOT format for later evaluation.

The second set of algorithms used to perform this analysis were written primarily by the author, except for the algorithms pertaining to the kinematic fitter. The second set of algorithms were built off of the ROOT platform. The kinematic fitter algorithms were written by Dustin Keller and the procedure of kinematic fitting is discussed in Sec. 4.6.

4.1 DATA REDUCTION AND EVENT SELECTION

4.1.1 EXCLUDED RUNS

For this analysis 165 production runs, all single-prong runs and all special calibration runs were excluded. Table 14 contains a list of the runs that are excluded along with the reason of exclusion.

TABLE 14. $g12$ production runs excluded from current analysis and the reasoning

Excluded Run	Exclusion Reason	Excluded Run	Exclusion Reason
56476	Single-prong Run	56408	Lepton TrigBit (6) Not Set
56502	Single-prong Run	56410	Lepton TrigBit (6) Not Set
56520	Single-prong Run	56420-56422	Lepton TrigBit (6) Not Set
56544	Single-prong Run	56435-56436	Lepton TrigBit (6) Not Set
56559	Single-prong Run	56441	Lepton TrigBit (6) Not Set
56585	Single-prong Run	56442-56443	Lepton TrigBit (6) Not Set
56619	Single-prong Run	56445-56450	Lepton TrigBit (6) Not Set
56637	Single-prong Run	56453-56462	Lepton TrigBit (6) Not Set
56663	Single-prong Run	56465	Lepton TrigBit (6) Not Set
56664	Single-prong Run	56467-56472	Lepton TrigBit (6) Not Set
56697	Single-prong Run	56476	Lepton TrigBit (6) Not Set
56725	Single-prong Run	56478-56483	Lepton TrigBit (6) Not Set
56747	Single-prong Run	56485-56487	Lepton TrigBit (6) Not Set
56769	Single-prong Run	56489-56490	Lepton TrigBit (6) Not Set
56804	Single-prong Run	56499	Lepton TrigBit (6) Not Set
56835	Single-prong Run	56501-56506	Lepton TrigBit (6) Not Set
56869	Single-prong Run	56508-56510	Lepton TrigBit (6) Not Set
56910-56913	Single-prong Run	56513-56517	Lepton TrigBit (6) Not Set
56933-56934	Single-prong Run	56519-56542	Lepton TrigBit (6) Not Set
56981-56983	Single-prong Run	56544-56550	Lepton TrigBit (6) Not Set
56985-56986	Single-prong Run	56555-56556	Lepton TrigBit (6) Not Set
56989	Single-prong Run	56559-56564	Lepton TrigBit (6) Not Set
57028	Single-prong Run	56573-56583	Lepton TrigBit (6) Not Set
57061	Single-prong Run	56586-56594	Lepton TrigBit (6) Not Set
57094	Single-prong Run	56608-56636	Lepton TrigBit (6) Not Set
57129	Single-prong Run	56638-56646	Lepton TrigBit (6) Not Set
57155-57156	Single-prong Run	56397	normalization
57237-57238	Single-prong Run	56475	zero-field
57312	No Flux Information	56511	normalization
57314-57316	No Flux Information	56512	normalization
57273	No Flux Information	56584	normalization
57241	No Flux Information	56682	normalization
56906	No Flux Information	56790	normalization
56363	Lepton TrigBit (6) Not Set	56931	normalization
56365	Lepton TrigBit (6) Not Set	56947	normalization
56369	Lepton TrigBit (6) Not Set	57169	normalization
56384	Lepton TrigBit (6) Not Set	57239	empty-target
56386	Lepton TrigBit (6) Not Set	57241	empty-target
56400-56401	Lepton TrigBit (6) Not Set	57248	normalization
56403-56406	Lepton TrigBit (6) Not Set		

4.1.2 EVENT SELECTION

During the skimming process, CLASEVENT employs several corrections to the data that are necessary to analyze the data. Such corrections are “energy-loss” and “tagger-sag” correction which are discussed in Sec. 4.2.1 and Sec. 4.2.2 respectively.

The skim performed on the BOS files included the criteria of Table 15 using the PART reconstruction scheme. There is another particle reconstruction scheme, EVNT. However this method was first reported unreliable for $g12$ by the author of this manuscript and then later confirmed by various other users. Pions were skimmed initially and then

TABLE 15. Requirements of initial skim

Requirement	Section Discussed
One in-time beam photon	Sec. 4.1.3
One proton	Sec. 3.3
One π^+ or “unknown” of q^+	Sec. 3.3
One π^- or “unknown” of q^-	Sec. 3.3

re-identified as leptons by changing the mass of the pion. This method is sufficient when the decaying particle’s mass, i.e. m_{π^0} , is less than that of pions. If the event satisfied the requirements listed in Table 15, then all TOF, ST, momentum and vertex information was outputted as well as CC and EC information for the π^\pm particles to be used to identify leptons, as discussed in Sec 4.1.4. To reduce the size of the data set, a cut was placed on the total missing mass of $\gamma p \rightarrow p\pi^+\pi^-$ to be less than 275 MeV. This cut was broad enough to not interfere with π^0 selection from single π^0 production i.e. $\gamma p \rightarrow p\pi^0$ when assigned the pion the lighter mass of a electron/positron. This broad cut also does not interfere with π^0 production from light meson decay, i.e $\gamma p \rightarrow p\omega \rightarrow p\pi^+\pi^-\pi^0$.

4.1.3 BEAM PHOTON IDENTIFICATION

As described in Sec. 4.1.1, only runs in which the beam current was 60-65 nA were used. This high current incident on the radiator can create multiple tagger hits within the time gate of the trigger. To determine which beam photon interacted with the target creating the event, a tagger time best matching the average ST time is chosen to be the time of the interacting photon that created the triggered event.

Due to the 2.004 ns CEBAF beam bunching spacing, there are possibilities in which a beam bunch will contain multiple bremsstrahlung photons that are indistinguishable in timing, within 2.004 ns, that satisfy the best tagger time. Figs 41 and 42 show that $\simeq 86\%$

of events have a single in-time tagger-ST coincidence, $\simeq 11.5\%$ of events have two in-time tagger-ST coincidences, $\simeq 2\%$ of events have three in-time tagger-ST coincidences and $< .5\%$ of events have more than three in-time tagger-ST coincidences. For the events in which there are multiple photons within the 2.004 ns window that are in time with the ST, the best photon is chosen at random with no preference to the energies of each photon. This method of random choice allows for a 7% background increase due to the mismatching of the photon. The 7% is due to randomly choosing the incorrect photon $\frac{1}{2}$ of the 14%.

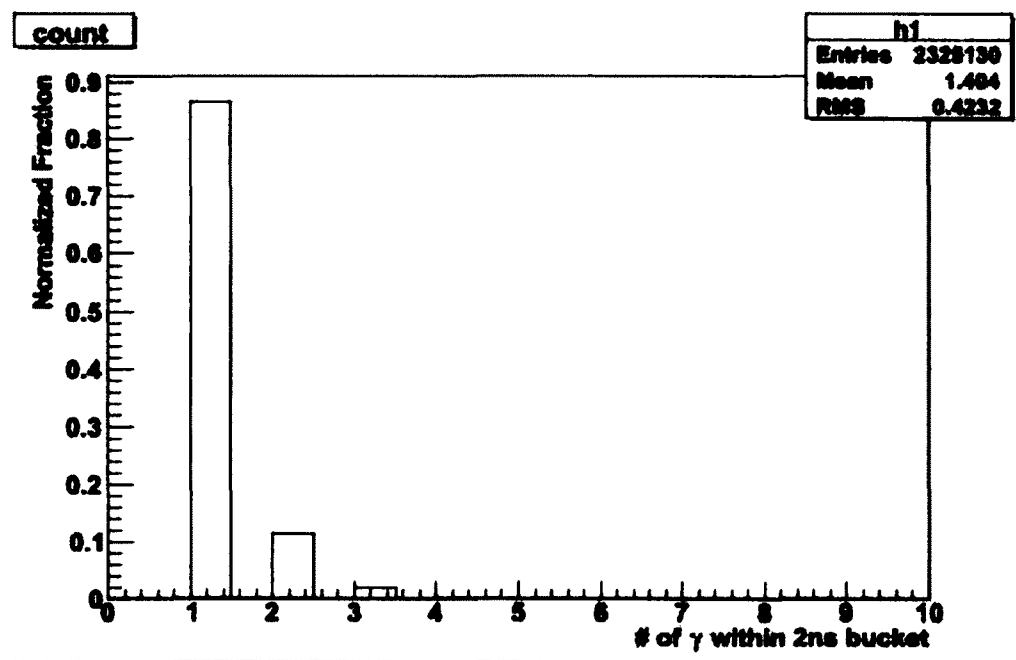


FIG. 41. Probability of single and multiple photons within the CEBAF timing window of 2.004 ns.

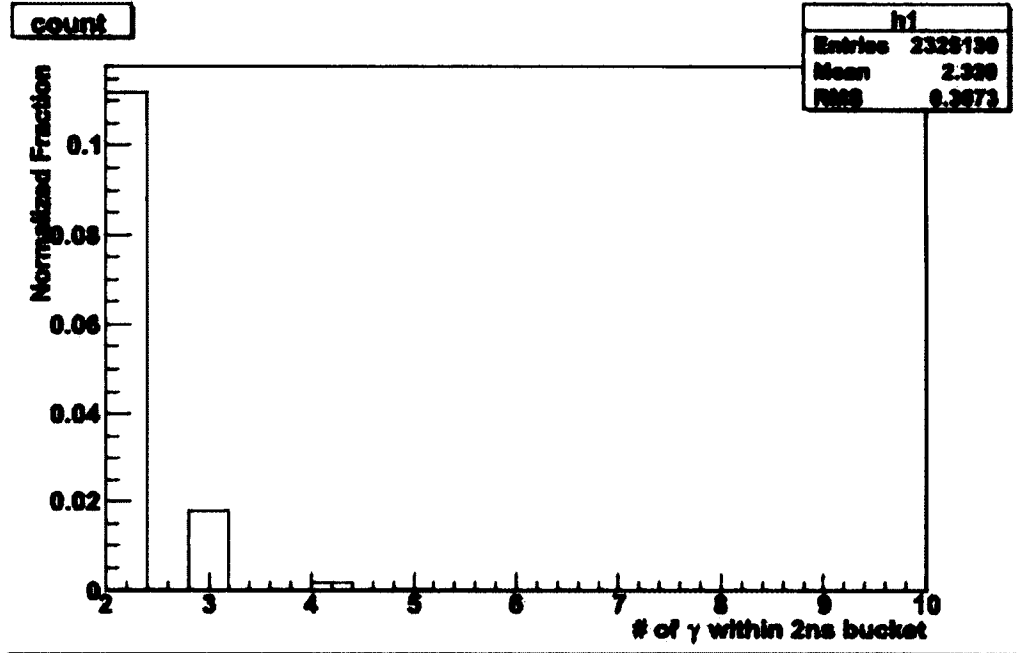


FIG. 42. Probability of multiple photons within the CEBAF timing window of 2.004 ns.

4.1.4 PARTICLE IDENTIFICATION

Lepton identification was based on conservation of mass. Once the data is skimmed according to Table 15, all particles that were π^+ , π^- , unknown with q^+ or unknown with q^- were tentatively assigned to be electrons or positrons based on their charge. This meant that the mass term of the particle's 4-vector was set to be the mass of an electron instead of that of a pion. This technique works because the mass of the π^0 (0.135 GeV) is less than the mass of π^+ or π^- (0.139 GeV) and by laws of conservation of energy-momentum, a lighter particle cannot decay into heavier particle's.

For particles with higher masses that can decay into two-pions or into e^+e^- , such as η , ω , etc., the CC and EC provide a $\frac{e^+e^-}{\pi^+\pi^-}$ rejection factor of $\approx 10^6$. The method to achieve this rejection factor was developed by Mike Wood and is based on using various cuts placed on the CC and EC measured quantities. This method was not used in this analysis, the $\gamma p \rightarrow p\pi^0 \rightarrow pe^+e^-\gamma$ reaction provides insight into the validity of the method. The Mike Wood method of $\frac{e^+e^-}{\pi^+\pi^-}$ rejection factor is discussed in [41].

4.2 g_{12} CORRECTIONS

There were three corrections that were implemented onto the *g12* data set. The first correction was applied to the tagger subsystem due to a magnetic field problem that affected only the *g12* experiment. The second correction corrects for the “energy-loss” of a particle through matter. These corrections are discussed further in the proceeding subsections. The third correction was the tagger sag correction that was handled in the tagger calibration.

4.2.1 ENERGY LOSS

Since tracking began after the particle had already traversed through the target and ST, the measured momentum was decreased by the “energy-loss” the particle underwent before entering the Region 1 DC. This “energy-loss” is due to charged particles losing their energy through atomic excitation and ionization while traveling through materials in the CLAS detector. The effect of “energy-loss”, in CLAS, is only indicative to all charged particles. However, using the Bethe-Bloch equation:

$$\frac{dE}{dx} \sim \frac{\ln \gamma}{\beta^2}, \quad (87)$$

where γ and β have their usual meanings, it is seen that for electrons with $\beta \approx 1$ lose less energy than protons. Therefore “energy-loss” corrections are not applied to electrons or positrons. For those charged particles that are subject to “energy-loss”, such as the proton for this analysis, corrections were made to account for energy lost in the target material (ℓH_2), kapton target walls, the beam pipe, the start counter and the air between the start counter and the Region 1 DC. The corrections were applied by the *e loss* software package written by Eugene Pasyuk for the CLAS detector [43] as an add-on to the CLASEVENT software package.

4.2.2 BEAM CORRECTIONS

Initially, missing masses computed for *g12* were systematically low. It was realized while investigating the issue that the low missing mass depended on run number and varied by as much as 10 MeV. The run dependent missing mass showed a constant low mass (run<56550) followed by a higher mass which remained constant (56500<run<56920) until another increase in mass (run>56920). To analyze and correct for the problem, two reactions were chosen to select missing protons and neutrons. The first reaction;

$$\gamma p \rightarrow \pi^+ \pi^- p \quad (88)$$

was used to derive the correction, while the second reaction;

$$\gamma p \rightarrow \pi^+ \pi^+ \pi^- (n) \quad (89)$$

was chosen to verify the corrections. The reaction of Eq. 88 was used to derive the correction because all three particles can be detected. Thus

$$(P_\gamma + P_{target} - (P_{\pi^+} + P_{\pi^-}))^2 = P_p^2 = m_p^2 \quad (90)$$

where P_γ , P_{target} , P_{π^\pm} and P_p are the 4-vectors of the incident photon, target, π^\pm and proton respectively and m_p is the mass of the proton. We selected events for the correction with one CLAS PID π^+ , one CLAS PID π^- , one CLAS PID proton and nothing else. Exclusive cuts were then placed by requiring the missing energy, $M_E(\gamma p \rightarrow p\pi^+\pi^-) < 0.025$ GeV and the missing mass squared of $M_x^2(\gamma p \rightarrow p\pi^+\pi^-) < 0.015$ GeV². These cuts assure that the selected events did not have a undetected $p\pi^0$, since the mass squared of $\pi^0 = 0.0182$ GeV².

The first step chosen was to verify whether the “energy-loss” correction was causing the discrepancy. This can be seen in Figs. 43, 44. It was concluded that the “energy-loss” correction was not the problem. From Fig. 43, two runs were chosen, 56515 and 57130, in which the difference in the missing mass was ≈ 10 MeV. Inspecting the invariant mass, $M(\pi^+\pi^-)$, Fig 45, for runs 56515 and 57130 revealed only a mass deviation of ≈ 1.4 MeV. This implies that the problem is caused by the photon beam energy.

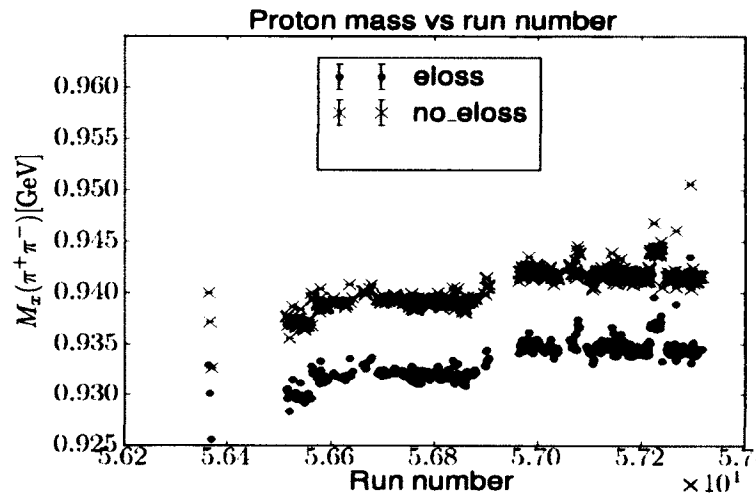


FIG. 43. Plot of $g12$ run number vs. undetected proton mass with and without the “energy-loss” applied.

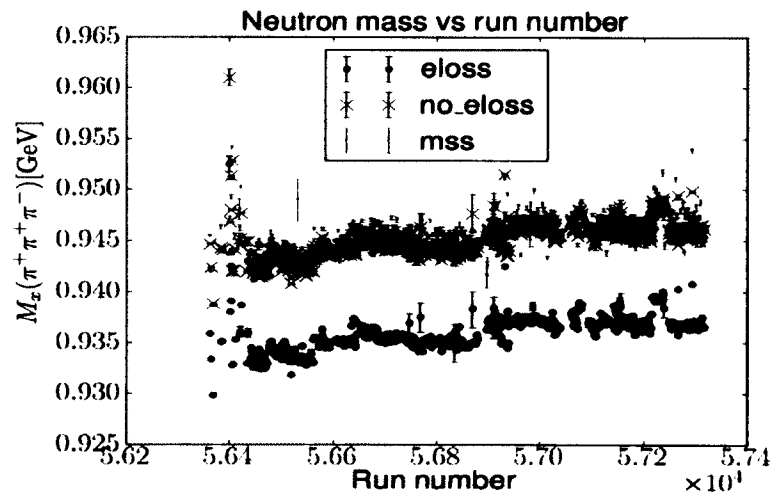


FIG. 44. Plot of $g12$ run number vs. undetected neutron mass with and without the “energy-loss” applied. The red data points labeled “mss” are data taken directly from tape. Image Source: [42]

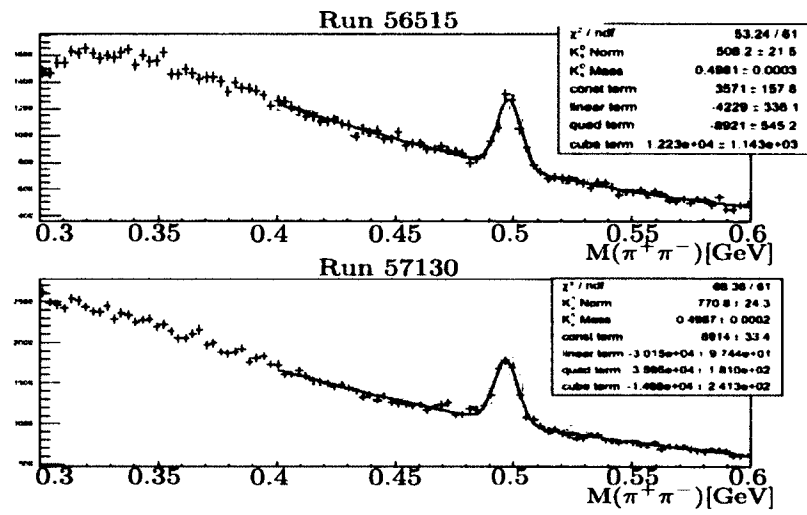


FIG. 45. Plot of $\pi^+\pi^-$ mass for runs 56515 and 57130. $m_{K_0} = 0.4976 \text{ GeV}/c^2$.

Several tagger quantities were analyzed. The tagger magnet current was apparently constant (see Fig. 46) but had been turned off around run=56920 (May 12, 2008). When the tagger magnet was turned on, the current was set to its previous setting. The tagger magnet current was recorded by the accelerator group shown in Fig. 47, it was also stable throughout the running of *g12*. The beam current was also stable (see Fig. 48)

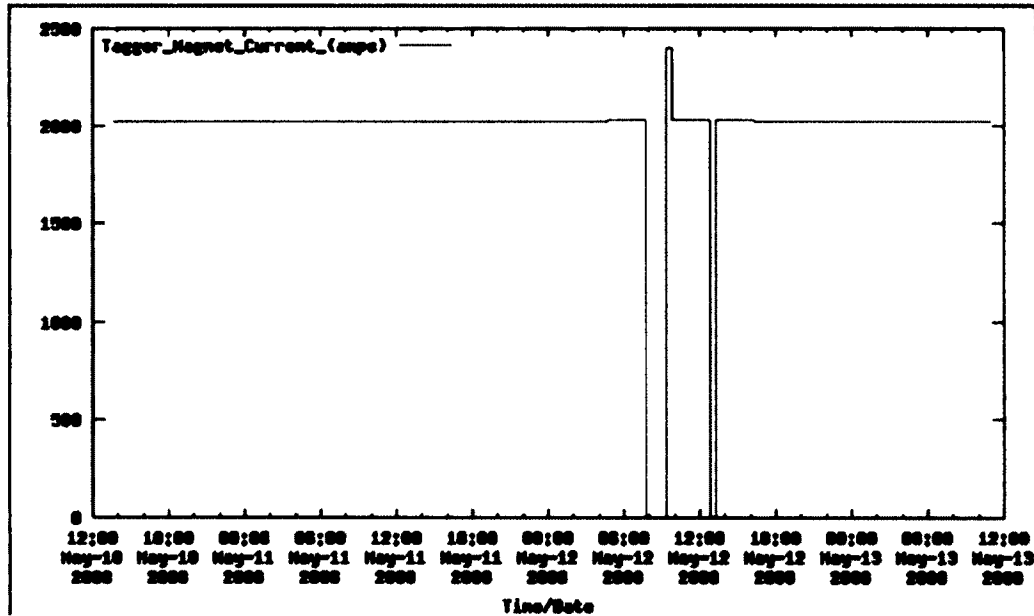


FIG. 46. Tagger magnet current according to EPICS

The next quantity investigated was the positioning of the beam spot on the tagger dump. This quantity was used in place of the tagger magnetic field strength because hall B does not measure the tagger magnetic field strength. However since the radius of curvature of a charged particle is inversely proportional to the magnetic field this quantity is suitable.

$$p = qrB \text{ (if } \vec{p} \perp \vec{B} \text{)} \quad (91)$$

The y-position of the tagger beam spot on the dump jumps on or about May 12, 2008 (see Fig. 49). The change in y-position can only be due to the magnetic field changing. The phenomena in magnetism that allows for a steady current but a change in magnetic field is known as hysteresis (see Fig. 50).

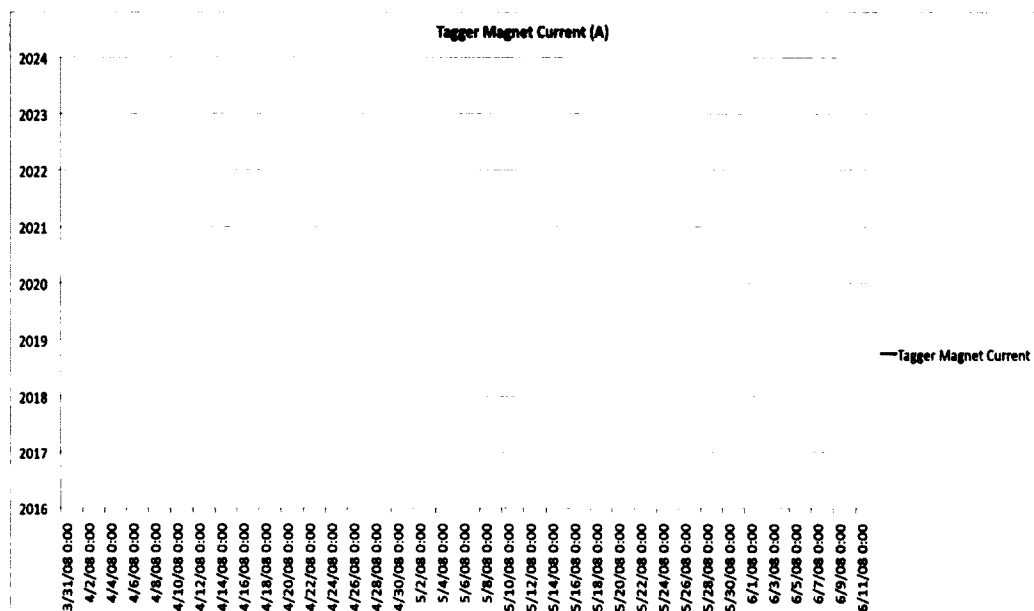


FIG. 47. Tagger magnet current according to accelerator group via EPICS

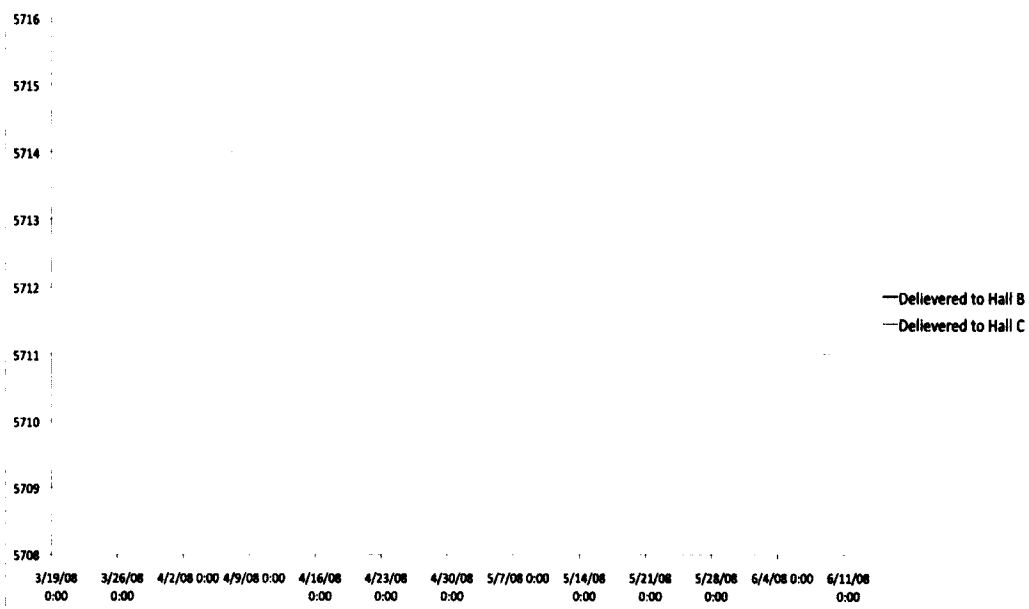


FIG. 48. Electron beam current delivered to hall B (red) and hall C (green) according to the accelerator group during $g12$. The green line overlays the red line except during the time around April, 03, 2008.

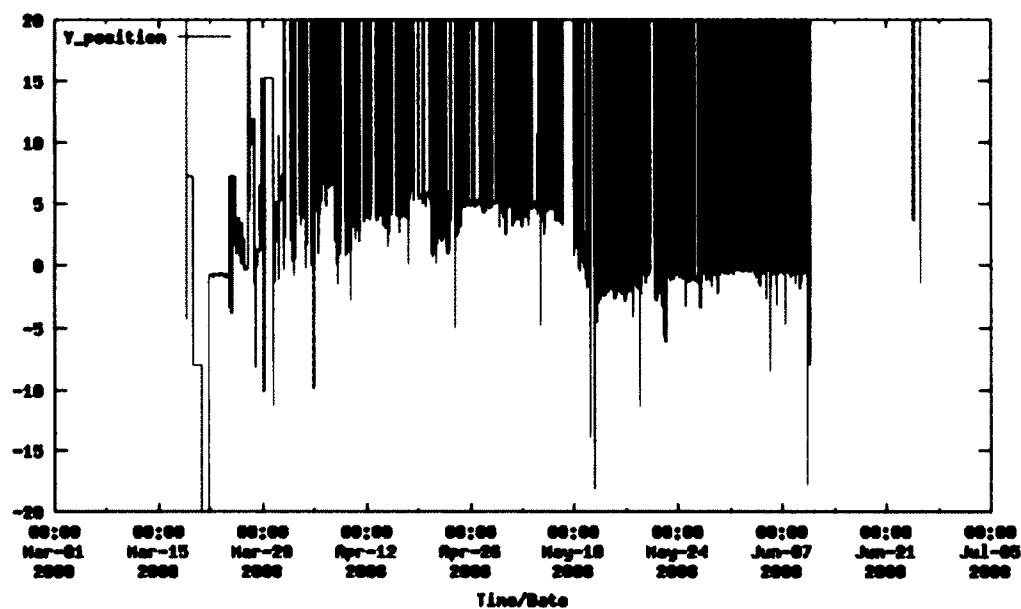


FIG. 49. Tagger dump beam spot y-position according to EPICS

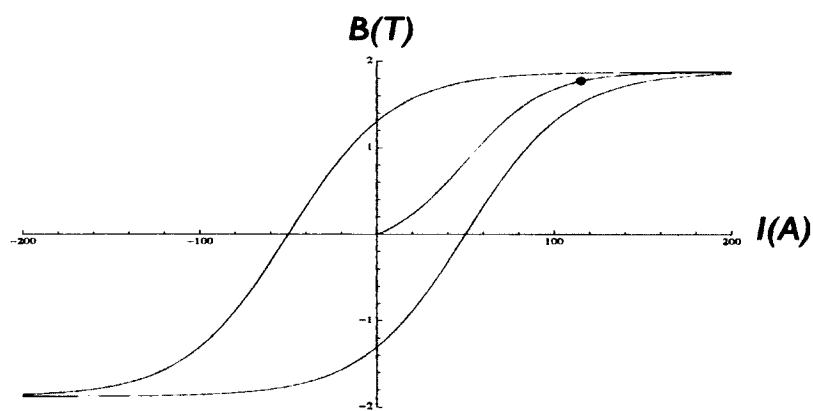


FIG. 50. Plot depicting magnetic field strength vs. magnet current showing the process of hysteresis. For a current of strength I , there could exist many magnetic fields of strength B .

It appeared that the $g12$ missing mass fluctuations are due to tagger magnet hysteresis and the effect it would be on the scattered electron and hence the tagged photon. The tagged photon energies were corrected as follows;

$$P_{\pi^+} + P_{\pi^-} = P_{\pi^+\pi^-}$$

where P_{π^+} , P_{π^-} are the 4-momenta of the π^+ , π^- respectively and $P_{\pi^+\pi^-}$ is the sum of π^+ and π^- 4-momenta. Therefore;

$$(P_\gamma + P_{target} - (P_{\pi^+\pi^-}))^2 = m_p^2 \quad (92)$$

$$P_\gamma^2 + P_{target}^2 + P_{\pi^+\pi^-}^2 + 2P_\gamma P_{target} - 2P_\gamma P_{\pi^+\pi^-} - 2P_{target} P_{\pi^+\pi^-} = m_p^2 \quad (93)$$

collecting terms of P_γ to one side and using $P_{target}^2 = m_p^2$ and $P_\gamma^2 = 0$

$$P_{\pi^+\pi^-}^2 - 2P_{target} P_{\pi^+\pi^-} = 2P_\gamma (P_{\pi^+\pi^-} - P_{target}) \quad (94)$$

From this using Eq. 65 in 4-vector notation

$$P_\gamma = P_{E_0} - P_e$$

where P_{E_0} is the four vector of the incident electron and P_e is the four vector of the scattered electron in the bremsstrahlung process that is measured by the tagger. Applying a scalar correction to P_e as xP_e and solving for x for all known quantities, Eq. 94 simplifies to;

$$x = \frac{P_{E_0}(P_{target} - P_{\pi^+\pi^-}) + P_{\pi^+\pi^-}^2/2 - P_{target}P_{\pi^+\pi^-}}{(P_{E_0} - P_\gamma)(P_{target} - P_{\pi^+\pi^-})} \quad (95)$$

To reduce statistical fluctuations $\frac{1}{10}$ of run 56515 was analyzed to obtain the correction factor x . The correction factor was fitted using a Gaussian to establish an accurate measurement of the peak, this is shown in Fig 51. After the correction factor was extracted for run 56515, it was applied to both the reactions listed in Eq. 88 and Eq. 89 by recalculating the photon beam energy as;

$$E_e = E_{E_0} - E_\gamma$$

$$E_\gamma^{new} = E_{E_0} - xE_e.$$

Figures 52, 53 illustrate the missing masses after the tagger correction and show that the new calculated missing masses are less than 1 MeV from PDG values. Since both the missing proton mass and missing neutron mass were adjusted properly to the correct mass

by using the same beam correction factor, it shows that the correction factor is independent of reaction and therefore can be applied to all $g12$ analyses. The procedure to calculate x was repeated for every run in $g12$, Fig 54, with $\frac{1}{10}$ of the data used. To validate the corrections of the entire $g12$ data set, the missing neutron mass was recalculated for each run, shown in Fig. 55, using several correction schemes, i.e. a scheme of just “energy-loss” corrections, a scheme of “energy-loss” and momentum corrections (JTG PCor), a scheme of “energy-loss”, momentum corrections (JTG PCor) and beam corrections (MK BeamCor) and a scheme of “energy-loss” and beam corrections (MK BeamCor). It can be seen in Fig. 55 that the only scheme that sufficed was the combination of “energy-loss” and beam corrections.

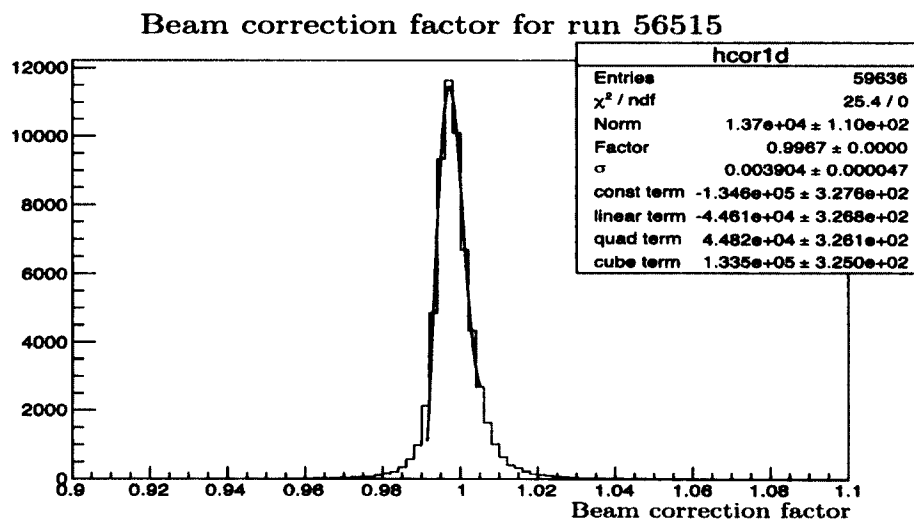


FIG. 51. Beam correction factor for run 56515. The fit is a Gaussian function.

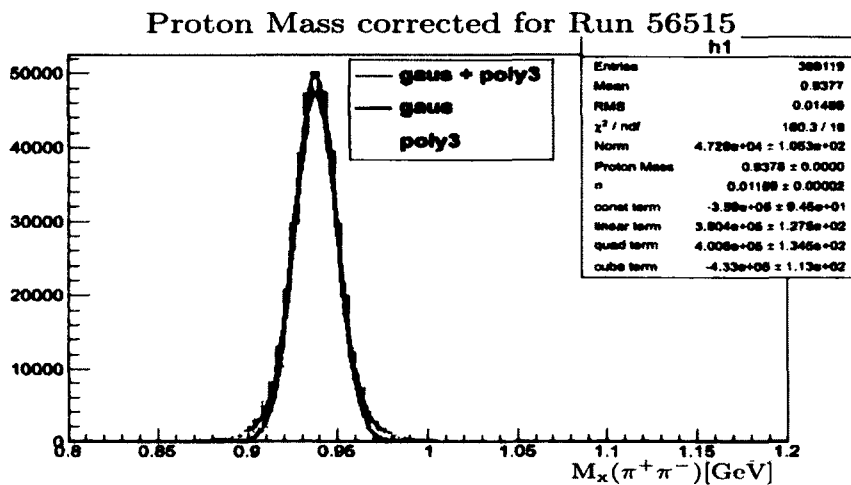


FIG. 52. Plot of proton mass for runs 56515 after beam correction was applied. PDG mass for the proton is 0.938272 GeV/c.

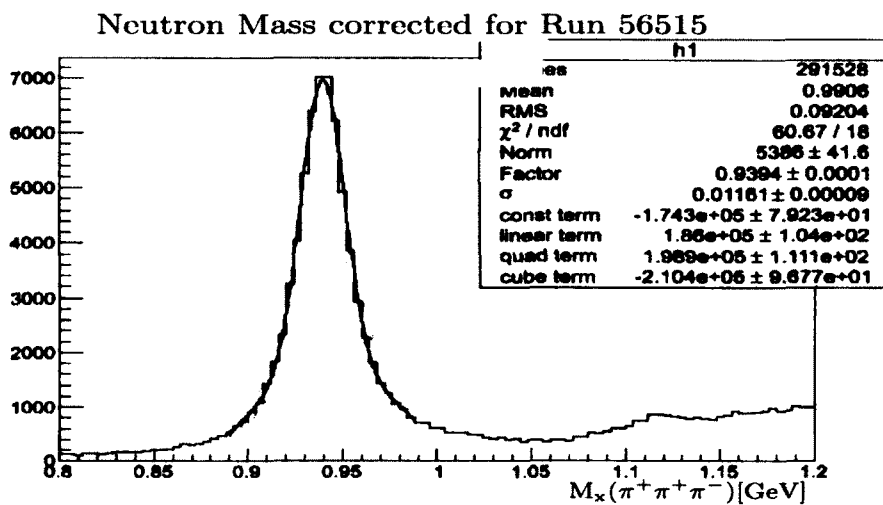


FIG. 53. Plot of neutron mass for runs 56515 after beam correction was applied. PDG mass for the neutron is 0.939565 GeV/c.

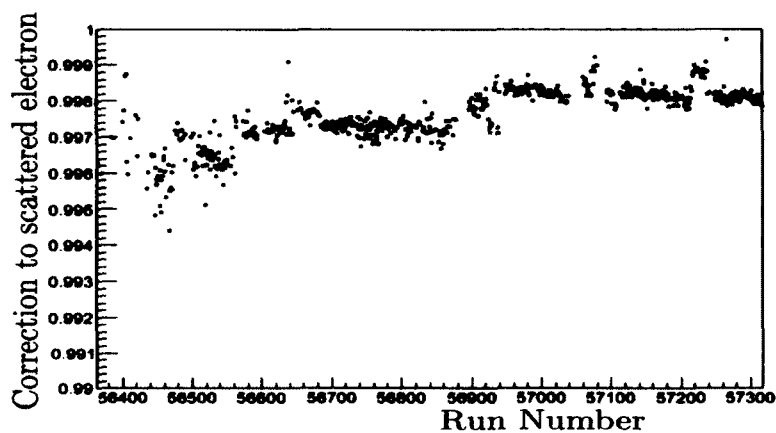


FIG. 54. Plot of the correction factor x as a function of run number.

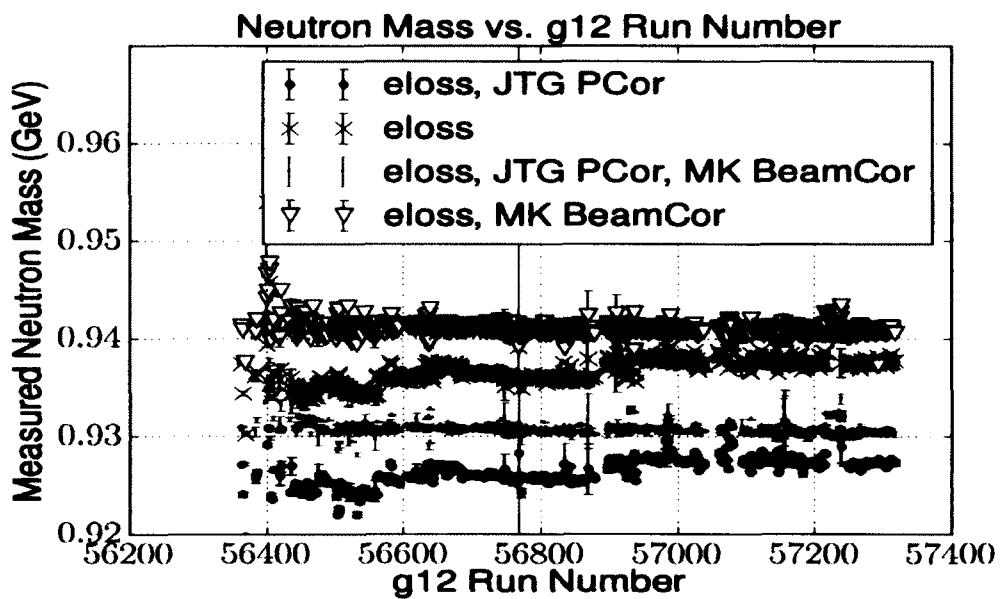


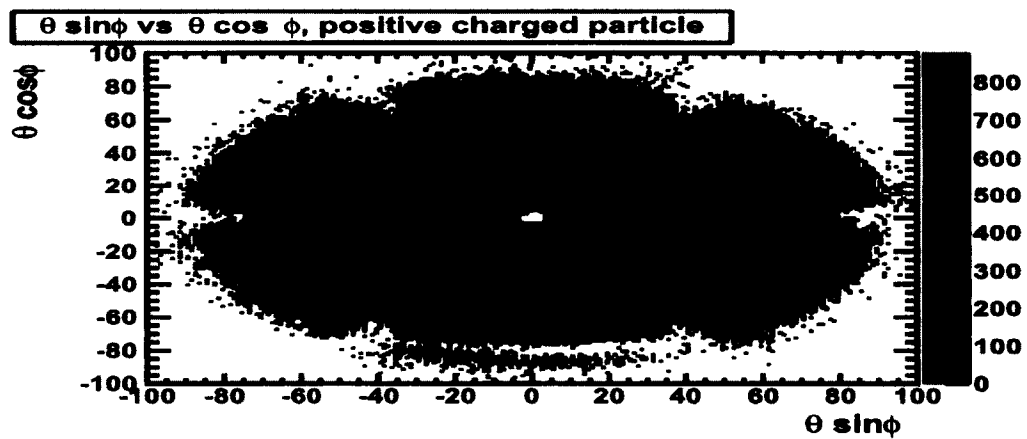
FIG. 55. Plot of missing neutron mass vs. run number using various corrections. The yellow triangles show a missing neutron mass with only “energy-loss” and beam correction applied (MK BeamCor) which was the only corrections needed to correct the $g12$ data stream.

4.3 FIDUCIAL CUTS

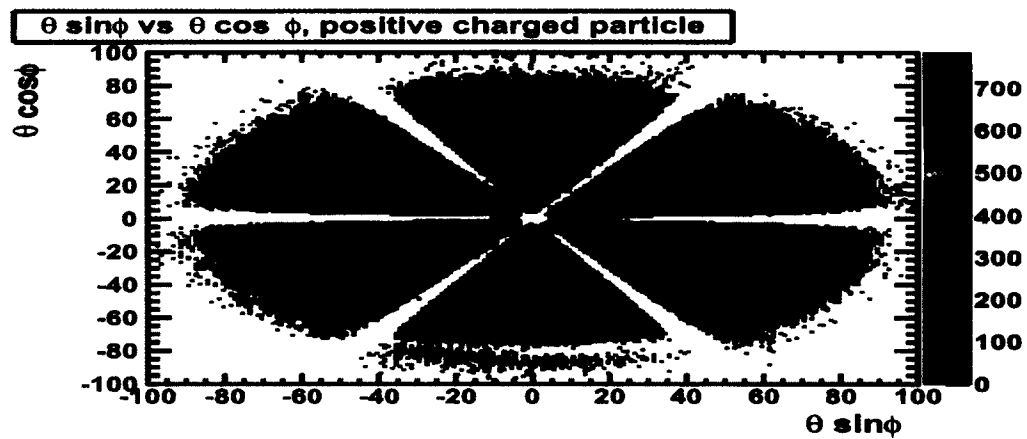
This section will describe the various detector performance cuts that were used in this analysis to clean the data due to various subsystems deficiencies. These deficiencies are not understood well enough to be modeled in the MC, therefore some events must be removed from the analysis.

4.3.1 GEOMETRIC FIDUCIAL CUTS

A fiducial cut is required to prevent a significant systematic error contribution from either gaining or losing events that lie in nonuniform regions, such as space between sectors. This cut, shown in Figs. 56, 57, was applied to all data, real and simulated, presented in the final result shown in Sec. 5. The geometric fiducial cuts analysis was performed by Jason Bono of the FIU group. The package for performing these fiducial cuts has three options for the parameters involved in the removal process. These options are “loose”, “nominal” and “tight” and refer to the amount of area that is to be cut in the space between the drift chambers. A detailed specification of this cut is given in [41]. This analysis used the nominal option. To understand the systematic error caused in this fiducial, the measurement from the “tight” option was compared to the measurement at the nominal option. This is discussed in Sec. 5.4.

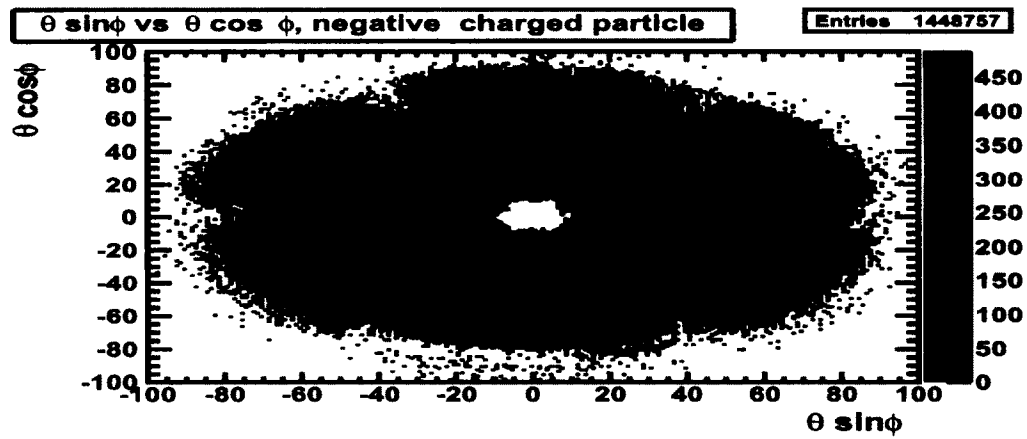


(a)

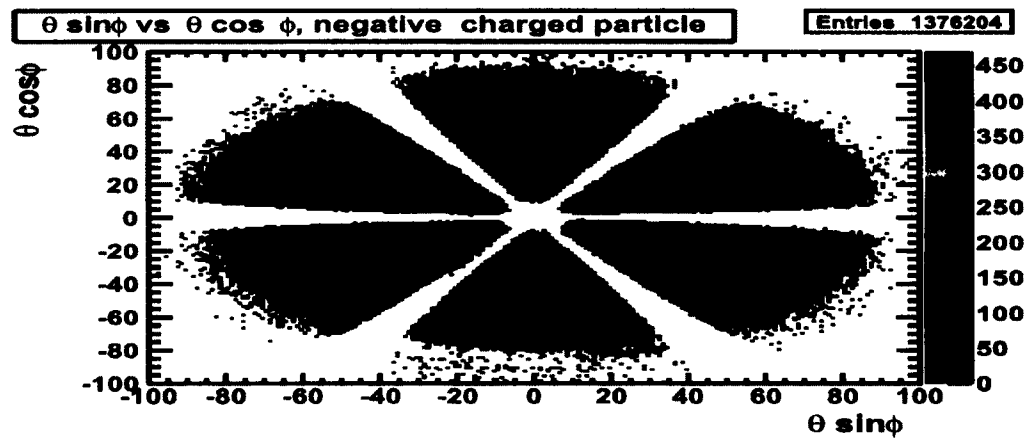


(b)

FIG. 56. Positive charged tracks in CLAS DC prior to fiducial cuts (a) being applied, and after (b) being applied.



(a)



(b)

FIG. 57. Negative charged tracks in CLAS DC prior to fiducial cuts (a) being applied, and after (b) being applied.

4.3.2 TOF FIDUCIAL CUTS

The efficiency for the TOF subsystem, described in Sec. 2.9, is different for each paddle for each section. As a result, there are regions of detection in which are inefficient. The program GPP, Sec. 4.4, was constructed to account for these inefficiencies in the simulation. However the MC indicated a greater efficiency than we measured in the data. Therefore we measured the efficiency of CLAS as a function of particle angle and momentum. The particles π^+ , π^- and proton momentum and angular measurements were selected from data and MC to analyze these functions. When an inefficiency was observed in the data, but not the MC, equations were derived in θ and ϕ to use as a cut to account for the inefficiency. Example of such an inefficiency can be seen in Fig 58, where the top panel depicts the π^+ azimuthal angle (ϕ) vs. polar angle (θ) and the bottom panel illustrates momentum (p) vs. polar angle (θ) for sector 3. Fig. 58 shows a band of low efficiency pertaining to a inefficient TOF paddle between $\approx 15^\circ < \theta < 21^\circ$. Fig. 58 also shows a “rib” like structure on the bottom plot, θ vs. p , which is not present in the π^- data, therefore was not further investigated as a bad paddle. The inefficient section of sector 3 was removed in data and MC. The effect of this cut can be seen in Fig. 59. The statistical sample used in Fig. 59 was 1/5 of the data used to derive the cut equation shown in Fig 58. There also existed an inefficiency in sector 1. The plots showing the inefficiency along with the other 5 sectors can be found in App. A. The parameters for the TOF cuts are listed in Tab. 16. Placing the cuts described in Tab. 16 is equivalent to knocking out TOF paddle by ID number. The variable ϕ_s is ϕ represented in the interval of $-30 \leq \phi \leq 30$ in which the term f_{mod} is the $C++$ function used to perform the operation.

TABLE 16. TOF cut parameters.

Sector	$\phi [^\circ]$	θ Upper Limit (\leq)	θ Lower Limit (\geq)
1	$\phi < 0$	$24 - \phi(26 - 24)/30$	$21.5 - \phi(23.5 - 21.5)/30$
1	$\phi \geq 0$	$24 + \phi(26 - 24)/30$	$21.5 + \phi(23.5 - 21.5)/30$
3	$\phi_s < 0$	$20.5 - \phi_s(22. - 20.5)/30$	$16 - \phi_s(17.5 - 16)/30$
3	$\phi_s \geq 0$	$20.5 + \phi_s(22 - 20.5)/30$	$16. + \phi_s(17.5 - 16)/30$
$\phi_s = f_{mod}(f_{mod}((\phi + 390), 360), 60) - 30$			

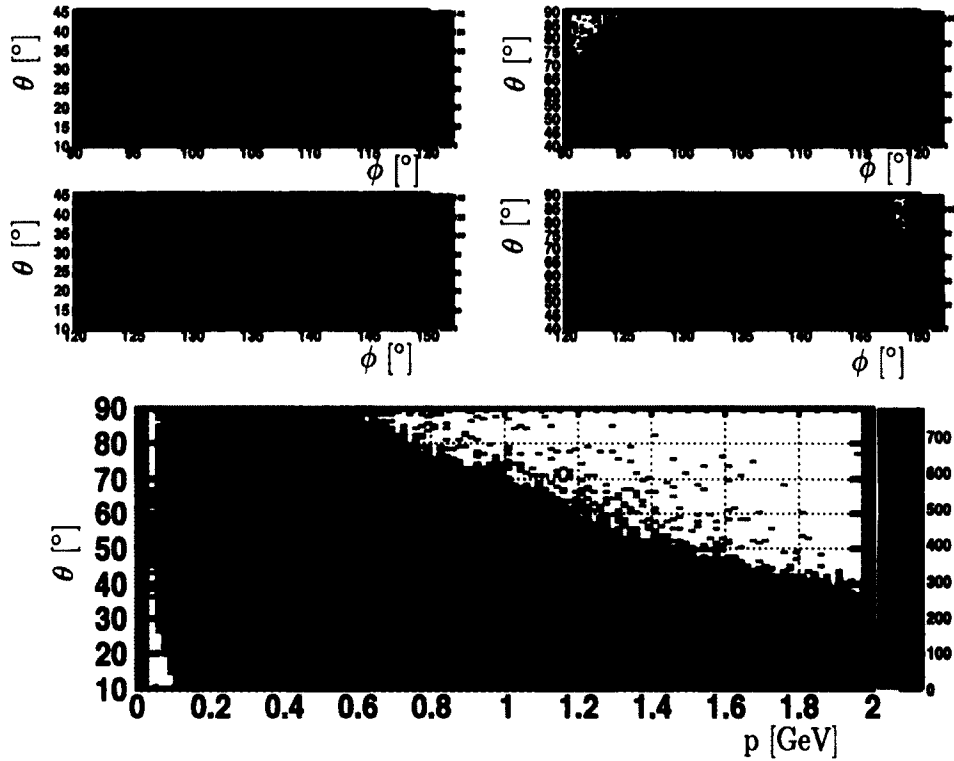


FIG. 58. (Top Left) θ vs. ϕ of π^+ data. Angular range $90^\circ < \phi < 120^\circ$ and $10^\circ < \theta < 45^\circ$. (Top Right) θ vs. ϕ of π^+ data. Angular range $90^\circ < \phi < 120^\circ$ and $40^\circ < \theta < 90^\circ$. (Middle Left) θ vs. ϕ of π^+ data. Angular range $120^\circ < \phi < 150^\circ$ and $10^\circ < \theta < 45^\circ$. (Middle Right) θ vs. ϕ of π^+ data. Angular range $120^\circ < \phi < 150^\circ$ and $40^\circ < \theta < 90^\circ$. (Bottom) θ vs. P of π^+ data. Momentum range $0 < P < 2$ GeV and θ range $10^\circ < \theta < 90^\circ$. The z-axis on all plots illustrate the yield of data used in the plot. Inefficiency seen in CLAS π^+ data, due to an inefficient TOF paddle.

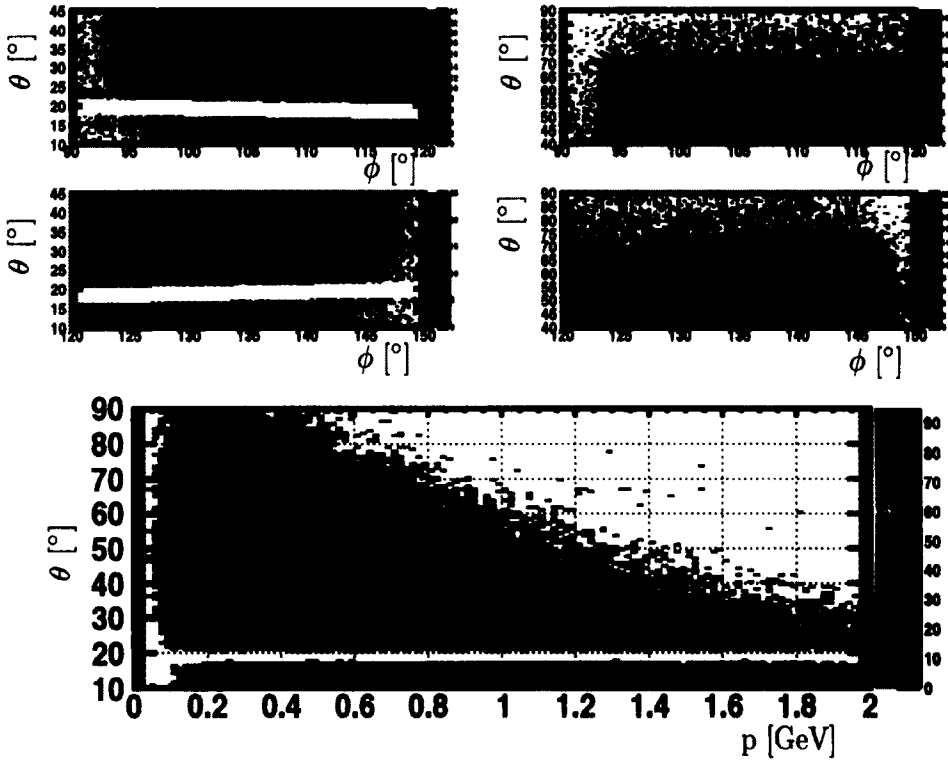


FIG. 59. Inefficiency cut for π^+ and proton data. Notation same as in Fig. 58.

4.3.3 EC FIDUCIAL CUTS

The efficiency for the EC subsystem, described in Sec. 2.10, is different for each strip in the u , v , w arrangement. As a result, there are regions of detection which are inefficient. An extreme example of this is illustrated in Fig. 60, where the EC *inner* (top row) and *outer* (bottom row) strips are plotted as a function of the azimuthal angle (ϕ) for sector 5. A dead or inefficient strip is seen as a horizontal band in Fig. 60. The curvature of inefficient strips seen are reflections of inefficiency in another orientation. For example, the curves seen in the top left plot, u orientation, of Fig. 60 is a reflection of dead or inefficient strips from v and w orientations respectively. The projection of Fig. 60 onto the y -axis can be

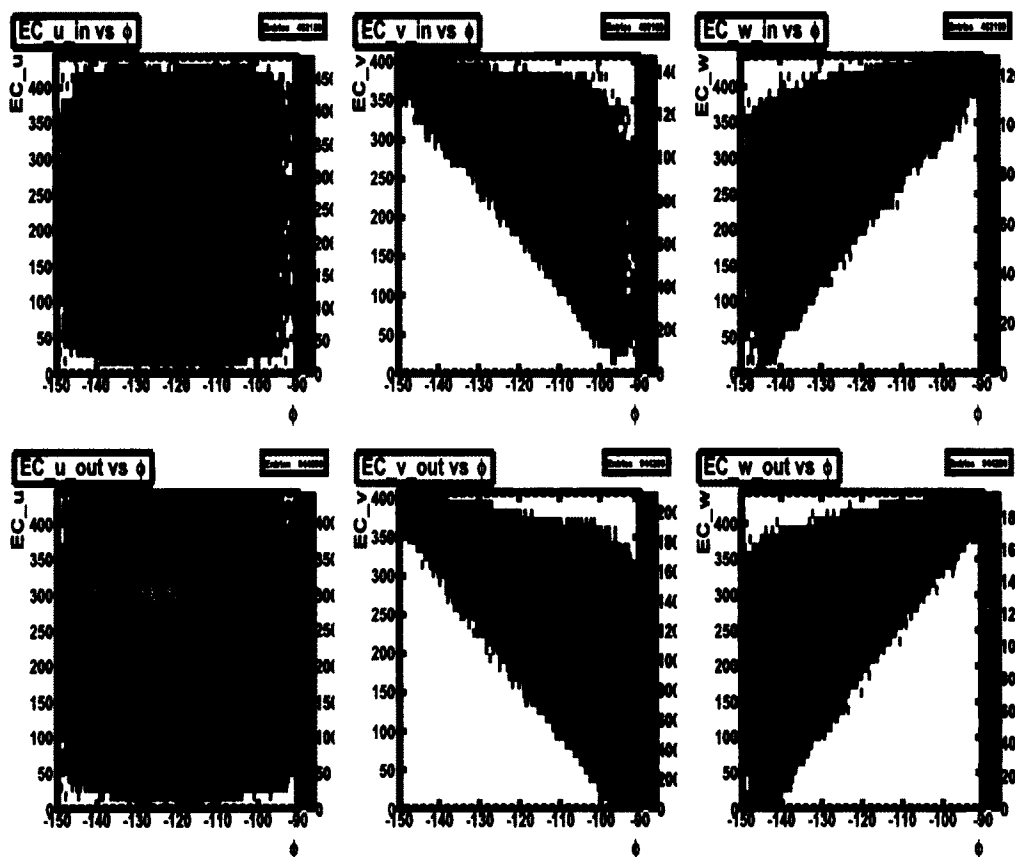


FIG. 60. Inefficient EC u , v , w strips vs. ϕ for sector 5 in CLAS e^- data. Top row depicts the u , v , w strips for the *inner* EC, while the bottom row depicts the u , v , w strips for the *outer* EC. The z-axis illustrates the number of hits in the plot.

seen in Fig. 61. This view depicts the actual paddles that are dead or inefficient. It can be seen in either Figs. 60 and 61 that there exists inefficient EC strips for sector 5. The inefficient strips were removed in data and MC. The effect of the inefficient strip cut, along

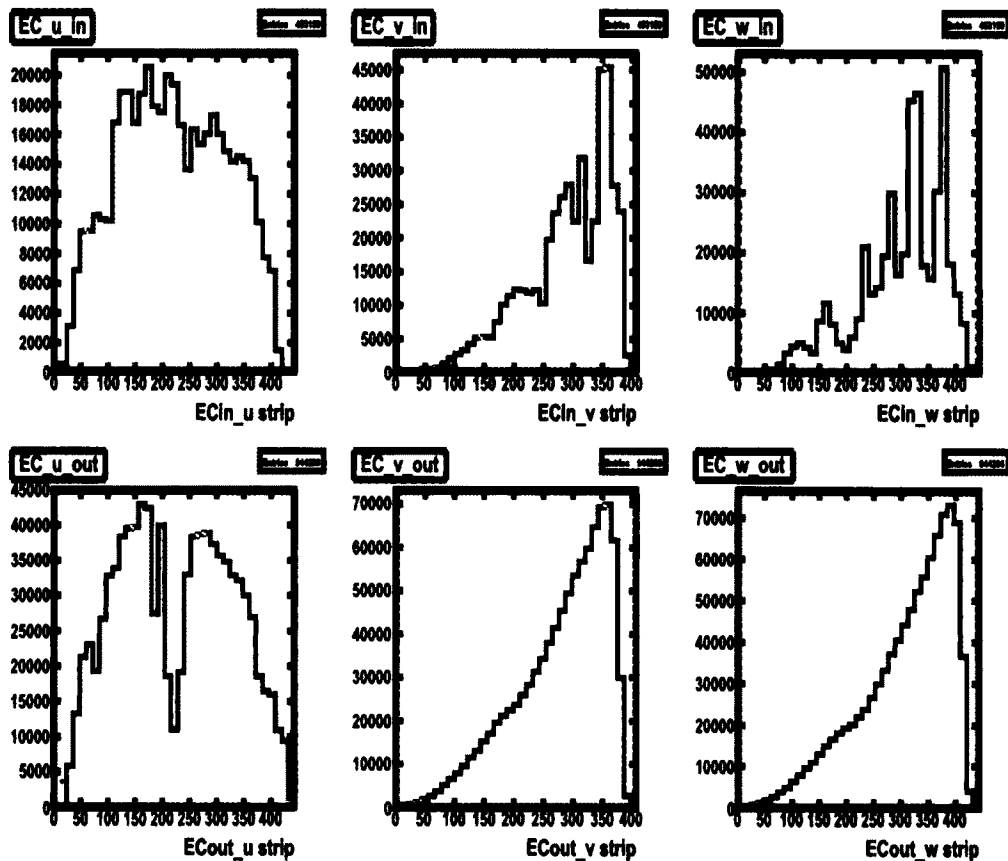


FIG. 61. Number of hit vs. inefficient EC u , v , w strips for sector 5 for e^- data. Top row depicts the u , v , w strips for the *inner* EC, while the bottom row depicts the u , v , w strips for the *outer* EC

with the standard CLAS EC geometric fiducial cuts can be seen in Fig. 62 and Fig. 63. There also existed an inefficiency in other sectors. The plots to show the total inefficiency of the EC can be found in App. A. The parameters for the EC strip cuts are listed in Tab. 17 and the parameters for the good EC fiducial range can be found in Tab. 18.

TABLE 17. EC UVW cut parameters.

Sector	EC _{inner/outer}	U
2	EC _{inner}	$96 \leq U \leq 108 \parallel 324 \leq U \leq 336$
3	EC _{inner}	$324 \leq U \leq 336 \parallel 180 \leq U \leq 216 \parallel 324 \leq U \leq 337$
2	EC _{outer}	$324 \leq U \leq 336.$
3	EC _{outer}	$131 \leq U \leq 142 \parallel 204 \leq U \leq 216 \parallel 324 \leq U \leq 336$
5	EC _{outer}	$180 \leq U \leq 192 \parallel 204 \leq U \leq 240$
		V
5	EC _{inner}	$320 \leq V \leq 342 \parallel 254 \leq V \leq 242$
		W
1	EC _{inner}	$312 \leq W \leq 324$
2	EC _{inner}	$396 \leq W \leq 408$
3	EC _{inner}	$396 \leq W \leq 408$
5	EC _{inner}	$336 \leq W \leq 372 \parallel 288 \leq W \leq 312 \parallel 240 \leq W \leq 276$ $\parallel 168 \leq W \leq 228 \parallel 132 \leq W \leq 144$
6	EC _{inner}	$W \geq 396$

TABLE 18. EC UVW good fiducial parameters.

EC Good Fiducial Range	U	V	W
	$20 \leq U \leq 400$	$V \leq 375.0$	$W \leq 405.0$

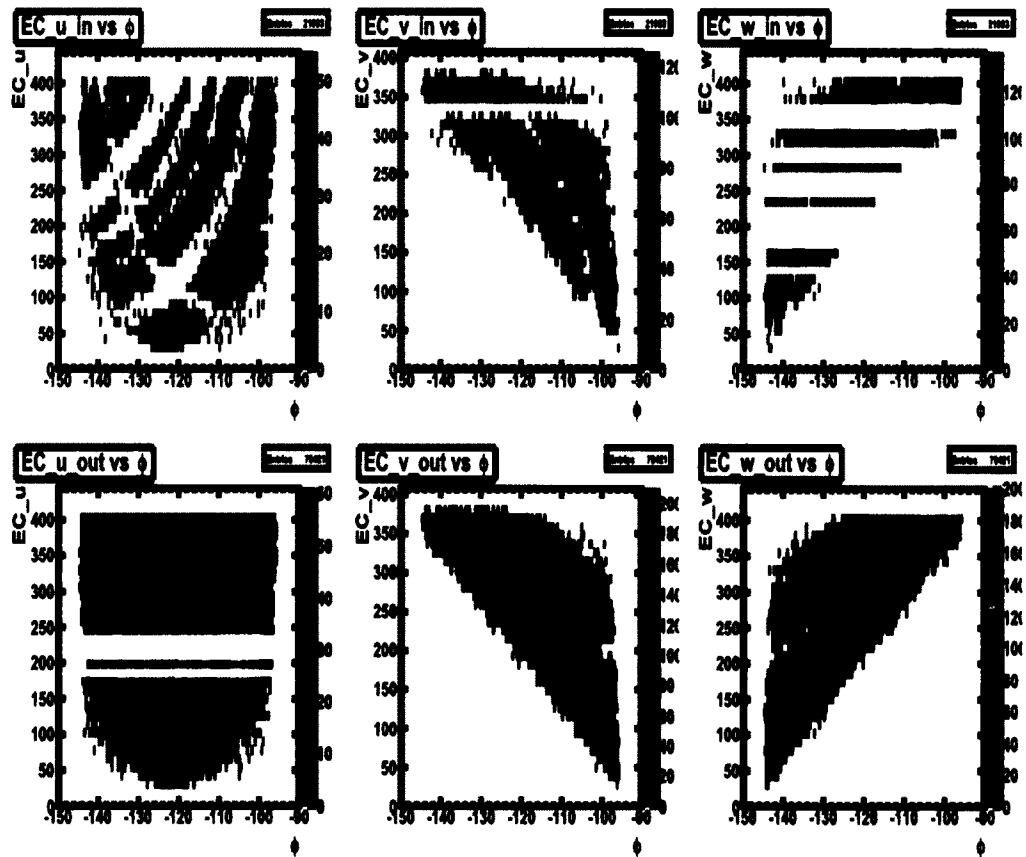


FIG. 62. EC u , v , w strips vs. ϕ for sector 5 with fiducial cuts and inefficient paddle knockouts applied to e^- data. Top row depicts the u , v , w strips for the *inner* EC, while the bottom row depicts the u , v , w strips for the *outer* EC. The z -axis illustrates the number of hits in the plot.

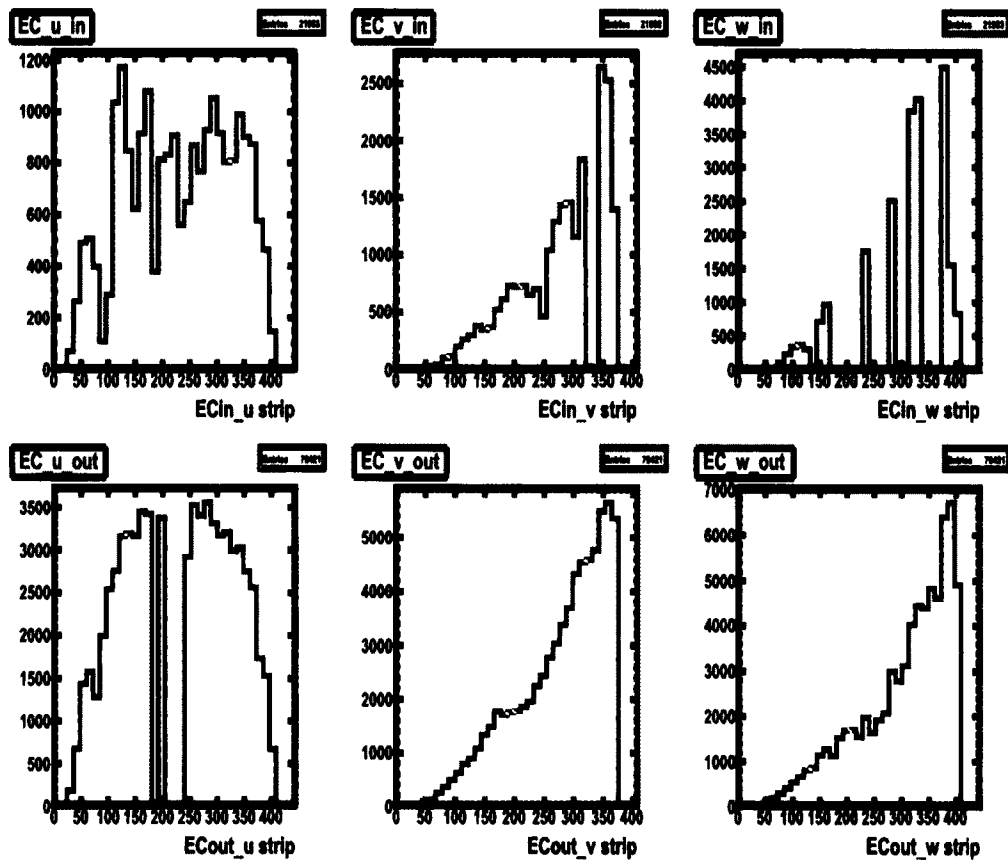


FIG. 63. Number of hits vs. EC u , v , w strips for sector 5 with fiducial cuts and inefficient paddle knockouts applied to e^- data. Top row depicts the u , v , w strips for the *inner* EC, while the bottom row depicts the u , v , w strips for the *outer* EC

4.4 SIMULATION

There are certain kinematic regions of CLAS in which physics events are not being recorded properly i.e. the area dividing each sector in CLAS. Furthermore each sector in CLAS is asymmetric in the acceptance of events due to subsystem inefficiencies such as inoperable DC wires, PMT inefficiencies, dead scintillator strips the the TOF and ST subsystems. When a triggered event is recorded and reconstructed these asymmetric inefficiencies factors are reflected and must be carefully understood because these factors are properties of the CLAS detector and independent of any physics that occurred. To properly understand the detector effects on the data, CLAS utilizes a GEANT simulation package know as GSIM. To prepare an event for GSIM the program GAMP2PART converts a text file, containing the 4-momentum of the generated event, into a suitable file format for GSIM. GSIM then simulates the passage of these particles through the CLAS detector and generates the associated ADC and TDC information from detector hits. GSIM takes into account detector inefficiencies described in the CLAS_CALDB_RUNINDEX. The CLAS_CALDB_RUNINDEX is an array of information about each subsystem's inefficiency that was derived during the *g12* calibration process. The GSIM simulated hits are then "post-processed" by smearing the TDC and ADC hits to imitate the observed resolution of the detector subsystems using the program GPP (GSIM post-processor). GPP also removes detector hits due to inefficient DC wires. The simulation output processed with GPP is then reconstructed with a1c, the same program used to reconstruct data events. The reconstructed simulation is subject to the same scrutiny as real data events, undergoing all the cuts (Sec. 4.3), corrections (Sec. 4.2), and kinematic fitting (Sec. 4.6), as the real data except for beam corrections (Sec. 4.2.2).

4.4.1 SIMULATION VERIFICATION

Part of understanding the simulation output is understanding how well the simulation mimics the real data. To investigate this, 26000 real e^+e^- events were treated as generated events and inputted into the GAM2PART→GSIM→GPP→a1c chain. Of the 26000 inputted, only 100 were successfully reconstructed through the simulation chain. The source of this low efficiency was due to the calibrations entries for the CC and EC in the CLAS_CALDB_RUNINDEX not having values in which would set the "PEDESTAL" values appropriately for simulation. The calibrations constants in the CLAS_CALDB_RUNINDEX were correct for data reconstruction, but not for simulation reconstruction of e^+e^- in the CC and EC subsystems. It was also discovered that the CC and EC subsystems should be simulated with "RUN 10" constants instead of the normal "RUN 56855" used by

the $g12$ group. “RUN 56855” is a special run benchmarked to have the best calibrations and required to properly simulate the ST, DC, and TOF subsystems. To rectify this, a special CLAS_CALDB_RUNINDEX was created, changing “RUN 10” for to have “RUN 56855” constants for all subsystems except the CC and EC subsystems which were kept at “RUN 10” constants. Inputting the 26000 real e^+e^- events into the simulation chain using the CLAS_CALDB_RUNINDEX *RunIndexg12 leptons_and_photons* outputted $\approx 24700 e^+e^-$ reconstructed events, a $\approx 95\%$ efficiency.

The missing 5% was a result of “time-based” and “hit-based” tracking failures as briefly mentioned in Sec. 3.3. The events that failed “hit-based” tracking contributes a 3.75% overall event inefficiency. The cause of the “hit-based” failure was never determined, but it was thought to have also occur in the cooking of the data. Therefore since it did occur in the data reconstruction this was considered to cancel the inefficiency of the simulation.

The “time-based” failure was due to a random bug in the processing of the TDC element information of ST (STN0) and the ADC element information of ST (STN1) raw data banks. The bug miscalculated the tracks sector exiting the ST even as the hit element of the ST matched that to the track in the DC. If the track failed due to this error, it usually passed “time-based” on the second or third pass of the “time-based” tracking if another particle passed “time-based” during the initial pass. The probability that a track failed initial “time-based” tracking was $\approx .23\%$. The probability that this failed event would pass “time-based” tracking after another pass was $\approx 99.78\%$. The average inefficiency for three charged track events for data was 0.0125%

4.4.2 SIMULATING THE LEPTON TRIGGER

During the collection process, for an event to be written by the DAQ it must have passed at least one of the trigger “bits” defined in Sec. 3.1. As discussed in Sec. 3.1.1, the process of lepton triggering required a coincidence between the EC and the CC subsystems. This coincidence was established by using the voltage sum of the CC for a sector and the voltage sum of the EC for the same sector and comparing each sum to a preset threshold described in Table 10. However when GSIM simulates tracks through the CC and EC, it does not account for the minimum voltage threshold that was required for data collection, moreover the simulation of the trigger must match the trigger efficiency discussed in Sec. 4.10.

Simulation of the CC and EC trigger “bit 6”, Sec. 3.1.1, was performed by writing an algorithm that attempted to mimic the method in which triggered data was recorded. To accomplish this a modified function, written by Simeon McAleer from FSU, was written into the simulation reconstruction algorithm. The routine returned the sector and a boolean of 0 or 1 (pass or fail), that simulated the trigger based on the following criteria;

1. The sector with the highest EC summed energy over threshold.
2. The sector with the highest EC Inner Layer summed energy over threshold.
3. The sector with the highest CC summed energy over threshold.
4. All three above conditions must be in same sector.

Thresholds as described in Table 10 are 80 mV, 60 mV and 20 mV for EC *inner*, EC *total* and CC respectively. The CC trigger threshold was applied to groups of eight CC PMTs, called “sim bits”. The “sim bits” were staggered by four PMTs so that each PMT goes into two “sim bits”, after which all “sim bits” were “OR”’d together. If any “sim bit” calculated as above threshold, that specific sector was then compared to the remaining sectors to establish the condition listed in 3.

The EC *inner* and EC *total* trigger thresholds were applied to all EC strips in a sector. This was done by summing over the energy for every strip in every orientation of the EC per sector. If the energy summation for the EC *inner* was above threshold, that specific sector was then compared to the remaining sectors to establish the condition listed in 2. If the energy summation for the EC *total* was above threshold, that specific sector was then compared to the remaining sectors to establish the condition of the sector with the highest EC summed energy over threshold.

Validity of Trigger Simulation

The actual triggered data could have been triggered by the following sceneries;

1. e^- CC and EC hit above preset thresholds,
2. e^+ CC and EC hit above preset thresholds,
3. e^- CC hit above preset thresholds and e^+ EC hit above preset thresholds in the same sector,
4. e^- EC hit above preset thresholds and e^+ CC hit above preset thresholds in the same sector.

The lepton trigger “bit 6” was 100% efficient (see Sec. 4.10) when the data was cut using all the conditions listed above (1, 2, 3, 4) using an “OR” flag. This means that a $\gamma p \rightarrow pe^+e^-$ event must satisfy at least one of the listed conditions. The reduction in events when at least one of the conditions was satisfied was 69.91%. Prior to simulating the trigger, cutting the MC with the listed conditions reduced the event yield by 81.91%. Simulating the trigger and cutting on the MC events with the listed conditions reduced that event yield to 69.48%.

This indicates that the trigger simulation is properly mimicking the trigger configuration used when data is collected.

4.5 PLUTO++ EVENT GENERATOR

Pluto [44] is a Monte-Carlo event generator designed for the study of hadronic interactions and heavy ion reactions in HADES, FAIR and upcoming PANDA collaborations. The versatility of Pluto enables its use as an event generator for photoproduction in CLAS. For hadronic interactions, Pluto can generate interactions from pion production threshold to intermediate energies of a few GeV per nucleon. The entire software package is based on ROOT and uses ROOT's embedded C++ interpreter to control the generation of events. Programming event reaction can be set up with a few lines of ROOT macro code without detailed knowledge of programming. Some features in Pluto are, but not limited to;

- Ability to generate events in phase space.
- Ability to generate events with a continuous bremsstrahlung photon beam.
- Ability to generate events weighted by a user defined t -slope.
- Ability to generate events weighted by a user defined cross-section.
 - Total cross section can be inputted via functional form or histogram.
 - Differential cross sections can be inputted via functional forms or histograms for specific beam energies up to 110 histograms relating to intervals of beam energy.
- Ability to generate events that decay via already established physics parameters, i.e. transition form factors.
- Ability to generate events that decay via modified established physics parameters.
- Ability to generate events with multiple production channels, weighted by user inputted cross-section probability.
- Ability to generate events with multiple decay channels, weighted by user inputted branching ratio.
- Ability to perform vertex smearing.
- Ability to create virtual detectors.

For the analysis presented in this work, Pluto was used in conjunction with known differential cross sections to verify simulation momentum smearing and tagger resolution, Sec. 4.9. Pluto was also utilized as a phase space generator in this analysis, to perform a “tune” on the kinematic fitter, Sec. 4.6, to calculate the acceptance corrections Sec. 5.2, and to calculate the normalization Sec. 4.13.

4.6 KINEMATIC FITTING

When CLAS records a triggered event, there is always an error associated with the measurement of the vector $\vec{\eta}$ in the form of,

$$\vec{\eta} = \vec{y} + \vec{\epsilon}, \quad (96)$$

where \vec{y} are the actual values that would have been measured by CLAS in the absence of measurement errors $\vec{\epsilon}$. To improve the precision of the measurement on $\vec{\eta}$, kinematic fitting is used to impose kinematic constraints by using the method of Lagrange multipliers to perform a least-squares fit of a hypothesis. The hypothesis is dictated by physics constraints, e.g. conservation of 4-momenta. Depending on the physics of interest, the kinematic fitter is able to solve for constraint fits listed in Table 19. In Table 19, the “Topology” column lists the physics of interest with the constraint particle in parenthesis while the “Extra Constraint” column lists a secondary inputted constraint used in the fitting process. The

TABLE 19. Examples of constraint fits

Type of Fit	Topology	Extra Constraint
4-C	$\gamma p \rightarrow p\pi^+\pi^-$	-
1-C	$\gamma p \rightarrow pe^+e^-(\gamma)$	-
2-C	$\gamma p \rightarrow pe^+e^-(\gamma)$	$e^+e^-(\gamma) \rightarrow \pi^0$
2-C	$\gamma p \rightarrow K^+\Sigma^{*0} \rightarrow K^+\Lambda(\pi^0) \rightarrow K^+p\pi^-(\pi^0)$	$p\pi^- \rightarrow \Lambda$

method of kinematic fitting is described in great detail in [45]. The kinematic fitter used in *g12* analyses has been written by Dustin Keller [45].

Confidence Levels and Pull Distributions

Using the kinematic fitter to select events requires the determination of a “quality of fit” for a given physics hypothesis. The “quality of fit” is the minimization quantity interpreted

from the χ^2 distribution of $(q - d)$ degrees of freedom, where q is the number of measurements and d is the number of unknown parameters. The systematic measure of probability that a χ^2 of the ideal theoretical distribution is greater than or equal to the χ^2 value found from the fit for a full distribution of events is defined as a “confidence level” and expressed as

$$P(\chi^2) = \int_{\chi^2}^{\infty} f(x, n) dx \quad (97)$$

where the function $f(x, n)$ is the χ^2 probability density function for n degrees of freedom. “Confidence levels” range from 0 to 1 when the fit hypothesis is satisfied, correspondingly the “confidence level” is small for events that are poorly described by the fit hypothesis. The method of checking the quality of the covariance matrix and ensuring the kinematic fit is working properly was done by examining the “pull” distributions for quantities of a “test fit”, see Sec. 4.6. The pull distribution is defined as the difference between the measured and the final parameters obtained by the kinematic fit and normalized by the quadratic error difference [45]. Defining $\vec{\eta}_i$ and $\vec{\eta}_f$ as the initial and final vector values of the measured quantities and $\sigma_{\vec{\eta}_i}$ and $\sigma_{\vec{\eta}_f}$ as the errors of vectors $\vec{\eta}_i$ and $\vec{\eta}_f$, the pull distribution is defined as,

$$\vec{z} = \frac{\vec{\eta}_i - \vec{\eta}_f}{\sqrt{\sigma_{\vec{\eta}_i}^2 - \sigma_{\vec{\eta}_f}^2}}. \quad (98)$$

If the covariance matrix errors are correctly estimated, the pulls will be normally distributed with zero mean and have a unit standard deviation.

Tuning

In order for the kinematic fitter to perform a χ^2 minimization properly, it has to be provided with an initial covariance matrix that contains the correlations between the kinematic variables of each track as determined during the reconstruction of the track. The covariance matrix recorded by CLAS is inadequate to use in the kinematic fitter because the covariance matrix does not incorporate multiple scattering errors, “energy loss” or the error approximation is misrepresented by a systematic. To correct for this, the elements of the covariance matrix are scaled appropriately by the kinematic fitter routine by means of what is called “tuning”. The process of “tuning” determines the nature of the misrepresented errors as a function of a measured variable by studying the shift from the zero mean at different ranges of dependent variables. To perform a “tune”, a test channel must be chosen in which the event selection must be background free. The multiple scattering option used in this

analysis was set to false, therefore an algorithm which attempts to incorporate multiple scattering is not utilized. Instead a directory of parameterization files are called for the scaling of individual particle covariance matrix elements, such as p , π^+ , π^- , e^+ and e^- . This was done because the multiple scattering algorithm did not perform well for events involving electrons and positrons.

For this analysis, the channels

$$\gamma p \rightarrow \pi^+ \pi^- (p) \quad (99)$$

$$\gamma p \rightarrow p \pi^- (\pi^+) \quad (100)$$

$$\gamma p \rightarrow \pi^+ p (\pi^-) \quad (101)$$

$$\gamma p \rightarrow p \omega / \rho \rightarrow p e^+ e^- \quad (102)$$

were chosen as the “tune” channels because these channels incorporate the physics and background of the analysis performed. The reactions 99, 100, 101 were “tunes” done individually for the proton, π^+ and π^- respectively, while 102 “tuned” the electrons and positrons together because of the limit in statistics needed to tune each lepton individually. Once the “tuning” for 99, 100, 101 was complete, the “tune” was verified by checking the pull distributions and confidence level for the topology,

$$\gamma p \rightarrow p \pi^+ \pi^- . \quad (103)$$

Figures 64 and 65 illustrate the quality of the “tuned” covariance matrix for $g12$ data and $g12$ simulation of electrons and positrons from “tune” 102 and Fig. 66 illustrates the “confidence levels” for $g12$ data and simulation of electrons and positrons from “tune” 102. Figures 67 and 68 illustrate the quality of the “tuned” covariance matrix for $g12$ data and $g12$ simulation of π^+ and π^- from “tune” 103 and Fig. 69 illustrates the “confidence levels” for $g12$ data and simulation of π^+ and π^- from “tune” 103. The variables p used in Figs. 64, 65, 67 and 68 represent the lab frame momentum. The λ variable is the angle between the track and the (x_{track}, y_{track}) plane. The ϕ variable is the angle in the sector’s (x_{track}, y_{track}) plane relative to the x_{track} -axis, or between the track and the beam line [45].

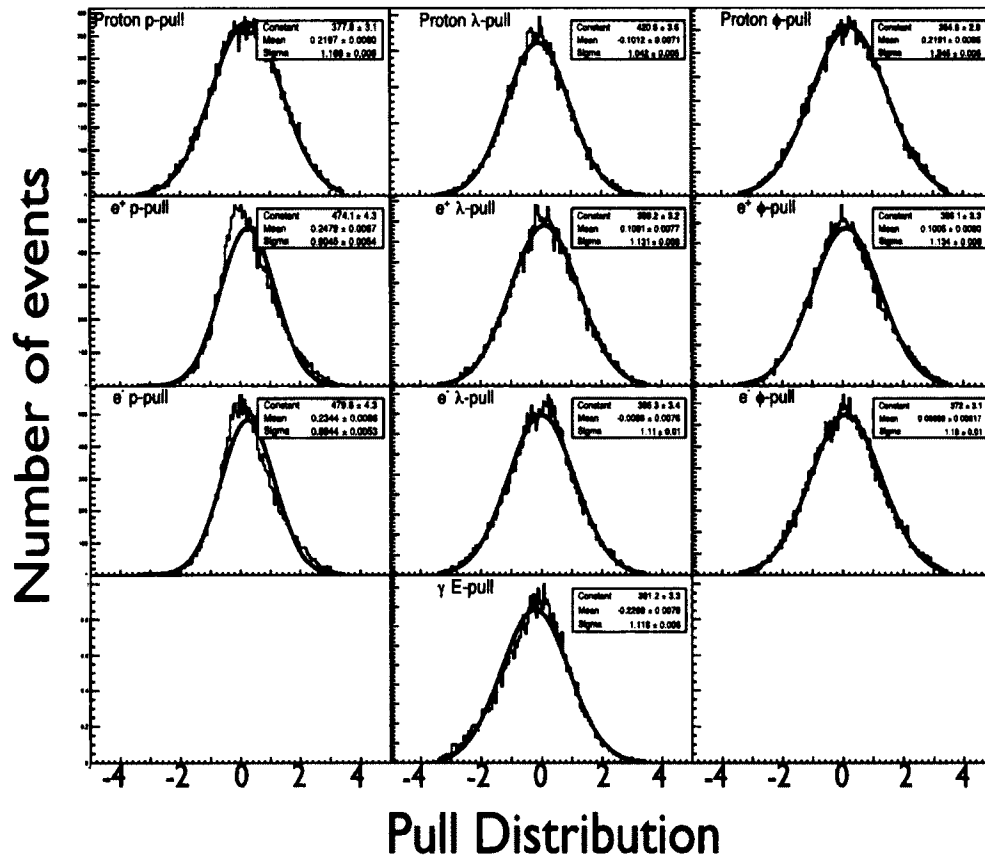


FIG. 64. Number of events vs. Pull distribution for the (4-C) kinematic fit for $\gamma p \rightarrow pe^+e^-$ for $g12$ data with a 1% Confidence Level cut applied, and a Gaussian fit to each.

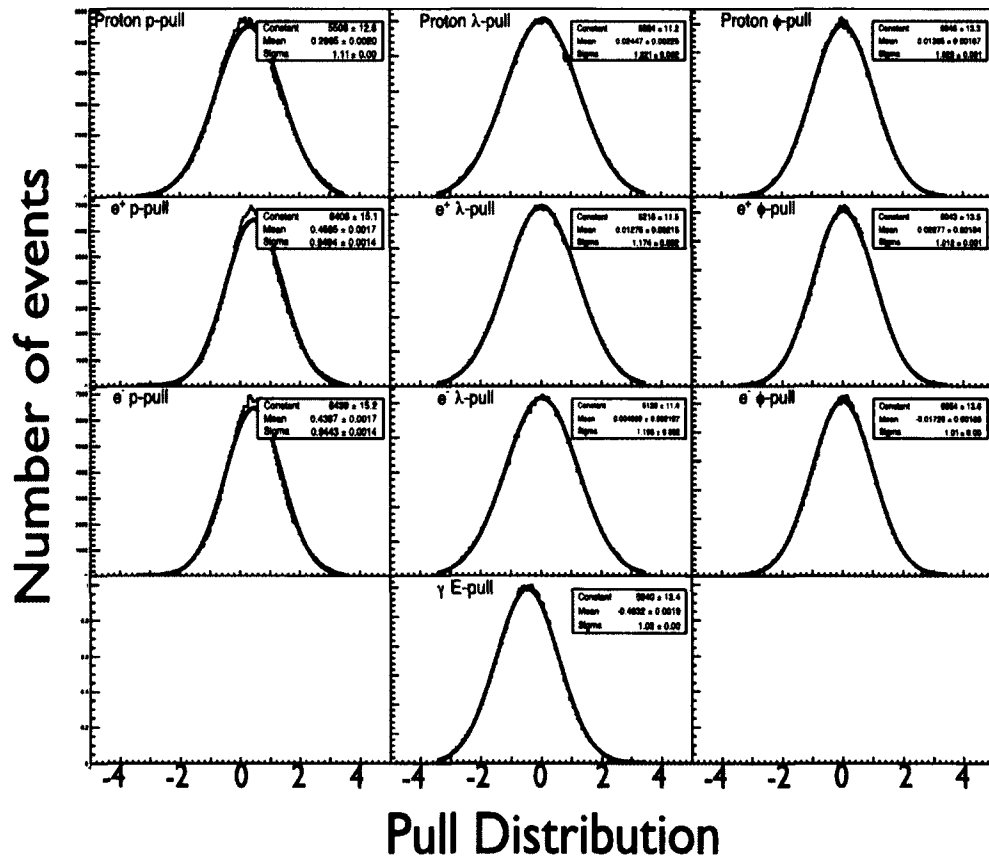


FIG. 65. Number of events vs. Pull distribution for the (4-C) kinematic fit for $\gamma p \rightarrow pe^+e^-$ for $g12$ simulation with a 1% Confidence Level cut applied, and a Gaussian fit to each.

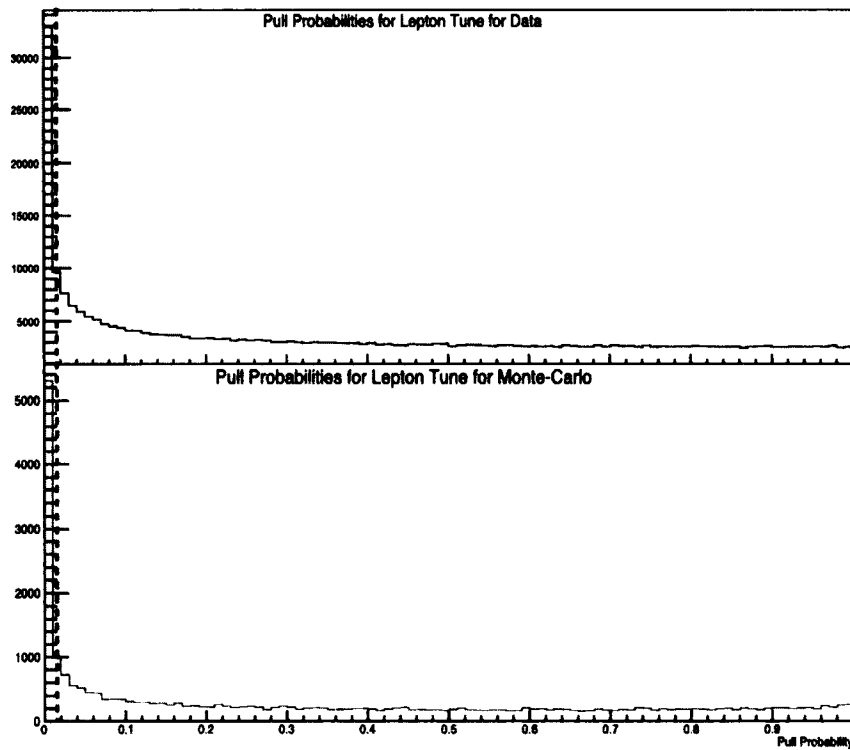


FIG. 66. Number of events vs. Confidence Level for $g12$ (top) data and $g12$ simulation (bottom) for a (4-C) fit using $\gamma p \rightarrow pe^+e^-$. The black dashed line indicates the cut taken, events with probability $<1\%$ are rejected.

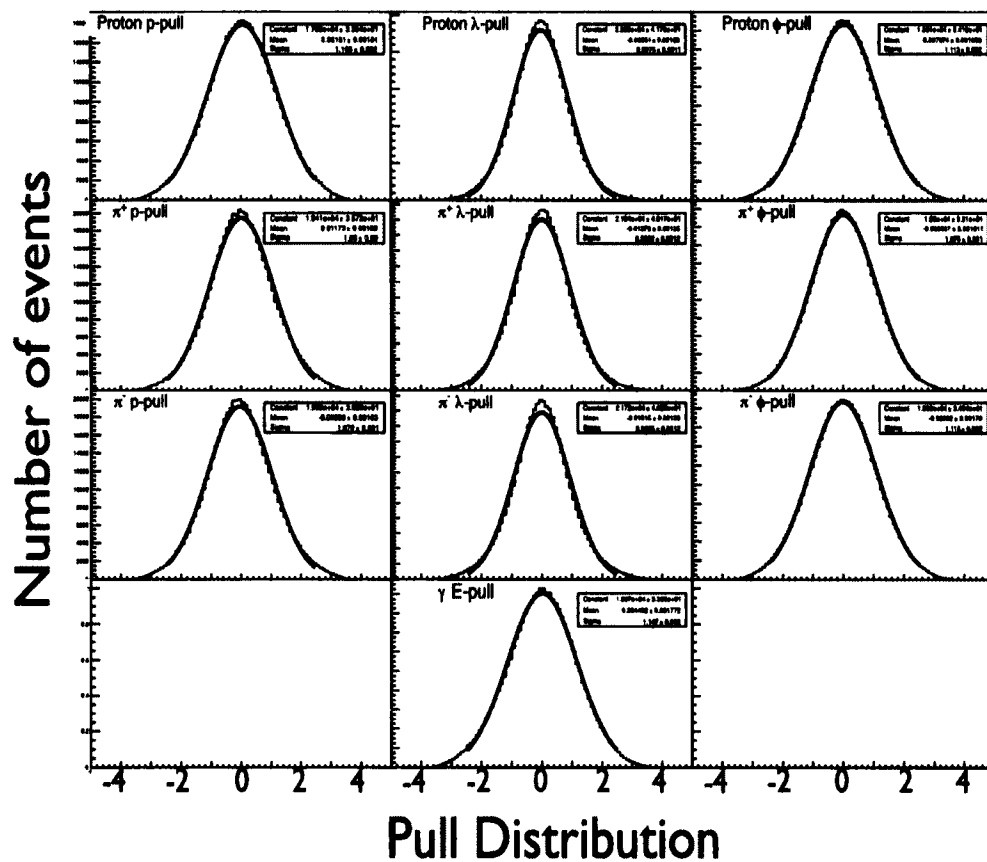


FIG. 67. Number of events vs. Pull distribution for the (4-C) kinematic fit for $\gamma p \rightarrow p\pi^+\pi^-$ for $g12$ data with a 1% Confidence Level cut applied, and a Gaussian fit to each.

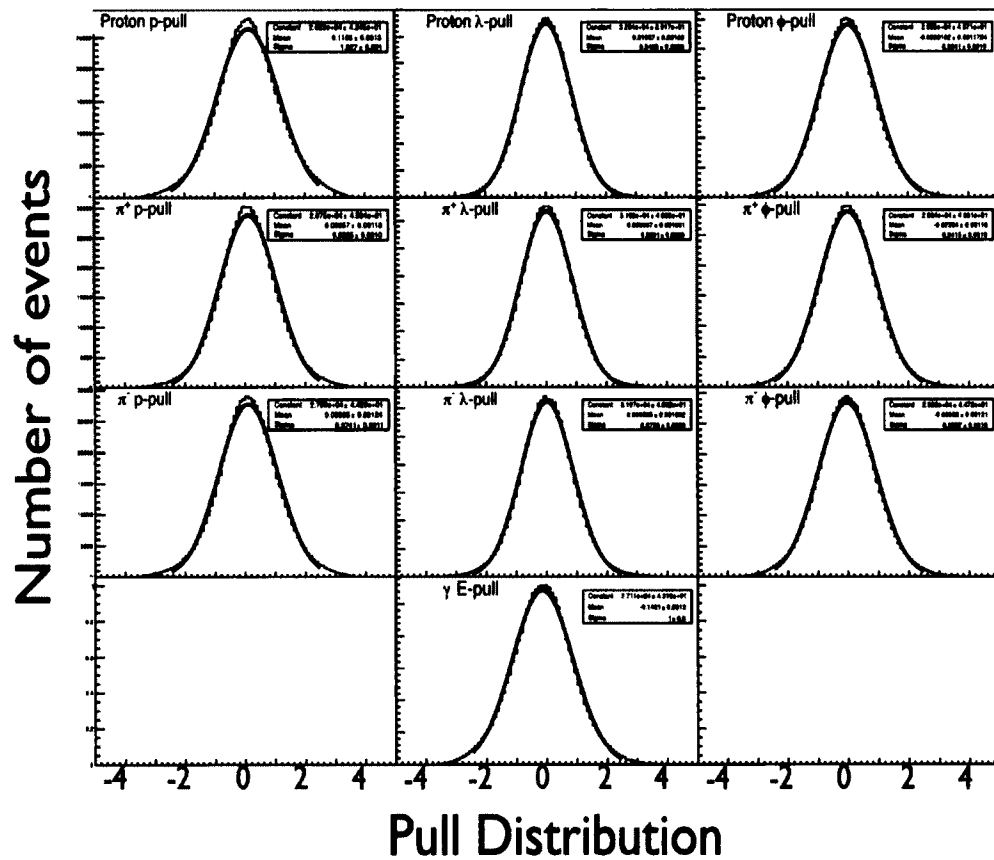


FIG. 68. Number of events vs. Pull distribution for the (4-C) kinematic fit for $\gamma p \rightarrow p\pi^+\pi^-$ for $g12$ simulation with a 1% Confidence Level cut applied, and a Gaussian fit to each.

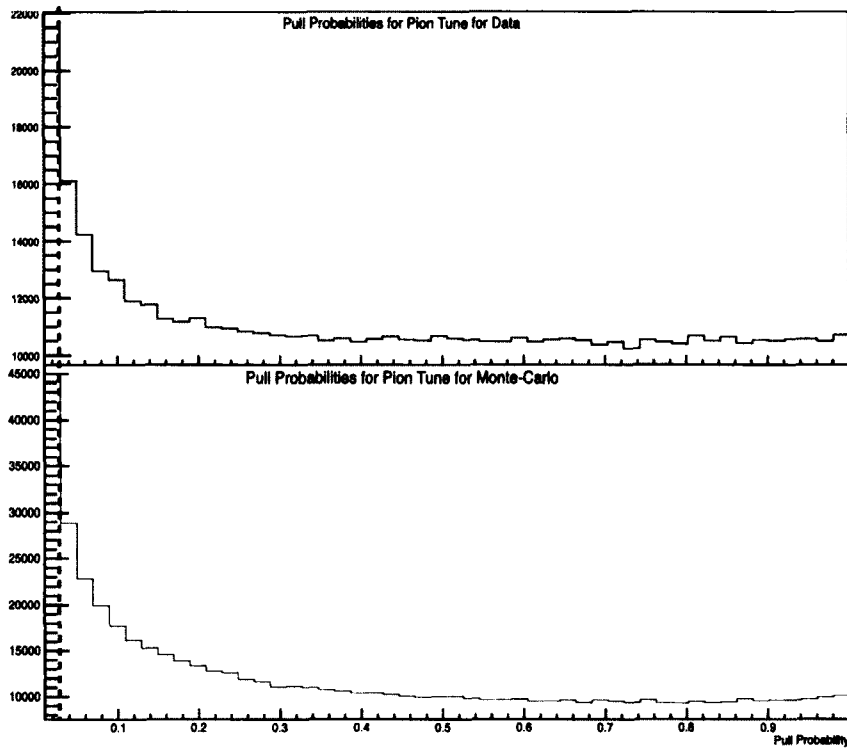


FIG. 69. Number of events vs. Confidence Level for $g12$ (top) data and $g12$ simulation (bottom) for a (4-C) fit using $\gamma p \rightarrow p\pi^+\pi^-$. The black dashed line indicates the cut taken, events with probability $<1\%$ are rejected.

4.6.1 ANALYSIS FITTING

This analysis performed three separate kinematic fitting hypotheses, 4-C, 1-C and 2-C. The 4-C fit used the $\gamma p \rightarrow p\pi^+\pi^-$ channel to filter background from double charged pion production from single π^0 production. The 1-C fit was used to the topology of $\gamma p \rightarrow pe^+e^-(\gamma)$ to fit to a missing final state photon. The constraint equation for this 1-C fit is given in Eq. 104.

$$\mathcal{F} = \begin{bmatrix} E_{beam} + M_p - (E_p + E_{e^+} + E_{e^-} + E_x) \\ \vec{p}_{beam} - (\vec{p}_p + \vec{p}_{e^+} + \vec{p}_{e^-} + \vec{p}_x) \end{bmatrix} = \vec{0} \quad (104)$$

The constraint equation for this 4-C fit is given in Eq. 105.

$$\mathcal{F} = \begin{bmatrix} E_{beam} + M_p - (E_p + E_{\pi^+} + E_{\pi^-}) \\ \vec{p}_{beam} - (\vec{p}_p + \vec{p}_{\pi^+} + \vec{p}_{\pi^-}) \end{bmatrix} = \vec{0} \quad (105)$$

The 2-C fit was used to the topology of $\gamma p \rightarrow pe^+e^-(\gamma)$ to fit to a missing final state photon but also to constrain the invariant mass of $e^+e^-(\gamma) = m_{\pi^0}^2$. The constraint equation for this 2-C fit is given in Eq. 106.

$$\mathcal{F} = \begin{bmatrix} (E_{e^+} + E_{e^-} + E_x)^2 - (\vec{p}_{e^+} + \vec{p}_{e^-} + \vec{p}_x)^2 - M_{\pi^0}^2 \\ E_{beam} + M_p - (E_p + E_{e^+} + E_{e^-} + E_x) \\ \vec{p}_{beam} - (\vec{p}_p + \vec{p}_{e^+} + \vec{p}_{e^-} + \vec{p}_x) \end{bmatrix} = \vec{0} \quad (106)$$

The ‘‘confidence levels’’ for each constraint Eq. 104, 105, 106 are shown in Fig. 70 and Fig. 71 for $g12$ data and simulation respectively. These quantities ensure proper mass and energy constraints for this analysis. Cuts on these quantities are discussed in Sec. 4.6.2. The sparseness of the 4-C fit for simulation is due because background was not simulated for the analysis for reasons discussed in Sec. 4.3.

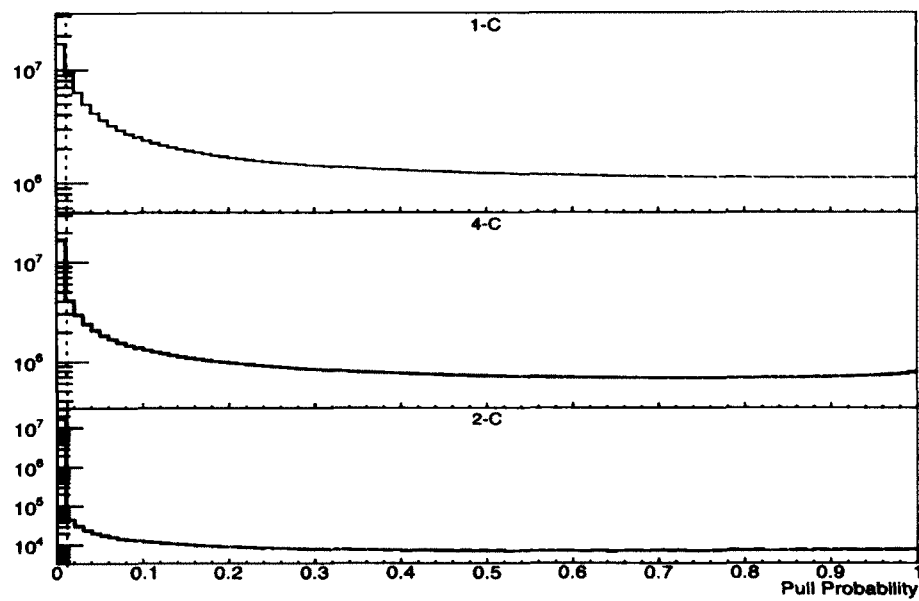


FIG. 70. Number of data events plotted vs. Pull distribution for the 1-C(red,Eq. 104), 4-C(black,Eq. 105), 2-C(blue,Eq. 106) for $g12$ data. The orange dashed line illustrates the 1% cut for all pull distributions.

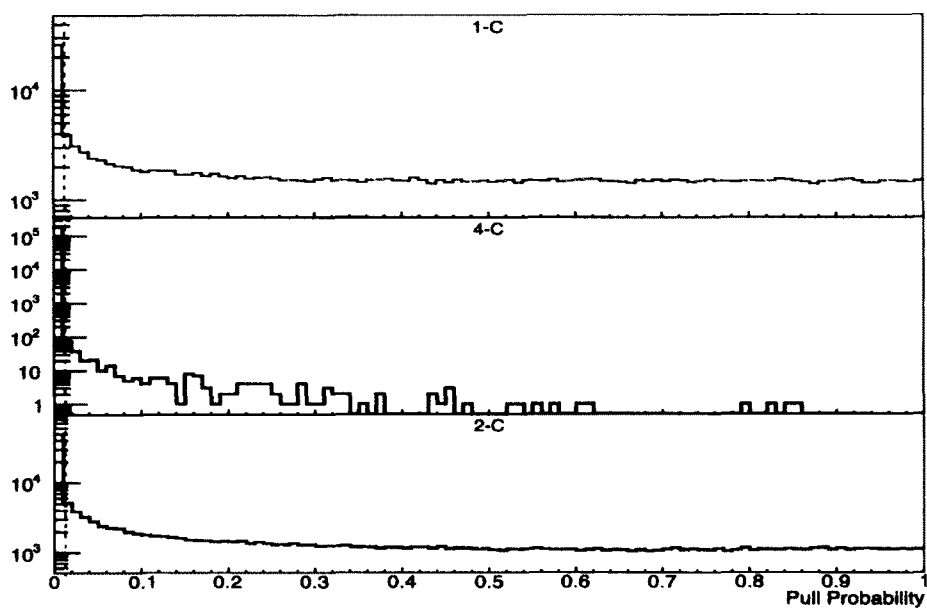


FIG. 71. Number of data events plotted vs. Pull distribution for the 1-C(red,Eq. 104), 4-C(black,Eq. 105), 2-C(blue,Eq. 106) for $g12$ simulation. The orange dashed line illustrates the 1% cut for all pull distributions.

4.6.2 KINEMATIC FITTING ANALYSIS AND CUTS

The base hypothesis of all corrections performed to the data by the kinematic fitter was the 1-C constraint equation found in Eq. 104. This means that all fitted data will be presented in quantities based upon the hypothesis of a missing photon. The effect of 1-C kinematic fitting for events, prior to any topological cuts, with beam energies less than 3.6 GeV can be seen in Fig. 72, while for beam energies greater than 3.6 GeV can be seen in Fig. 73. The top panel depicts the unfitted data and the bottom panel depicts the data output from the kinematic fitter. The red data line represents all data while the blue line depicts the data where cuts were placed on CC and EC hits in order to satisfy the trigger as discussed in Sec 3.1.1. The red, vertical dashed-dotted line illustrates the production point for two charged pion production. The MC counterpart plots of Figs. 72, 73 can be seen in Figs. 74, 75, where only the π^0 signal was simulated.

It can be seen that the effects of the 1-C fit, prior to topological cuts, narrows the π^0 signal for events with beam energies less than 3.6 GeV, while for energies greater than 3.6 GeV, the 1-C fit reveals a signal that appears hidden without further cuts for the data.

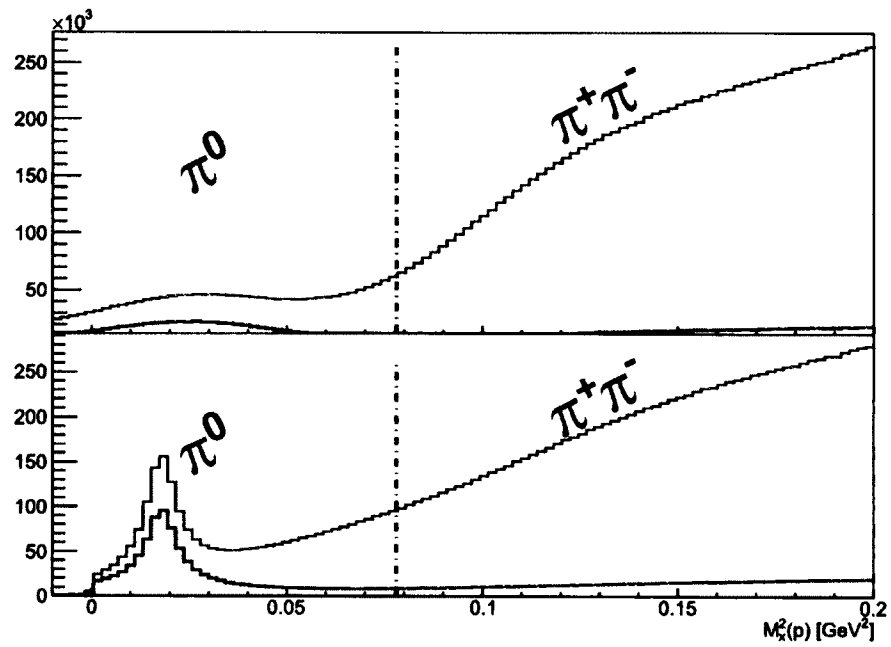


FIG. 72. Number of data events plotted vs. missing mass $M_x(\gamma p \rightarrow pX)$ for uncut data and $E_\gamma < 3.6$ GeV. The top panel depicts the unfitted data, where the red data line represents all data while the blue line depicts all data with cuts placed on CC and EC. The bottom panel depicts the data output from the kinematic fitter 1-C fit, where the red data line represents all data while the blue line depicts all data with cuts placed on CC and EC.

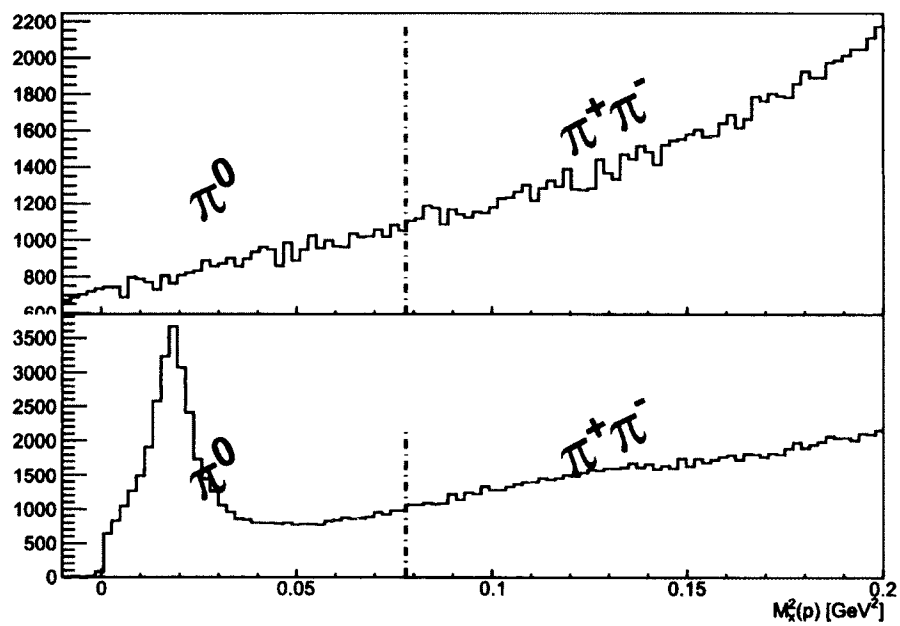


FIG. 73. Number of data events plotted vs. missing mass $M_x(\gamma p \rightarrow pX)$ for uncut data and $E_\gamma > 3.6$ GeV. The top panel depicts the unfitted data. The bottom panel depicts the data output from the kinematic fitter 1-C fit.

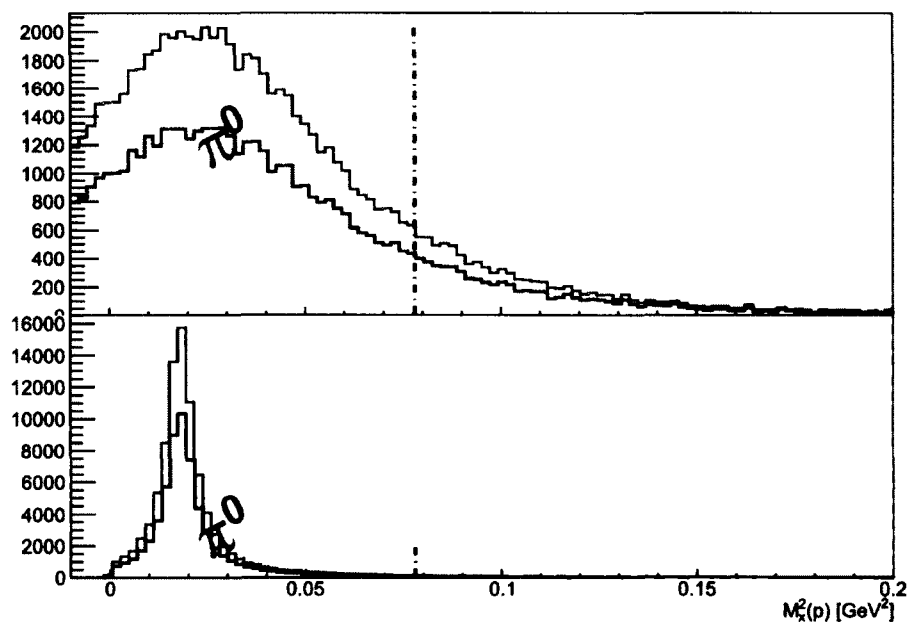


FIG. 74. Number of MC events plotted vs. missing mass $M_x(\gamma p \rightarrow pX)$ for uncut data and $E_\gamma < 3.6 \text{ GeV}$. The top panel depicts the unfitted data, where the red data line represents all data while the blue line depicts all data with cuts placed on CC and EC hits to be present. The bottom panel depicts the data output from the kinematic fitter 1-C fit, where the red data line represents all data while the blue line depicts all data with cuts placed on CC and EC hits to be present.

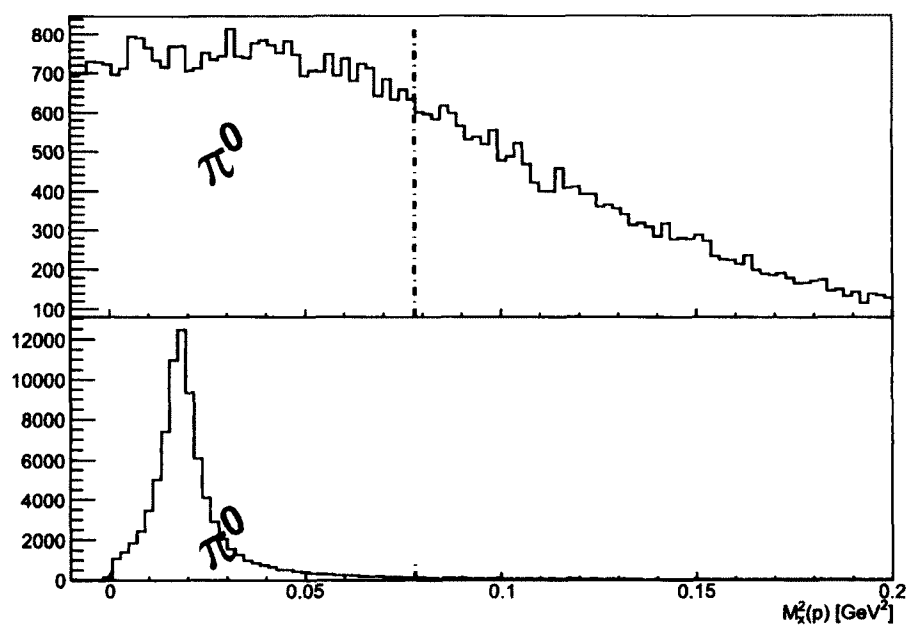
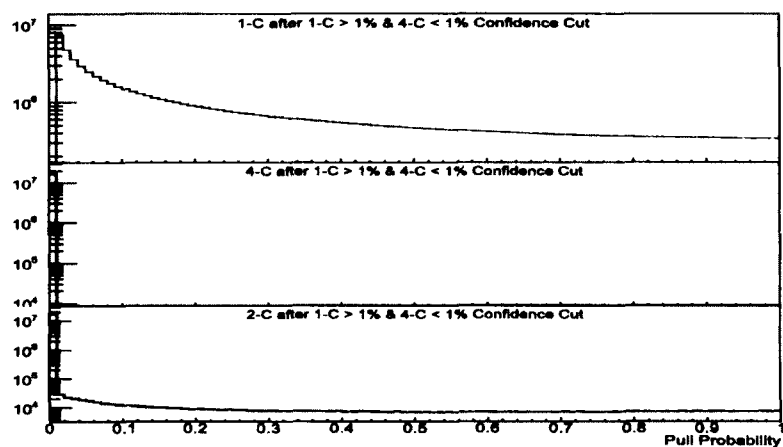


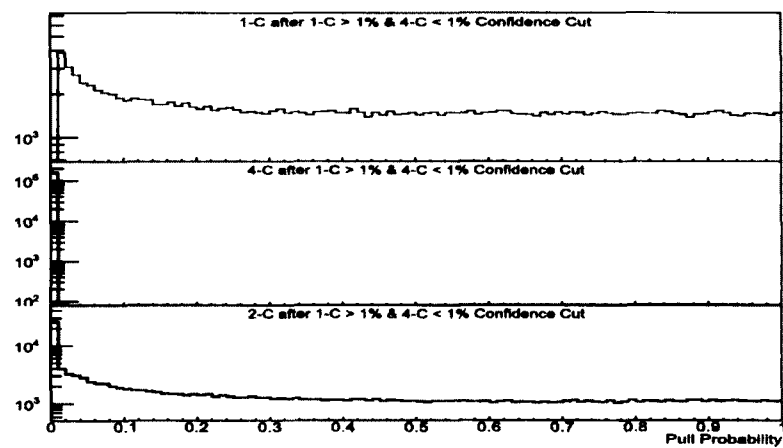
FIG. 75. Number of MC events plotted vs. missing mass $M_x(\gamma p \rightarrow pX)$ for uncut data and $E_\gamma > 3.6$ GeV. The top panel depicts the unfitted data. The bottom panel depicts the data output from the kinematic fitter 1-C fit.

1-C & 4-C Cuts

As mentioned in Sec 4.6.1, there were 3 constraint equations used in this analysis. The 1-C fit utilizes a constraint equation to a missing photon, while the 4-C fit assumed a $\pi^+\pi^-$ topology instead of the e^+e^- topology. In this analysis a $>1\%$ confidence level cut was placed on the 1-C fit to ensure the missing photon is in the event. However, a $<1\%$ confidence level cut was placed on the 4-C fit to remove the $\pi^+\pi^-$ background. The effect of the pull distributions after placing these cuts can be seen in Fig. 76. The effect of the 1-C and 4-C cut on the data can be seen in Fig. 77, where the blue line depicts the uncut fitted data spectrum, except the trigger cut, the black line depicts after a $>1\%$ cut placed on the 1-C and green line depicts the effect of the $<1\%$ 4-C fit cut. Top panel illustrates the effect of the cuts on recorded data, bottom panel illustrates the effect of the cuts on MC. The top plot of each panel depicts events of beam energies less than 3.6 GeV, while the bottom plot of each panel depicts events of beam energies greater than 3.6 GeV. It is shown in Fig. 77a that each cut depletes the background while maintaining signal.

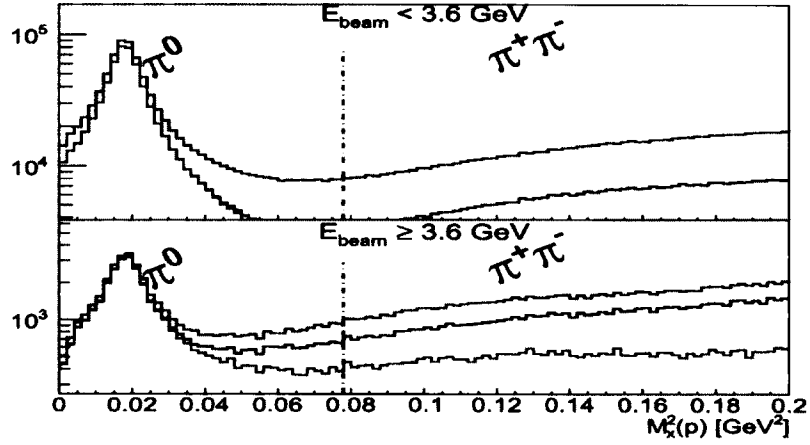


(a)

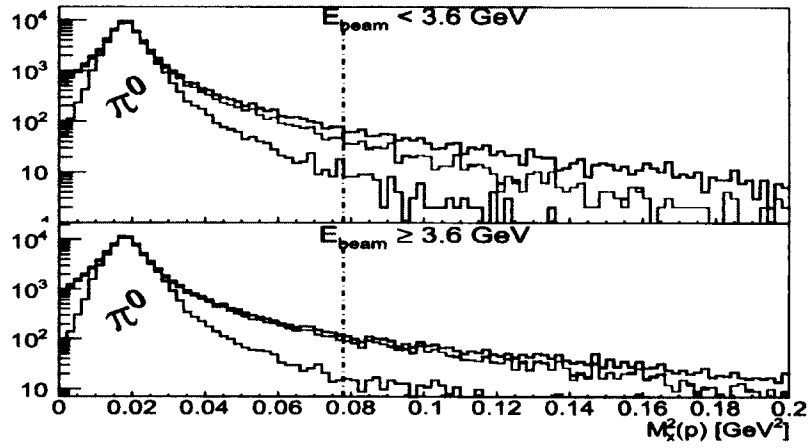


(b)

FIG. 76. Number of events vs. Pull distributions after a 1% cut placed on the 1-C (top plots) and 4-C fit (middle plots) for data (a) and MC (b).



(a)



(b)

FIG. 77. Number of data events plotted vs. missing mass $M_x(\gamma p \rightarrow pX)$. Blue lines depict the fitted data prior to pull distribution cuts, black line depicts after a 1% cut placed on the 1-C and green line depicts the effect of the 1% 4-C fit cut. Top panel (a) depicts data while bottom panel (b) depicts MC.

Missing Energy Cut

The remainder of the background can be attributed to $\pi^+\pi^-$ events. To reduce the background further, a comparison of the missing mass squared off of the proton and the missing energy of the system was performed. This comparison is plotted in Fig. 78, where it can be seen that the majority of $\pi^+\pi^-$ background has missing energy less than 75 MeV. To eliminate this background all events with a missing energy less than 75 MeV were cut out.

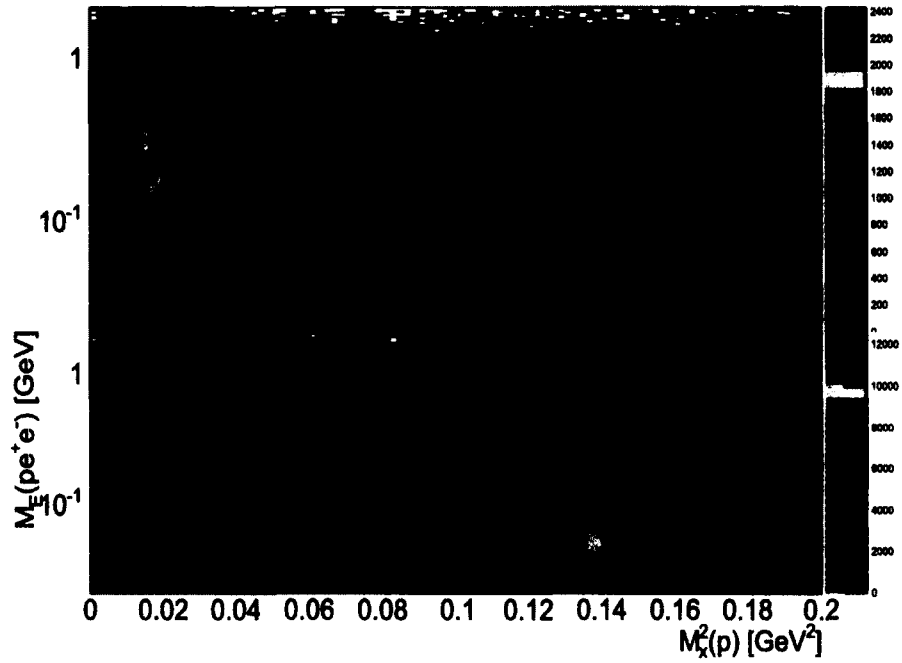
The effect of the 75 MeV missing energy cut on the $M_x^2(p)$ spectrum can be seen in Fig. 79. The signal function (red solid) is the *Crystal Ball Function* [46], [47] and the background (black) a 3rd order polynomial. The contamination of the background under the π^0 signal for data events where the beam energy is less than 3.6 GeV is 1.3 %. The contamination of the background under the π^0 signal for data events where the beam energy is greater than 3.6 GeV is 2.1 %. This background can be reduced more with the 2-C cut. The Crystal Ball function, named after the Crystal Ball Collaboration, is a probability density function commonly used to model various lossy processes in high-energy physics. It consists of a Gaussian core portion and a power-law low-end tail, below a certain threshold. The function itself and its first derivative are both continuous [47].

$$f(x; \alpha, n, \bar{x}, \sigma) = N \cdot \begin{cases} \exp\left(-\frac{(x-\bar{x})^2}{2\sigma^2}\right), & \text{for } \frac{x-\bar{x}}{\sigma} > -\alpha \\ A \cdot \left(B - \frac{x-\bar{x}}{\sigma}\right)^{-n}, & \text{for } \frac{x-\bar{x}}{\sigma} \leq -\alpha \end{cases} \quad (107)$$

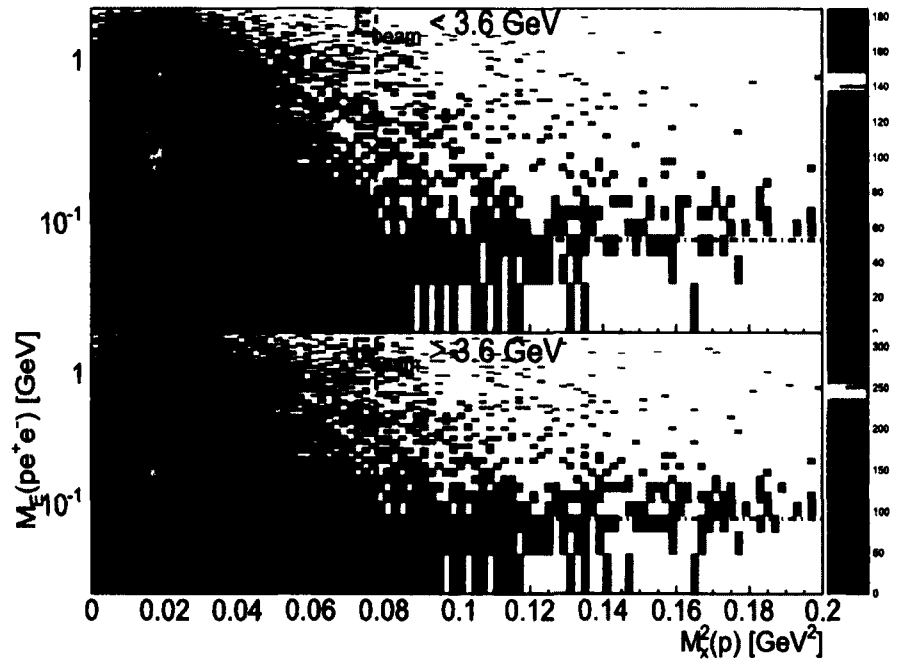
where

$$A = \left(\frac{n}{|\alpha|}\right)^n \cdot \exp\left(-\frac{|\alpha|^2}{2}\right) \\ B = \frac{n}{|\alpha|} - |\alpha| \quad (108)$$

N is a normalization factor and α , n , x and σ are parameters which are fitted with the data.

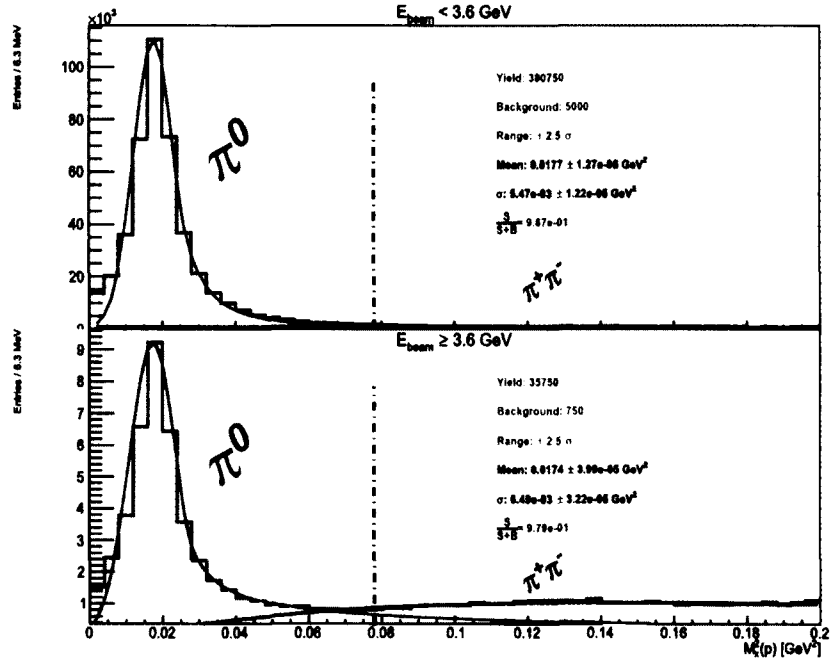


(a)

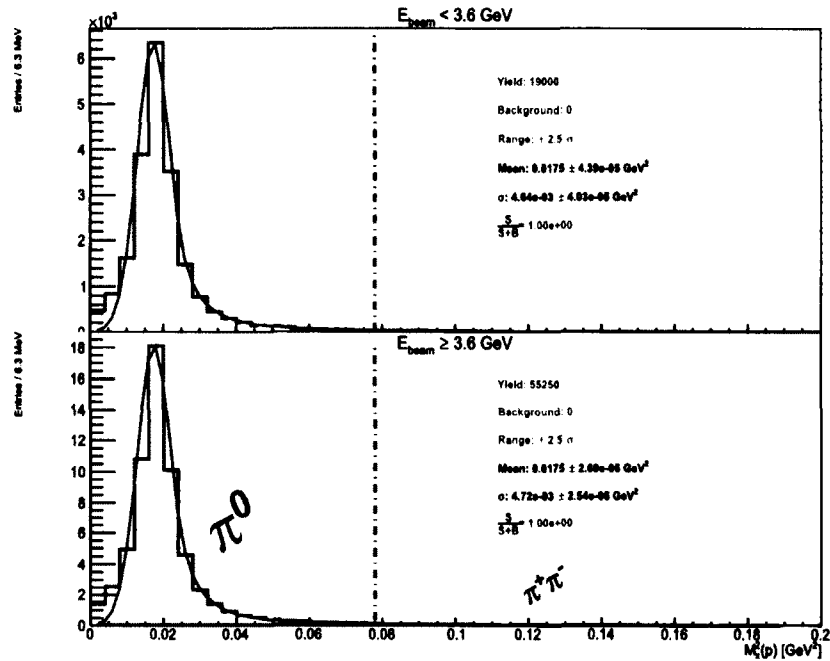


(b)

FIG. 78. $M_x^2(\gamma p \rightarrow pX)$ vs. $M_E(\gamma p \rightarrow pe^+e^-X)$. The horizontal red dashed-dotted line depicts the 75 MeV cut used in this analysis. The vertical red dashed-dotted line depicts boundary of single π^0 to $\pi^+\pi^-$ production. Top panel depicts data, while the bottom panel depicts MC.



(a)

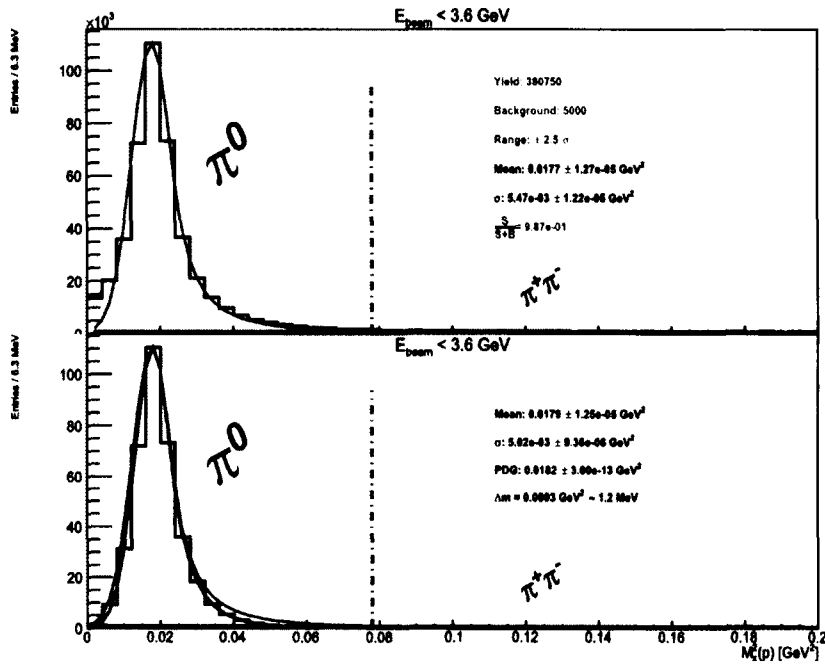


(b)

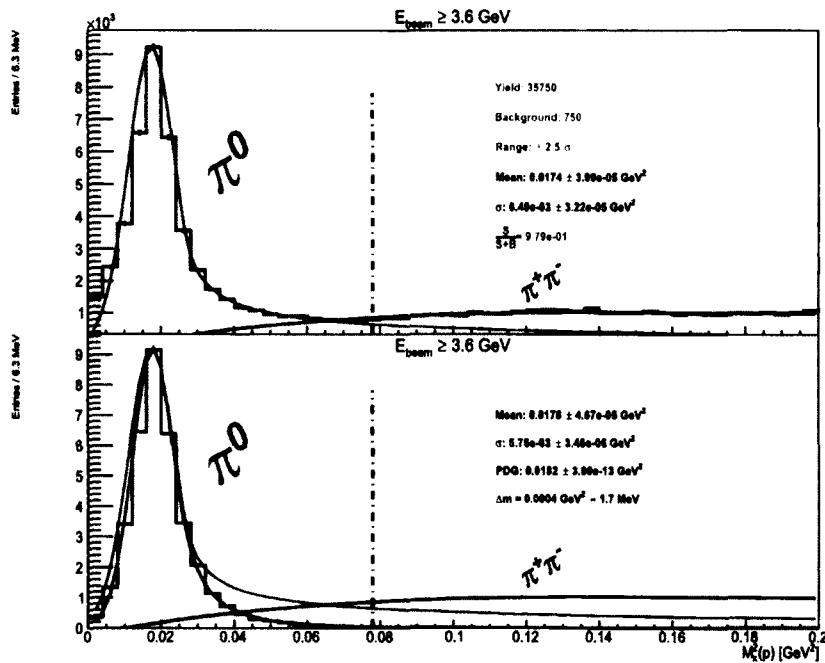
FIG. 79. Number of data events plotted vs. missing mass $M_x(\gamma p \rightarrow pX)$ after the 1-C, 4-C and 75 MeV missing energy cut. Top plots depicts the data. Bottom plot depicts the MC. For both panels, the top plots illustrate events with beam energies less than 3.6 GeV, while the bottom plot illustrates events with beam energies greater than 3.6 GeV. The red solid line are fits using the *Crystal Ball Function*, while the black line illustrates the 3rd order polynomial background function.

2-C Cut

The final cut that was utilized in the analysis was the 2-C constraint. The 2-C constraint fits to a missing final state photon but also constrains the invariant mass of $e^+e^-(\gamma) = m_{\pi^0}^2$. The constraint equation for this 2-C fit is given in Eq. 106. This analysis used a $> 1\%$ confidence level cut on the 2-C fit, this translates to a 2.5σ cut of a Gaussian function if a Gaussian was assumed for the signal instead of the *Crystal Ball Function*. The effect of the 2-C cut after the 1-C, 4-C and missing energy cut on the data can be seen in Fig. 80, where the top plot of each panel illustrates the mass spectrum prior to the $> 1\%$ 2-C cut and the bottom plot of each panel illustrates the mass spectrum after to the $> 1\%$ 2-C cut along with the other cuts. To show the full effect for the 2-C fit, the bottom plot of each panel has the fits of their top plots superimposed. For events under 3.6 GeV in beam energy, the 2-C cut has little effect, which is expected because this spectrum presented itself almost background free due to the CC and EC trigger constraints. For events above 3.6 GeV in beam energy, the 2-C cut has greater effect, which is expected because this spectrum presented itself with an irreducible $\pi^+\pi^-$ background. The effect of the 2-C cut on MC, Fig. 81, is minimal as well due to the π^0 spectrum being the only topology simulated. The blue lines atop of the data spectrum for each plot in which the 2-C cuts was taken, shows the new fit using the *Crystal Ball Function*. The mass differences from the accepted value [4] to the fitted value are 1.2 MeV and 1.7 MeV for the events below 3.6 GeV and above 3.6 GeV respectively.

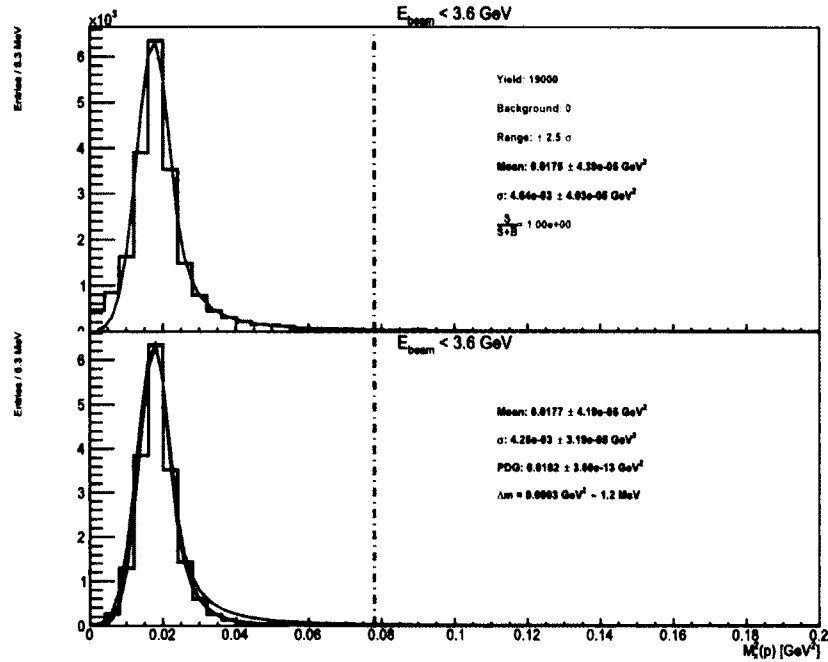


(a)

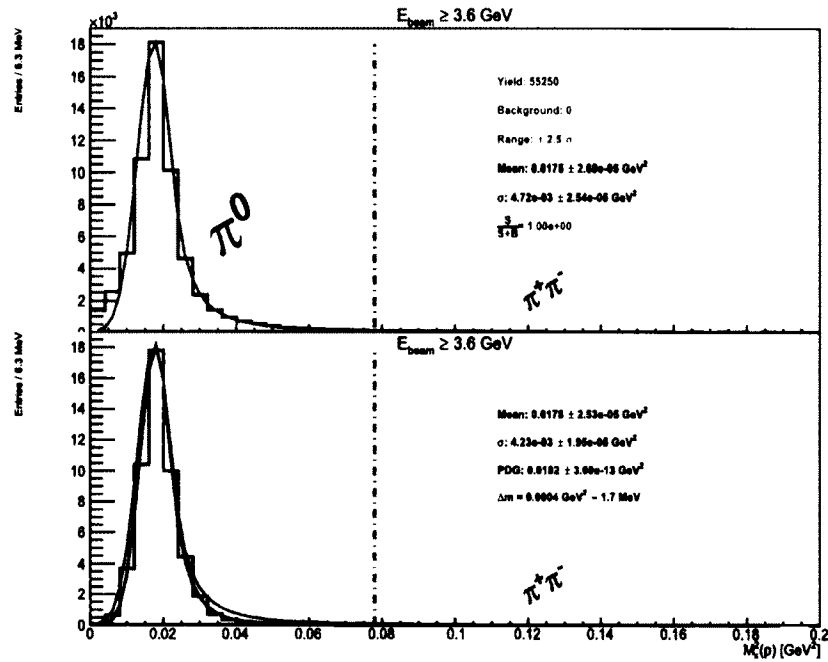


(b)

FIG. 80. Number of data events plotted vs. missing mass $M_x(\gamma p \rightarrow pX)$ after the 1-C, 4-C and 75 MeV missing energy cut. For both panels, the top plots illustrates events with beam energies less than 3.6 GeV, while the bottom plot illustrates events with beam energies greater than 3.6 GeV. The red solid line are fits using the *Crystal Ball Function*, while the black line illustrates the 3rd order polynomial background function. The bottom plot on the bottom panel shows what the background and signal function parameters were without the 2-C cut for comparison.



(a)



(b)

FIG. 81. Number of MC events plotted vs. missing mass $M_x(\gamma p \rightarrow pX)$ after the 1-C, 4-C, 2-C and 75 MeV missing energy cut. For both panels, the top plots illustrates events with beam energies less than 3.6 GeV, while the bottom plot illustrates events with beam energies greater than 3.6 GeV. The red solid line are fits using the *Crystal Ball Function*, while the black line illustrates the 3rd order polynomial background function. The bottom plot on the bottom panel shows what the background and signal function parameters were without the 2-C cut for comparison.

4.7 PARTICLE VERTEX TIMING CUTS

Another quantity that is used for PID and data cleanliness is the vertex timing t_{vert} , which is the time the particle left the target. It can be calculated as;

$$t_{vert} = t_{TOF} - l_{TOF}/(c\beta) \quad (109)$$

where t_{TOF} and l_{TOF} are the time and length measurement, respectively, recorded at the TOF subsystem, and c is the speed of light. The value of β is calculated using the particles mass, m , and momentum, p , as measured from the DC. Therefore $\beta = \frac{p}{E} = \frac{p}{\sqrt{p^2+m^2}}$. Another means of calculating t_{vert} is to use the timing of the tagger hit using the RF-corrected tagger time, see tagger calibration in [41]. In this method t_{vert} is calculated as;

$$t_{vert} = t_{pho} + t_{prop} \quad (110)$$

where t_{pho} is the RF-corrected time that the photon crossed the center of the target and t_{prop} is the propagation time from the center of the target to the track's vertex. Comparing the two quantities of t_{vert} from Eq. 109 and Eq. 110 gives information of proper particle timing as well as the PID. In Fig. 82, the comparison of the difference $t_{(vert, tagger)} - t_{(vert, TOF)}$ is shown for the detected proton, e^- , and e^+ for data and MC after all geometric, TOF, EC fiducial cuts as well as all analysis cuts mentioned previously. A cut of ± 1.2 ns was placed on all particles, the effect is minimal.

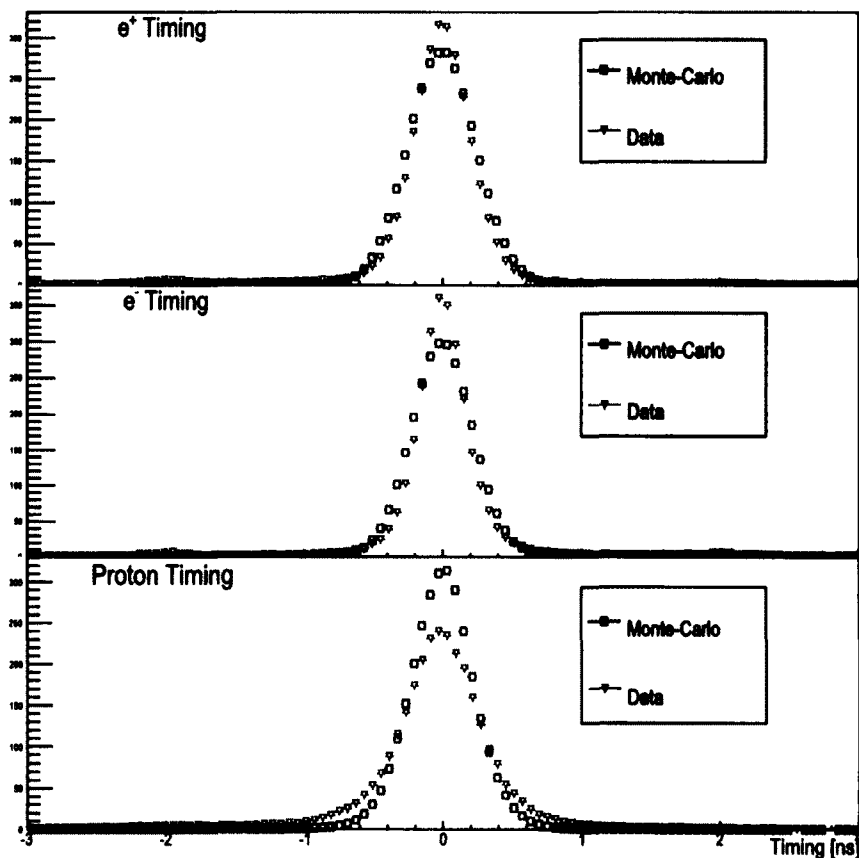


FIG. 82. Number of events vs. $t_{pho} + t_{prop} - (t_{TOF} - l_{TOF}/(c\beta))$ for MC and data for proton, e^- , and e^+ .

4.8 Z VERTEX CUTS

To ensure that π^0 production occurred on the ℓH_2 target, a cut was placed on the z -vertex position to be $-110 \leq z \leq -70$ (see Fig.). Since the vertex resolution of CLAS is 1 cm, there is a probability of π^0 production on the Kapton endcaps of the target. This effect was studied as a systematic uncertainty (see Sec 5.4). The z -vertex is not flat because of acceptance. At large angles(backward) the acceptance in $g12$ was reduced to ≈ 100 degrees for single particle detection. For multi-particle detection, the acceptance, at large angles, was reduced to ≈ 70 degrees (see Fig. 84). For particles that originated from the start of the target, this acceptance effect was prominent. For π^0 production in $g12$, in which the decay of π^0 was identified with e^+e^- (γ) events, the acceptance was largest when production occurred near the center of the target. When production happened in

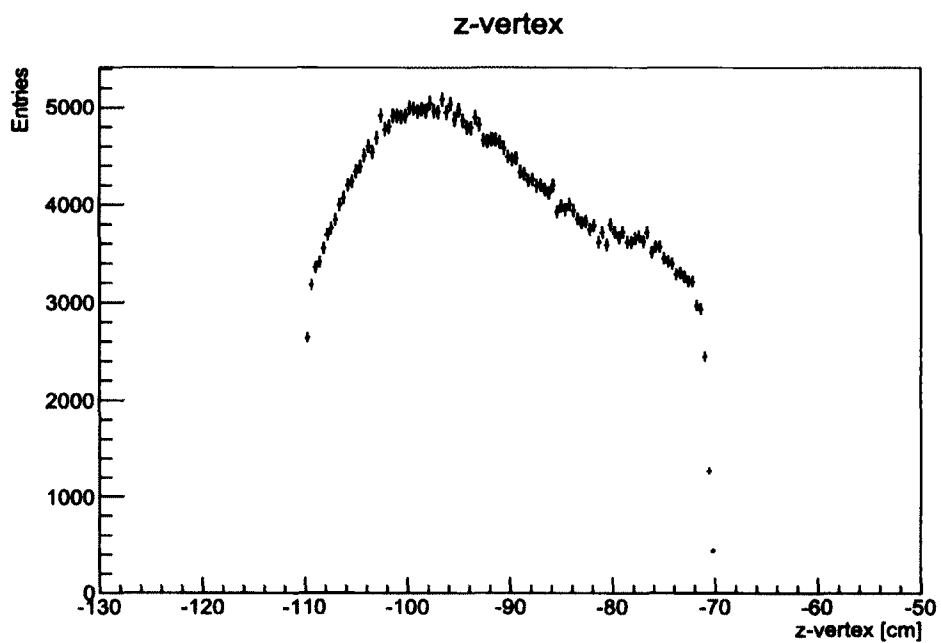


FIG. 83. Number of data events plotted vs. z-vertex

the forward part of the target, the dilepton acceptance was reduced.

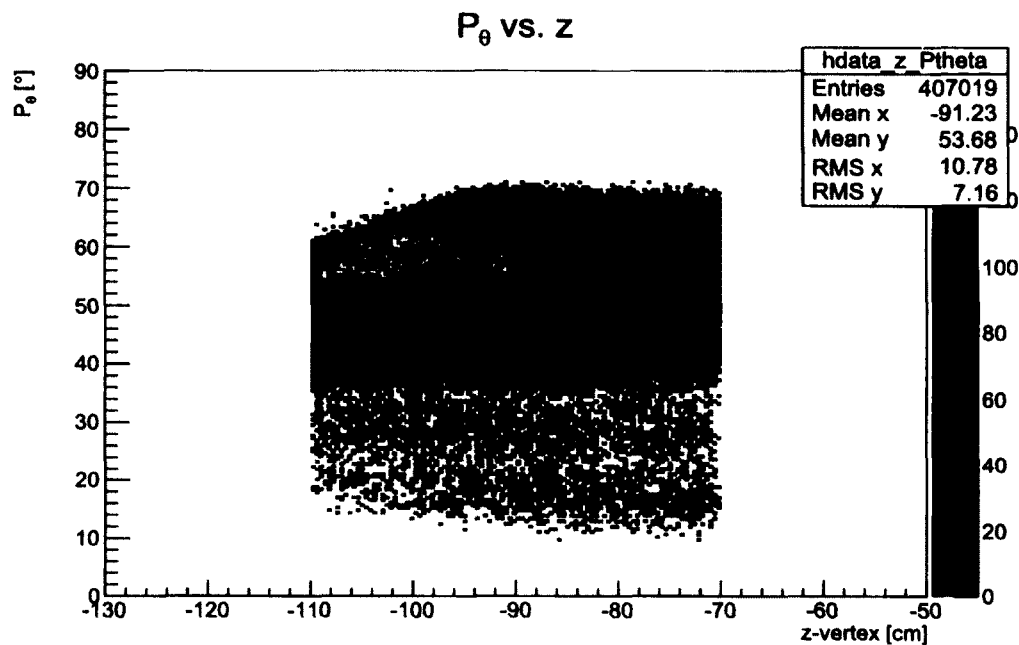


FIG. 84. Proton θ vs. z -vertex. The z -axis depicts the total number of events.

Final Data Distribution

The final data selection used for measuring of physics variables from π^0 production for this analysis can be seen in Fig. 85.

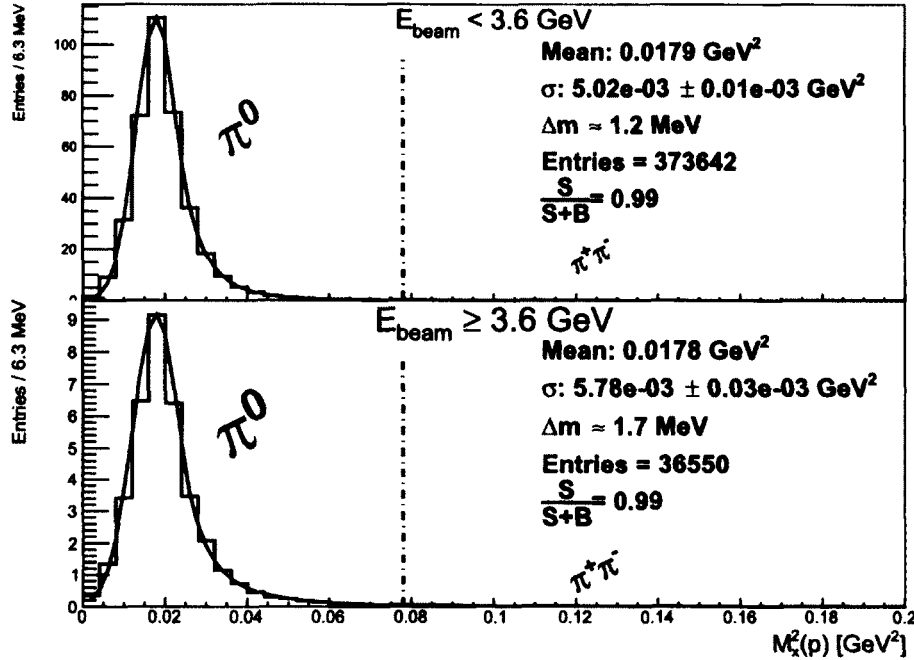


FIG. 85. Number of data events plotted vs. missing mass $M_x(\gamma p \rightarrow pX)$ for $\gamma p \rightarrow pe^+e^-(\gamma)$ events after all cuts and corrections.

4.9 SIMULATION KINEMATIC VARIABLES VERIFICATION

In the Sec. 4.4.1 the simulation was verified for efficiency. Another systematic check on the simulation was performed to investigate the validity of the kinematic variables outputted from the simulation package 4.4. This procedure was also performed as a means to double check the conclusion about the simulation efficiency found in Sec. 4.4.1 and to verify whether *GSIM* simulates *pair-production* properly. To perform this check, first the total number of expected π^0 events as well as $\pi^+\pi^-$ events were calculated for the beam energy range 1.1 GeV-2.8 GeV using the total cross-section, σ , for π^0 and $\pi^+\pi^-$ production found in [48] and using

$$N_{events} = \sigma \rho L, \quad (111)$$

where ρ and L are the target density and photon flux respectively. The total number of π^0 and $\pi^+\pi^-$ events can be seen in Fig. 86, where the left axis depicts the number of π^0 events and the right axis depicts the number of $\pi^+\pi^-$ events.

Once the total amount of π^0 was determined, it was necessary to determine the amount

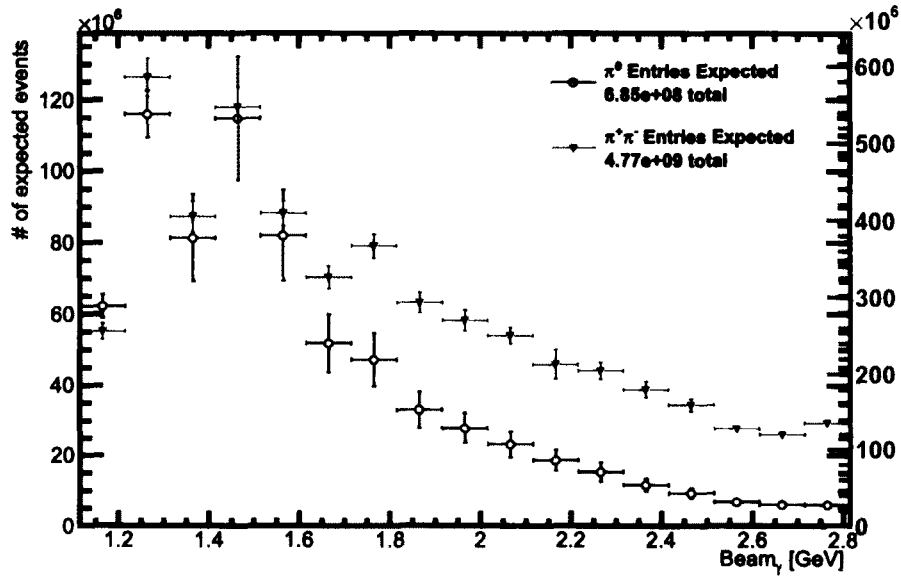
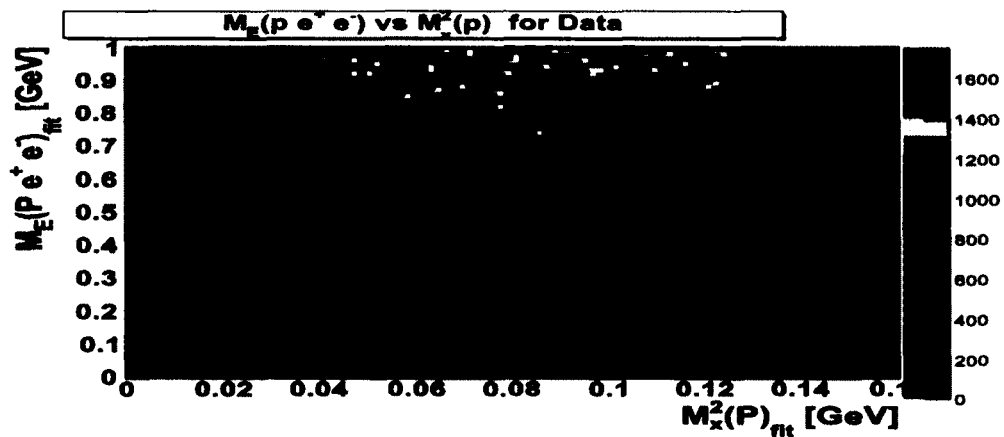


FIG. 86. Total Number of π^0 (black open circles) and $\pi^+\pi^-$ (black closed triangles) events expected between E_γ 1.1 GeV-2.8 GeV. The left axis depicts the events expected for π^0 production while the right axis depicts the events expected from $\pi^+\pi^-$ production.

of $\pi^0 \rightarrow \gamma\gamma$ and $\pi^0 \rightarrow e^+e^-\gamma$ to generate. This was done via the branching ratios of π^0 decay. The $\pi^0 \rightarrow \gamma\gamma$ has a branching ratio of $98.823 \pm 0.034\%$ while $\pi^0 \rightarrow e^+e^-\gamma$ has a branching ratio of $1.174 \pm 0.035\%$ [4] which lead to $7.03914 \cdot 10^8$ $\pi^0 \rightarrow \gamma\gamma$ events generated and $8.36237 \cdot 10^6$ $\pi^0 \rightarrow e^+e^-\gamma$ events generated. Moreover, once the total amount of events were determined, the generation of the events was weighted using the π^0 differential cross-section found in the SAID [11] database and the $\pi^+\pi^-$ differential cross-section found in the Durham [48] database. After the events were generated, they were processed using the simulation package described in 4.4 in which afterward were given the same fiducial cuts described in Sec. 4.3, kinematic constraint cuts Sec. 4.6.2 and trigger simulation cuts Sec. 4.4.2.

In Figs. 88, 89, 90, 91 it is shown that the simulation procedure appears to give an accurate representation of physics events for the incident beam, detected proton positron and electron within CLAS. Furthermore, the overall acceptance and simulation of *pair-production* is within a normalization factor of 1.011, meaning that the number of generated events was correct within 1.1% or the simulation has an acceptance inefficiency of 1.1%.

The different sources contributing to the final detected e^+e^- topology can be seen in Fig. 92.



(a)

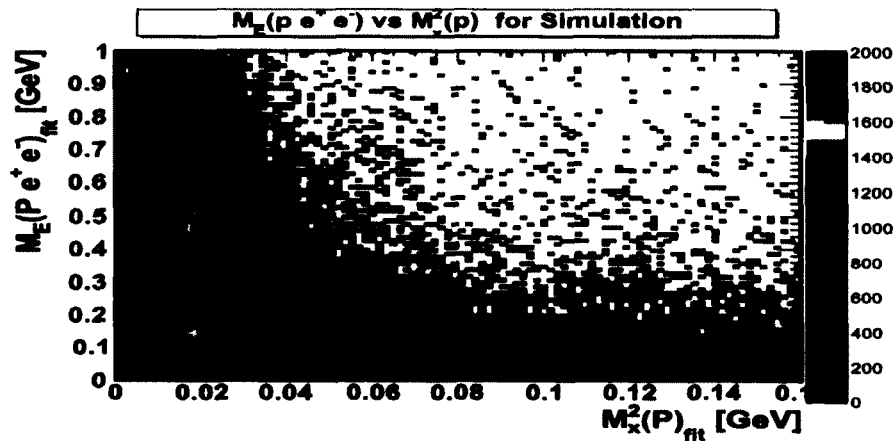
(b) $M_x^2(p)$ vs. $M_E^2(pe^+e^-)$ for MC

FIG. 87. $M_x^2(\gamma p \rightarrow pX)$ vs. $M_E^2(\gamma p \rightarrow pe^+e^-X)$ for simulation systematic check. Top panel depicts data, while the bottom panel depicts MC.

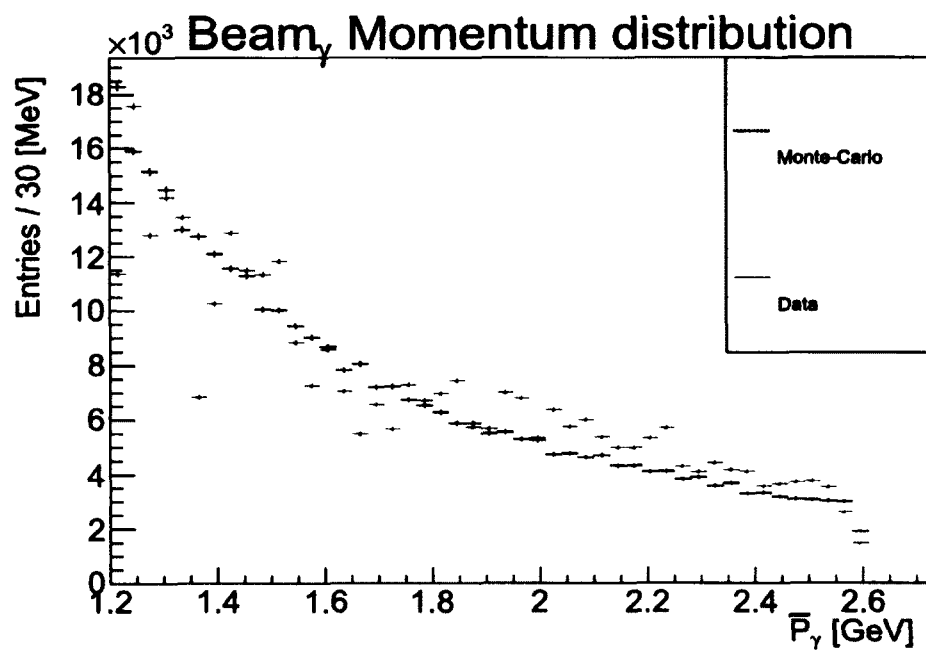


FIG. 88. Number of events vs. beam momentum for simulation systematic check. Comparison of incident photon beam kinematics for MC (black) events and data (red) when generating MC via differential cross-sections. Normalization factor is 1.011.

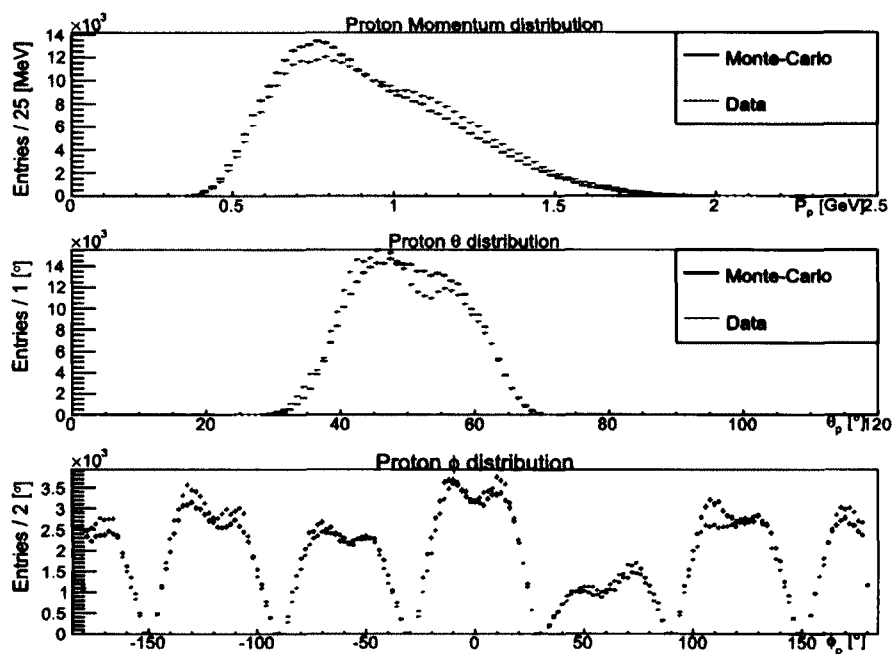


FIG. 89. Number of events vs. proton momentum (top), proton θ (middle) and proton ϕ kinematics for MC (black) events and data (red) when generating MC via differential cross-sections. Normalization factor is 1.011.

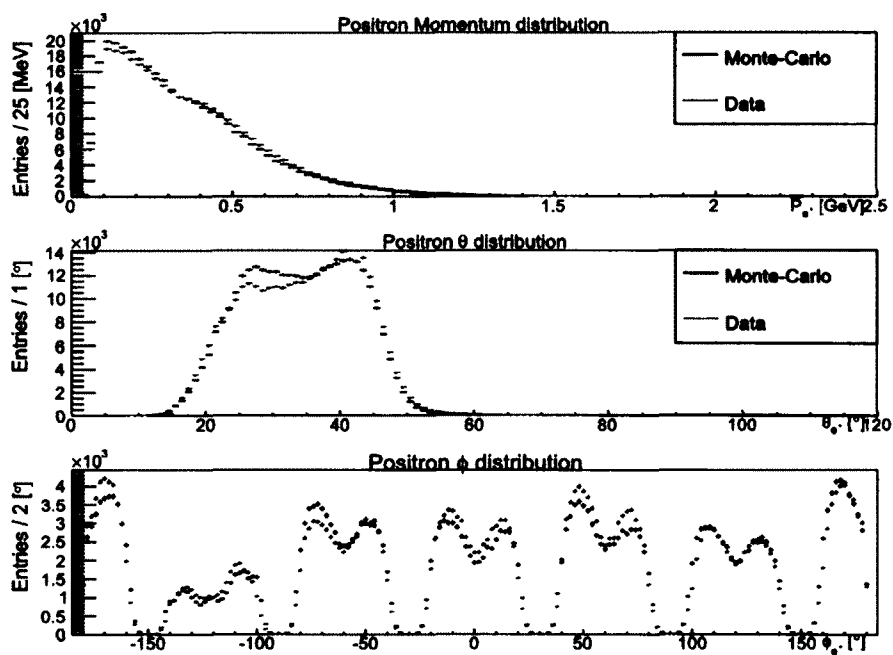


FIG. 90. Number of events vs. positron momentum (top), positron θ (middle) and positron ϕ kinematics for MC (black) events and data (red) when generating MC via differential cross-sections. Normalization factor is 1.011.

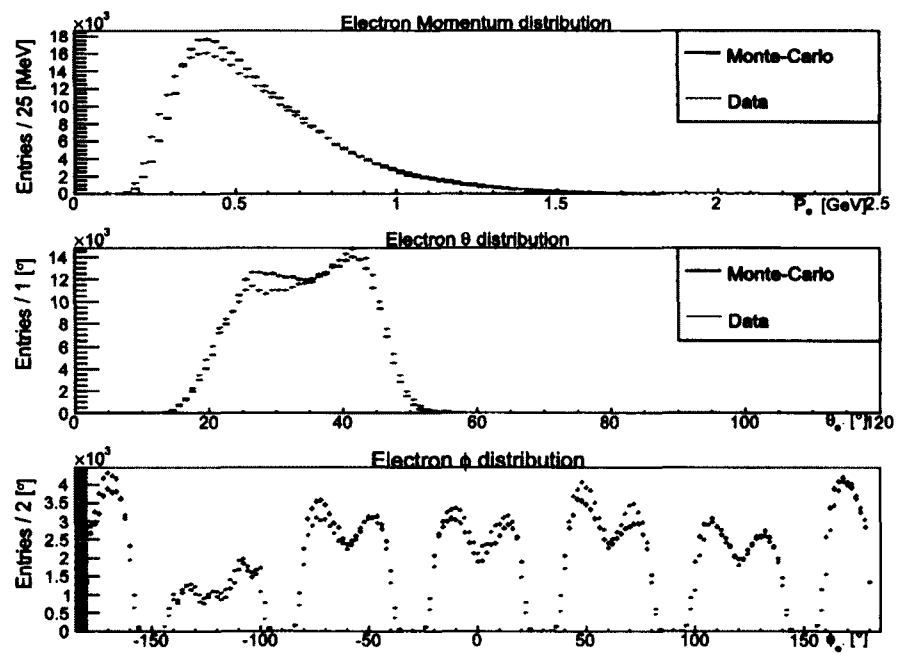


FIG. 91. Number of events vs. electron momentum (top), electron θ (middle) and electron ϕ kinematics for MC (black) events and data (red) when generating MC via differential cross-sections. Normalization factor is 1.011.

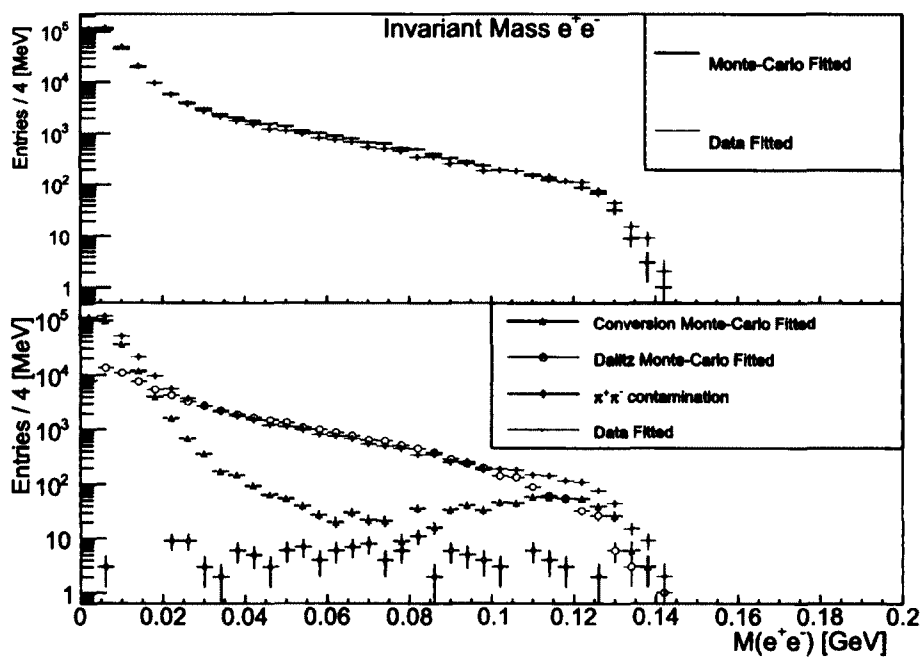


FIG. 92. Top Panel: Number of events vs. e^+e^- mass distribution for all MC (black) events and data (red). Bottom Panel: Number of events vs. e^+e^- mass distribution showing the sources of the MC e^+e^- topology overlaid to the data. Normalization factor is 1.011.

4.10 LEPTON TRIGGER EFFICIENCY FOR π^0 CANDIDATES

Using all π^0 candidates for incident beam energies less than 3.6 GeV, a trigger analysis was performed to investigate the lepton trigger “bit 6” efficiency. The normalization is the total number of π^0 events as seen in the top panel of Fig. 85 in Sec. 4.8. The normalization is done by calculating the total amount of entries for each trigger “bit” and normalizing by the total amount of events. Since there was no hierarchy in the trigger configuration, a event can be triggered on multiple triggers. It can be seen in Fig 93 that for π^0 candidates, below 3.6 GeV beam energy, the trigger “bit 6” efficiency is $\approx 100\%$.

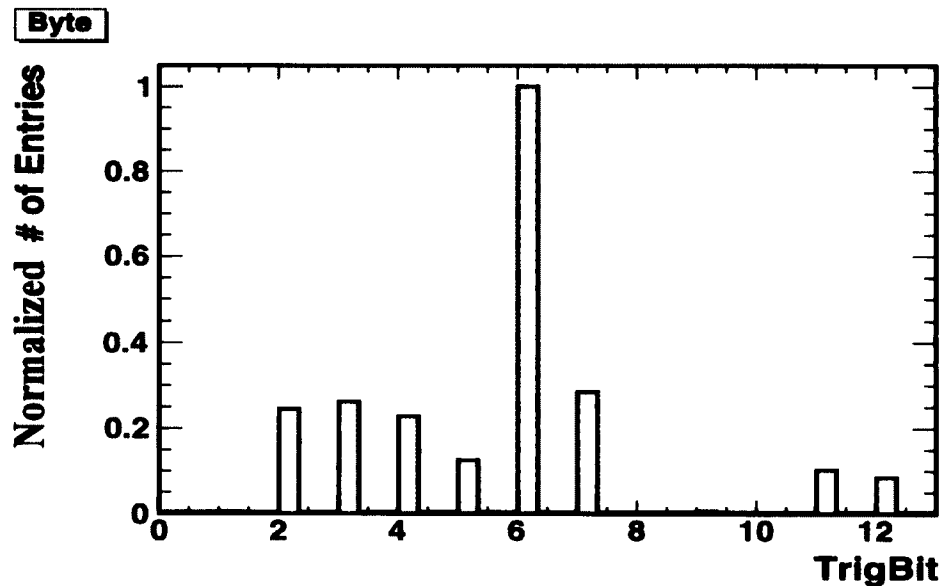


FIG. 93. Normalized lepton trigger “bit 6” for π^0 candidates. The normalization is based upon the total number of π^0 candidates.

4.11 TARGET DENSITY

We need to know the target density to calculate the differential cross-section. The procedure for determining the density of ℓH_2 target in CLAS has already been established in [49]. In the $g12$ experiment, the target temperature and pressure was measured periodically during each run. Each run contained at least 3 measurements of the pressure and temperature. The formula for calculating the target density is;

$$\rho = a_1 T^2 + a_2 P + a_3 , \quad (112)$$

where T and P represent the temperature and pressure respectively and a_1 , a_2 , a_3 are constants given in Tab. 20 taken from [50]. Fig. 94 shows the average target density, $\bar{\rho}$, for each run along with the $\sqrt{\sigma^2}$. The average density, for each run, was calculated as;

TABLE 20. Constants used in target density measurements

Parameter	Value
a_1	$-2.89 \cdot 10^{-5} \frac{g}{cm^3 K^2}$
a_2	$1.0 \cdot 10^{-7} \frac{g}{cm^3 mbar}$
a_3	$8.249 \cdot 10^{-2} \frac{g}{cm^3}$

$$\bar{\rho}_{run} = \frac{1}{N} \sum_i^N \rho_i, \quad (113)$$

while the variance σ^2 is calculated, for each run, as;

$$\sigma^2 = \frac{1}{N-1} \sum_i^N (\rho_i - \bar{\rho})^2. \quad (114)$$

Once the target density was calculated for each run, the average target density for all $g12$ runs was calculated using;

$$\bar{\rho}_{tot} = \frac{1}{N_{run}} \sum_i^{N_{run}} \bar{\rho}_{run} = 0.0711398 \pm 1.74 \cdot 10^{-5}, \quad (115)$$

while the variance σ^2 is calculated, for all $g12$ run, as;

$$\sigma_{tot}^2 = \frac{1}{N_{run}-1} \sum_i^{N_{run}} (\bar{\rho}_{run} - \bar{\rho}_{tot})^2 = 0.00024. \quad (116)$$

Since the uncertainty, σ , in the target density is lower than the uncertainty of the physical in the target materials, the target density uncertainty will not be a factor in the total systematic errors, Sec.5.4. The target length has an inaccuracy of $40 \text{ cm} \pm 0.2 \text{ cm}$. This gives a systematic of 0.5%.

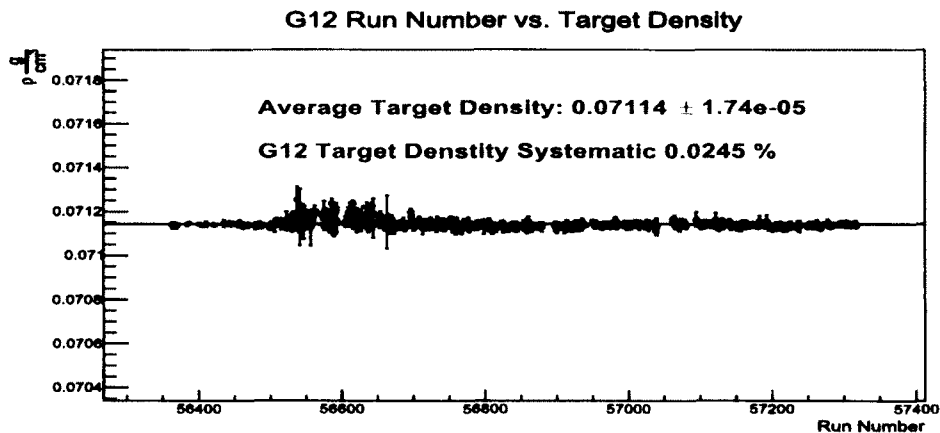


FIG. 94. Target density for $g12$

4.12 PHOTON NORMALIZATION

In the calculation of the differential cross-section, Sec. 5, accuracy of the total number of photons incident on the target will determine the accuracy of the cross-section measurement. The procedure for determining the total number of photons in CLAS has already been established in [51]. This procedure was performed for the $g12$ data set and is discussed further in [41]. In this analysis, only events which were in the “good” scalar interval were considered. A “good” scalar interval relates to data recorded when the photon flux was recorded in “live-time”. “Live-time” is the time that the data acquisition was ready to record events in conjunction with CLAS. For this analysis the photon flux, $gflux$, was binned in increments of 25 MeV and can be seen in Fig. 95. The 25 MeV binning was chosen to compare past experiments differential cross-sections with this analysis.

It should be noted that beam energies with values 3.025 ± 25 MeV, 3.075 ± 25 MeV, 3.125 ± 25 MeV and 3.525 ± 25 MeV bins are excluded from the analysis due to flux calculation problems that arose from dead scintillators in the tagger.

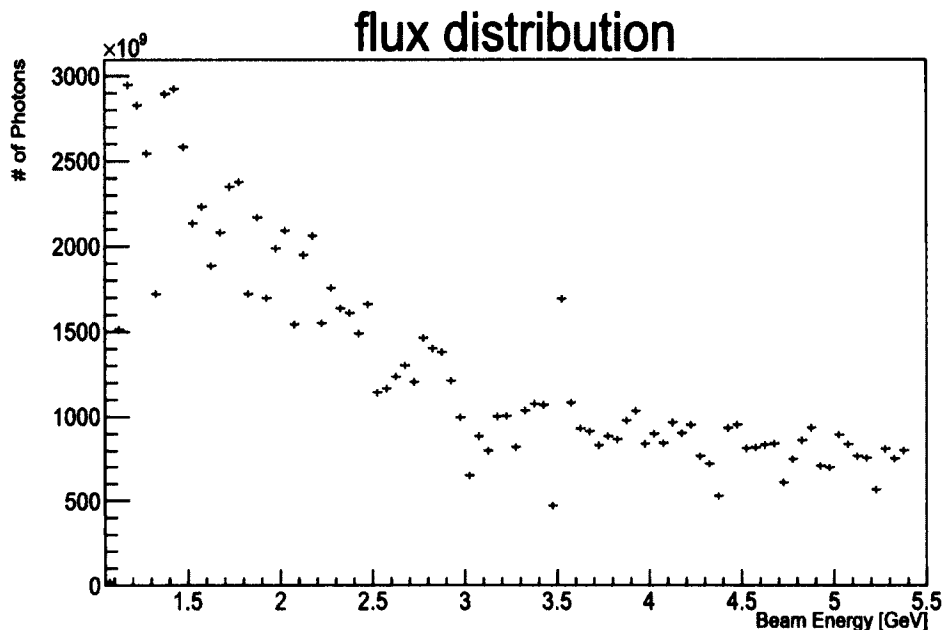


FIG. 95. Photon flux for analysis

4.13 NORMALIZATION

4.13.1 NORMALIZATION HISTORY

In the *g11* experiment there is an 18% discrepancy between the differential cross-sections of $\gamma p \rightarrow p\omega$ measured channels $\gamma p \rightarrow p\pi^+\pi^-(\pi^0)$ and $\gamma p \rightarrow p\pi^+(\pi^-\pi^0)$. One method of correction for this effect was to apply a global scale factor to the two track topology. The scale factor was on the order of 18%. The cause of the inefficiency was unknown but is believed to be due to the high current of the electron beam in conjunction with requiring 3 charged tracks from a 2-prong trigger.

4.13.2 *g12* NORMALIZATION PROCEDURE

In this analysis, a normalization constant on the order of 18% was also needed. The cause of this effect is unknown, but it is also believed to be related to using 3 charged tracks from 2-prong triggers at high current. *GPP* is responsible for smearing and dropping inefficient parts of the detector but not trigger efficiency. Therefore the normalization could be simulated if it was a trigger effect or another happenstance related to requiring 3

charged tracks in the analysis. To investigate this effect the following 3 topologies;

$$\begin{aligned}
 \gamma p &\rightarrow p\pi^+(\pi^-) \\
 \gamma p &\rightarrow p\pi^-(\pi^+) \\
 \gamma p &\rightarrow \pi^+\pi^-(p)
 \end{aligned}
 \tag{117}$$

were skimmed from data and simulated using the prescription chain in Sec. 4.4. In order to eliminate any statistical effects, $\frac{1}{4}$ of the entire *g12* data set was used and over 1 billion events were generated for simulation. Table 21 lists the number of events analyzed for each of the topologies listed in eq. 117. The data had two orders of magnitude higher

TABLE 21. Number of Events Used in Efficiency Study

Topology	Data Reconstructed	Monte-Carlo Generated/Reconstructed
$\gamma p \rightarrow p\pi^+(\pi^-)$	$5.09 \cdot 10^{10}$	$1.2 \cdot 10^9 / 2.16 \cdot 10^8$
$\gamma p \rightarrow p\pi^-(\pi^+)$	$5.43 \cdot 10^{10}$	$1.2 \cdot 10^9 / 2.17 \cdot 10^8$
$\gamma p \rightarrow \pi^+\pi^-(p)$	$5.34 \cdot 10^{10}$	$1.2 \cdot 10^9 / 1.08 \cdot 10^8$

statistics than the simulation, this was done to ensure enough events to analyze in the high momentum spectrum. The simulation generated the listed reactions in phase space using PLUTO++ [44]. The data and simulation were analyzed in the same manner.

The data was skimmed under the conditions of eq. 117. If the missing particle (particle in parenthesis) was detected, then this information was also recorded. After the data was skimmed, kinematic fits were performed to the missing particles. Nominal geometric fiducial cuts were employed for all detected particles along with a pull probability for each topology $> 1\%$, see Fig. 96.

The z-vertex of the two needed particles was determined by method of distance of closest approach of the two vectors. The data was then binned for the fitted missing particle according to the z-vertex position, momentum, $\theta \sin \phi$, and $\theta \cos \phi$. The z-vertex and momentum binning used can be seen in Table 22. If the particle to be fit was detected by CLAS, the information was also binned according z-vertex, momentum, $\theta \sin \phi$, and $\theta \cos \phi$. However to ensure that the detected particle and the fitted missing particle were the same, the detected particle must have been in the same momentum bin as the fitted missing particle.

The $\theta \sin \phi$ and $\theta \cos \phi$ binning was chosen to interpret the geometric x and y space the particle travels, independent of momentum and x and y vertex. These $\theta \sin \phi$ and

Pull Probabilities for Normalization Study

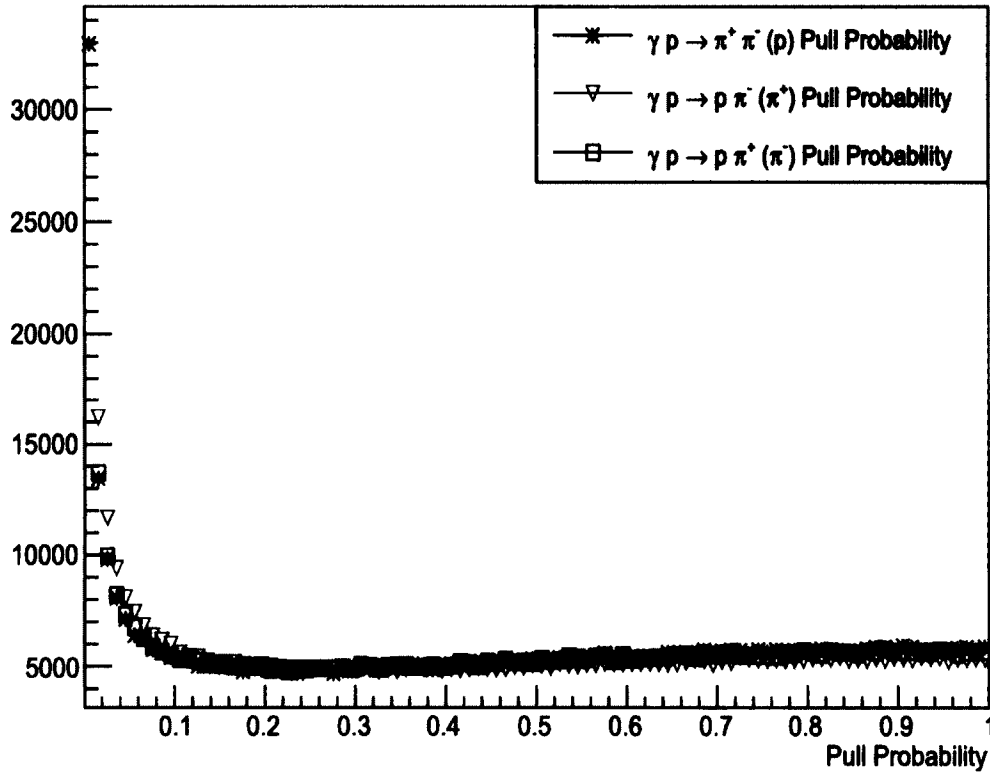


FIG. 96. Number of events vs. the pull distribution for the reactions used in the normalization study for data.

$\theta \cos \phi$ quantities are plotted as x and y variable of a histogram. To better illustrate this interpretation consider a spherical coordinate system where;

$$r = \sqrt{x^2 + y^2 + z^2} \quad (118)$$

$$x = r \sin \theta \cos \phi \quad (119)$$

$$y = r \sin \theta \sin \phi \quad (120)$$

therefore,

$$\theta \sin \phi = \left(\frac{\theta}{r \sin \theta} \right) y \quad (121)$$

$$\theta \cos \phi = \left(\frac{\theta}{r \sin \theta} \right) x . \quad (122)$$

Pull Probabilities for Normalization Study for Monte-Carlo

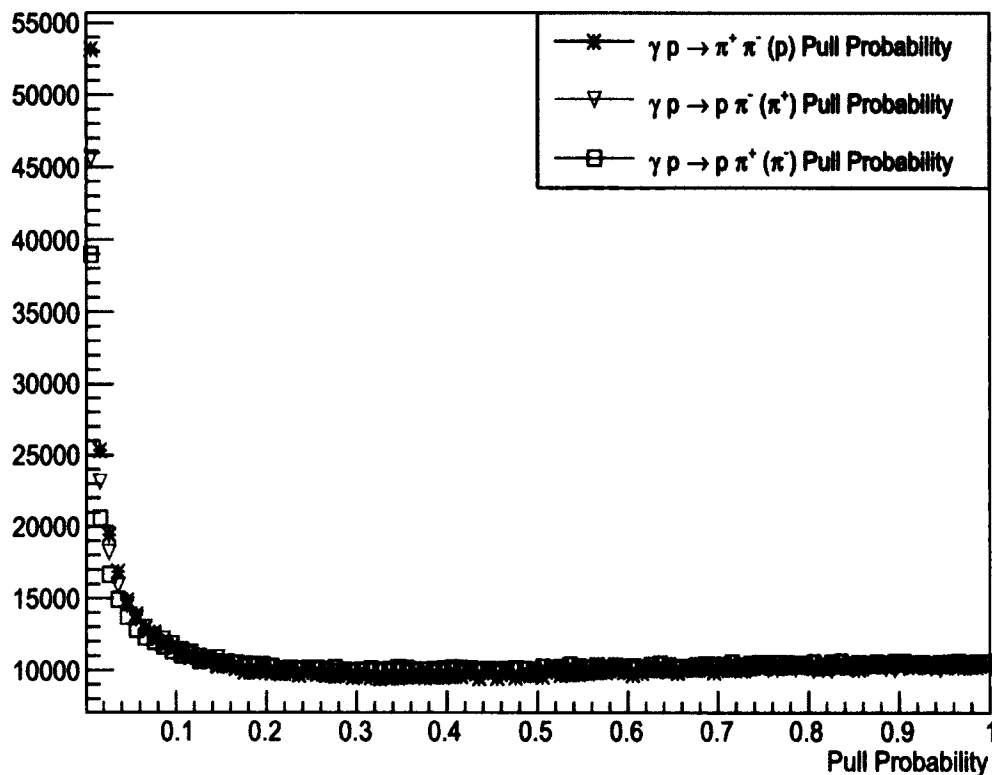


FIG. 97. Number of events vs. the pull distribution for the reactions used in the normalization study for MC.

It can be seen that plotting Eq 122 versus Eq 121 projects $x - y$ space.

For each type of missing particle, we plotted the number of events versus $\theta \sin \phi$ and $\theta \cos \phi$. We then plotted the number of events where the “missing” particle was detected. The ratio of the number of detected “missing” particle to the total number of “missing” particles is the detection efficiency for that bin in z -vertex, p , $\theta \sin \phi$ and $\theta \cos \phi$ (see Figs 98, 101 and 104). This process was repeated for simulated data (see Figs 99, 102 and 105). The ratio of the simulated efficiency to the measured efficiency for each particle was used to correct the data (see Figs 100, 103 and 106).

TABLE 22. Binning Used in Efficiency Study

z bins [cm] (5 cm increments)	Momentum bins [GeV]
$-70 \text{ cm} < z < -110 \text{ cm}$	0 - 0.5
	0.5 - 0.75
	0.75 - 1
	1 - 1.5
	1.5 - 2
	2 - 2.5
	2.5 - 3
	3 - 5

4.13.3 *g12* NORMALIZATION RESULTS

It was noticed that the simulation was over-efficient as compared to the data and the ratio of the efficiency of reconstruction should suffice as a correction to the data. Figures 98, 101, 104 depict the efficiency of data reconstruction for the proton π^+ and π^- respectively. Figures 99, 102, 105 depict the efficiency of the simulation reconstruction for the proton π^+ and π^- respectively. Figures 100, 103, 106 depict the over-efficiency of the simulation to data reconstruction for the proton π^+ and π^- respectively. The total over-efficiency was calculated as the product of each track's over-efficiency, i.e.,

$$\epsilon = \epsilon_{proton} \cdot \epsilon_{\pi^+} \cdot \epsilon_{\pi^-}. \quad (123)$$

The value of ϵ from eq. 123 is the same quantity used in the cross-section calculation in eq. 124.

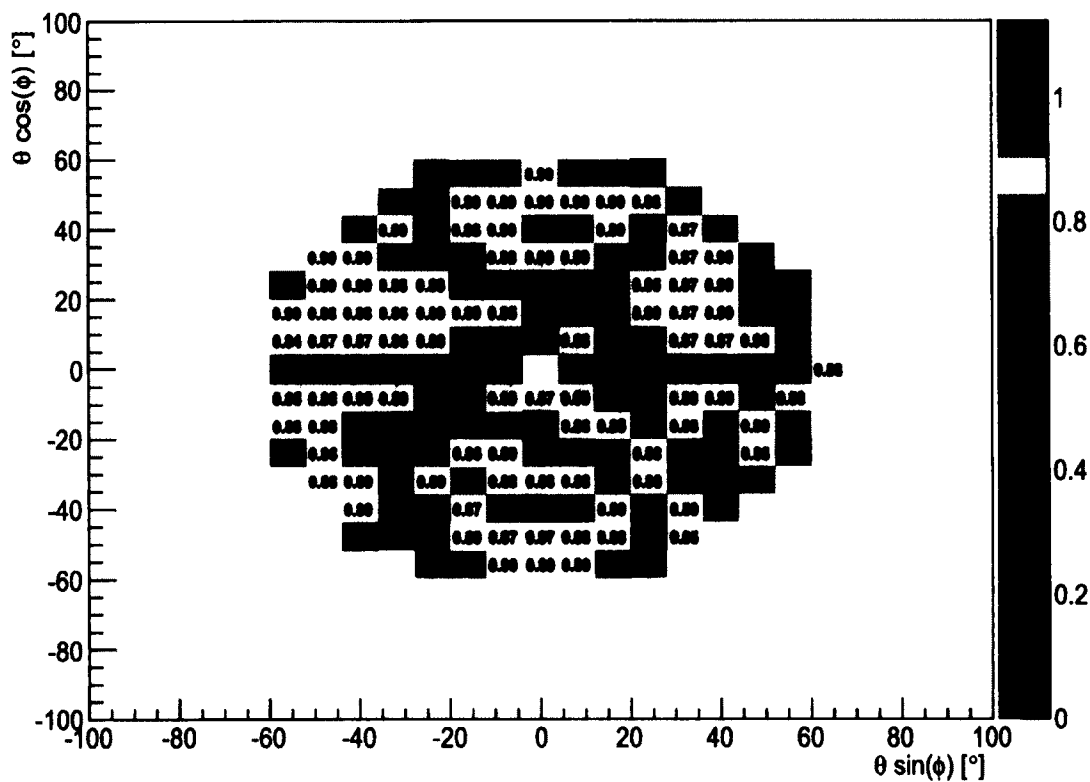
Proton Data Efficiency at $-90. < z < -85. \text{ cm}$ at $0.75 < P < 1 \text{ GeV}$ 

FIG. 98. $\theta \cos \phi$ vs. $\theta \sin \phi$ plot showing the efficiency of detecting the proton with z -vertex $-90 < z < -85 \text{ cm}$ and momentum $0.75 < p < 1 \text{ GeV}$ from a 2 charged track reaction using CLAS detection for $g12$.

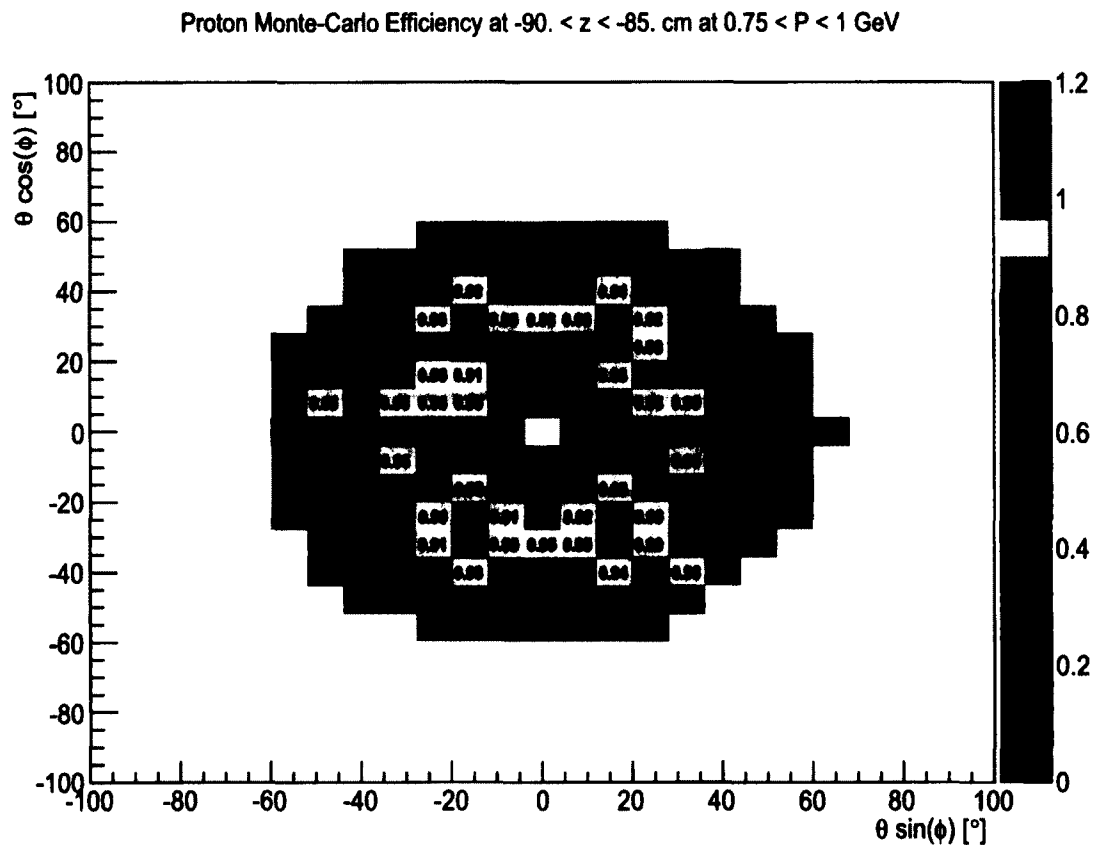


FIG. 99. $\theta \cos \phi$ vs. $\theta \sin \phi$ plot showing the efficiency of reconstructing the proton with z -vertex $-90 < z < -85$ cm and momentum $0.75 < p < 1$ GeV from a 2 charged track reaction using CLAS Monte-Carlo for $g12$.

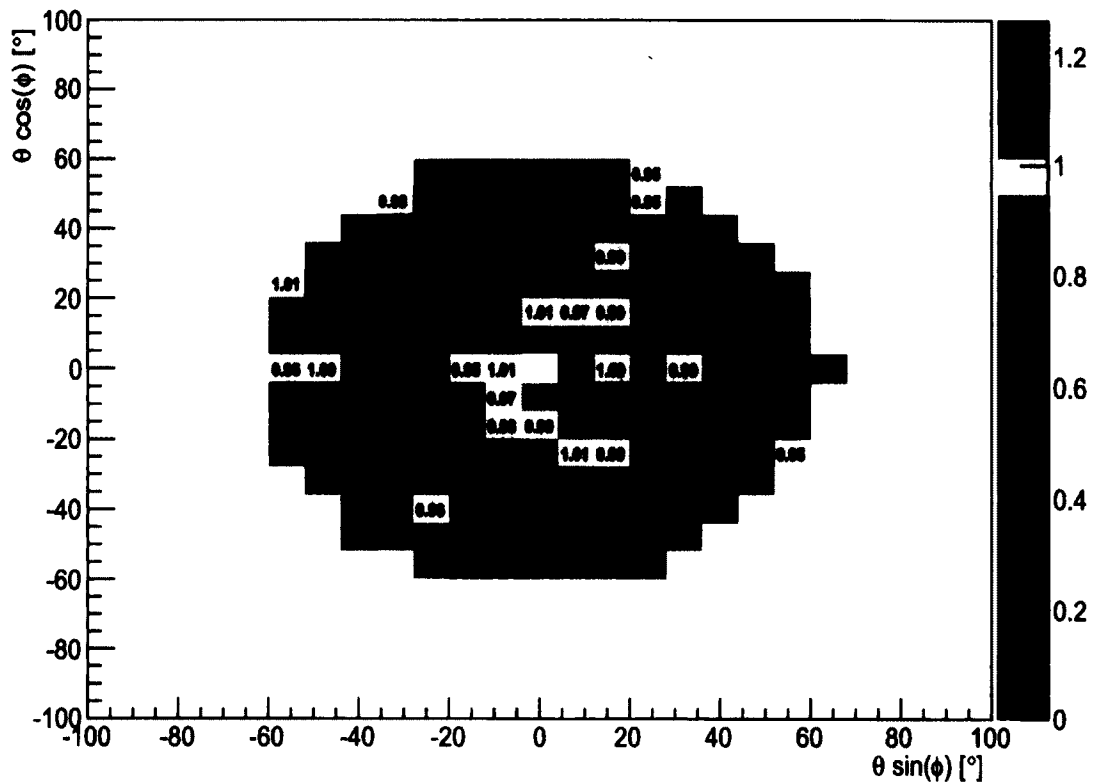
Proton Over-Efficiency at $-90. < z < -85. \text{ cm}$ at $0.75 < P < 1 \text{ GeV}$ 

FIG. 100. $\theta \cos \phi$ vs. $\theta \sin \phi$ plot showing the over-efficiency of simulating the proton with z -vertex $-90 < z < -85 \text{ cm}$ and momentum $0.75 < p < 1 \text{ GeV}$ from a 2 charged track reaction.

π^+ Data Efficiency at $-90. < z < -85. \text{ cm}$ at $0.75 < P < 1 \text{ GeV}$

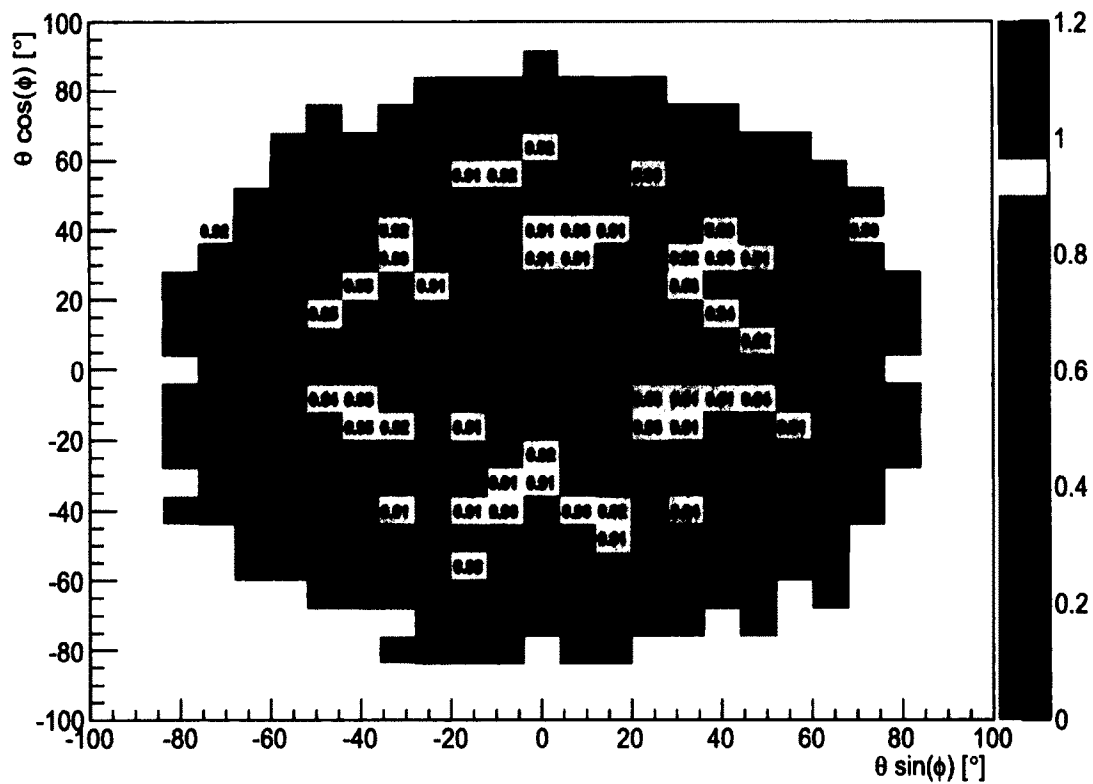


FIG. 101. $\theta \cos \phi$ vs. $\theta \sin \phi$ plot showing the efficiency of detecting the π^+ with z -vertex $-90 < z < -85 \text{ cm}$ and momentum $0.75 < p < 1 \text{ GeV}$ from a 2 charged track reaction using CLAS detection for $g12$.

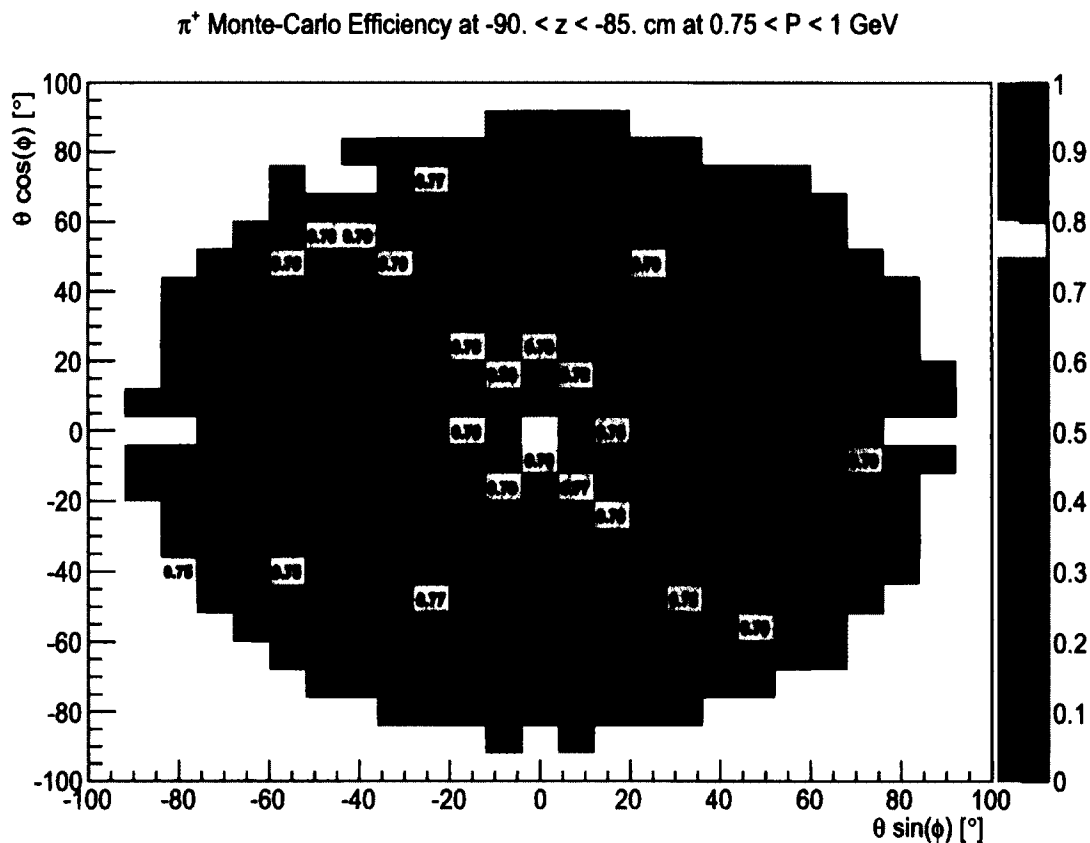


FIG. 102. $\theta \cos \phi$ vs. $\theta \sin \phi$ plot showing the efficiency of reconstructing the π^+ with z -vertex $-90 < z < -85 \text{ cm}$ and momentum $0.75 < p < 1 \text{ GeV}$ from a 2 charged track reaction using CLAS Monte-Carlo for $g12$.

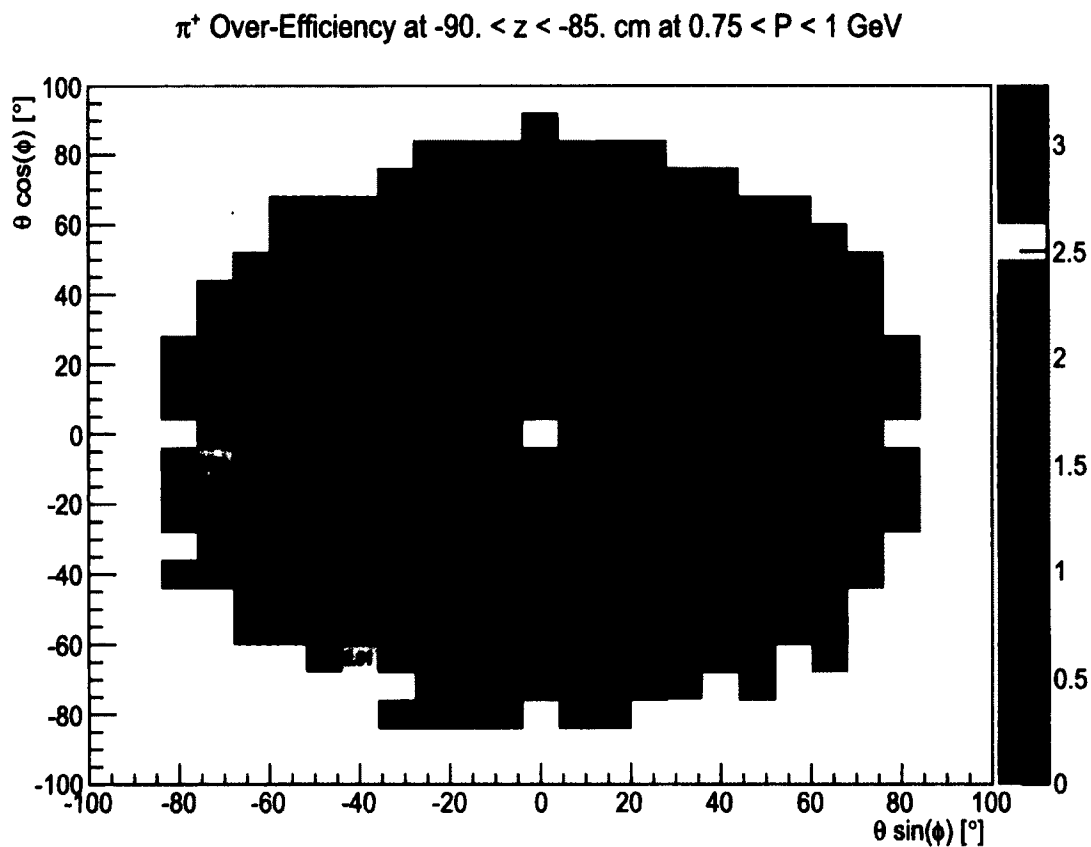


FIG. 103. $\theta \cos \phi$ vs. $\theta \sin \phi$ plot showing the over-efficiency of simulating the π^+ with z -vertex $-90 < z < -85 \text{ cm}$ and momentum $0.75 < p < 1 \text{ GeV}$ from a 2 charged track reaction.

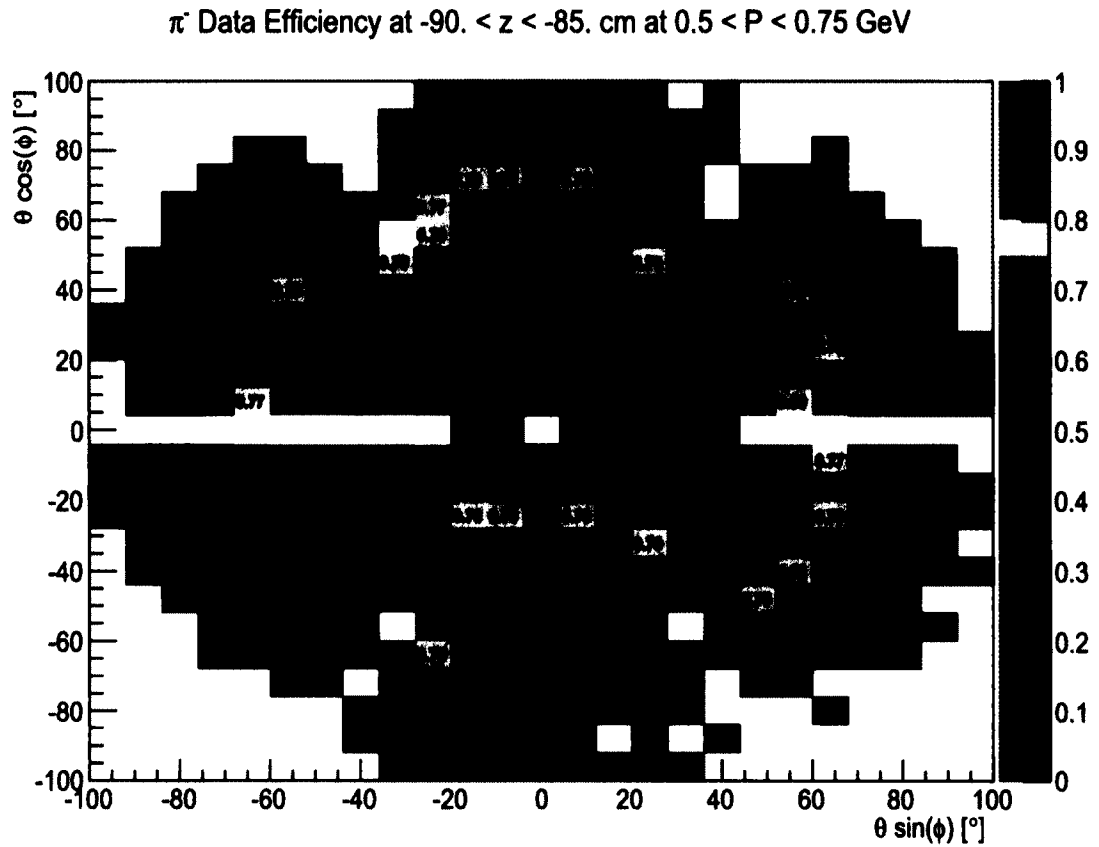


FIG. 104. $\theta \cos \phi$ vs. $\theta \sin \phi$ plot showing the efficiency of detecting the π^- with z -vertex $-90 < z < -85 \text{ cm}$ and momentum $0.75 < p < 1 \text{ GeV}$ from a 2 charged track reaction using CLAS detection for $g12$.

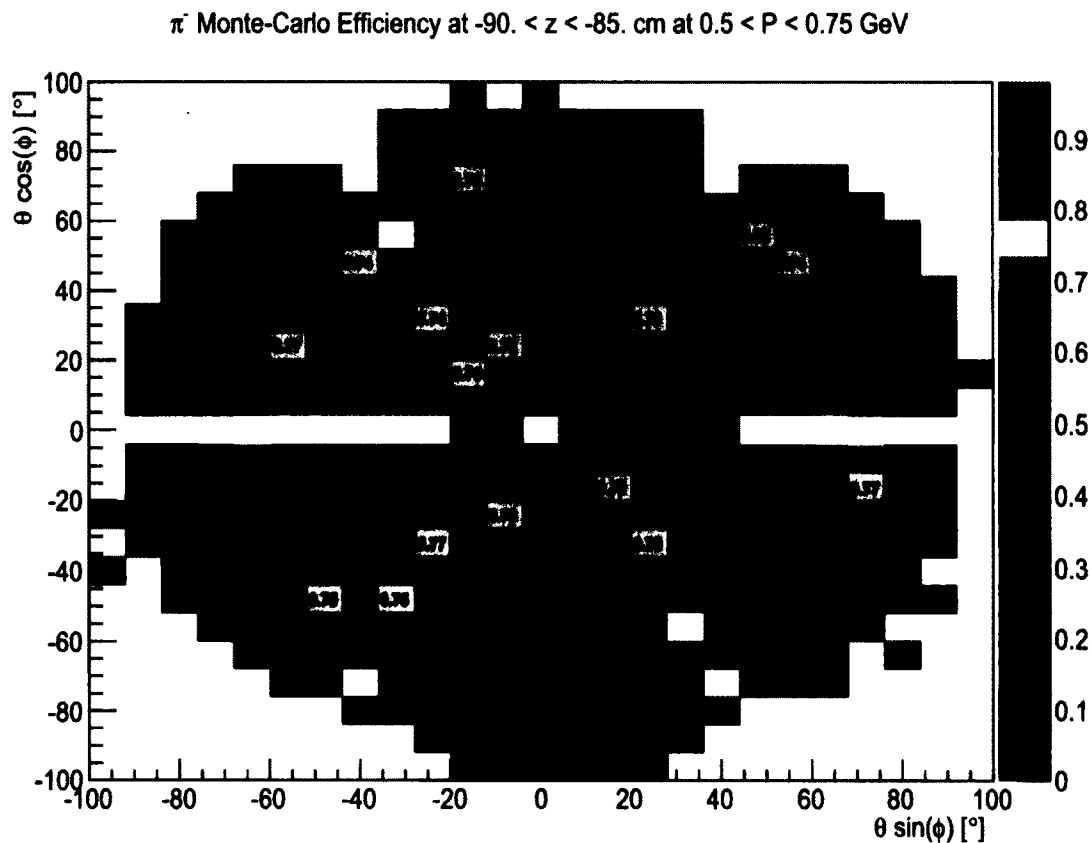


FIG. 105. $\theta \cos \phi$ vs. $\theta \sin \phi$ plot showing the efficiency of reconstructing the π^- with z -vertex $-90 < z < -85 \text{ cm}$ and momentum $0.75 < p < 1 \text{ GeV}$ from a 2 charged track reaction using CLAS Monte-Carlo for $g12$.

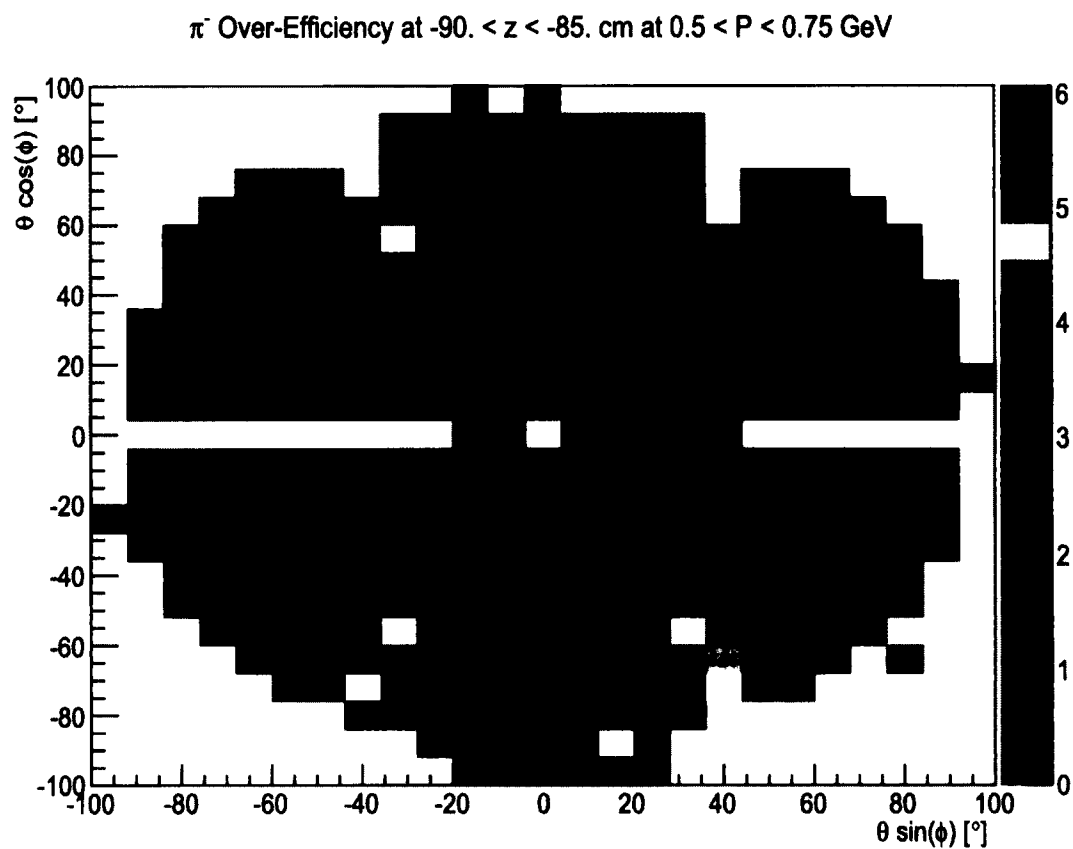


FIG. 106. $\theta \cos \phi$ vs. $\theta \sin \phi$ plot showing the over-efficiency of simulating the π^- with z -vertex $-90 < z < -85 \text{ cm}$ and momentum $0.75 < p < 1 \text{ GeV}$ from a 2 charged track reaction.

4.13.4 NORMALIZATION COMPARISON

To validate the $g12$ normalization results, the $g12$ π^0 differential cross-section was calculated using the $g11$ global normalization factor and then compared to the $g12$ π^0 differential cross-section using the $g12$ normalization procedure results. It is shown in Fig. 107 and Fig. 108 that the 2 methods agree with one another except for the very forward regions of $\cos\theta_{C.M.}^{\pi^0}$, where the cross-section using the dynamic normalization is larger than the cross-section measured with the $g11$ global normalization, however the larger cross-sections at forward $\cos\theta_{C.M.}^{\pi^0}$ agree very well with the past results of [55].

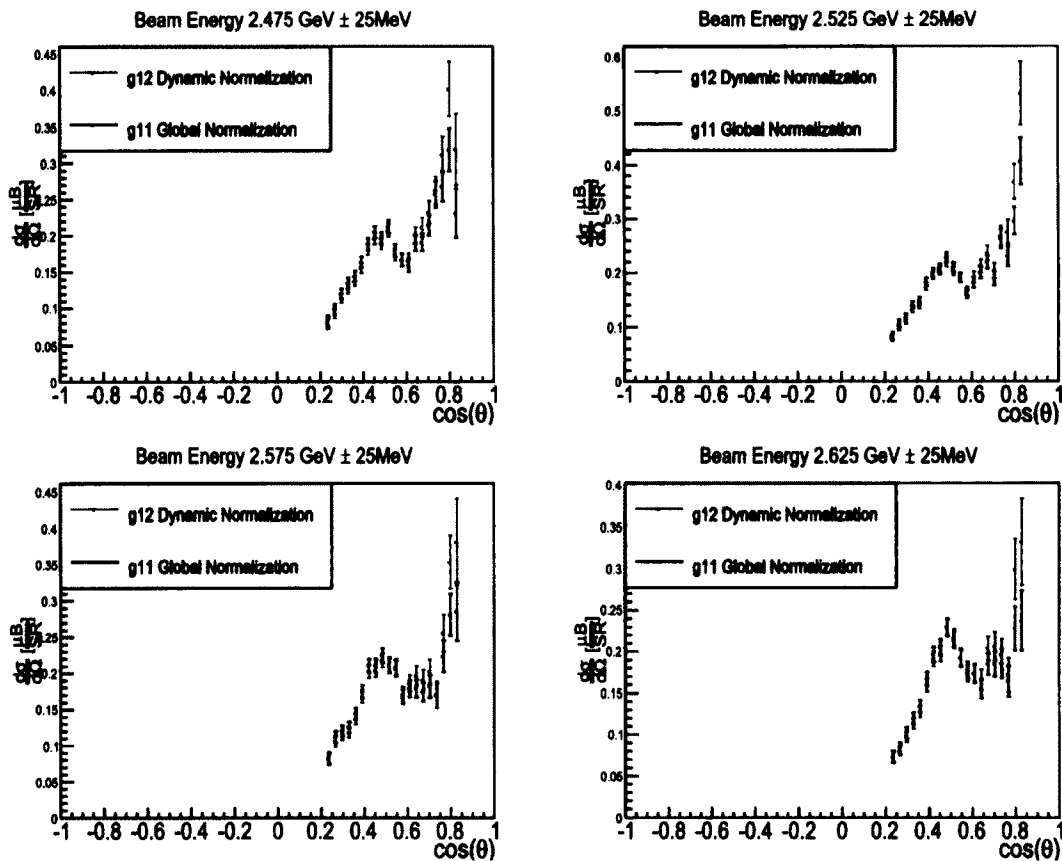


FIG. 107. $\frac{d\sigma}{d\Omega}$ vs. $\cos\theta$ plot showing the $g12$ π^0 differential cross-section when the $g11$ global normalization is used (blue) and when the $g12$ dynamic normalization is used (red) for various bins of beam energy inside lepton trigger acceptance.

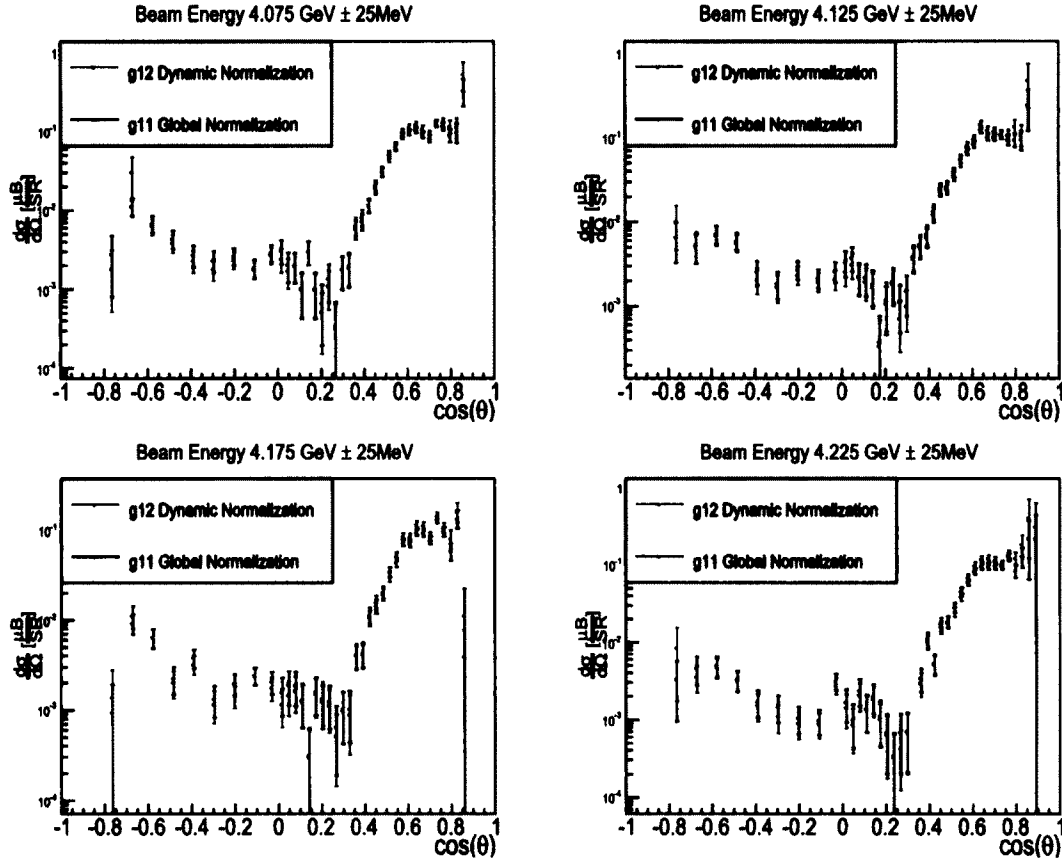


FIG. 108. $\frac{d\sigma}{d\Omega}$ vs. $\cos\theta$ plot showing the $g12 \pi^0$ differential cross-section when the $g11$ global normalization is used (blue) and when the $g12$ dynamic normalization is used (red) for various bins of beam energy above MORB threshold.

4.13.5 NORMALIZATION UNCERTAINTIES

The statistical uncertainties of the normalization correction was minimized by ensuring that the statistical sample of the data and MC was sufficient in each bin of z -vertex, momentum, $\theta \sin \phi$ and $\theta \cos \phi$. The maximum statistical uncertainty was 0.01%. The systematic uncertainties of the normalization correction was not calculated, but it is intended to be.

CHAPTER 5

RESULTS

This chapter will discuss the results of the cross-sections with comparisons to previous world data, as well as a comparison of SAID fits to the previous data sets and this analysis data. Also a comparison to the Bonn-Gatchina solution is presented.

5.1 CROSS-SECTION

In this section, the calculations leading up to the cross-section measurement of the π^0 are described in detail. The number of particles detected in any apparatus in photoproduction, Υ , can be described as,

$$\Upsilon(E_\gamma) = \sigma(E_\gamma) \left(\frac{F(E_\gamma) \rho_{target} \ell_{target} N_A}{A_{target}} \right) \eta(E_\gamma) \epsilon \quad (124)$$

where ρ_{target} , ℓ_{target} and A_{target} are the target density, length and atomic weight respectively, N_A is Avogadro's number. The quantities $\sigma(E_\gamma)$, $F(E_\gamma)$, $\eta(E_\gamma)$ are the cross-section for the particle to be produced, the number of photons incident on the target, and the detector acceptance at beam energy E_γ . The factor ϵ is the total efficiency of detecting the particle, sometimes also referred to as normalization. For this analysis ϵ was derived independently of any cross-section, see Sec. 4.13

If the particle of interest decays into daughters, i.e. $P_{mother} \rightarrow P_{daughter_1} + P_{daughter_2} + \dots + P_{daughter_N}$, then Eq. 124 must be normalized by the branching ratio of the decay $\Gamma_{P_m \rightarrow P_{d_1} + P_{d_2} + \dots + P_{d_N}}$. For this analysis, the detected final state particles were proton, electron and positron with a missing photon. The electron, positron and missing photon are the daughter particles of the π^0 . However the final state of this decay was a mixture of the π^0 dalitz decay and the π^0 two photon radiative decay with one photon converting into an electron-positron pair, see Sec 1.3.1. Since the detected final state is a mixture of branching ratios, Eq. 124 must be normalized by the sum of the normalized branching ratios contributing

$$\frac{\Gamma}{\Gamma_{tot}} = \frac{\Gamma_{\pi^0 \rightarrow e^+ e^- \gamma}}{\Gamma_{tot}} + \frac{\Gamma_{\pi^0 \rightarrow \gamma \gamma}}{\Gamma_{tot}}, \quad (125)$$

and the detector acceptance $\eta(E_\gamma)$ also becomes a mixture of the branching ratios.

$$\eta(E_\gamma) = \eta_{dalitz} + \eta_{conversion} \quad (126)$$

which is described in Sec. 5.2

The differential cross-section in the center-of-mass system of a particle can be obtained by differentiating eq. 124 with respect to the observables $\cos\theta$ and ϕ , where $\cos\theta$ is the polar angular distribution and ϕ the azimuthal distribution. Since there are no physical observables with respect to ϕ , we can rewrite Eq. 124 as,

$$\frac{d\sigma}{d\cos\theta_{C.M.}^{\pi^0}d\phi} = \frac{1}{2\pi\Delta\cos\theta_{C.M.}^{\pi^0}} \frac{\Upsilon(E_\gamma, \cos\theta_{C.M.}^{\pi^0})}{\eta(E_\gamma, \cos\theta_{C.M.}^{\pi^0})\epsilon} \left(\frac{A_{target}}{F(E_\gamma)\rho_{target}\ell_{target}N_A} \right) \frac{1}{\Gamma} \quad (127)$$

where $\Delta\cos\theta_{C.M.}^{\pi^0}$ is the width of each $\cos\theta_{C.M.}^{\pi^0}$ bin. In this analysis there were two bin widths used

$$\Delta\cos\theta_{C.M.}^{\pi^0} = 0.09375 \quad -1 < \cos\theta_{C.M.}^{\pi^0} < 0 \quad (128a)$$

$$\Delta\cos\theta_{C.M.}^{\pi^0} = 0.03125 \quad 0 < \cos\theta_{C.M.}^{\pi^0} < 1, \quad (128b)$$

in order to minimize statistical errors in the backward direction, Sec. 5.3. The values of the constants used in eq. 127 can be found in Table 23.

TABLE 23. Constants used in $\frac{d\sigma}{d\cos\theta_{C.M.}^{\pi^0}d\phi}$ measurements

Quantity	Value	Description
A_{target}	1.00794 g/mol	Target atomic number
ρ_{target}	0.0711398 g/cm ³	Target density Sec. 4.11
ℓ_{target}	40 cm	Length of target [52] , Fig. 19
N_A	6.022·10 ²³	Avogadro's number
$\Gamma_{\pi^0 \rightarrow \gamma\gamma}$	0.98823	Branching ratio of $\pi^0 \rightarrow \gamma\gamma$
$\Gamma_{\pi^0 \rightarrow e^+e^-\gamma}$	0.01174	Branching ratio of $\pi^0 \rightarrow e^+e^-\gamma$
$\frac{\Gamma}{\Gamma_{tot}}$	0.99997	Sum of branching ratios used in this analysis

5.2 ACCEPTANCE

The simulation package was verified for both geometry and detector response efficiency in Sec 4.4. The acceptance for the cross-sections presented in this work was measured using phase-space Monte-Carlo (MC) simulation, using PLUTO++ [44] as the generator, for the reaction channels,



A total of events, N_g , was generated and this number was weighted by the relative branching ratios found in Table 23 to resemble the conditions of the data. The number of events generated for the reaction channel 129a can be found in Table 24 as N_c . The number of events generated for the reaction channel n 129b can be found in Table 24 as N_d . Af-

TABLE 24. Number of generated events in each decay spectrum

Quantity	Value	Description
N_g	$2.39869 \cdot 10^9$	Total number of π^0 events generated
N_c	$2.37039 \cdot 10^9$	Total number of $\pi^0 \rightarrow \gamma\gamma$ events generated
N_d	$2.80647 \cdot 10^7$	Total number of $\pi^0 \rightarrow e^+e^-\gamma$ generated

ter the events are generated, they are inputted into the CLAS simulation chain **GAMP2BOS**, **GSIM**, **GPP**, and then reconstructed with the same program used to reconstruct the data, **a1c**, all programs in the simulation chain use the parameters and the run index described in Sec. 4.4,. For a detailed explanation of this chain, refer to Sec. 4.4. Once the events are processed through **a1c**, the cuts described in Secs. 4.3, 4.6.2, are applied as they are to the real data. The acceptance $\eta(E_\gamma, \theta_{C.M.}^{\pi^0})$ is then determined by adding the simulations for the conversion and the dalitz, then for photon energy bins of 25 MeV increments and $\Delta \cos \theta_{C.M.}^{\pi^0} = 0.0125$ increments, the ratio of reconstructed events (N_R) to generated events (N_G) yields,

$$\eta(E_\gamma, \cos \theta_{C.M.}^{\pi^0}) = \frac{N_R(E_\gamma, \cos \theta_{C.M.}^{\pi^0})}{N_G(E_\gamma, \cos \theta_{C.M.}^{\pi^0})}.
\tag{130}$$

The $\Delta \cos \theta_{C.M.}^{\pi^0}$ binning in the acceptance is a factor of 2.4 finer than the smallest $\Delta \cos \theta_{C.M.}^{\pi^0}$ increment used in the cross-section measurement. If an accurate physics model for the generator had been used, as was in Sec. 4.4, the binning for the acceptance would not have had to be so fine.

5.3 STATISTICAL UNCERTAINTIES

In this section, the calculations leading up to the statistical uncertainty of the cross-section measurement will be discussed. Statistical fluctuations of the measurement will depend solely on the variables in eq. 127 that are not constant and can vary depending on bin width or calculation methods. For this analysis, discrete binning was employed allowing to utilize Poisson distribution error estimation. A Poisson distribution $P(\lambda, k)$ is defined as,

$$P(\lambda, k) = \frac{\lambda^k e^{-\lambda}}{k!} \quad (131)$$

with k being the observed occurrences, λ being the rate of occurrences and also the variance, is a discrete probability distribution that expresses the probability of a given number of events occurring in a fixed interval of time and/or space if these events occur with a known average rate and independently of the time since the last event [53]. With λ as the variance of the measurement the standard deviation (σ), or error of the measurement is described by $\sigma = \sqrt{\lambda}$. For data samples of uncorrelated variables, the error propagation can be described as

$$\left(\frac{\sigma_f}{f}\right)^2 = \sum_{i=1}^M \left(\frac{\sigma_i}{f_i}\right)^2 \quad (132)$$

Let's denote the differential cross-section as

$$\frac{d\sigma}{d \cos \theta_{C.M.}^{\pi^0} d\phi} = \Xi$$

and the error of Ξ to be

$$\sigma_{\Xi} = \Xi \left(\left(\frac{\sigma_{\Upsilon}}{\Upsilon}\right)^2 + \left(\frac{\sigma_{\eta(E_{\gamma}, \cos \theta_{C.M.}^{\pi^0})}}{\eta(E_{\gamma}, \cos \theta_{C.M.}^{\pi^0})}\right)^2 + \left(\frac{\sigma_{F(E_{\gamma})}}{F(E_{\gamma})}\right)^2 \right)^{\frac{1}{2}} \quad (133)$$

where the statistical error of the flux $F(E_{\gamma})$ and detected particles Υ is given by Poisson statistics,

$$\sigma_{F(E_{\gamma})} = \sqrt{F(E_{\gamma})} \quad (134a)$$

$$\sigma_{\Upsilon} = \sqrt{\Upsilon}. \quad (134b)$$

From eq. 130

$$\left(\frac{\sigma_{\eta}}{\eta}\right) = \left(\left(\frac{\sigma_R}{N_R}\right)^2 + \left(\frac{\sigma_G}{N_G}\right)^2 \right)^{\frac{1}{2}} \quad (135)$$

where the statistical error of the reconstructed events, σ_R , and generated events, σ_G , is

given by Poisson statistics

$$\begin{aligned}\sigma_R &= \sqrt{N_R} \\ \sigma_G &= \sqrt{N_G}\end{aligned}$$

therefore

$$\left(\frac{\sigma_\eta}{\eta}\right) = \left(\frac{1}{N_R} + \frac{1}{N_G}\right)^{\frac{1}{2}} \quad (137)$$

The number of events reconstructed, N_R for the simulation was chosen to be such that $N_R \sim 4\Upsilon$, while the pair-production rate combined with the acceptance made it such that $N_R \ll N_G$, simplifying eq. 137 to be

$$\left(\frac{\sigma_\eta}{\eta}\right) = \left(\frac{1}{4\Upsilon}\right)^{\frac{1}{2}}. \quad (138)$$

It should also be noted that the beam energy binning chosen reflects that $\Upsilon \ll F(E_\gamma)$ and so substituting Eqs. 134b, 134a, 138 into Eq. 133 yields

$$\sigma_\Xi = \Xi \left(\frac{1}{\Upsilon} + \frac{1}{4\Upsilon}\right)^{\frac{1}{2}} \quad (139)$$

The backward angle binning discussed in Sec 5.1 eq. 128a was chosen to minimize the statistical error by maximizing

$$\left(\frac{1}{\Upsilon} + \frac{1}{4\Upsilon}\right)^{\frac{1}{2}} \quad (140)$$

The contribution of eq. 140 is shown in Fig. 109 for values of $\Upsilon < 100$ which is typical at high beam energies, large backward $\cos\theta_{C.M.}^{\pi^0}$.

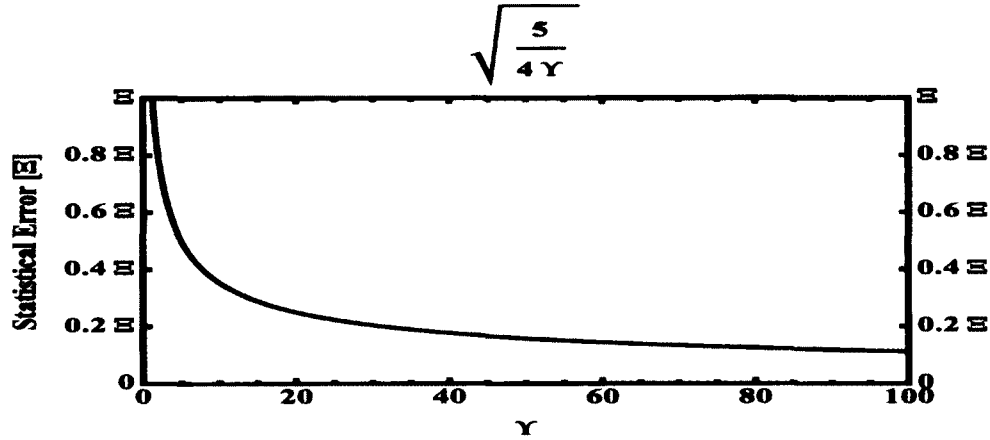


FIG. 109. The uncertainty plotted vs. the total number of detected events and reconstructed events from MC, for small values of Υ . The binning in the backward direction was chosen to maximize Υ to reduce the overall statistical error

5.4 SYSTEMATIC UNCERTAINTY

In this section, the calculations leading up to the systematic of the measurement will be discussed. Systematic errors are caused the controls of the experiment, such as flux, simulation, density and length of the ℓH_2 target and also systematic errors are caused by various analytical tools used, such as the kinematic fitter.

5.4.1 BRANCHING RATIO SYSTEMATIC UNCERTAINTY

The branching ratios for the two topologies used to measure the cross-section were obtained from PDG [54] and are listed again in Table 25 with their associated errors. Uncorrelated quantities that are summed as,

$$f = \sum_{i=1}^M a_i P_i \quad (141)$$

have errors as

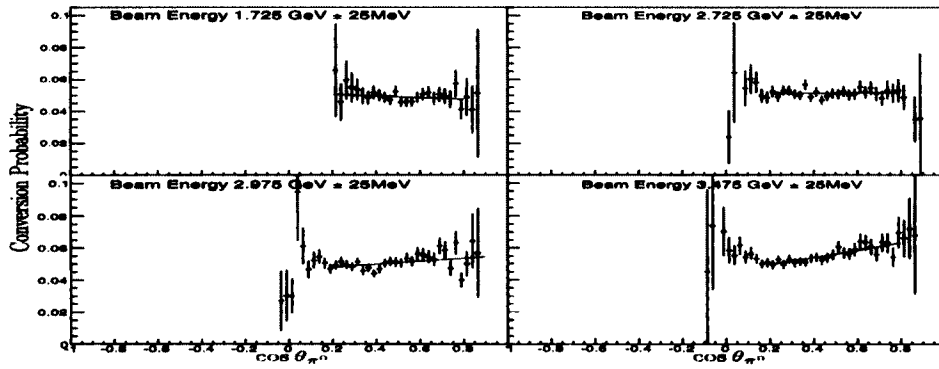
$$\sigma_f = \sqrt{\sum_{i=1}^M (a_i \sigma_i)^2}. \quad (142)$$

Therefore

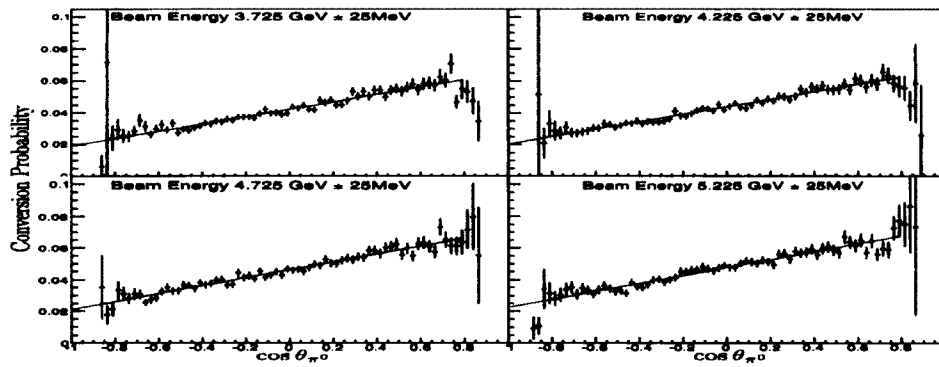
$$\frac{\Gamma}{\Gamma_{tot}} = \frac{\Gamma_{\pi^0 \rightarrow e^+e^-\gamma}}{\Gamma_{tot}} + \frac{\Gamma_{\pi^0 \rightarrow \gamma\gamma \rightarrow e^+e^-\gamma}}{\Gamma_{tot}} \quad (143)$$

$$= \frac{\Gamma_{\pi^0 \rightarrow e^+e^-\gamma}}{\Gamma_{tot}} + \frac{\Gamma_{\pi^0 \rightarrow \gamma\gamma} P(\gamma \rightarrow e^+e^-)}{\Gamma_{tot}}, \quad (144)$$

where $P(\gamma \rightarrow e^+e^-)$ is the probability of photon conversion into e^+e^- . To measure $P(\gamma \rightarrow e^+e^-)$, the acceptance for conversion ($P(\gamma \rightarrow e^+e^-) \cdot \eta_{e^+e^-}$) is divided by the acceptance for Dalitz ($\eta_{e^+e^-}$). Fig. 110 shows that the conversion probability depends on incident photon energy. A maximum probability of 8% per-photon was measured, shown in Fig 110b top left plot. Therefore



(a)



(b)

FIG. 110. Probability of Photon Conversion vs. $\cos \theta$ for various values of E_γ . The maximum probability for this analysis was measured in the top left plot of b.

$$\frac{\Gamma}{\Gamma_{tot}} = \frac{\Gamma_{\pi^0 \rightarrow e^+e^-\gamma}}{\Gamma_{tot}} + \frac{\Gamma_{\pi^0 \rightarrow \gamma\gamma} P(\gamma \rightarrow e^+e^-)}{\Gamma_{tot}} = 0.09, \quad (145)$$

and has error

$$\sigma_f = \sqrt{\left(\frac{1}{\Gamma_{tot}}\right)^2 (\sigma_{\pi^0 \rightarrow e^+e^-\gamma}^2 + \sigma_{\pi^0 \rightarrow \gamma\gamma}^2)} = 0.0037. \quad (146)$$

The energy and $\cos\theta$ dependence of the conversion is accounted for in the acceptance, which is E_γ and $\cos\theta$ bin-dependent.

TABLE 25. Branching ratio and errors used in $\frac{d\sigma}{d\cos\theta_{C.M.}^{*\pi^0} d\phi}$ measurements

Quantity	Value	Error
$\Gamma_{\pi^0 \rightarrow \gamma\gamma}$	0.98823	0.00034
$\Gamma_{\pi^0 \rightarrow e^+e^-\gamma}$	0.01174	0.00035
$\frac{\Gamma}{\Gamma_{tot}}$	0.13	0.0037

5.4.2 CUT BASED SYSTEMATIC UNCERTAINTY

The procedure to determine the systematic uncertainty of the cuts placed on the various kinematic fits was first to calculate an acceptance with a different cut, then to calculate a new total cross-section measurement applying the different cut to the data. The total cross-section was computed at various photon beam energies. Lets denote the original measured total cross-section as Ξ_1 and the new total cross-section determined by the new cut as Ξ_n , then the systematic error was calculated as.

$$\sigma_{cut} = \frac{|\Xi_1 - \Xi_n|}{\Xi_1} \quad (147)$$

Some systematic uncertainty depended on the photon energy. All cut based systematics were performed individually, meaning when a cut was changed, the remaining cuts retained their original value, see Table 26 for the values of the cuts that were changed to calculate the systematic error.

TABLE 26. Different Cuts to analyze systematics

Cut	Original	Adjusted	Uncertainty
2-C Fit Pull Probability	1%	10%	0.0219
1-C Fit Pull Probability	1%	10%	$0.00216 + 0.01083E_\gamma$
4-C Fit Pull Probability	1%	10%	0.00031
Missing Energy Cut	75 MeV	100 MeV	0.02781

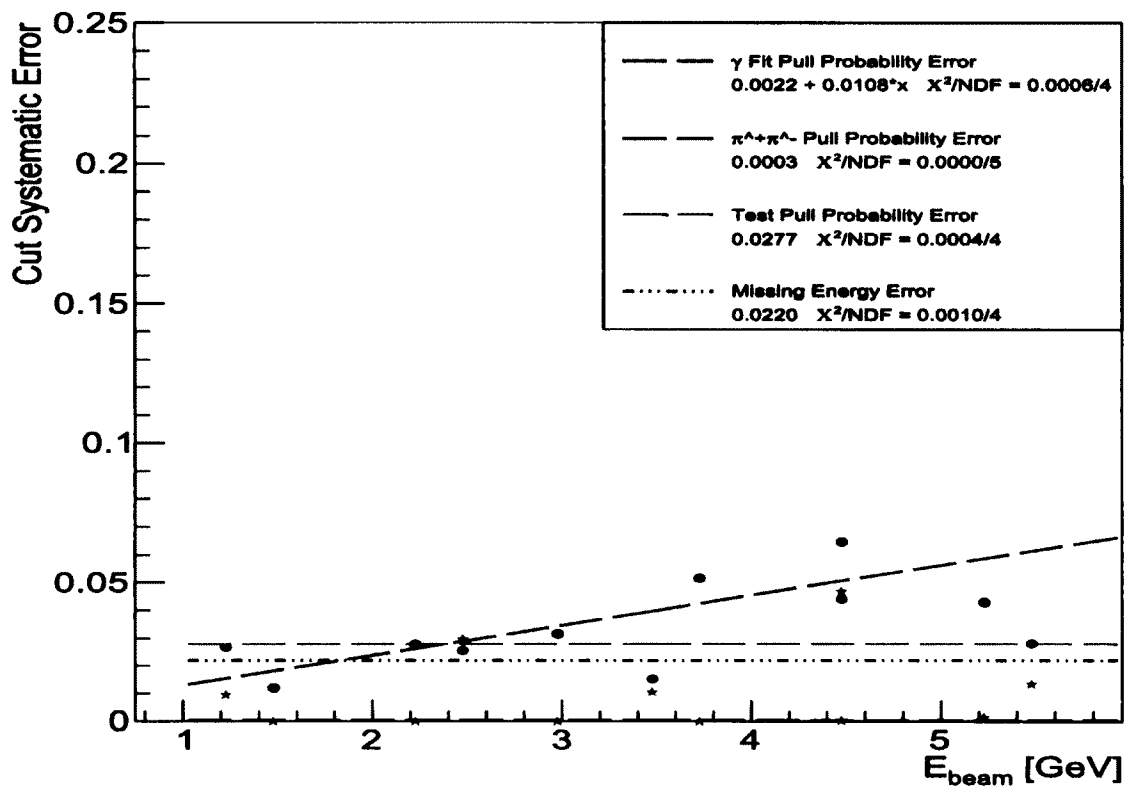


FIG. 111. Plot showing the contribution of the data cut systematic error and the incoming beam dependence of the error.

5.4.3 PHOTON FLUX SYSTEMATIC UNCERTAINTY

The photon flux calculation should be consistent throughout the experiment. If the flux measurement is not consistent due to corrections made with the live-time, beam corrections or fractional difference in the reported current to the actual current during the photon flux normalization run then a systematic uncertainty would be produced. To study this effect we divided the g12 run period into four groups. The change between group 2 and group 3 was at the run in which the tagger hysteresis was not present, see Sec 4.2.2. Table 27 lists the run groups used for this study.

TABLE 27. List of run groups used to determine photon flux systematic error.

Run Group	Range	Total Runs
1	56605-56798	116
2	56799-56980	116
3	56992-57173	116
4	57174-57317	115

The procedure to determine the systematic error, σ , of the flux is to calculate the accepted and flux corrected yield, Υ^c , for each run group and compare Υ^c to the average accepted and flux corrected yield of all 4 run groups, μ^c . After σ is calculated, it was normalized to $N\mu^c$ as to represent the error as a percentage, which later is added in quadrature and multiplied by the measured cross section to determine the appropriate error.

$$\sigma_{group} = \sqrt{\sum_{i=1}^{N=4} (\Upsilon_i^c - \mu^c)^2}, \quad (148)$$

where

$$\mu^c = \frac{1}{N} \sum_{i=1}^{N=4} \Upsilon_i^c \quad (149)$$

$$\sigma_{group}^{normalized} = \frac{\sigma_{group}}{N\mu^c} \quad (150)$$

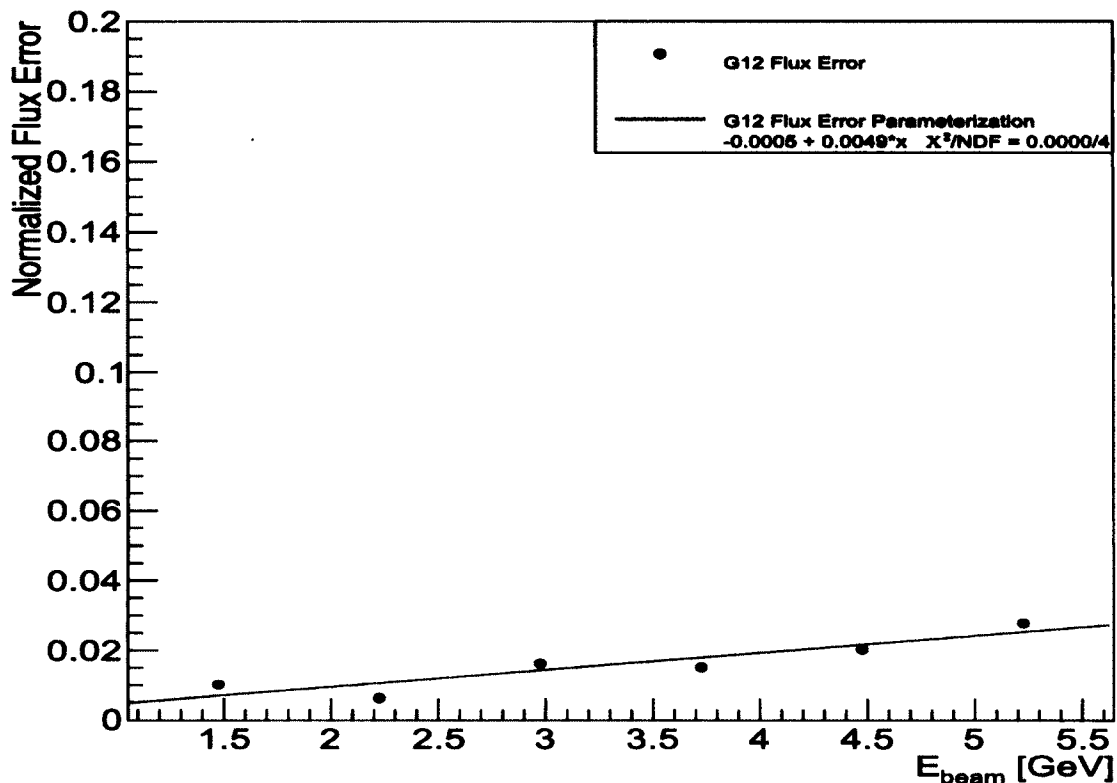


FIG. 112. Plot showing the contribution of the flux systematic error and the incoming beam dependence of the error.

5.4.4 DETECTOR EFFICIENCY SYSTEMATIC UNCERTAINTY

Each sector in CLAS can be treated as an individual detector, with its own efficiency and resolution. A systematic uncertainty could arise if one or more of the sectors is not simulated properly. The procedure to determine the systematic error, σ , of the sector is to calculate the accepted corrected yield, Υ^c , for each sector and compare Υ^c to the average accepted corrected yield of all 6 sectors, μ^c . After σ is calculated, it was normalized to $N\mu^c$ as to represent the error as a percentage, which later is multiplied by the measured cross section to determine the appropriate error.

$$\sigma_{\text{sector}} = \sqrt{\sum_{i=1}^{N=6} (\Upsilon_i^c - \mu^c)^2}, \quad (151)$$

where

$$\mu^c = \frac{1}{N} \sum_{i=1}^{N=6} \Upsilon_i^c \quad (152)$$

$$\sigma_{sector}^{normalized} = \frac{\sigma_{sector}}{N\mu^c} \quad (153)$$

This calculation was performed for various bins of incoming beam energy to determine the beam energy dependence (see Fig. 113).

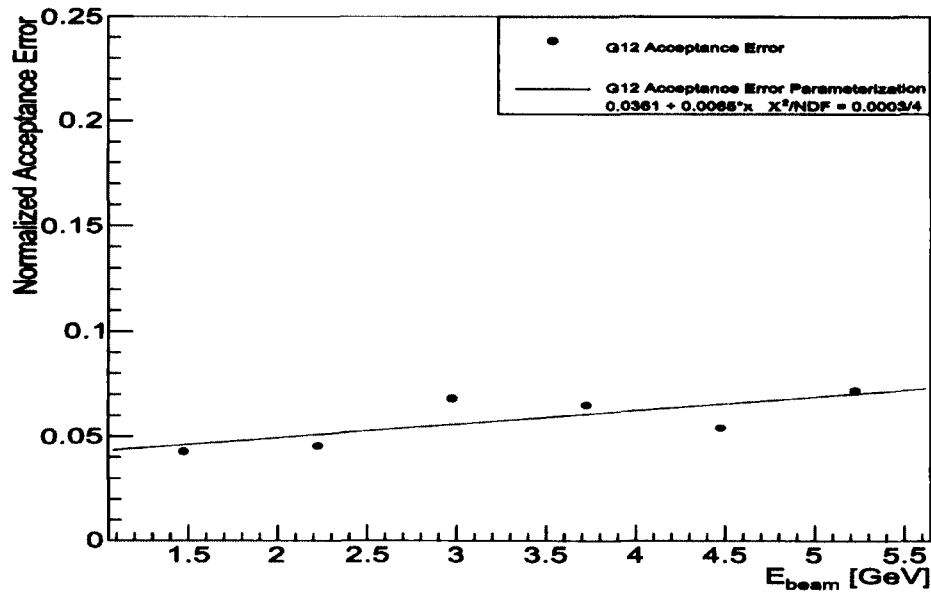


FIG. 113. The sector systematic uncertainty as a function of the incoming photon energy.

The sector systematic uncertainty is consistent with the extracted sector systematic uncertainty from the g11 data set [28](see Fig. 114).

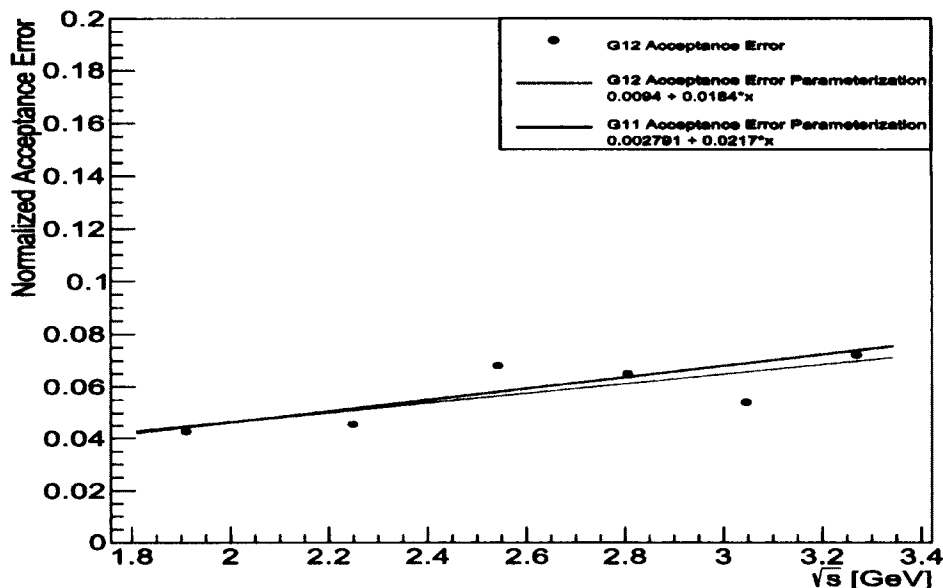


FIG. 114. Comparison of sector systematic uncertainty to g11 measurement.

5.4.5 Z-VERTEX CUT SYSTEMATIC UNCERTAINTY

The systematic uncertainty of the z -vertex cut was analyzed by varying the initial vertex cut from $-110 \leq z \leq -70$ to $-109 \leq z \leq -71$ for both data and MC. Afterward the procedure for determining the systematic was identical to the method used to determine the “Cut Based Systematic Uncertainty”. The systematic uncertainty from varying the z was 0.0041, shown in Fig. 115

5.4.6 TARGET SYSTEMATIC UNCERTAINTY

Since the systematic on the density is 0.02%, see Sec 4.11, the maximum systematic on the target is due to uncertainty in the length on the target which is $40 \text{ cm} \pm 0.2 \text{ cm}$. A total systematic on the target was assign to be 0.5%.

5.4.7 TOTAL SYSTEMATIC UNCERTAINTY

The total systematic uncertainty along with a list of the individual systematics is presented in this subsection. The calculation of the total systematic error is

$$\sigma_{tot}^{sys} = \sqrt{\sum_{i=1}^M \sigma_i^2} \quad (154)$$

Figure 115 is a pictorial version of Table 28.

TABLE 28. Systematic errors used in $\frac{d\sigma}{d \cos \theta_{C.M.}^0 d\phi}$ measurements

Systematic	Error
Sector	$0.0361 + 0.0065E_\gamma$
Flux	$-0.00051 + 0.00491E_\gamma$
Missing Energy Cut	0.02781
2-C Fit Pull Probability	0.0219
1-C Fit Pull Probability	$0.00216 + 0.01083E_\gamma$
4-C Fit Pull Probability	0.00031
Target	0.005
Branching Ratio	0.0037
Fiducial Cut	0.024
z-vertex Cut	0.0041
Total	$\sqrt{0.0032 + 0.00051E_\gamma + 0.000184E_\gamma^2}$

Systematics

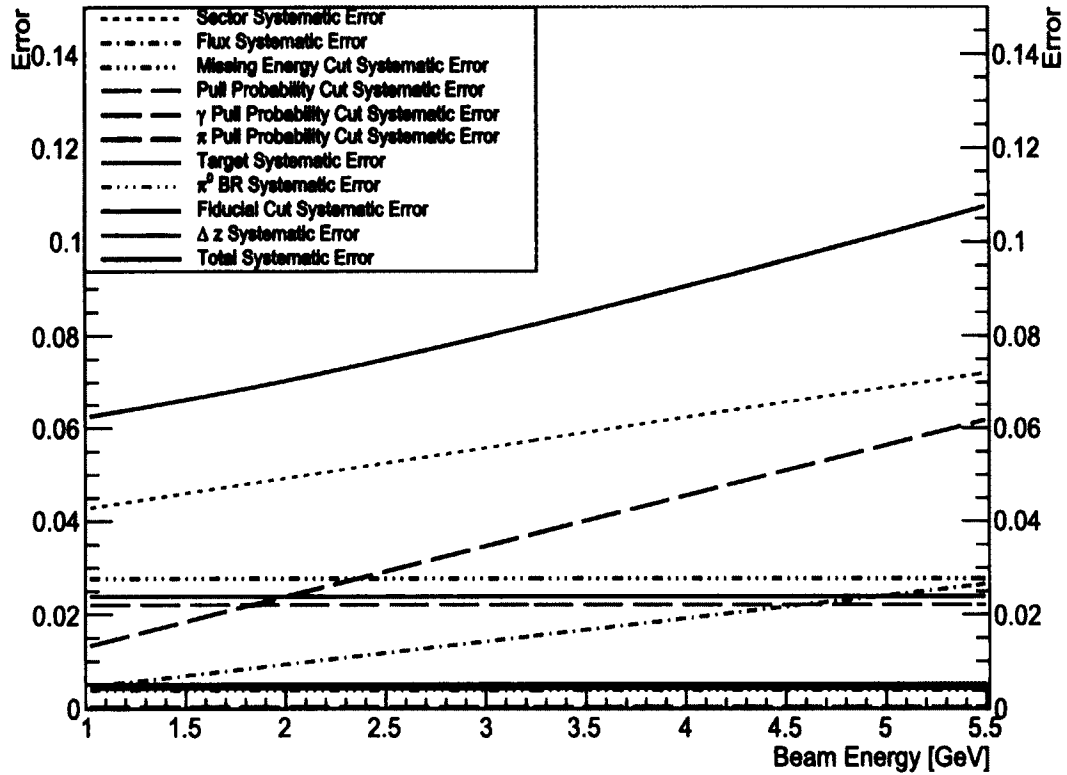


FIG. 115. The contribution of all systematic uncertainties.

5.5 COMPARISON TO WORLD DATA AND SAID FITS

This section will discuss comparisons of our data with SAID fits and the GPD handbag model. The SAID parameterization, discussed in Sec. 1.2.4, for this analysis was based upon previous data observables in conjunction with the new cross-section measurement presented in this analysis.

5.5.1 DIFFERENTIAL CROSS-SECTIONS $\frac{d\sigma}{d\Omega}$

The differential cross-sections $\frac{d\sigma}{d\Omega}$ are illustrated in Figs. 116, 117, 118, 119. A brief discussion is written in Sec. 5.5.5.

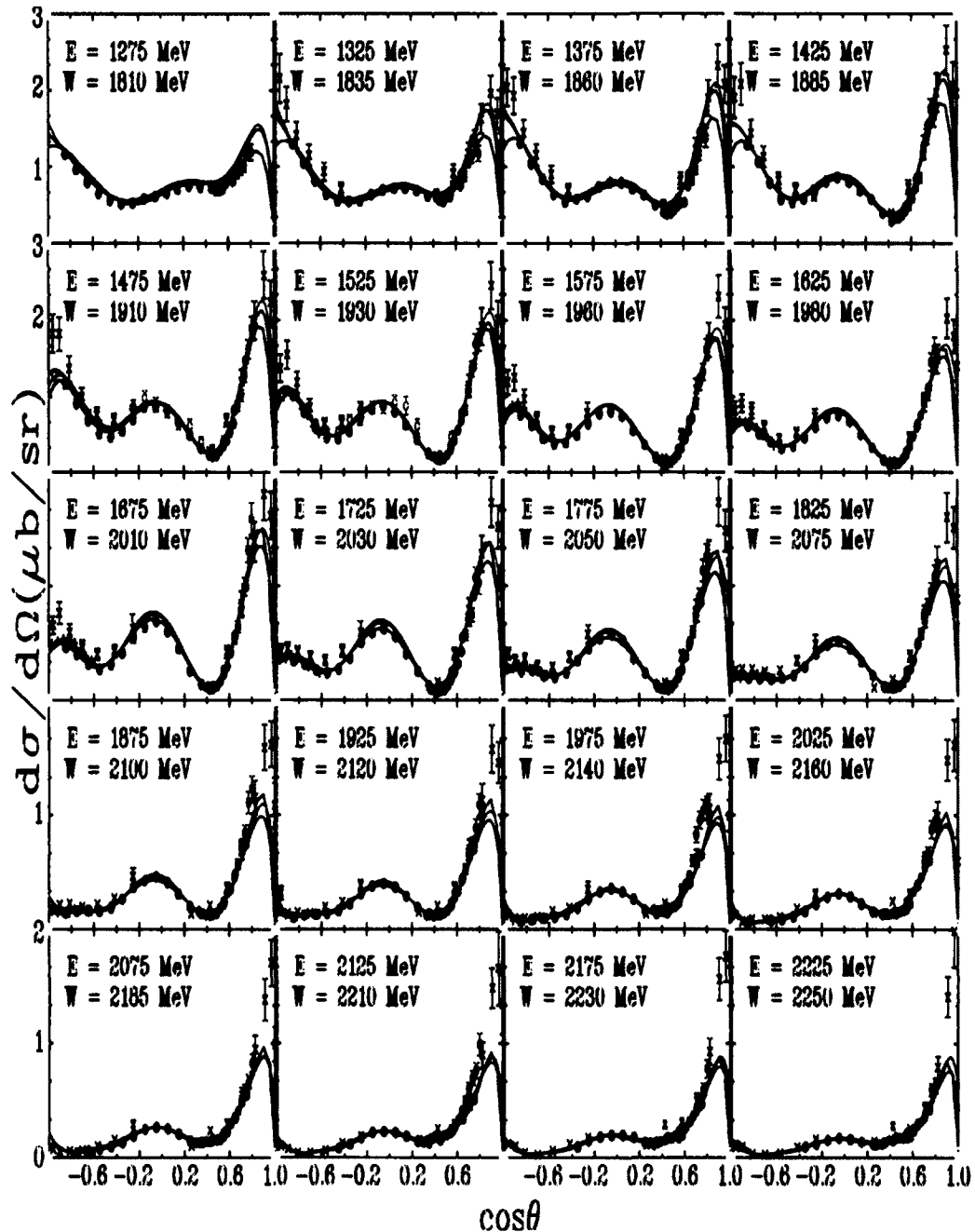


FIG. 116. (Color online) The π^0 proton photoproduction cross section, $(d\sigma/d\Omega)$, at $E_\gamma = 1.275 - 2.225$ GeV versus $\cos\theta$ where θ is the pion center-of-mass production angle. Photon energy is indicated by E , while the center-of-mass total energy is indicated by W . Red solid (blue solid) lines show the SAID KU14 (DU13 [56]) calculations. Black solid lines give the BG2011-02 BnGa [57] predictions. Experimental data are from the current measurement (red filled circles), CLAS [58] (black filled circles), GRAAL [59] (magenta open circles), LEPS [60] (blue plus), CB-ELSA [61] [55] (green crosses) and previous bremsstrahlung measurements [62] (black open circles). Plotted uncertainties are statistical. The plotted points from previously published experimental data are those data points within ± 3 MeV of the photon energy indicated on each panel.

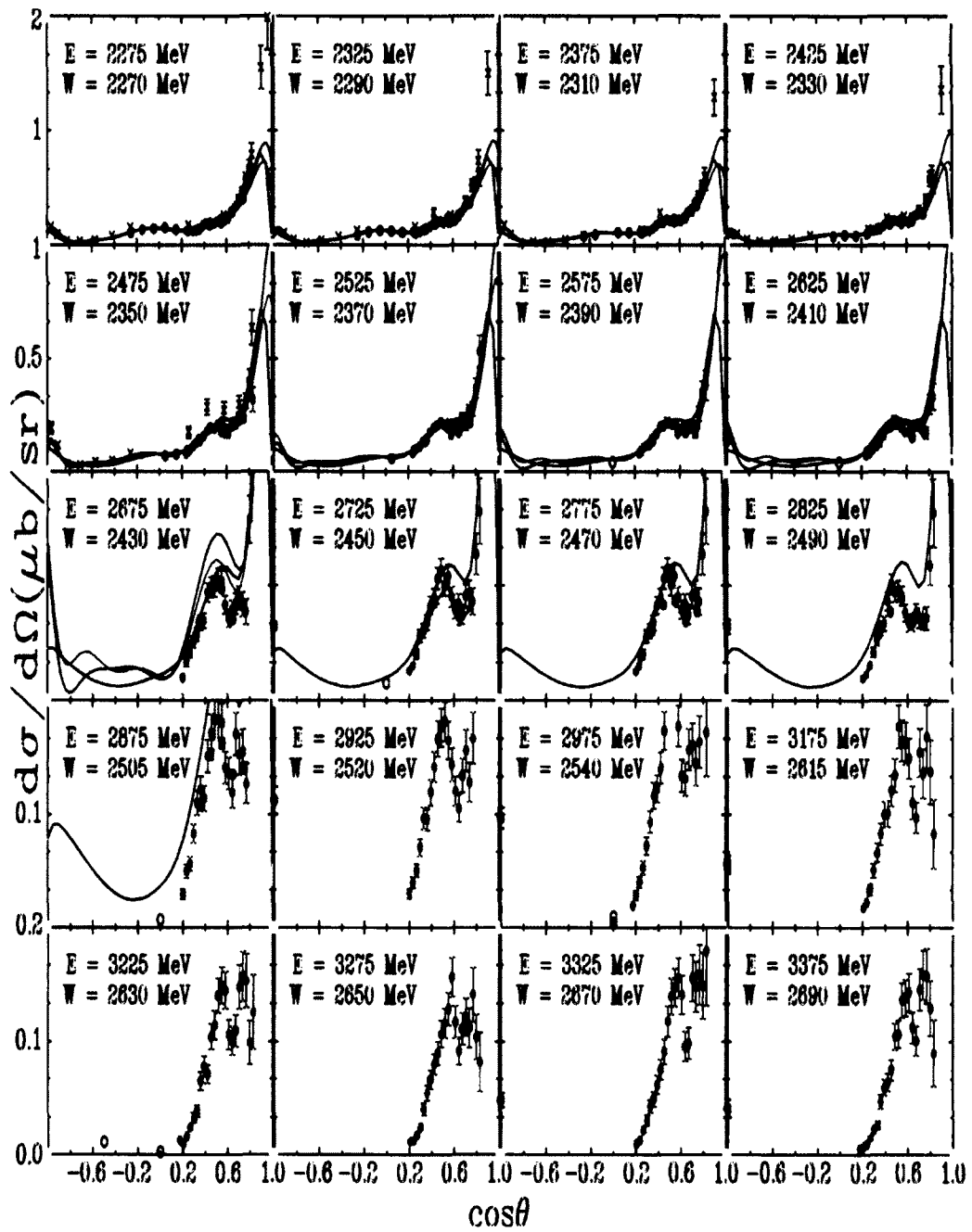


FIG. 117. (Color online) The π^0 proton photoproduction cross section at $E_\gamma = 2.275 - 3.375$ GeV versus cosine of the pion center-of-mass production angle. Notation as in Fig. 116.

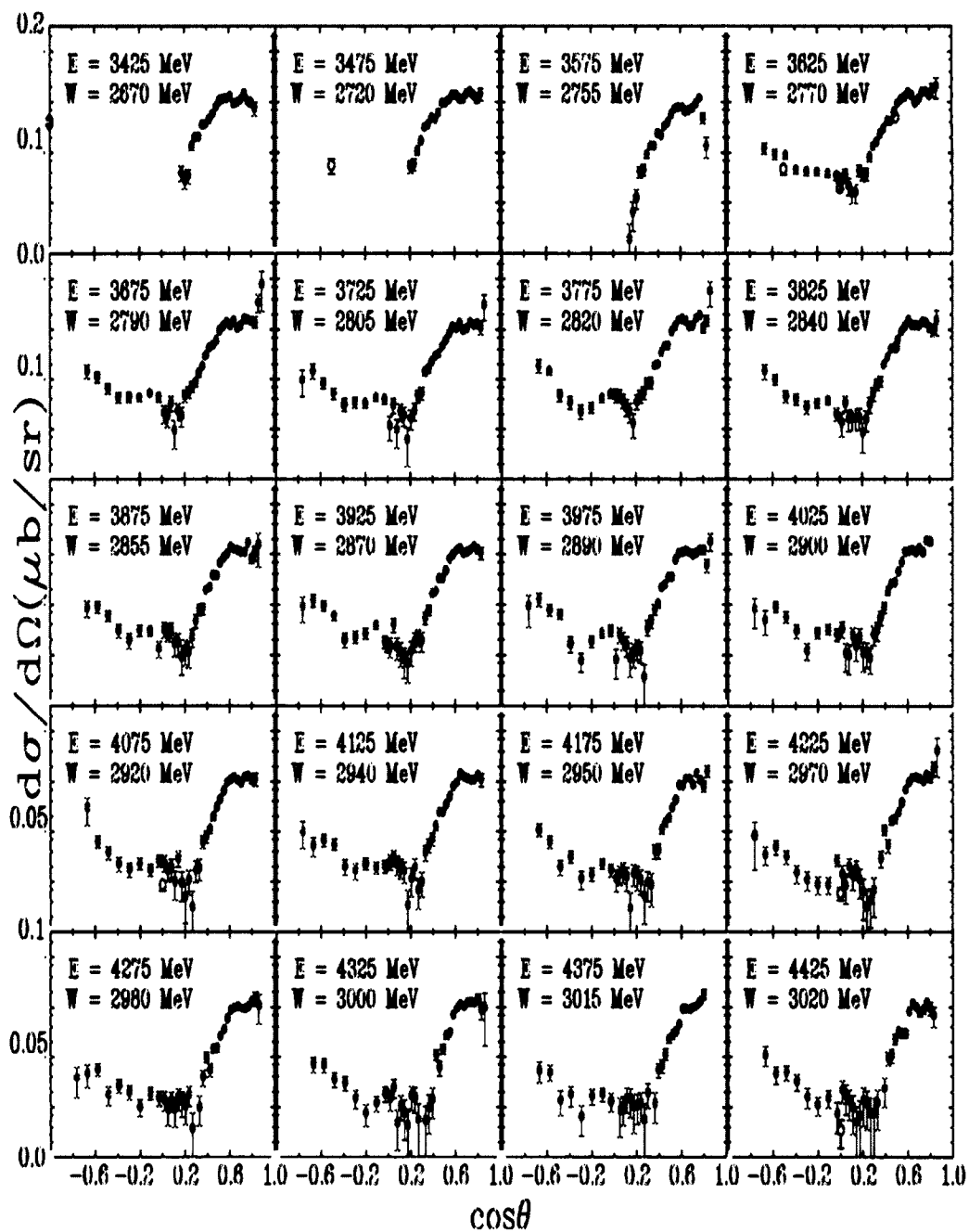


FIG. 118. (Color online) The π^0 proton photoproduction cross section at $E_\gamma = 3.425 - 4.425$ GeV versus cosine of the pion center-of-mass production angle. Notation as in Fig. 116.

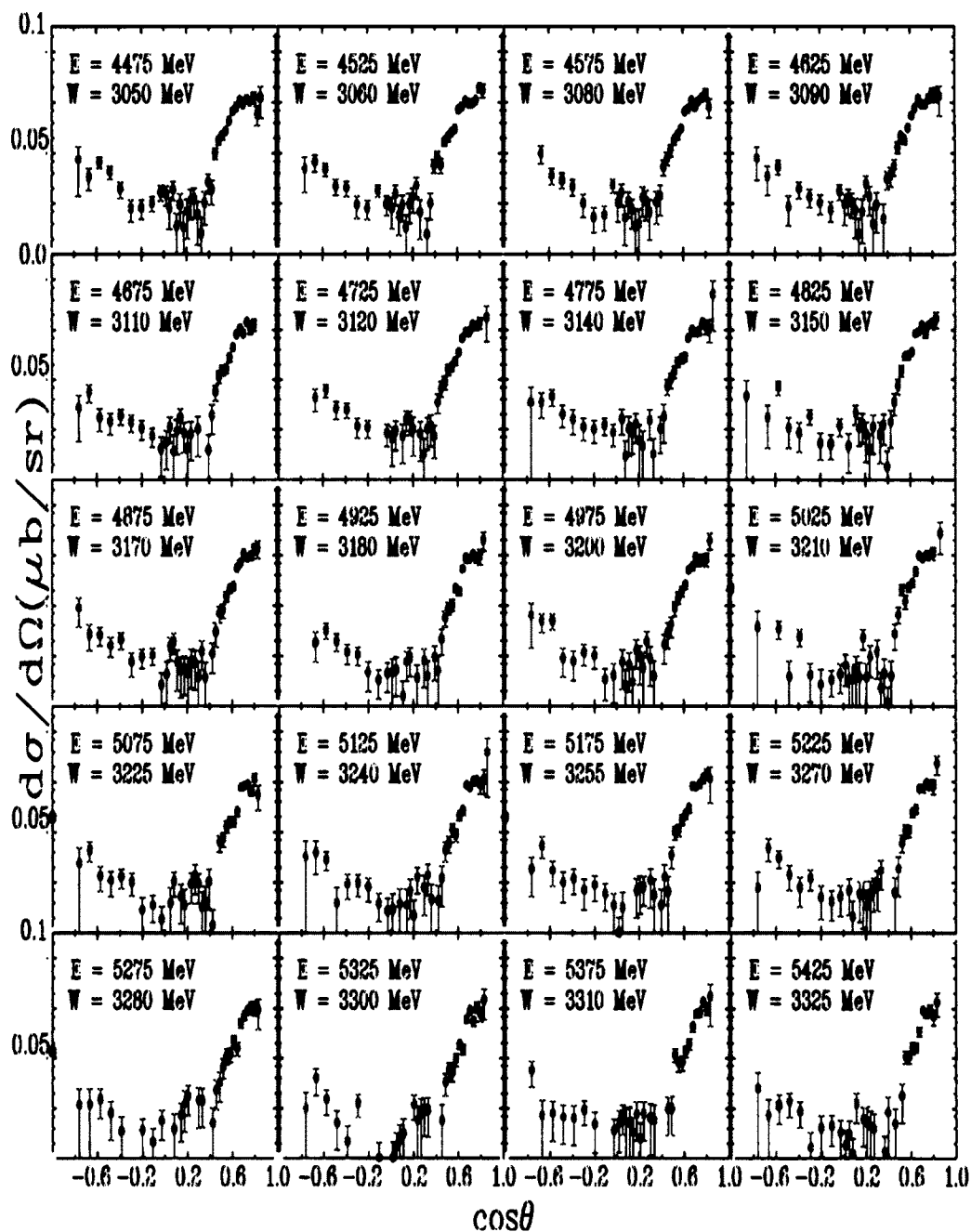


FIG. 119. (Color online) The π^0 proton photoproduction cross section at $E_\gamma = 4.475 - 5.425$ GeV versus cosine of the pion center-of-mass production angle. Notation as in Fig. 116.

5.5.2 EXCITATION FUNCTIONS

The excitation functions $\frac{d\sigma}{d\Omega}$ at fixed θ are illustrated in Figs. 120, 121. A brief discussion is written in Sec. 5.5.5.

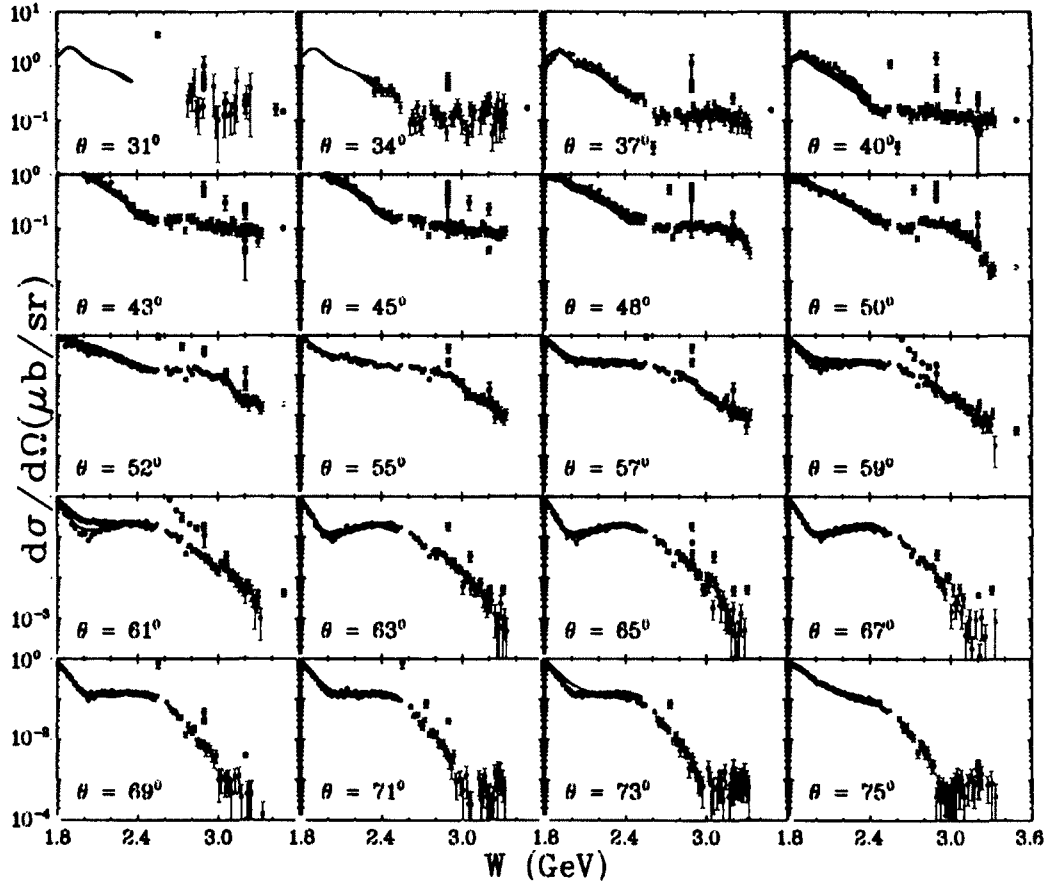


FIG. 120. (Color online) Fixed angle excitation functions of the π^0 photoproduction cross section, $(d\sigma/d\Omega)$, off the proton at $\theta = 31 - 75^\circ$ versus center-of-mass total energy W . The pion center-of-mass production angle is shown. Plotted uncertainties are statistical. The plotted points from previously published experimental data are those data points within $\pm 2^\circ$ of pion center-of-mass production angle indicated on each panel. Notation as in Fig. 116.

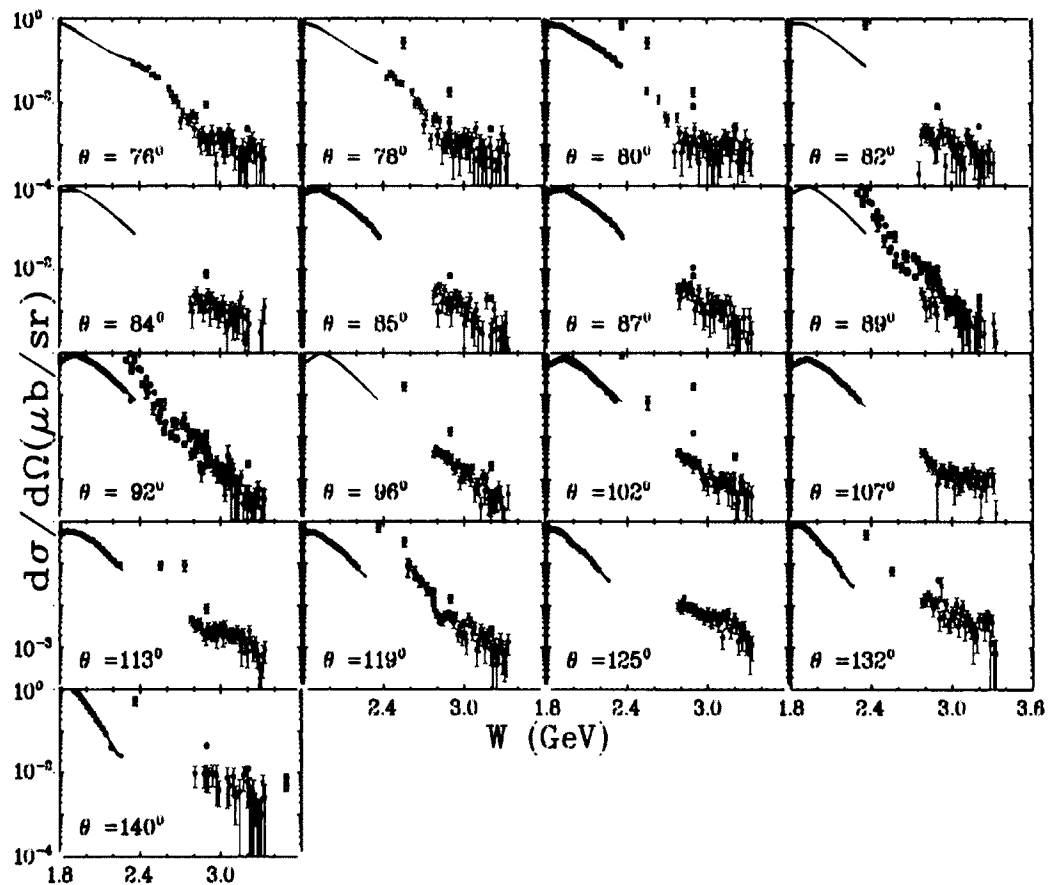


FIG. 121. (Color online) Fixed angle excitation functions of the π^0 photoproduction cross section, $(d\sigma/d\Omega)$, off the proton at $\theta = 76 - 140^\circ$ versus center-of-mass total energy W . Notation as in Fig. 116.

5.5.3 T -DEPENDENCE

The t -dependence of $\frac{d\sigma}{dt}$ at fixed E_γ are illustrated in Figs. 122, 123, 124, 125. A brief discussion is written in Sec. 5.5.5.

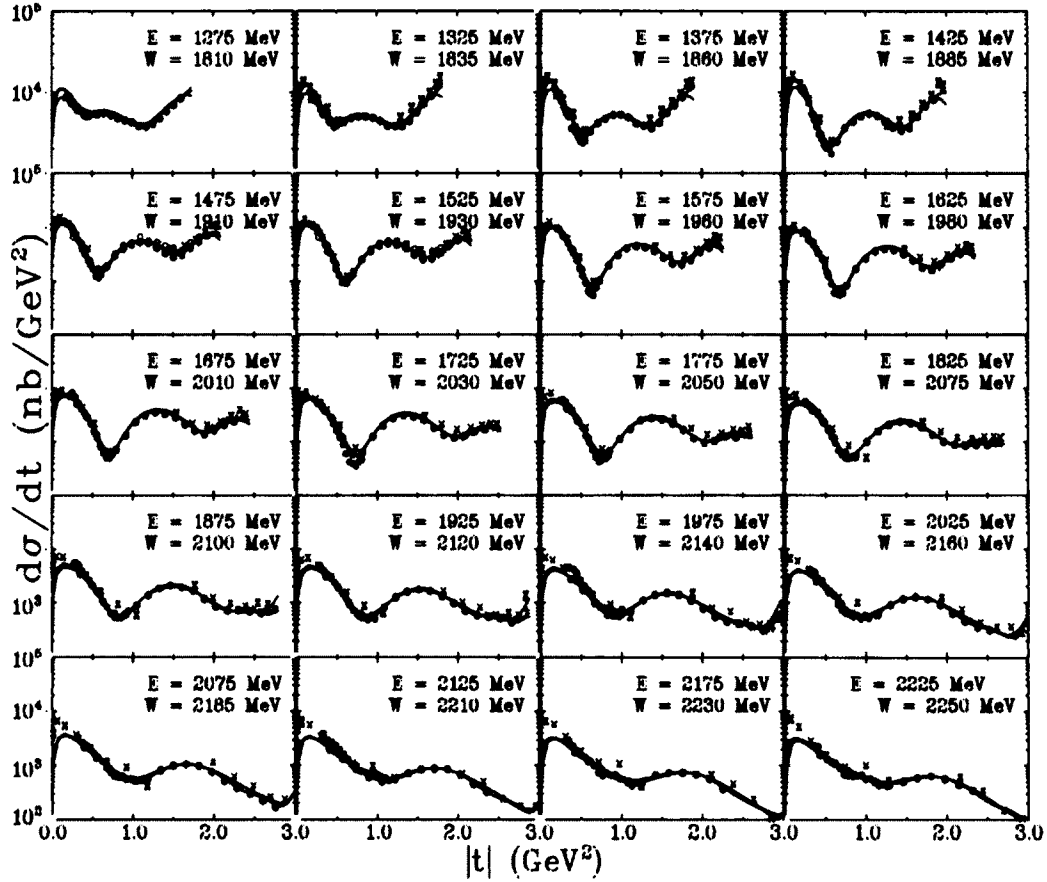


FIG. 122. (Color online) π^0 photoproduction cross section, $(d\sigma/dt)$, off the proton at $E_\gamma = 1275 - 2225$ MeV versus momentum transfer t . Notation as in Fig. 116.

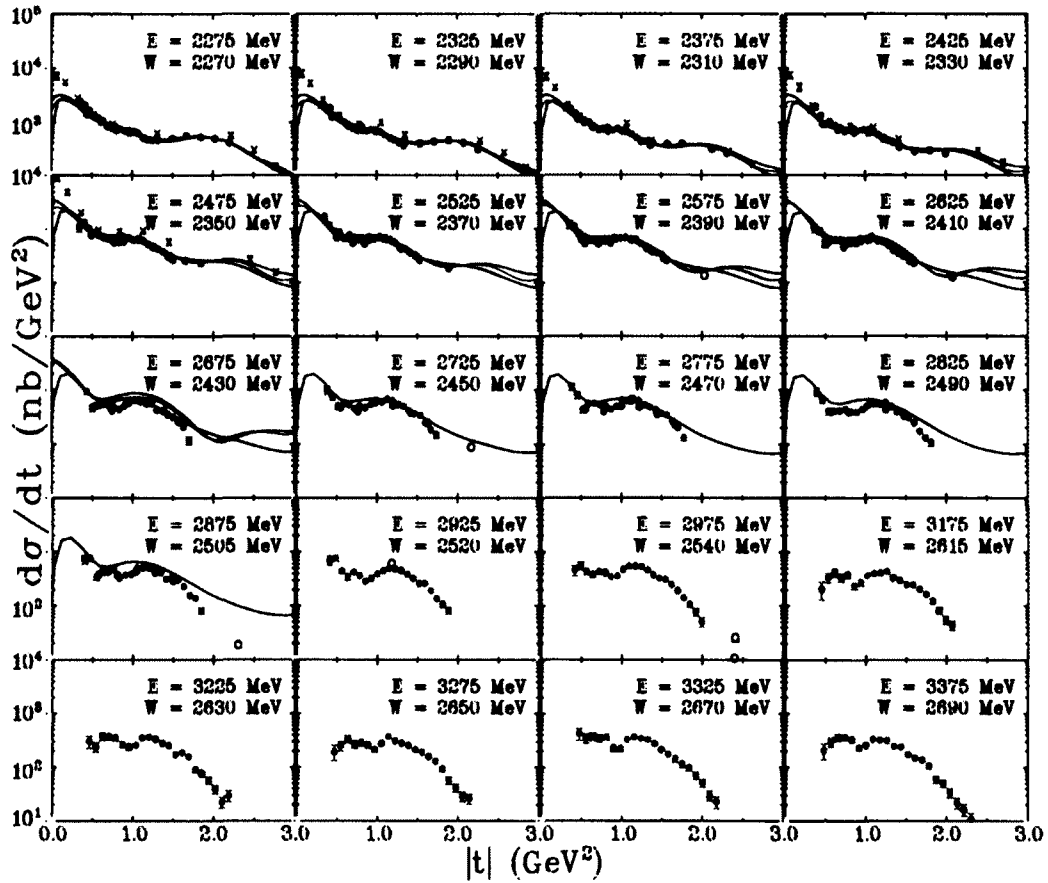


FIG. 123. (Color online) π^0 photoproduction cross section, $(d\sigma/dt)$, off the proton at $E_\gamma = 2275 - 3375$ MeV versus momentum transfer t . Notation as in Fig. 116.

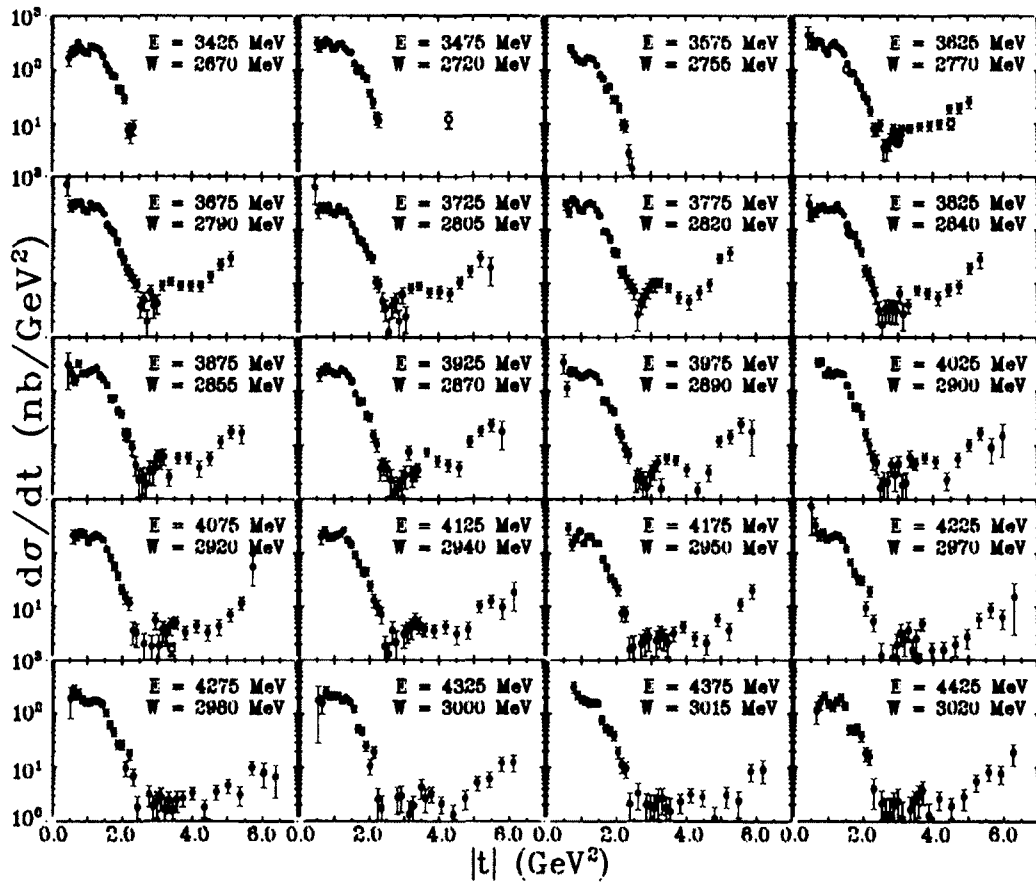


FIG. 124. (Color online) π^0 photoproduction cross section, $(d\sigma/dt)$, off the proton at $E_\gamma = 3425 - 4425$ MeV versus momentum transfer t . Notation as in Fig. 116.

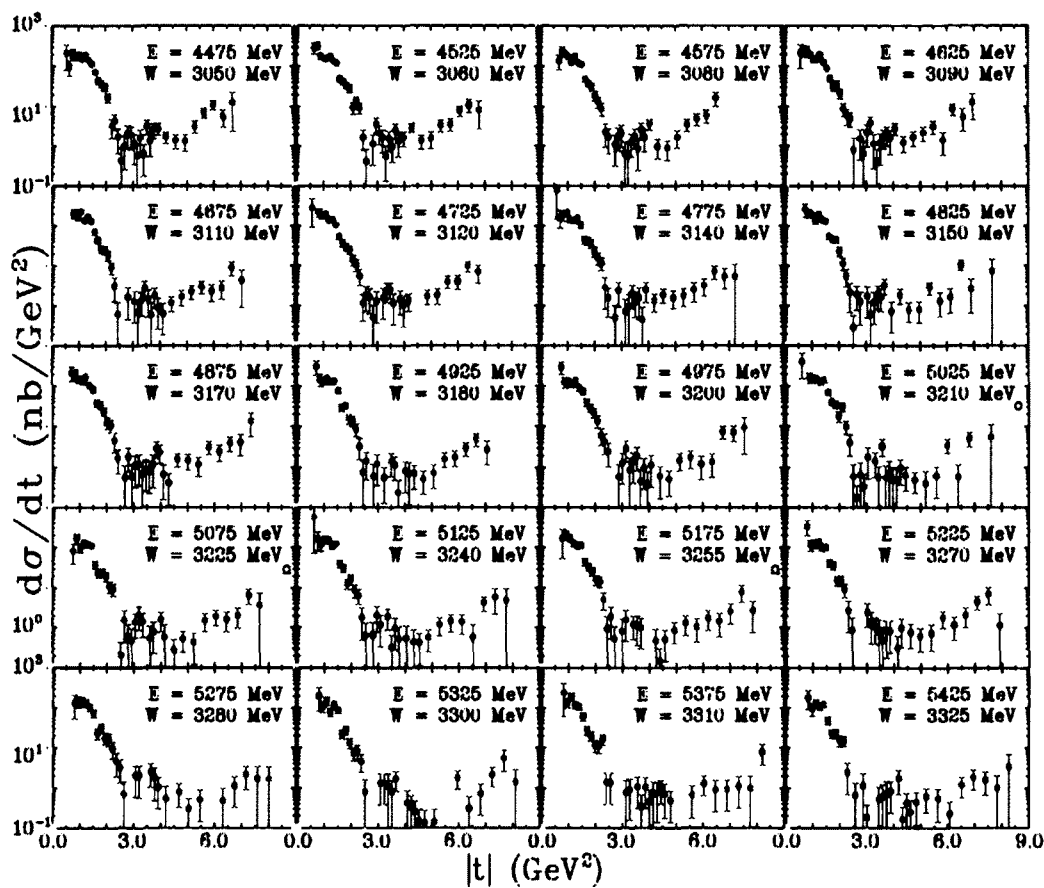


FIG. 125. (Color online) π^0 photoproduction cross section, $(d\sigma/dt)$, off the proton at $E_\gamma = 4475 - 5425$ MeV versus momentum transfer t . Notation as in Fig. 116.

5.5.4 IMPROVEMENT TO PREVIOUS SAID FITS

CGLN Amplitudes

To demonstrate the impact of our data on the global fit, in Fig. 126 we show, the distribution of amplitudes (see Sec.1.2.3) at one particular pion production angle $\Theta_{\pi^0}^{CM} = 60^\circ$ as a function of W . The blue lines are results of the fit to world data and the red lines are solutions with our data included. The dashed lines are for imaginary parts of amplitudes. For the real part of amplitudes the blue (dashed-dotted) lines are results of the fit to previous data and red (solid) are results of the fit with our data included. Vertical arrows show positions of N^* resonances listed as 4^* -resonances in PDG. As one can see, the main features of previous solution are preserved, however the strength of different groups of resonances are affected and for some the contributions almost negligible, questioning their overall existence.

Detailed amplitude analysis of the world data with the inclusion of our new data in entire kinematic range at all angles and invariant masses available will allow to constrain positions, Breit-Wigner widths and couplings of different resonances as well as dismiss and/or observe missing resonance states with high statistical confidence.

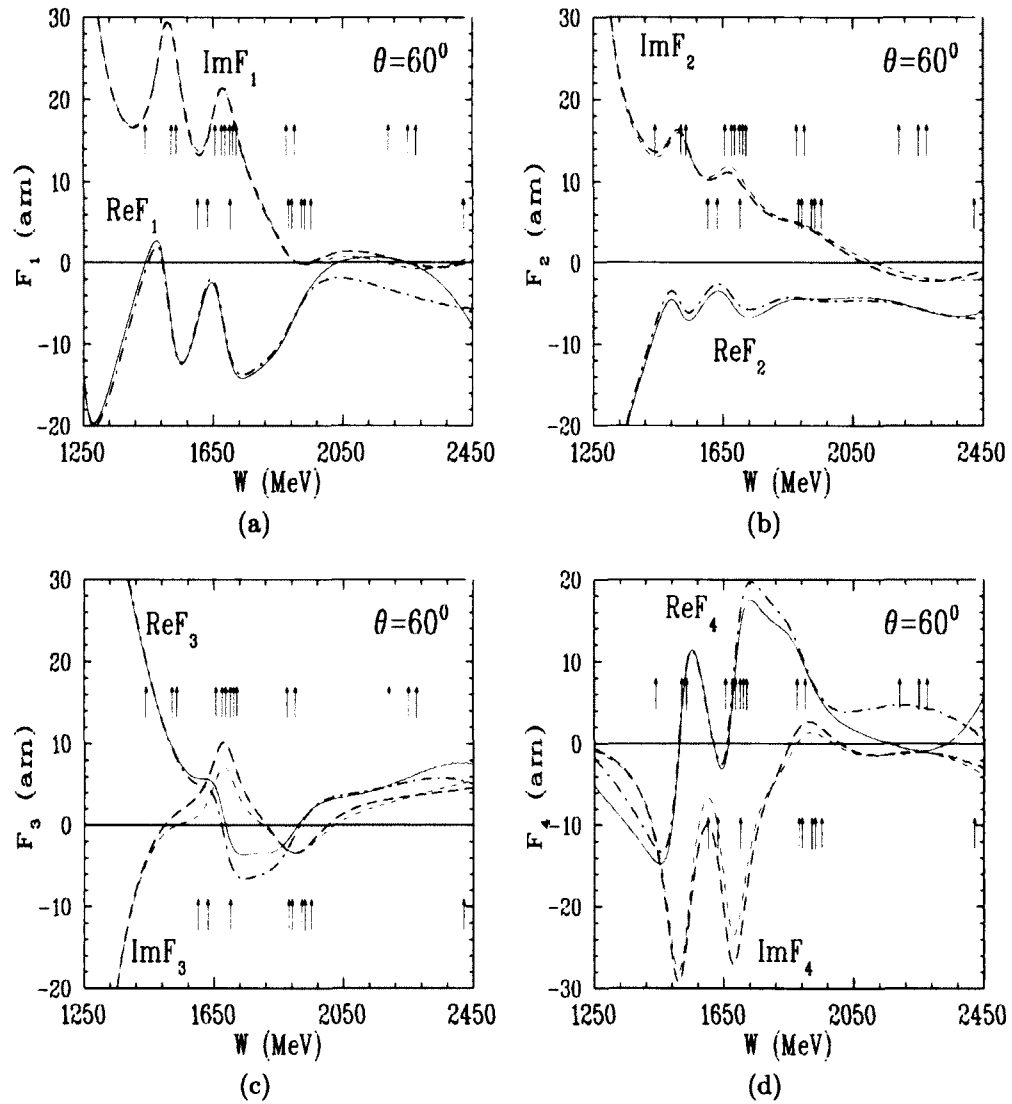


FIG. 126. (Color online) CGLN amplitude [8] at $\theta = 60^\circ$. Vertical arrows indicate resonance energies W_R (4^* -resonances) [4]. Notation as in Fig. 116.

χ^2 Improvements

The measured cross-section presented in this analysis yielded an improvement to the SAID fit. This improvement, in the form of a χ^2/dp , can be seen in Fig. 127, where the new cross-section measurement is depicted in red while the previous is depicted in blue. Decreasing the χ^2/dp reflects the “goodness” of fit and overall quality of fitting the data. This is important because if a fit determines a resonance or change in amplitude, the quality of the fit determines the accuracy of the of the solution.

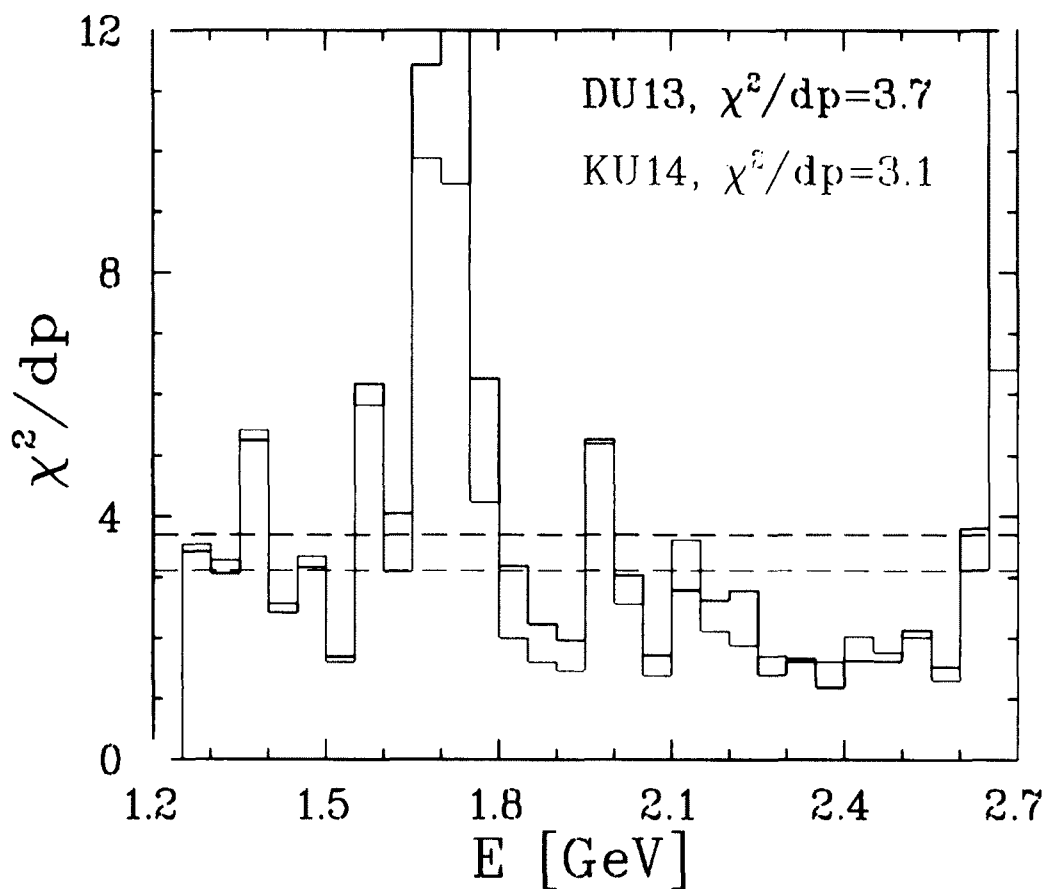


FIG. 127. Energy dependence of the χ^2/dp comparison to previous SAID fits. Blue points depict previous DU13 solution, while the red points depict the new KU14 solution.

5.5.5 DISCUSSION OF SAID FITS AND COMAPRISION TO WORLD DATA

This measurement agrees with existing world data at low energy where there are numerous previous measurements. At higher energies there appears to be partial disagreement

with [62] in which this data was taken from untagged bremsstrahlung beam. This disagreement can be seen in some of the low angle θ excitation functions in Sec. 5.5.2. However, with the same data presented in [62] there is agreement, noticeably at angles $\theta = 89^\circ$ and $\theta = 92^\circ$. Since the excitation function measurements performed in this analysis agree well in the low energy domain and also the data is congruent throughout the θ spectrum, further investigation is needed into the method of [62] to understand where or why the discrepancy exists.

5.5.6 COMPARISON WITH THEORY

The handbag model calculations by Kroll *et al.* [1] does not agree with the present data as seen in Fig. 128. There is no supporting material to explain why this model does not work well. Future models using Regge-parametrization are currently being formulated independently of this analysis. These high energy π^0 cross-sections will be the basis for all future models.

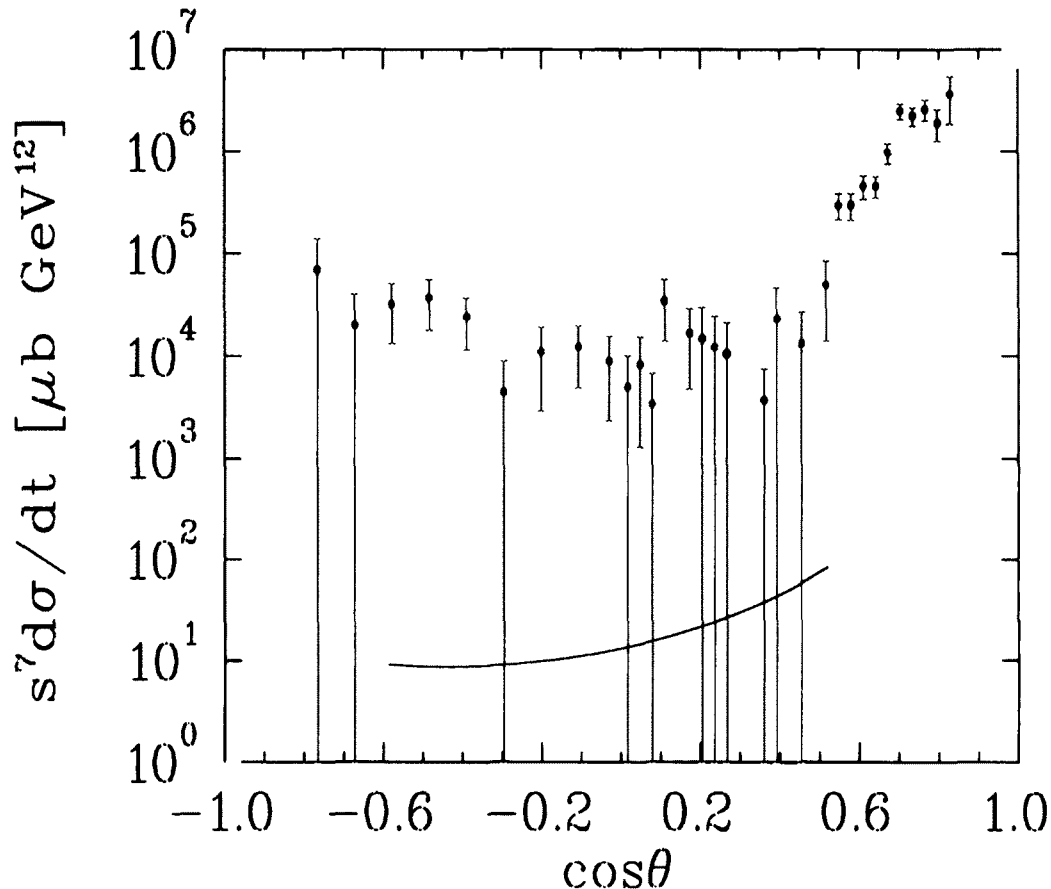


FIG. 128. Comparison of the π^0 differential cross section photoproduction data to GDP handbag model. Experimental data at $s = 11.08 \text{ GeV}^2$ are from the current (red filled circles). The theoretical prediction at $s = 10 \text{ GeV}^2$ by Kroll *et al.* [1] is given by blue solid line.

5.6 CONCLUSIONS

This manuscript explained the procedure of collecting data in the CLAS detector for the $g12$ experiment. Data corrections, kinematic fitting and fiducial cuts were used to clean the data to the order of $\approx 98\%$ signal. Differential cross-sections in two representation, $\frac{d\sigma}{d\Omega}$ and $\frac{d\sigma}{dt}$, were given along with comparisons to the existing world data, comparison existing Bonn-Gatchina fits and new SAID parameterization fits. The cross-sections measured in this analysis agreed well with the existing world data for low incident beam energies, while there was a slight discrepancy with the previous limited high energy cross-sections. The fits using the SAID parameterization yielded a χ^2/dp lower than previous existing fits. The data set explained in this analysis is now 10% of the world data for π^0 photoproduction.

More theory is need to properly explain π^0 production at incident photon beam energies higher than 2.8 GeV.

BIBLIOGRAPHY

- [1] Han Wen Huang and Peter Kroll. Large momentum transfer electroproduction of mesons. *Eur.Phys.J.*, C17:423–435, 2000.
- [2] Wikipedia. Pseudoscalar meson — wikipedia, the free encyclopedia, 2013. [Online; accessed 16-September-2013].
- [3] J.L. Goity, A.M. Bernstein, and B.R. Holstein. The Decay $\pi^0 \rightarrow \gamma\gamma$ to next to leading order in chiral perturbation theory. *Phys.Rev.*, D66:076014, 2002.
- [4] K.A. Olive et al. Review of particle physics. *Phys. Rev. C*, 38:090001, 2014.
- [5] J.M. Butterworth and M. Wing. High energy photoproduction. *Rept.Prog.Phys.*, 68:2773–2828, 2005.
- [6] Richard A. Arndt, Ron L. Workman, Zhujun Li, and L. David Roper. Pion photoproduction resonance couplings in the second resonance region. *Phys. Rev. C*, 42:1864–1866, Nov 1990.
- [7] R. L. Walker. Phenomenological analysis of single-pion photoproduction. *Phys. Rev.*, 182:1729–1748, Jun 1969.
- [8] G. F. Chew, M. L. Goldberger, F. E. Low, and Y. Nambu. Relativistic dispersion relation approach to photomeson production. *Phys. Rev.*, 106:1345–1355, Jun 1957.
- [9] Kenneth M. Watson. The hypothesis of charge independence for nuclear phenomena. *Phys. Rev.*, 85:852–857, Mar 1952.
- [10] R. G. Moorhouse, H. Oberlack, and A. H. Rosenfeld. Analysis of π^+ , π^- , and π^0 photoproduction from the first through the third resonance region. *Phys. Rev. D*, 9:1–41, Jan 1974.
- [11] Institute of nuclear studies of the george washington university database.
- [12] Xiang-Dong Ji. Gauge-Invariant Decomposition of Nucleon Spin. *Phys.Rev.Lett.*, 78:610–613, 1997.
- [13] Xiangdong Ji. Deeply virtual compton scattering. *Phys. Rev. D*, 55:7114–7125, Jun 1997.
- [14] A.V. Radyushkin. Scaling limit of deeply virtual Compton scattering. *Phys.Lett.*, B380:417–425, 1996.
- [15] M. Diehl, T. Feldmann, R. Jakob, and P. Kroll. Linking parton distributions to form-factors and Compton scattering. *Eur.Phys.J.*, C8:409–434, 1999.
- [16] M.E. Peskin and D.V. Schroeder. *An Introduction to Quantum Field Theory*. Advanced book classics. Addison-Wesley Publishing Company, 1995.

- [17] F. Halzen and A.D. Martin. *Quarks and leptons: an introductory course in modern particle physics*. Wiley, 1984.
- [18] Norman M. Kroll and Walter Wada. Internal pair production associated with the emission of high-energy gamma rays. *Phys. Rev.*, 98:1355–1359, Jun 1955.
- [19] Geoffrey Krafft Christoph Leemann, David Douglas. The continuous electron beam accelerator facility: Cebaf at the jefferson laboratory. *Annu. Rev. Nucl. Part. Sci.*, 51:413–450, 2001.
- [20] Wikipedia. Thomas jefferson national accelerator facility — Wikipedia, the free encyclopedia, 2004. [Online; accessed 12-June-2014].
- [21] CEBAF 2013_v2. <https://www.flickr.com/photos/jeffersonlab/12614907725/>. Accessed: 2013-06-12.
- [22] J. Goetz and D. Weygand. personal correspondance, 2009 - 2014.
- [23] H. Olsen and L. C. Maximon. Photon and electron polarization in high-energy bremsstrahlung and pair production with screening. *Phys. Rev.*, 114:887–904, 1959.
- [24] Goetz J. Ξ *Hyperon Photoproduction from Threshold to 5.4 GeV with the CEBAF Large Acceptance Spectrometer*. Doctoral, Univeristy of California, May 2010.
- [25] Sober D. I. et al. The bremsstrahlung tagged photon beam in Hall B at JLab. *Nucl. Instr. and Meth. A*, 440:263–284, 2000.
- [26] J. Li. The new tagger calibration program. JLab, March 2003.
- [27] B. A. Mecking et al. The CEBAF Large Acceptance Spectrometer (CLAS). *Nucl. Instr. and Meth. A*, 503:513, 2003.
- [28] Williams M. *Measurement of Differential Cross Sections and Spin Density Matrix Elements along with a Partial Wave Analysis for $\gamma p \rightarrow p\omega$ using CLAS at Jefferson Lab*. Doctoral, Carnegie Mellon University, May 2007.
- [29] Y. G. Sharabian et al. A new highly segmented start counter for the CLAS detector. *Nucl. Instr. and Meth. A*, 556:246–258, 2006.
- [30] P. Eugenio et al. Search for new forms of hadronic matter in photoproduction. Technical report, CLAS Analysis Proposal PR04-005, 2003.
- [31] D. Weygand et al. Study of pentaquark states in photoproduction off protons. Technical report, CLAS Analysis Proposal PR04-017, 2004.
- [32] W. Chen et al. The $\gamma p \rightarrow \pi^+ n$ single charged pion photoproduction. Technical report, CLAS Analysis Proposal PR08-003, 2008.
- [33] M. Mestayer et al. The clas drift chamber system. *Nucl. Instr. and Meth. A*, 449:81–111, 2000.

- [34] David Lawrence and Mac Mestayer. CLAS Drift Chamber Calibration: Software and Procedures. CLAS-NOTE 1999-018, 1999.
- [35] cherenkov dipole.
- [36] G. Adams et al. The clas cherenkov detector. *Nucl. Instr. and Meth. A*, 465:81–111, 2000.
- [37] C. Grupen and B. Shwartz. *Particle Detectors*. Cambridge Monographs on Particle Physics, Nuclear Physics and Cosmology. Cambridge University Press, 2008.
- [38] E. S. Smith et al. The time-of-flight system for CLAS. *Nucl. Instr. and Meth. A*, 432:265–298, 1999.
- [39] Dector-en.
- [40] M. Amarian et al. The CLAS forward electromagnetic calorimeter. *Nucl. Instr. and Meth. A*, 460, 2001.
- [41] C. Bookwalter et al. g12 analysis procedures, statistics and systematics. *CLAS-NOTE*, 2014.
- [42] Craig Bookwalter. *A SEARCH FOR EXOTIC MESONS IN $\gamma p \rightarrow \pi^+ \pi^+ \pi^- n$ WITH CLAS AT JEFFERSON LAB*. Doctoral, The Florida State University, 2012.
- [43] E. Pasyuk. Energy loss corrections for charged particles in clas. *CLAS-NOTE*, 2007-016.
- [44] I. Frohlich, I. Froehlich, Lorenzo Cazon, T. Galatyuk, V. Hejny, et al. Pluto: A Monte Carlo Simulation Tool for Hadronic Physics. *PoS, ACAT2007:076*, 2007.
- [45] K. Hicks D. Keller. Techniques in kinematic fitting. *CLAS-NOTE*, 2010-1.
- [46] Wikipedia. Crystal ball function — wikipedia, the free encyclopedia, 2013. [Online; accessed 2-September-2014].
- [47] Dmitry A Romanov. Crystal ball function, 2013. [Online; accessed 2-September-2014].
- [48] Durham Reaction DataBase. Durham reaction database, 2014.
- [49] R. Bradford and R.A. Schumacher. Liquid hydrogen density in the glc clas cryotarget. *CLAS-NOTE*, 2002-003.
- [50] R.D. McCarty, J. Hord, and H.M. Roder. *Selected Properties of Hydrogen (engineering Design Data)*. NBS monograph. U.S. Government Printing Office, 1981.
- [51] J.Ball and E. Pasyuk. Photon flux determination through sampling of "out-of-time" hits with the hall b photon tagger. *CLAS-NOTE*, 2005-002.
- [52] The g11a target cell.
- [53] Frank A. Haight. *Handbook of the Poisson Distribution*. John Wiley & Sons, 1967.

- [54] J. Beringer et al. Review of particle physics. *Phys. Rev. D*, 86:010001, 2012.
- [55] V. Crede et al. Photoproduction of Neutral Pions off Protons. *Phys.Rev.*, C84:055203, 2011.
- [56] M. Dugger et al. Beam asymmetry Σ for π^+ and π^0 photoproduction on the proton for photon energies from 1.102 to 1.862 GeV. *Phys.Rev.*, C88(6):065203, 2013.
- [57] A.V. Anisovich, E. Klempt, V.A. Nikonov, M.A. Matveev, A.V. Sarantsev, et al. Photoproduction of pions and properties of baryon resonances from a Bonn-Gatchina partial wave analysis. *Eur.Phys.J.*, A44:203–220, 2010.
- [58] M. Dugger, Barry G. Ritchie, J.P. Ball, P. Collins, Eugene Pasyuk, et al. π^0 photoproduction on the proton for photon energies from 0.675 to 2.875-GeV. *Phys.Rev.*, C76:025211, 2007.
- [59] O. Bartalini et al. Measurement of π^0 photoproduction on the proton from 550-MeV to 1500-MeV at GRAAL. *Eur.Phys.J.*, A26:399–419, 2005.
- [60] M. Sumihama, J.K. Ahn, H. Akimune, Y. Asano, W.C. Chang, et al. Backward-angle photoproduction of π^0 mesons on the proton at $E_{\gamma} = 1.5\text{-}2.4\text{-GeV}$. *Phys.Lett.*, B657:32–37, 2007.
- [61] O. Bartholomy et al. Neutral pion photoproduction off protons in the energy range $0.3\text{-GeV} < E(\gamma) < 3\text{-GeV}$. *Phys.Rev.Lett.*, 94:012003, 2005.
- [62] P. Joss. Compilation of photoproduction data above 1.2 gev, 1970.

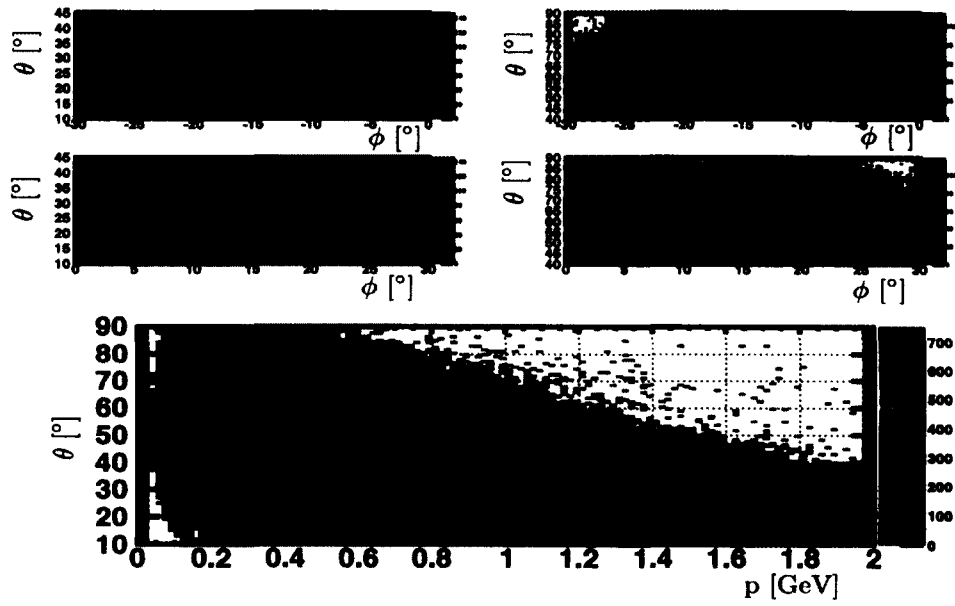
APPENDIX A

TOF AND EC PADDLE INEFFICIENCY STUDY PLOTS

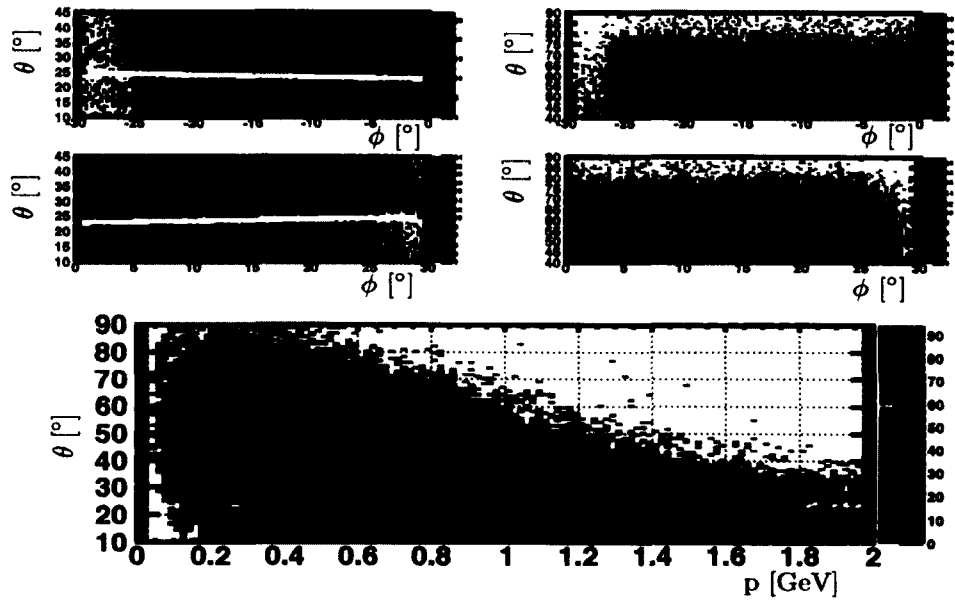
Shown below is are plots for the TOF and EC inefficiency studies. For completeness, all sectors are shown.

A.1 TOF INEFFICIENCY STUDY

Sec. 4.3.2 refers to this section for a complete view of the TOF study performed. All inefficiencies and cuts shown are for the π^+ and proton data. These inefficiencies and cuts are valid for the π^- and all other negative charged tracks.

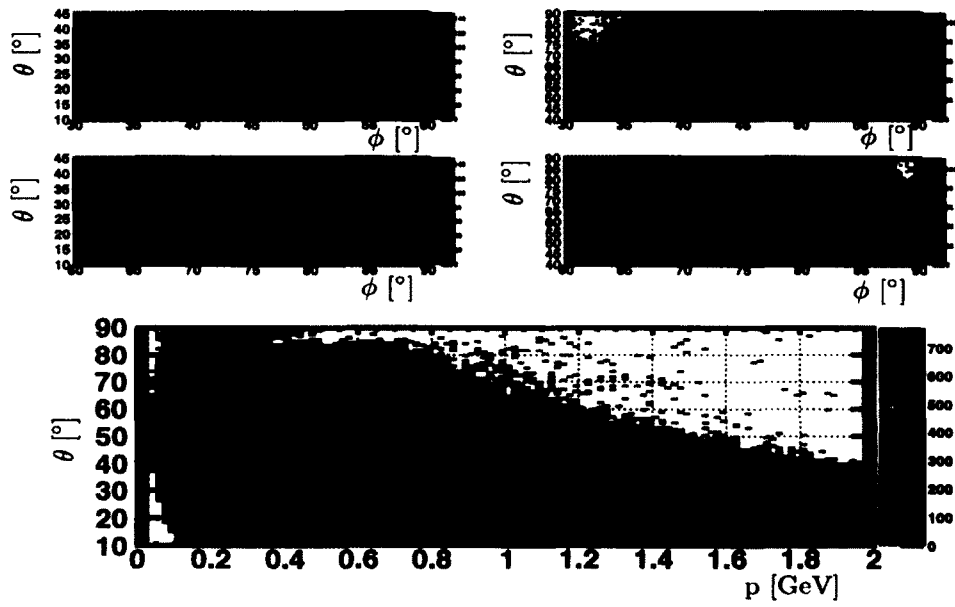


(a)

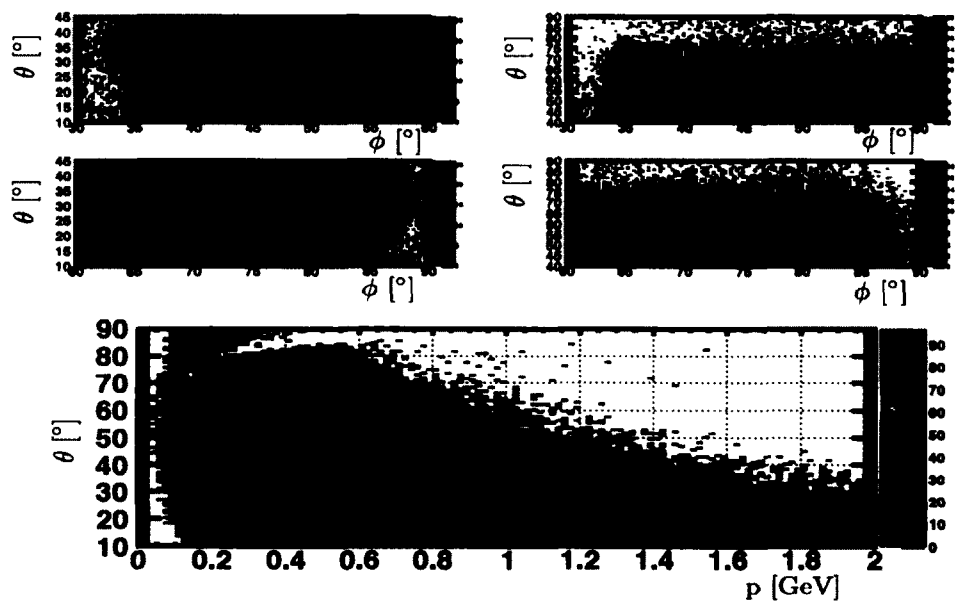


(b)

FIG. 129. TOF inefficiency Plot for sector 1 (129a). Inefficiency cut for π^+ and proton data (129b). Notation same as in Fig. 58.

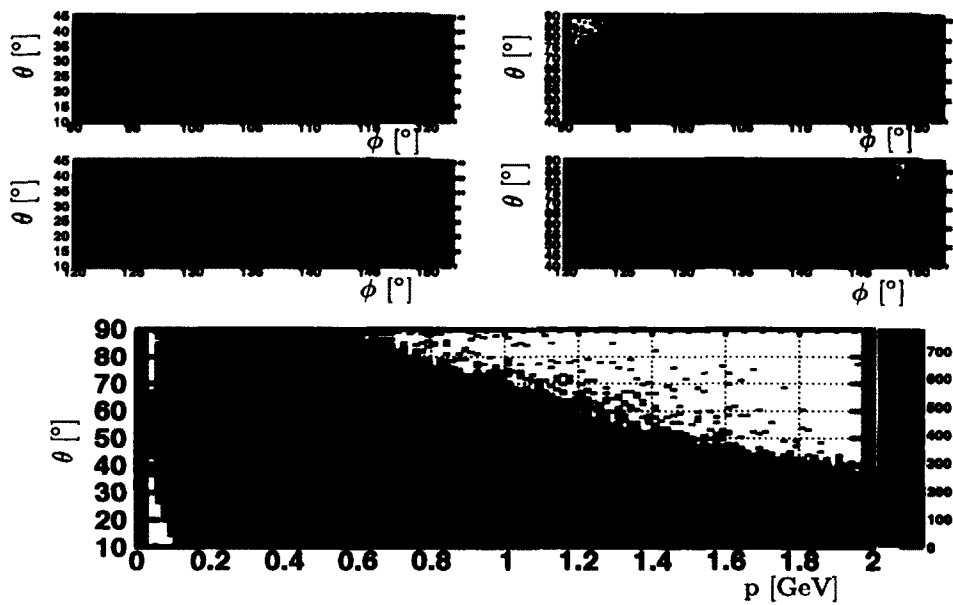


(a)

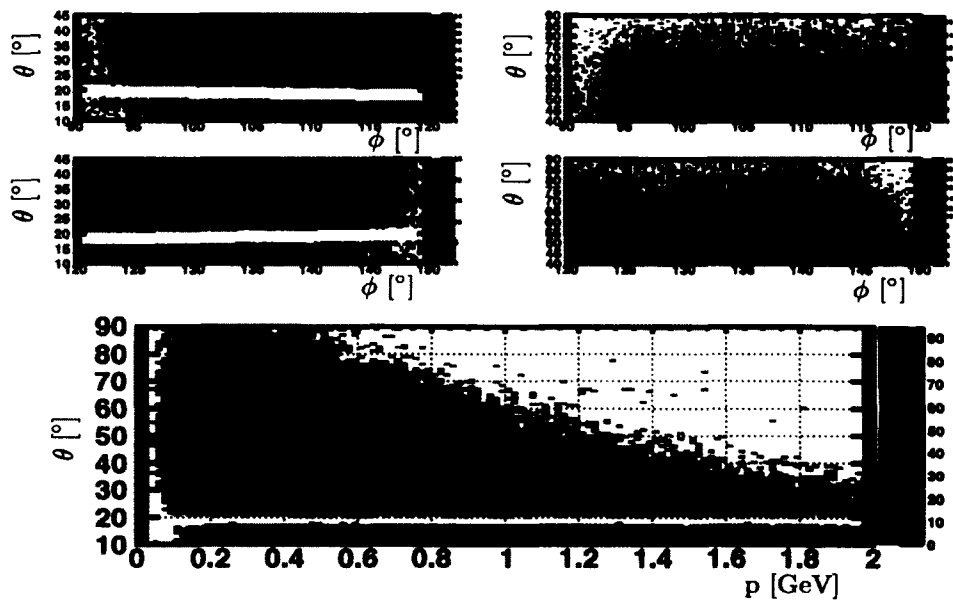


(b)

FIG. 130. TOF inefficiency Plot for sector 2 (130a). Inefficiency cut for π^+ and proton data (130b). Notation same as in Fig. 58.

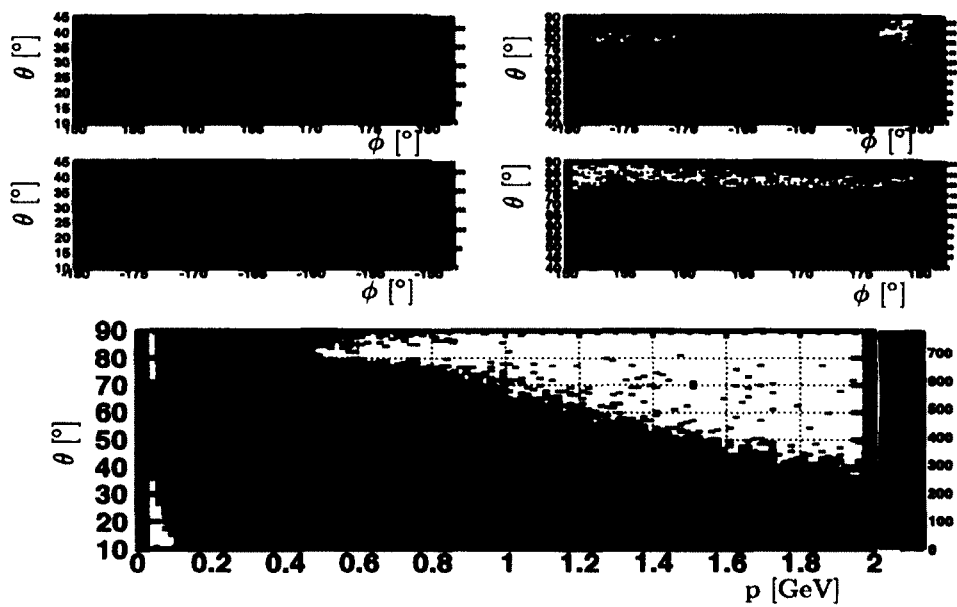


(a)

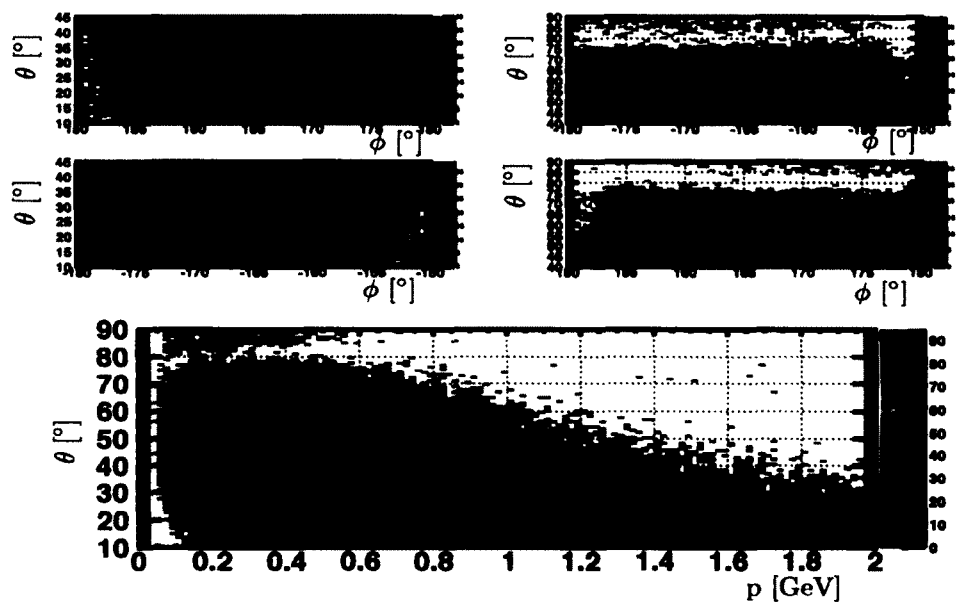


(b)

FIG. 131. TOF inefficiency Plot for sector 3 (131a). Inefficiency cut for π^+ and proton data (131b). Notation same as in Fig. 58.

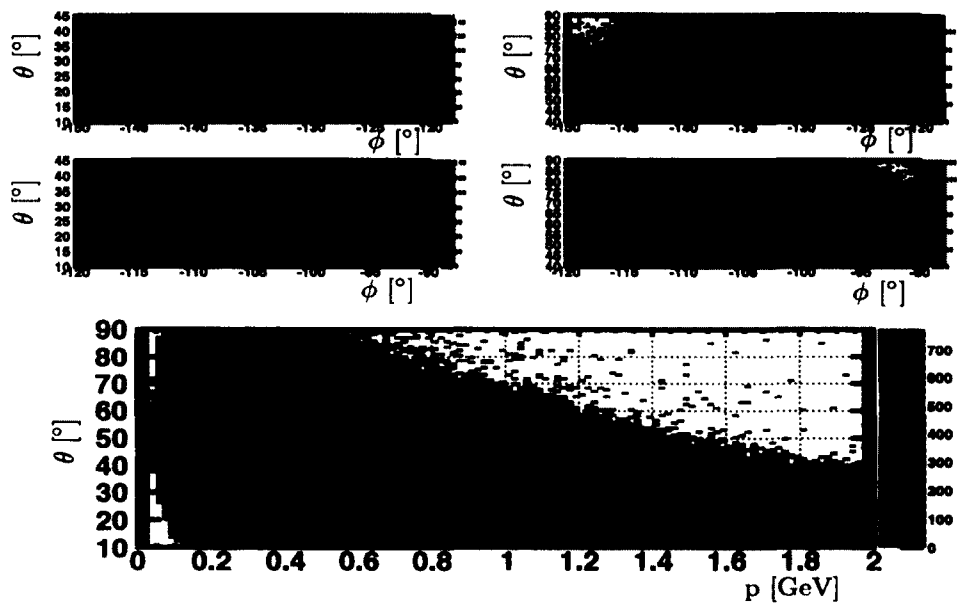


(a)

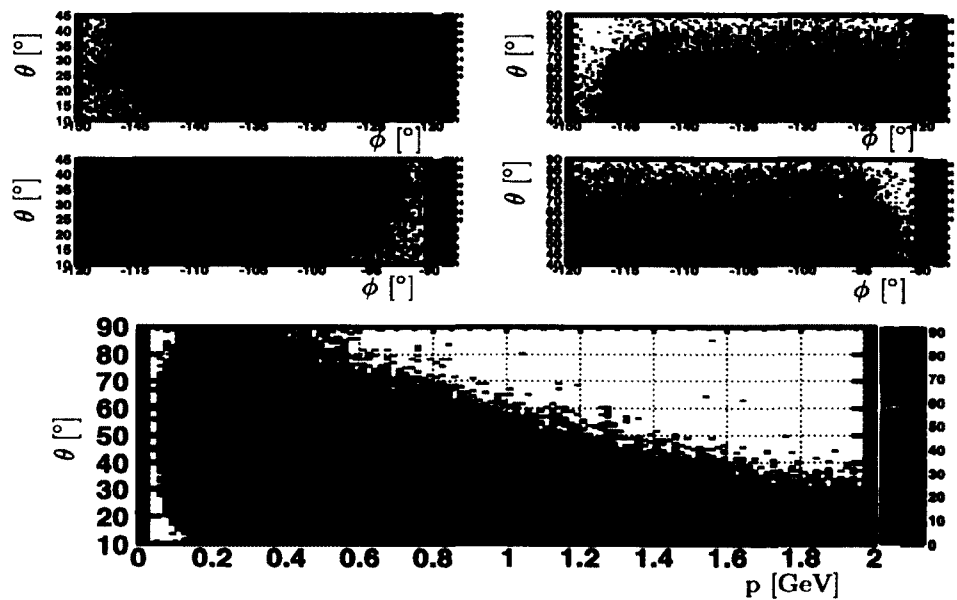


(b)

FIG. 132. TOF inefficiency Plot for sector 4 (132a). Inefficiency cut for π^+ and proton data (132b). Notation same as in Fig. 58.

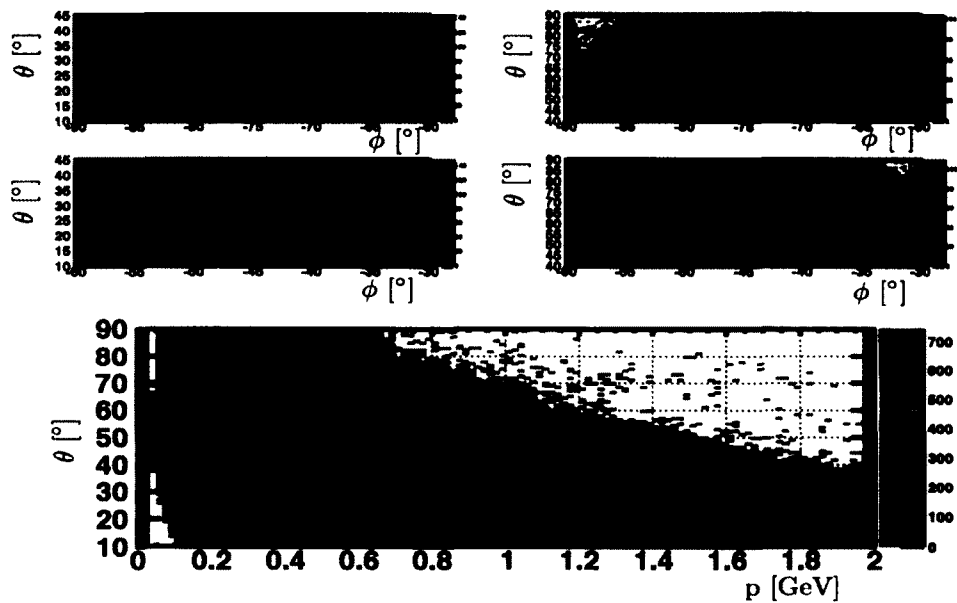


(a)

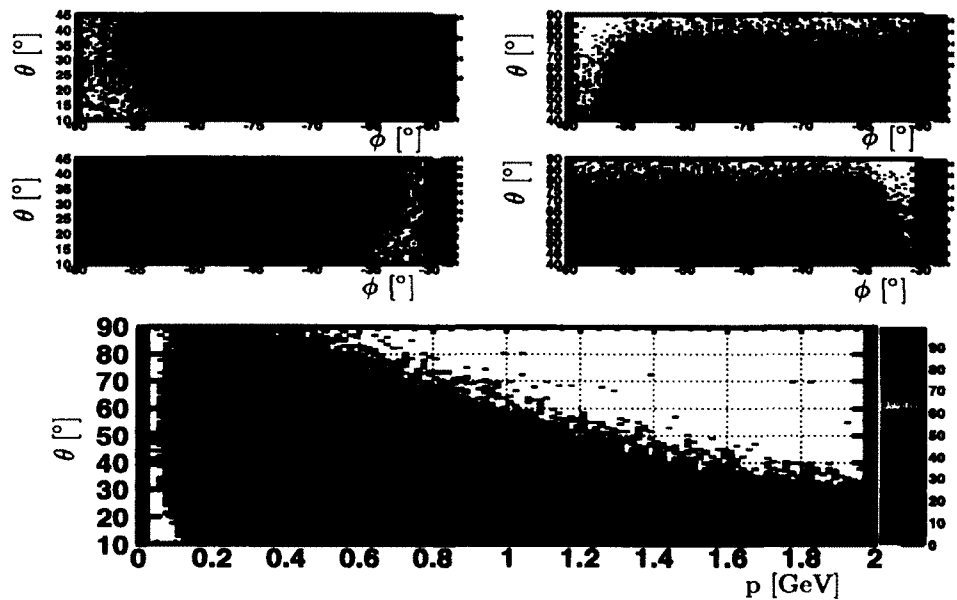


(b)

FIG. 133. TOF inefficiency Plot for sector 5 (133a). Inefficiency cut for π^+ and proton data (133b). Notation same as in Fig. 58.



(a)

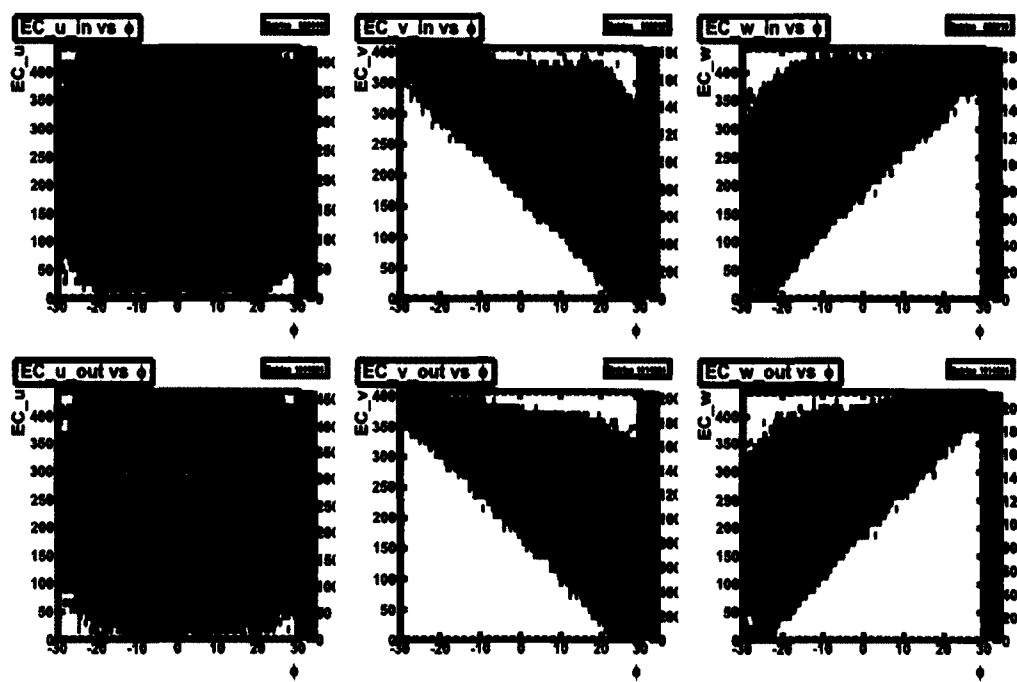


(b)

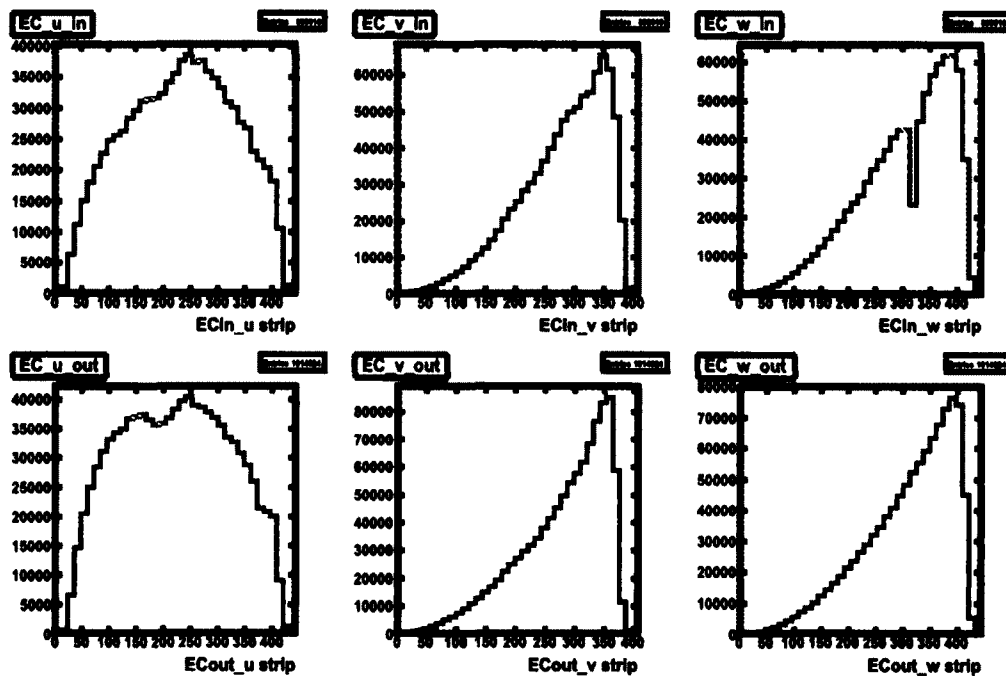
FIG. 134. TOF inefficiency Plot for sector 6 (134a). Inefficiency cut for π^+ and proton data (134b). Notation same as in Fig. 58.

A.2 EC INEFFICIENCY STUDY

Sec. 4.3.3 refers to this section for a complete view of the EC study performed. All inefficiencies and cuts shown are for the e^- data. These inefficiencies and cuts are valid for the e^+ data.

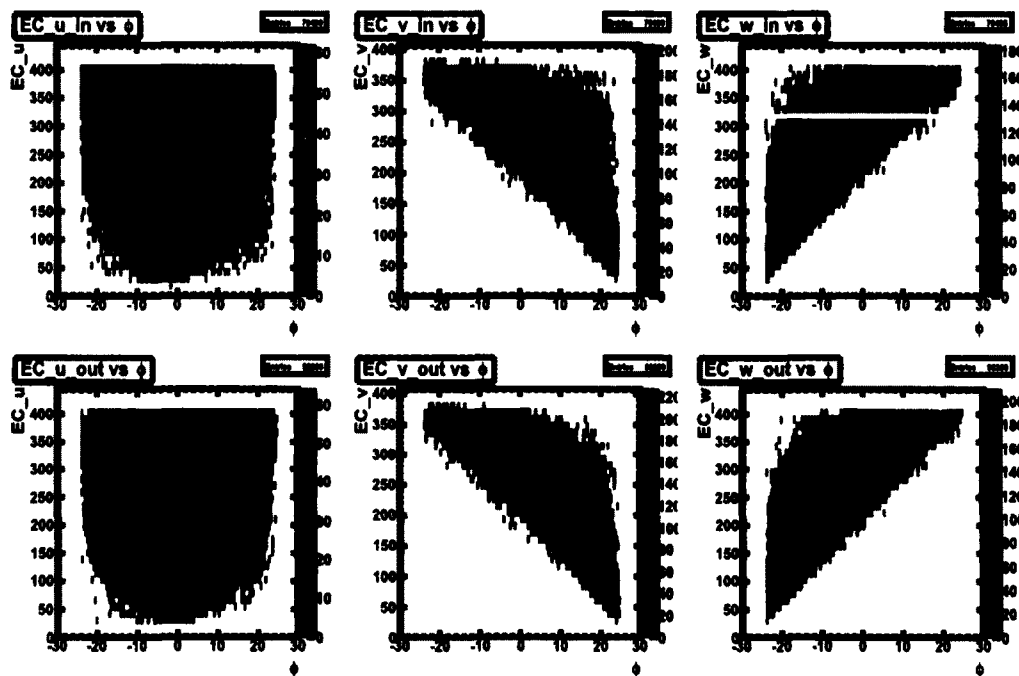


(a)

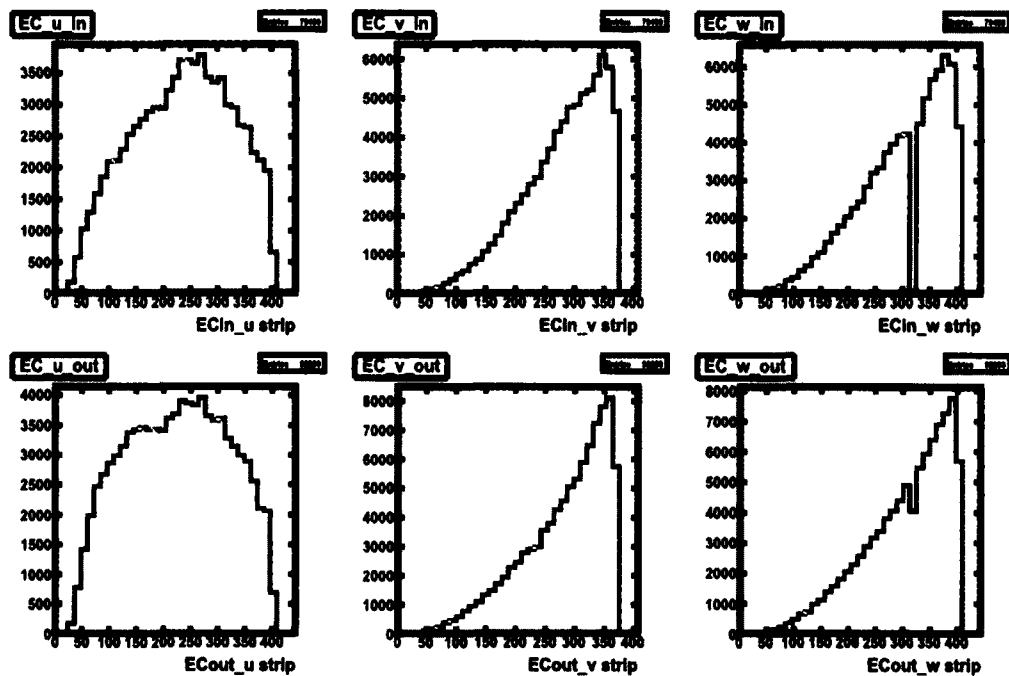


(b)

FIG. 135. Inefficient EC u , v , w strips vs. ϕ for sector 1 in CLAS e^- data (135a), notation the same as Fig. 60. Number of hits vs. inefficient EC u , v , w strips for sector 1 for e^- data (135b). Notation same as in Fig. 61.

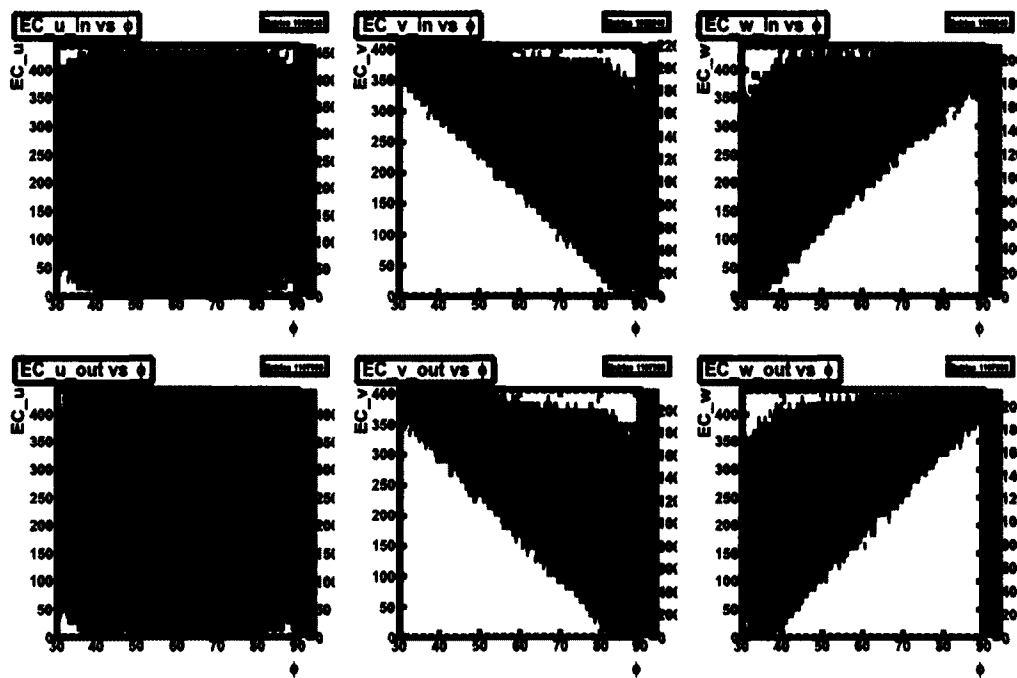


(a)

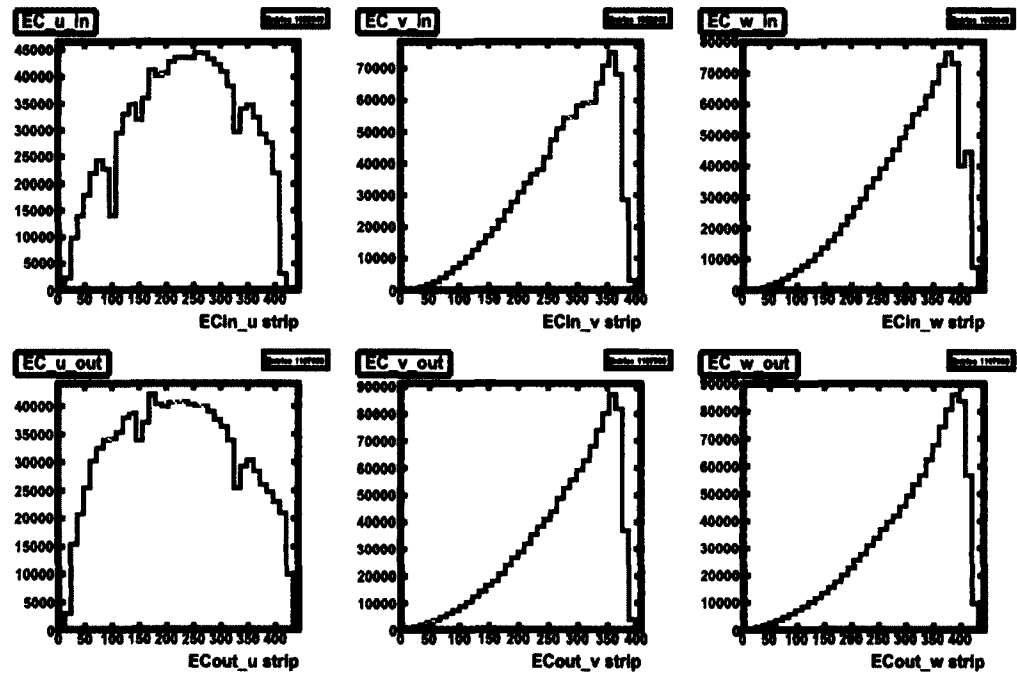


(b)

FIG. 136. EC u , v , w strips vs. ϕ for sector 1 with fiducial cuts and inefficient paddle knockouts applied to e^- data (136a), notation the same as Fig. 62. Number of hits vs. EC u , v , w strips for sector 1 with fiducial cuts and inefficient paddle knockouts applied to e^- data (136b). Notation same as in Fig. 63.

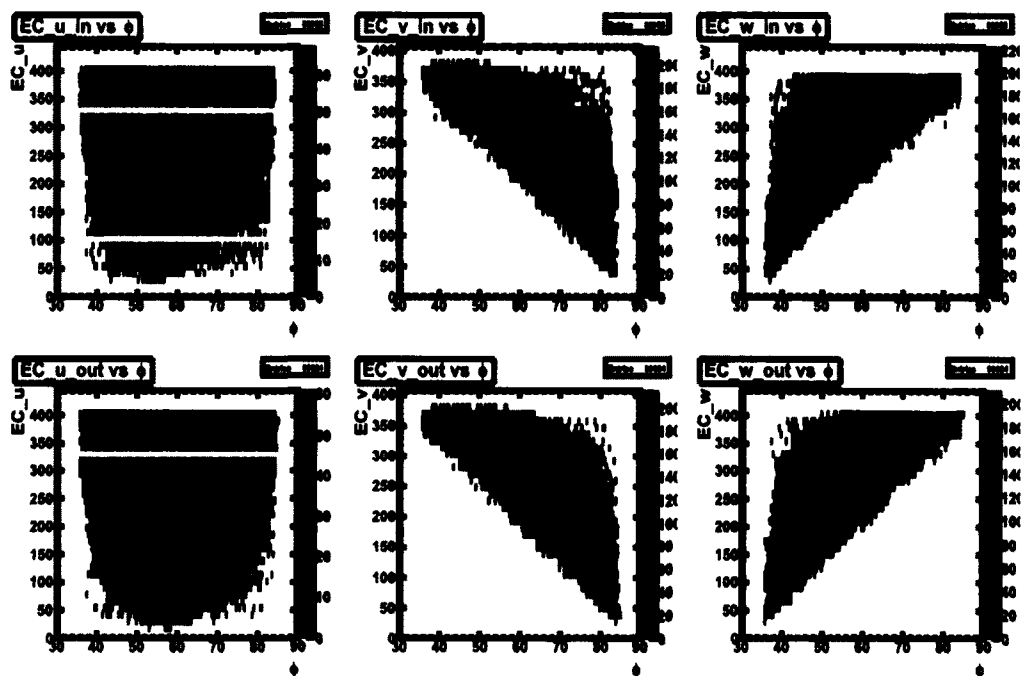


(a)

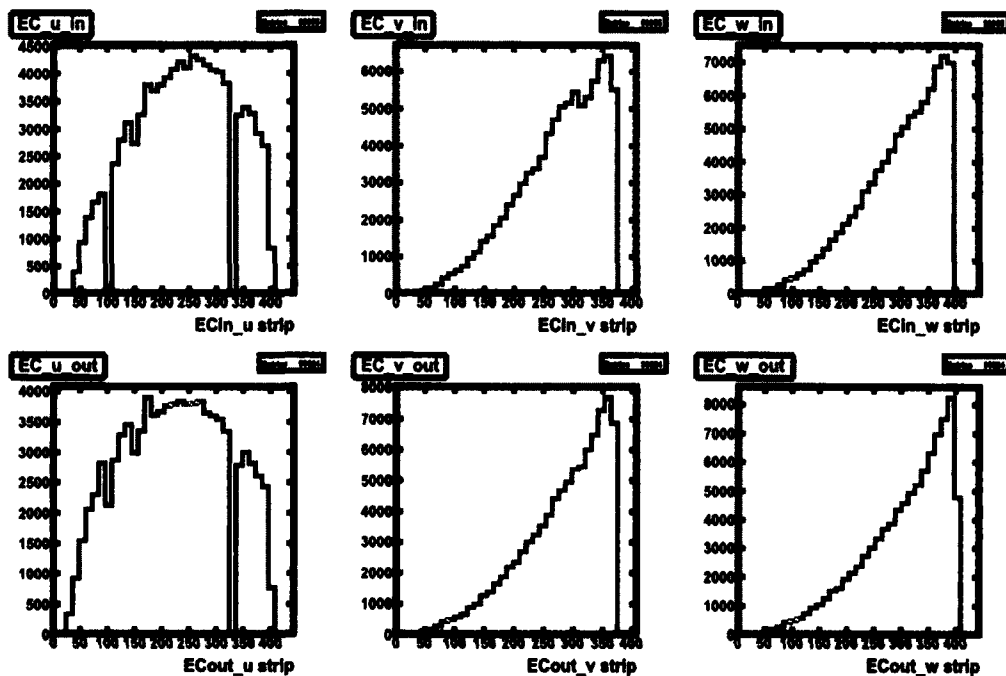


(b)

FIG. 137. Inefficient EC u , v , w strips vs. ϕ for sector 2 in CLAS e^- data (137a), notation the same as Fig. 60. Number of hits vs. inefficient EC u , v , w strips for sector 2 for e^- data (137b). Notation same as in Fig. 61.

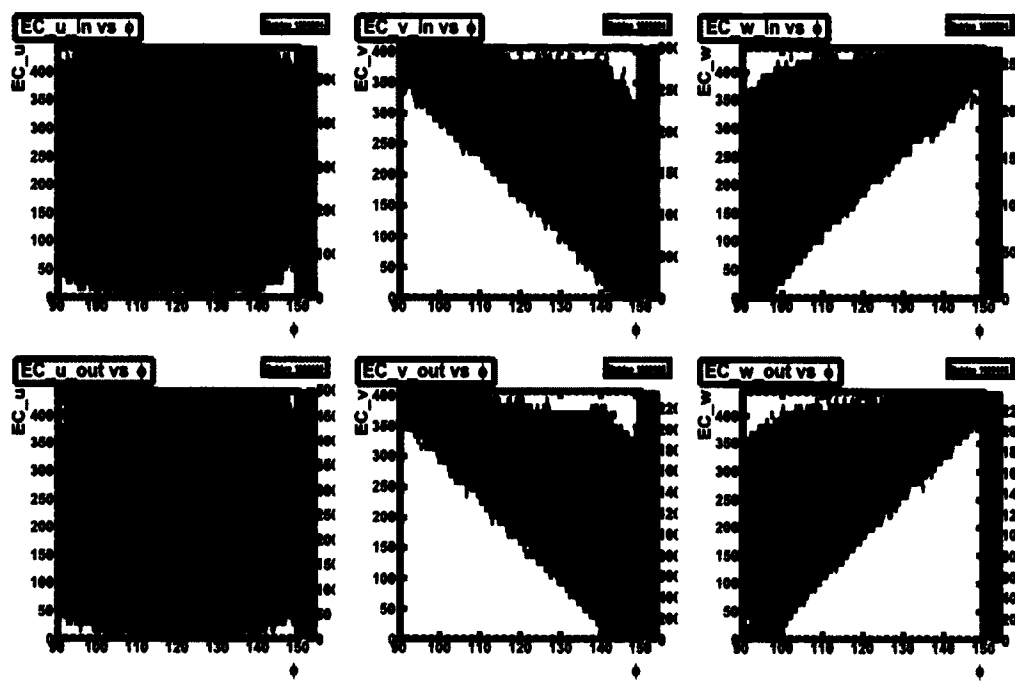


(a)

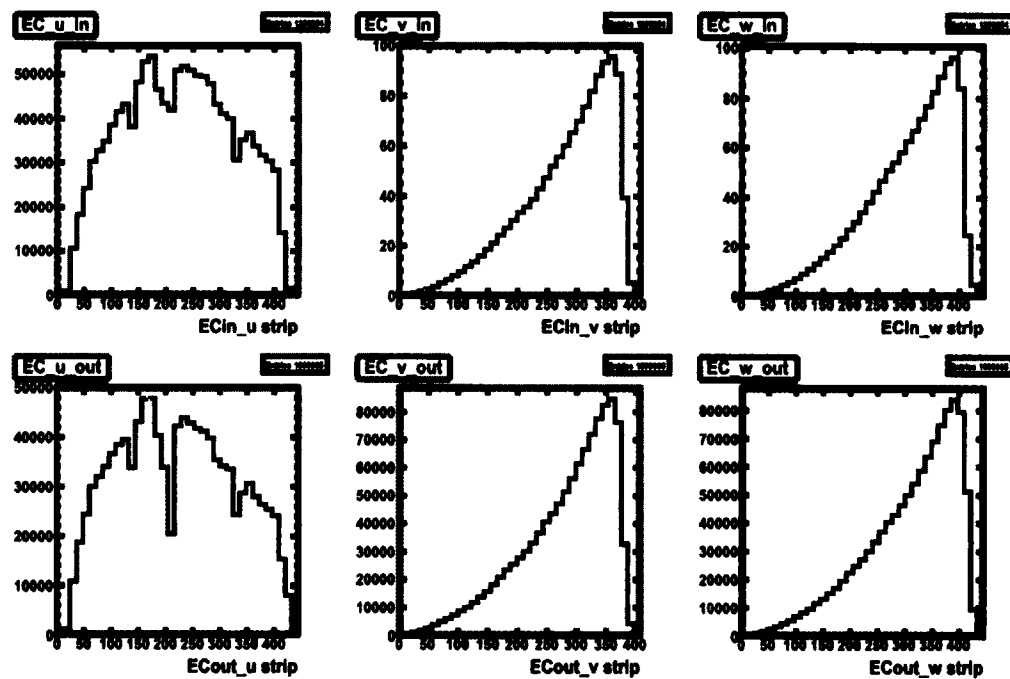


(b)

FIG. 138. EC u , v , w strips vs. ϕ for sector 2 with fiducial cuts and inefficient paddle knockouts applied to e^- data (138a), notation the same as Fig. 62. Number of hits vs. EC u , v , w strips for sector 2 with fiducial cuts and inefficient paddle knockouts applied to e^- data (138b). Notation same as in Fig. 63.

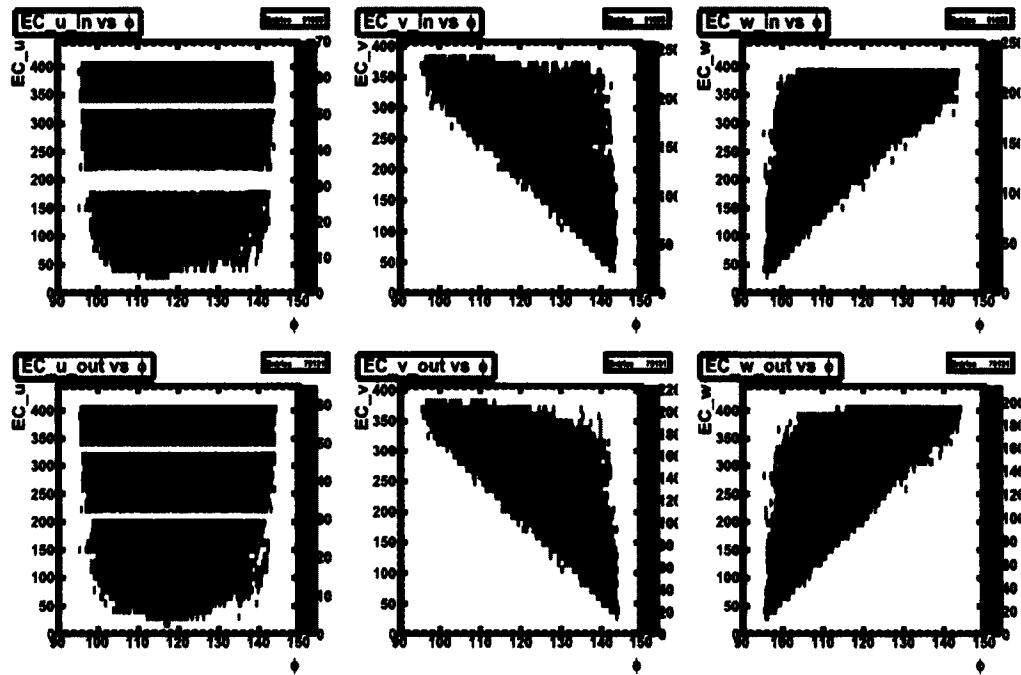


(a)

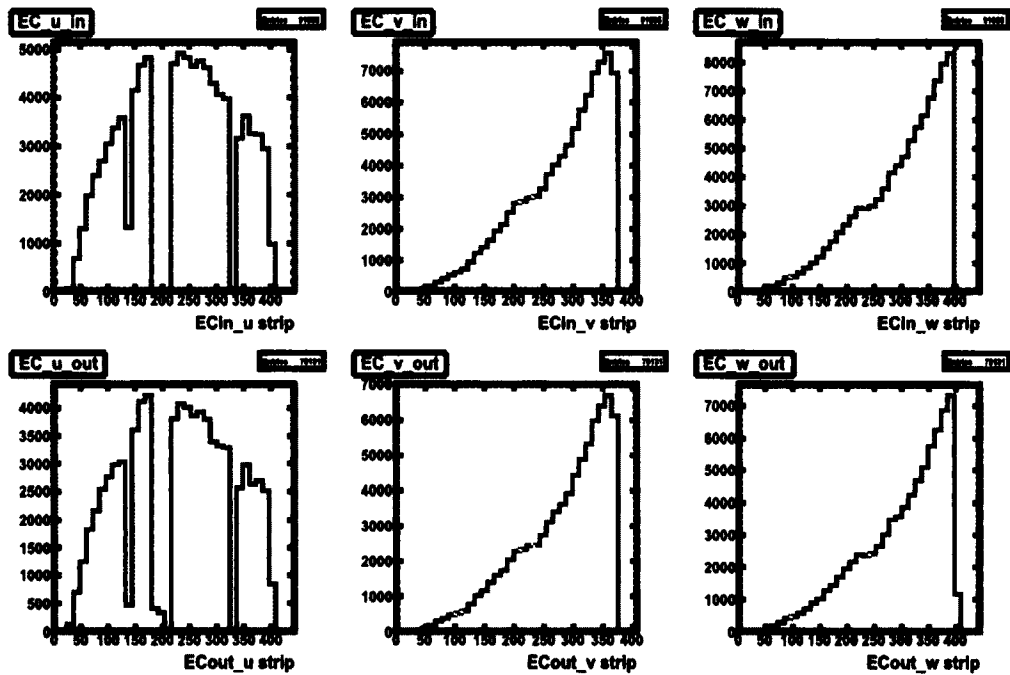


(b)

FIG. 139. Inefficient EC u , v , w strips vs. ϕ for sector 3 in CLAS e^- data (139a), notation the same as Fig. 60. Number of hits vs. inefficient EC u , v , w strips for sector 3 for e^- data (139b). Notation same as in Fig. 61.

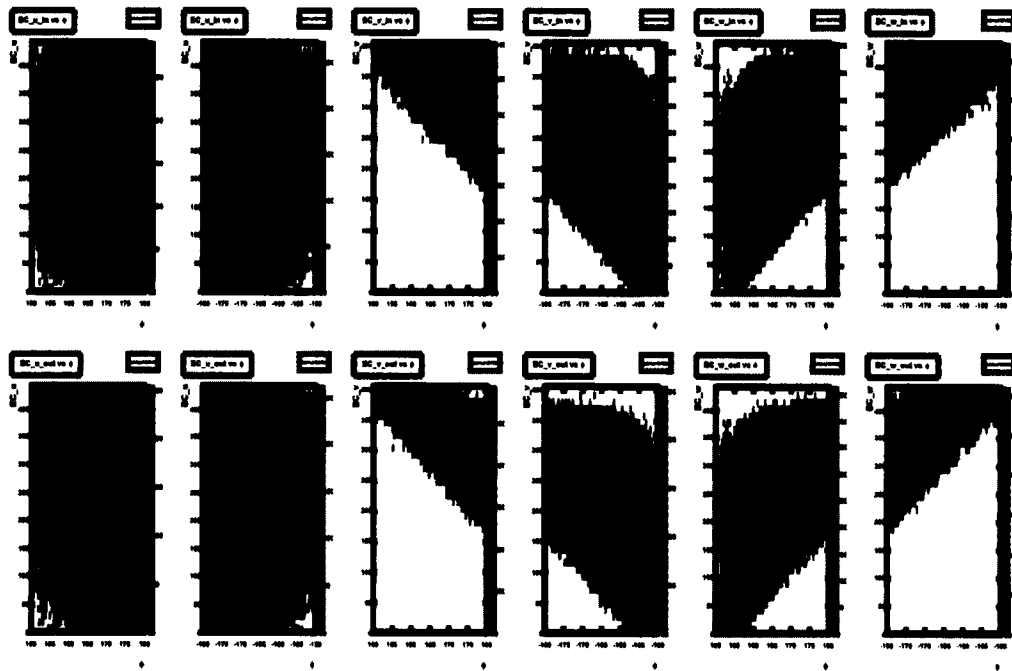


(a)

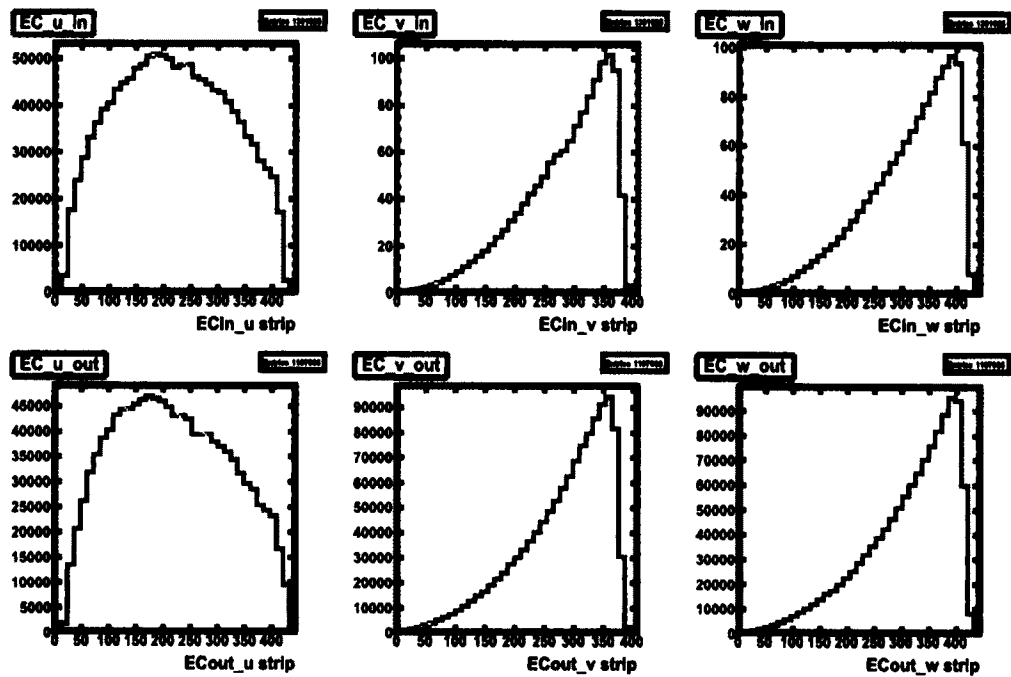


(b)

FIG. 140. EC u , v , w strips vs. ϕ for sector 3 with fiducial cuts and inefficient paddle knockouts applied to e^- data (140a), notation the same as Fig. 62. Number of hits vs. EC u , v , w strips for sector 3 with fiducial cuts and inefficient paddle knockouts applied to e^- data (140b). Notation same as in Fig. 63.

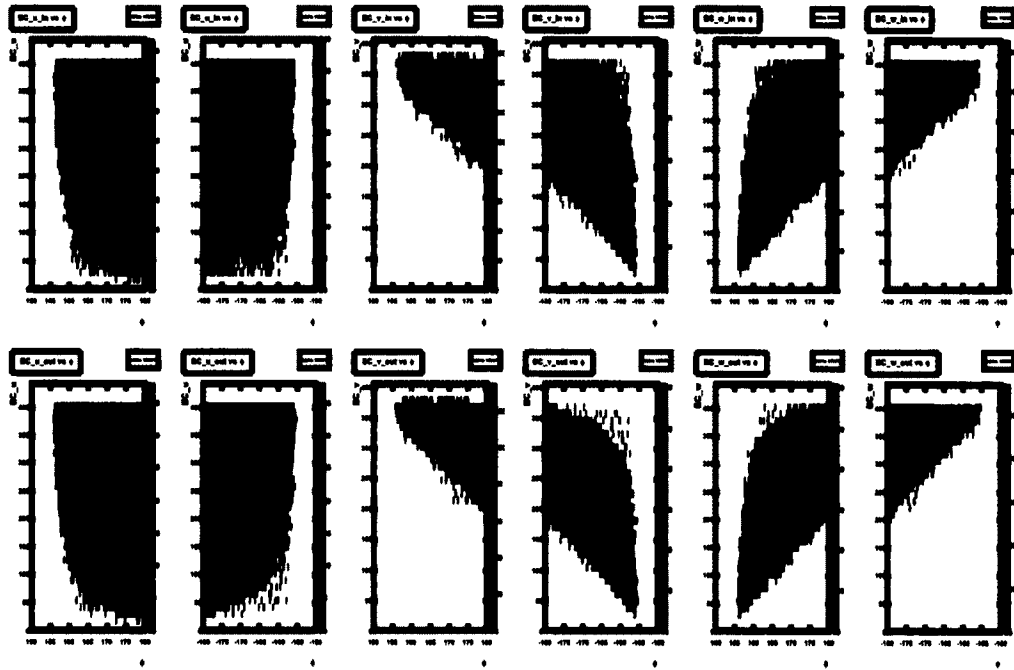


(a)

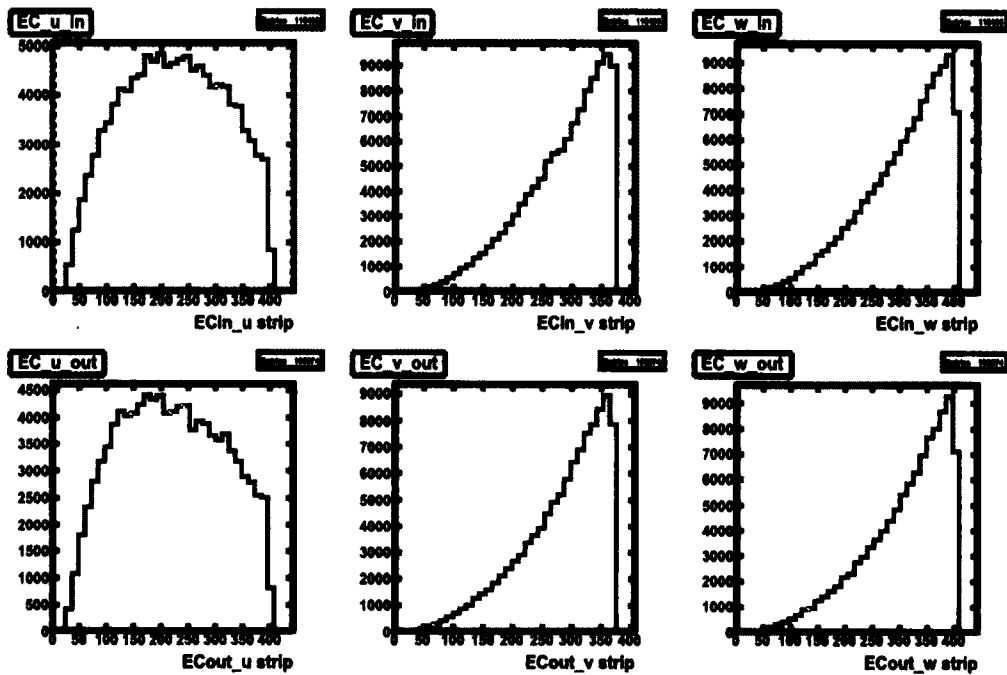


(b)

FIG. 141. Inefficient EC u , v , w strips vs. ϕ for sector 4 in CLAS e^- data (141a), notation the same as Fig. 60. Number of hits vs. inefficient EC u , v , w strips for sector 4 for e^- data (141b). Notation same as in Fig. 61.

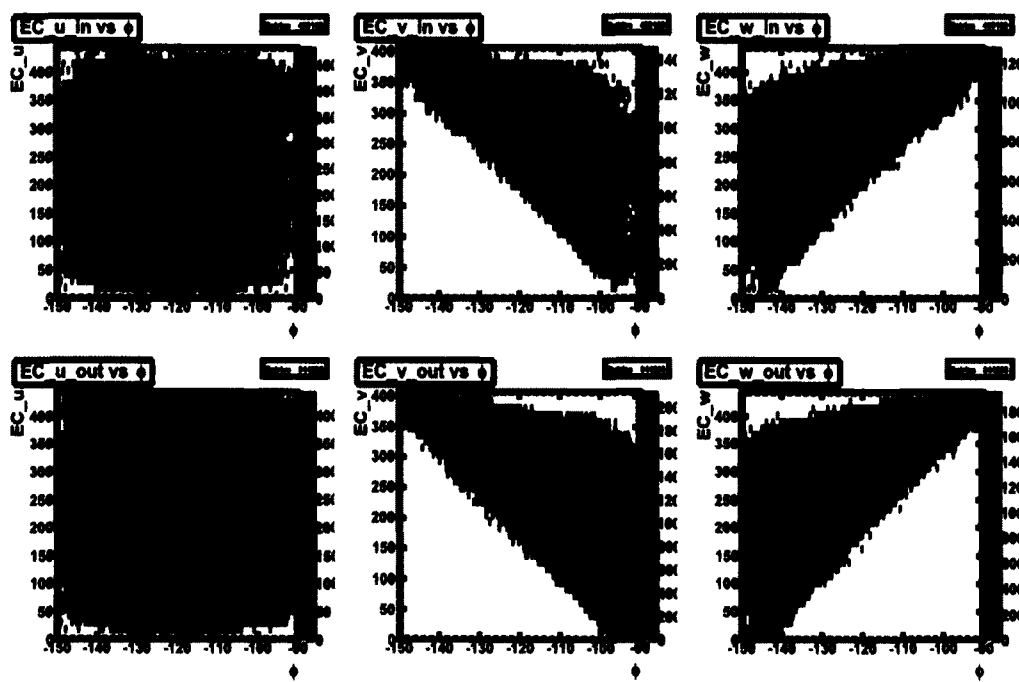


(a)

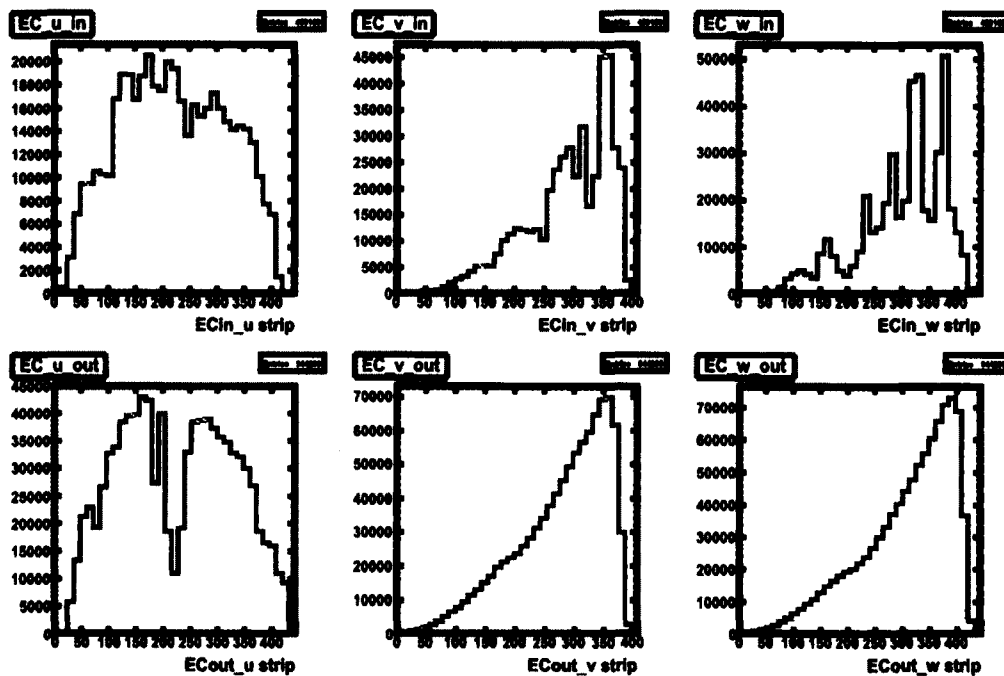


(b)

FIG. 142. EC u , v , w strips vs. ϕ for sector 4 with fiducial cuts and inefficient paddle knockouts applied to e^- data (142a), notation the same as Fig. 62. Number of hits vs. EC u , v , w strips for sector 4 with fiducial cuts and inefficient paddle knockouts applied to e^- data (142b). Notation same as in Fig. 63.

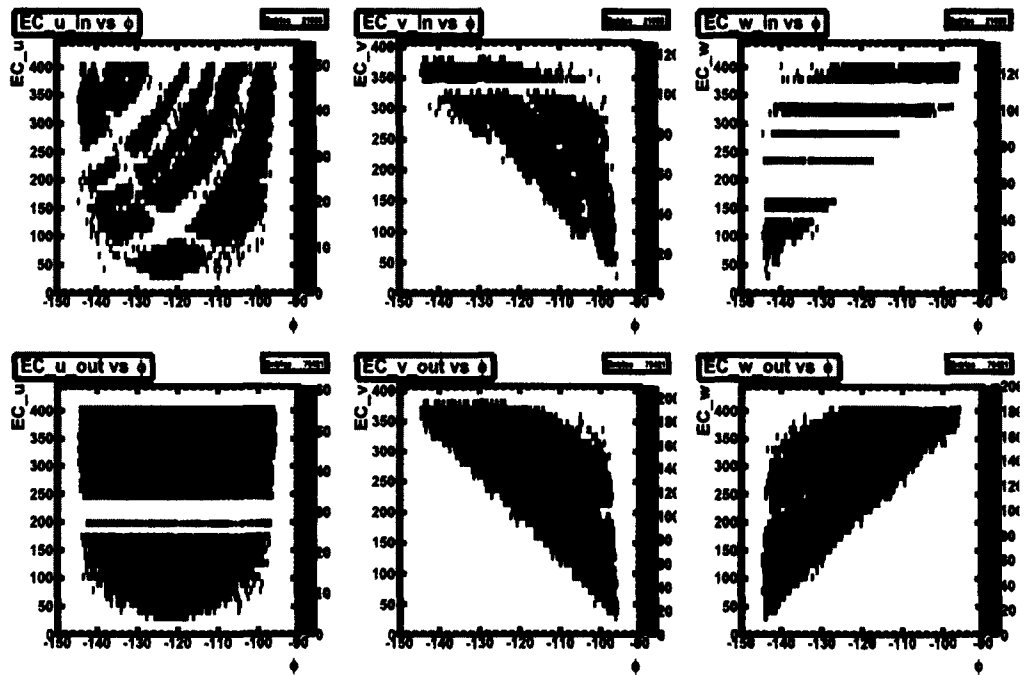


(a)

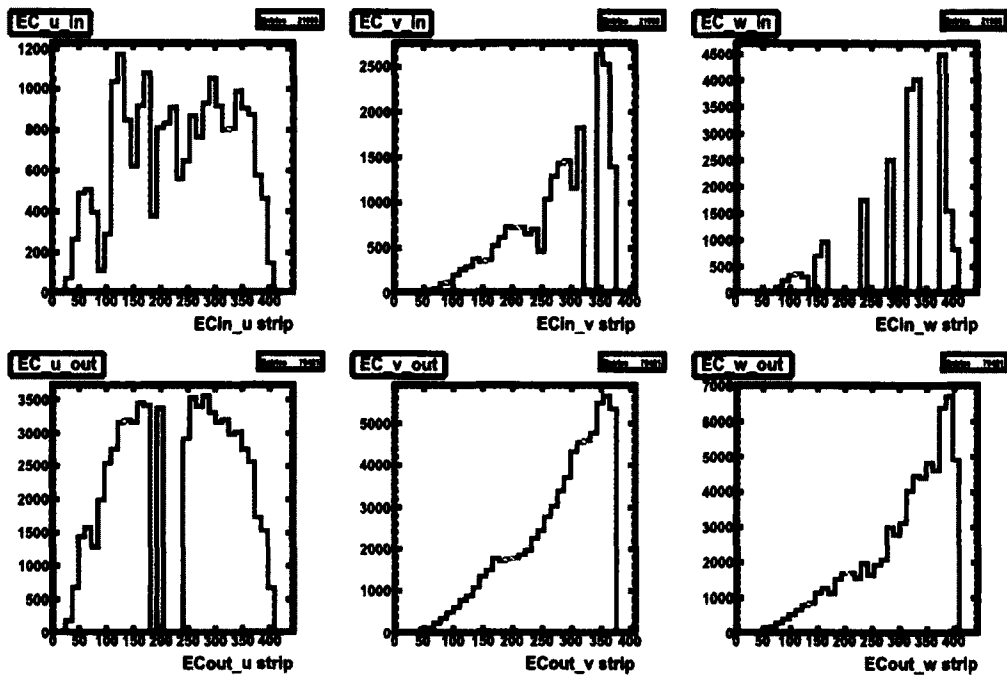


(b)

FIG. 143. Inefficient EC u , v , w strips vs. ϕ for sector 5 in CLAS e^- data (143a), notation the same as Fig. 60. Number of hits vs. inefficient EC u , v , w strips for sector 5 for e^- data (143b). Notation same as in Fig. 61.

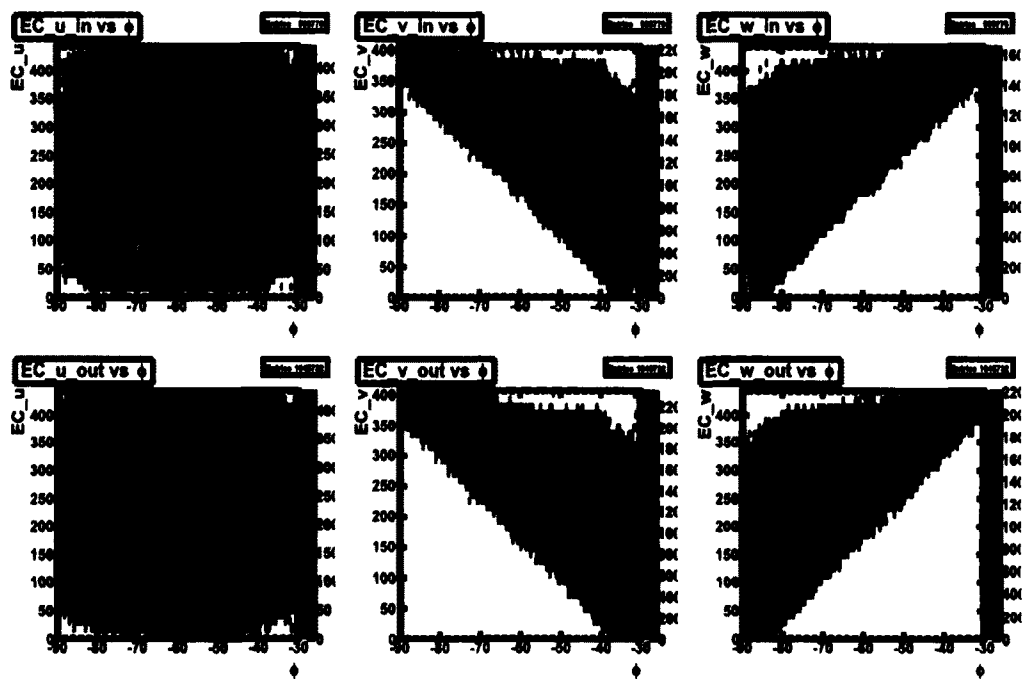


(a)

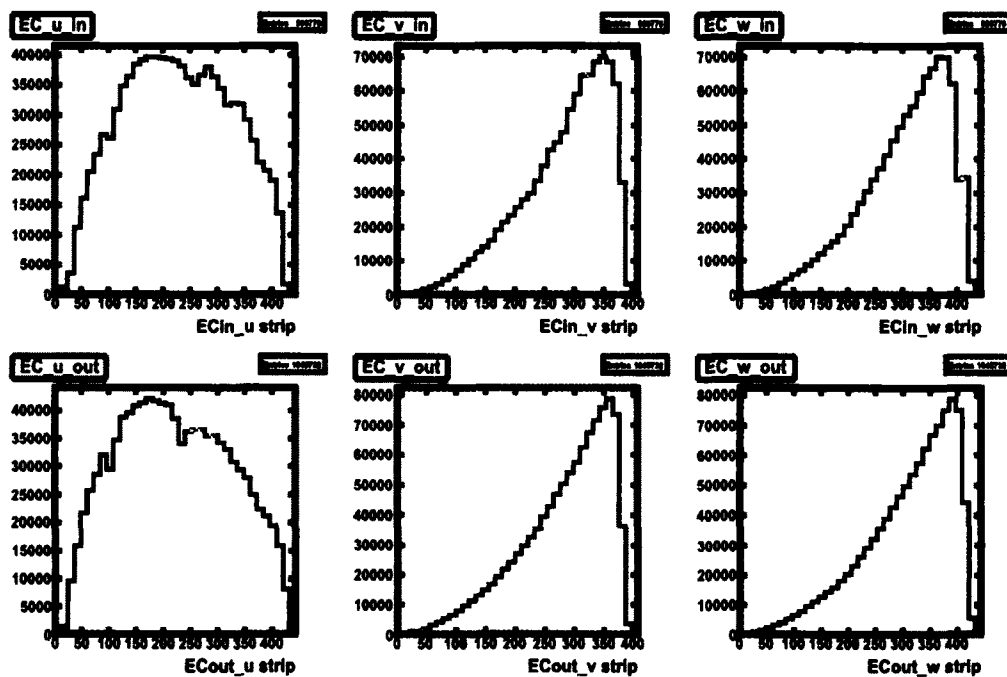


(b)

FIG. 144. EC u , v , w strips vs. ϕ for sector 5 with fiducial cuts and inefficient paddle knockouts applied to e^- data (144a), notation the same as Fig. 62. Number of hits vs. EC u , v , w strips for sector 5 with fiducial cuts and inefficient paddle knockouts applied to e^- data (144b). Notation same as in Fig. 63.

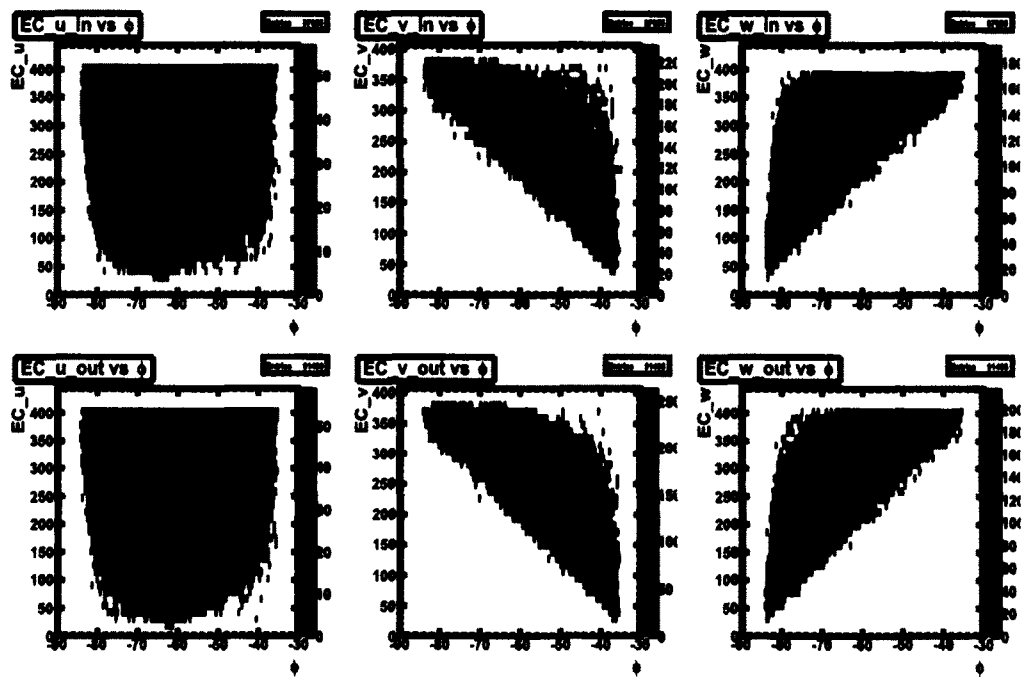


(a)

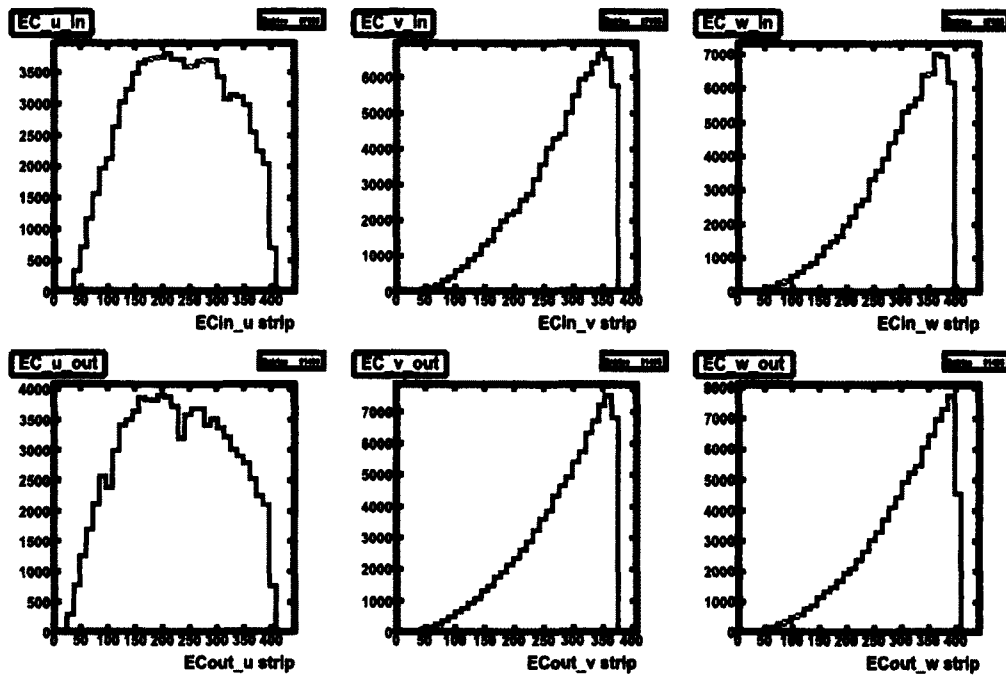


(b)

FIG. 145. Inefficient EC u , v , w strips vs. ϕ for sector 6 in CLAS e^- data (145a), notation the same as Fig. 60. Number of hits vs. inefficient EC u , v , w strips for sector 6 for e^- data (145b). Notation same as in Fig. 61.



(a)



(b)

FIG. 146. EC u , v , w strips vs. ϕ for sector 6 with fiducial cuts and inefficient paddle knockouts applied to e^- data (146a), notation the same as Fig. 62. Number of hits vs. EC u , v , w strips for sector 6 with fiducial cuts and inefficient paddle knockouts applied to e^- data (146b). Notation same as in Fig. 63.

APPENDIX B

TABULAR DATA

TABLE 29. $\frac{d\sigma}{d\Omega}$ Data for $\cos\theta_{\pi^0}^{C.M.}$.

E_{beam}^{lab} [GeV]	$\pm dE_{beam}^{lab}$	$\cos\theta_{\pi^0}^{C.M.}$	$\pm d\cos\theta_{\pi^0}^{C.M.}$	$\frac{d\sigma}{d\Omega}$ [$\frac{\mu b}{SR}$]	σ^{stat}	σ^{sys}
1.275	0.025	0.796875	0.015625	1.17715	0.0709938	0.0757257
1.275	0.025	0.765625	0.015625	1.19906	0.0502756	0.0771354
1.275	0.025	0.734375	0.015625	0.99729	0.0323912	0.0641553
1.275	0.025	0.703125	0.015625	0.954801	0.0260267	0.061422
1.275	0.025	0.671875	0.015625	0.907953	0.0224482	0.0584083
1.275	0.025	0.640625	0.015625	0.796032	0.0198173	0.0512085
1.275	0.025	0.609375	0.015625	0.834301	0.0198798	0.0536703
1.275	0.025	0.578125	0.015625	0.780085	0.0181191	0.0501826
1.275	0.025	0.546875	0.015625	0.700944	0.0171287	0.0450915
1.275	0.025	0.515625	0.015625	0.673026	0.0181679	0.0432955
1.275	0.025	0.484375	0.015625	0.673891	0.0197419	0.0433512
1.325	0.025	0.796875	0.015625	1.15936	0.0697721	0.0750256
1.325	0.025	0.765625	0.015625	1.36229	0.0538949	0.0881578
1.325	0.025	0.734375	0.015625	1.11529	0.0346604	0.072174
1.325	0.025	0.703125	0.015625	1.05633	0.0283207	0.0683581
1.325	0.025	0.671875	0.015625	0.867017	0.0220086	0.0561074
1.325	0.025	0.640625	0.015625	0.743081	0.0187581	0.0480871
1.325	0.025	0.609375	0.015625	0.767226	0.0189093	0.0496496
1.325	0.025	0.578125	0.015625	0.738712	0.0181357	0.0478044
1.325	0.025	0.546875	0.015625	0.598595	0.0158646	0.0387369
1.325	0.025	0.515625	0.015625	0.588626	0.0165172	0.0380918
1.325	0.025	0.484375	0.015625	0.5227	0.0170949	0.0338256
1.375	0.025	0.796875	0.015625	1.37011	0.0882144	0.0891962
1.375	0.025	0.765625	0.015625	1.42926	0.0651468	0.0930469
1.375	0.025	0.734375	0.015625	1.16296	0.0436071	0.0757105
1.375	0.025	0.703125	0.015625	0.965586	0.0321381	0.0628609
1.375	0.025	0.671875	0.015625	0.819163	0.0260331	0.0533286
1.375	0.025	0.640625	0.015625	0.742176	0.0233379	0.0483167
1.375	0.025	0.609375	0.015625	0.525371	0.0174937	0.0342023
1.375	0.025	0.578125	0.015625	0.513333	0.0169807	0.0334186
1.375	0.025	0.546875	0.015625	0.47092	0.0160935	0.0306575

TABLE 29 – Continued

E_{beam}^{lab} [GeV]	$\pm dE_{beam}^{lab}$	$\cos \theta_{n^0}^{C.M.}$	$\pm d \cos \theta_{n^0}^{C.M.}$	$\frac{d\sigma}{d\Omega} \left[\frac{\mu b}{SR} \right]$	σ^{stat}	σ^{sys}
1.375	0.025	0.515625	0.015625	0.41454	0.0159626	0.0269871
1.375	0.025	0.484375	0.015625	0.365593	0.0168338	0.0238006
1.375	0.025	0.453125	0.015625	0.351461	0.0177913	0.0228806
1.375	0.025	0.421875	0.015625	0.380386	0.0207232	0.0247636
1.425	0.025	0.796875	0.015625	1.65055	0.0766373	0.108102
1.425	0.025	0.765625	0.015625	1.74775	0.0569746	0.114468
1.425	0.025	0.734375	0.015625	1.38583	0.037427	0.0907637
1.425	0.025	0.703125	0.015625	1.17101	0.0274862	0.0766942
1.425	0.025	0.671875	0.015625	0.847092	0.0199913	0.0554797
1.425	0.025	0.640625	0.015625	0.714133	0.016997	0.0467716
1.425	0.025	0.609375	0.015625	0.586762	0.014323	0.0384295
1.425	0.025	0.578125	0.015625	0.472953	0.0120864	0.0309757
1.425	0.025	0.546875	0.015625	0.412689	0.0112162	0.0270288
1.425	0.025	0.515625	0.015625	0.343317	0.0106296	0.0224853
1.425	0.025	0.484375	0.015625	0.316198	0.0110859	0.0207092
1.425	0.025	0.453125	0.015625	0.315414	0.0127806	0.0206578
1.425	0.025	0.421875	0.015625	0.268373	0.0128728	0.0175769
1.475	0.025	0.796875	0.015625	1.88777	0.0901102	0.124388
1.475	0.025	0.765625	0.015625	1.61567	0.0513416	0.10646
1.475	0.025	0.734375	0.015625	1.28385	0.0345974	0.0845955
1.475	0.025	0.703125	0.015625	1.01308	0.0240816	0.0667538
1.475	0.025	0.671875	0.015625	0.873197	0.0203301	0.0575365
1.475	0.025	0.640625	0.015625	0.642263	0.0157471	0.0423199
1.475	0.025	0.609375	0.015625	0.530308	0.013083	0.034943
1.475	0.025	0.578125	0.015625	0.408821	0.0108199	0.026938
1.475	0.025	0.546875	0.015625	0.336221	0.00969344	0.0221542
1.475	0.025	0.515625	0.015625	0.273845	0.00913246	0.0180442
1.475	0.025	0.484375	0.015625	0.206542	0.00831113	0.0136094
1.475	0.025	0.453125	0.015625	0.187879	0.00869817	0.0123797
1.475	0.025	0.421875	0.015625	0.212553	0.0107649	0.0140055
1.525	0.025	0.796875	0.015625	1.73347	0.0787254	0.114918
1.525	0.025	0.765625	0.015625	1.68609	0.0541126	0.111777
1.525	0.025	0.734375	0.015625	1.35609	0.0367011	0.0899005
1.525	0.025	0.703125	0.015625	1.06554	0.0262172	0.0706385
1.525	0.025	0.671875	0.015625	0.817356	0.0203826	0.0541857
1.525	0.025	0.640625	0.015625	0.682503	0.0170462	0.0452458
1.525	0.025	0.609375	0.015625	0.556451	0.014274	0.0368893
1.525	0.025	0.578125	0.015625	0.409346	0.0112998	0.0271371
1.525	0.025	0.546875	0.015625	0.285617	0.00925407	0.0189347

TABLE 29 – Continued

E_{beam}^{lab} [GeV]	$\pm dE_{beam}^{lab}$	$\cos \theta_{\pi^0}^{C.M.}$	$\pm d \cos \theta_{\pi^0}^{C.M.}$	$\frac{d\sigma}{d\Omega}$ [$\frac{\mu b}{SR}$]	σ^{stat}	σ^{sys}
1.525	0.025	0.515625	0.015625	0.219524	0.00823636	0.0145531
1.525	0.025	0.484375	0.015625	0.163791	0.00748478	0.0108584
1.525	0.025	0.453125	0.015625	0.162011	0.008231	0.0107403
1.525	0.025	0.421875	0.015625	0.15661	0.0089078	0.0103823
1.525	0.025	0.390625	0.015625	0.194136	0.0110454	0.0128701
1.575	0.025	0.796875	0.015625	1.60995	0.083535	0.107384
1.575	0.025	0.765625	0.015625	1.31952	0.0519883	0.0880126
1.575	0.025	0.734375	0.015625	1.16908	0.0384025	0.077978
1.575	0.025	0.703125	0.015625	0.904046	0.0268399	0.0603003
1.575	0.025	0.671875	0.015625	0.712419	0.0211594	0.0475187
1.575	0.025	0.640625	0.015625	0.548582	0.0169667	0.0365907
1.575	0.025	0.609375	0.015625	0.433572	0.013586	0.0289195
1.575	0.025	0.578125	0.015625	0.307655	0.0106112	0.0205207
1.575	0.025	0.546875	0.015625	0.222173	0.00879238	0.014819
1.575	0.025	0.515625	0.015625	0.165025	0.00773108	0.0110073
1.575	0.025	0.484375	0.015625	0.115277	0.00668515	0.00768901
1.575	0.025	0.453125	0.015625	0.104249	0.00679368	0.00695344
1.575	0.025	0.421875	0.015625	0.0967771	0.00736062	0.00645508
1.575	0.025	0.390625	0.015625	0.136539	0.00994496	0.00910725
1.625	0.025	0.796875	0.015625	1.62741	0.0818542	0.109218
1.625	0.025	0.765625	0.015625	1.45477	0.0540166	0.0976316
1.625	0.025	0.734375	0.015625	1.02727	0.0324485	0.0689414
1.625	0.025	0.703125	0.015625	0.974735	0.0275827	0.0654158
1.625	0.025	0.671875	0.015625	0.750771	0.0209836	0.0503853
1.625	0.025	0.640625	0.015625	0.600858	0.0171123	0.0403245
1.625	0.025	0.609375	0.015625	0.481053	0.0140093	0.0322841
1.625	0.025	0.578125	0.015625	0.340674	0.0108999	0.0228631
1.625	0.025	0.546875	0.015625	0.229425	0.00867493	0.0153971
1.625	0.025	0.515625	0.015625	0.163899	0.0072717	0.0109995
1.625	0.025	0.484375	0.015625	0.113424	0.00631172	0.00761207
1.625	0.025	0.453125	0.015625	0.106813	0.00634563	0.00716835
1.625	0.025	0.421875	0.015625	0.104817	0.00697615	0.00703442
1.625	0.025	0.390625	0.015625	0.109502	0.00779834	0.00734881
1.675	0.025	0.796875	0.015625	1.58657	0.0838193	0.107136
1.675	0.025	0.765625	0.015625	1.31033	0.056382	0.088482
1.675	0.025	0.734375	0.015625	0.991016	0.036504	0.06692
1.675	0.025	0.703125	0.015625	0.784016	0.026145	0.052942
1.675	0.025	0.671875	0.015625	0.637413	0.0212089	0.0430424
1.675	0.025	0.640625	0.015625	0.533898	0.0174088	0.0360523

TABLE 29 – Continued

E_{beam}^{lab} [GeV]	$\pm dE_{beam}^{lab}$	$\cos \theta_{\pi^0}^{C.M.}$	$\pm d \cos \theta_{\pi^0}^{C.M.}$	$\frac{d\sigma}{d\Omega} \left[\frac{\mu b}{SR} \right]$	σ^{stat}	σ^{sys}
1.675	0.025	0.609375	0.015625	0.408581	0.0136565	0.0275901
1.675	0.025	0.578125	0.015625	0.290278	0.0107291	0.0196015
1.675	0.025	0.546875	0.015625	0.222211	0.00917828	0.0150052
1.675	0.025	0.515625	0.015625	0.154427	0.00752912	0.0104279
1.675	0.025	0.484375	0.015625	0.116568	0.00667331	0.00787148
1.675	0.025	0.453125	0.015625	0.0949076	0.00628981	0.00640879
1.675	0.025	0.421875	0.015625	0.0920195	0.00692552	0.00621377
1.675	0.025	0.390625	0.015625	0.109418	0.00818562	0.00738864
1.725	0.025	0.796875	0.015625	1.01814	0.0618608	0.0691785
1.725	0.025	0.765625	0.015625	1.06904	0.0471415	0.0726368
1.725	0.025	0.734375	0.015625	0.743224	0.0294712	0.0504992
1.725	0.025	0.703125	0.015625	0.697212	0.0243054	0.0473729
1.725	0.025	0.671875	0.015625	0.558644	0.019224	0.0379577
1.725	0.025	0.640625	0.015625	0.418945	0.0145189	0.0284657
1.725	0.025	0.609375	0.015625	0.312535	0.0112123	0.0212355
1.725	0.025	0.578125	0.015625	0.238825	0.00933903	0.0162272
1.725	0.025	0.546875	0.015625	0.174502	0.00756564	0.0118567
1.725	0.025	0.515625	0.015625	0.116833	0.00613825	0.00793837
1.725	0.025	0.484375	0.015625	0.0809106	0.00508409	0.00549756
1.725	0.025	0.453125	0.015625	0.0766862	0.00526298	0.00521053
1.725	0.025	0.421875	0.015625	0.0686384	0.00521649	0.00466371
1.725	0.025	0.390625	0.015625	0.0827605	0.00647625	0.00562326
1.725	0.025	0.359375	0.015625	0.0911173	0.00754032	0.00619107
1.775	0.025	0.796875	0.015625	1.24979	0.0670069	0.0854477
1.775	0.025	0.765625	0.015625	1.129	0.0451774	0.0771891
1.775	0.025	0.734375	0.015625	0.901153	0.0307848	0.0616116
1.775	0.025	0.703125	0.015625	0.73823	0.0233322	0.0504725
1.775	0.025	0.671875	0.015625	0.591562	0.01871	0.0404449
1.775	0.025	0.640625	0.015625	0.474236	0.0145542	0.0324234
1.775	0.025	0.609375	0.015625	0.371252	0.0118429	0.0253824
1.775	0.025	0.578125	0.015625	0.260302	0.00907602	0.0177968
1.775	0.025	0.546875	0.015625	0.194275	0.00749606	0.0132825
1.775	0.025	0.515625	0.015625	0.141213	0.00629534	0.0096547
1.775	0.025	0.484375	0.015625	0.103743	0.0054063	0.00709289
1.775	0.025	0.453125	0.015625	0.0857116	0.00500787	0.00586007
1.775	0.025	0.421875	0.015625	0.0934616	0.00569979	0.00638994
1.775	0.025	0.390625	0.015625	0.0972666	0.00631185	0.00665009
1.775	0.025	0.359375	0.015625	0.110595	0.00766392	0.00756134
1.825	0.025	0.796875	0.015625	1.0822	0.0562963	0.0744526

TABLE 29 – Continued

E_{beam}^{lab} [GeV]	$\pm dE_{beam}^{lab}$	$\cos \theta_{\pi_0}^{C.M.}$	$\pm d \cos \theta_{\pi_0}^{C.M.}$	$\frac{d\sigma}{d\Omega} \left[\frac{\mu b}{SR} \right]$	σ^{stat}	σ^{sys}
1.825	0.025	0.765625	0.015625	0.945719	0.0388202	0.065063
1.825	0.025	0.734375	0.015625	0.819402	0.0277509	0.0563727
1.825	0.025	0.703125	0.015625	0.728317	0.0231931	0.0501063
1.825	0.025	0.671875	0.015625	0.580529	0.0180903	0.0399389
1.825	0.025	0.640625	0.015625	0.481341	0.0143437	0.033115
1.825	0.025	0.609375	0.015625	0.343205	0.0108981	0.0236116
1.825	0.025	0.578125	0.015625	0.262518	0.00897413	0.0180605
1.825	0.025	0.546875	0.015625	0.200816	0.00758899	0.0138156
1.825	0.025	0.515625	0.015625	0.143481	0.00622244	0.0098711
1.825	0.025	0.484375	0.015625	0.120042	0.00566403	0.00825857
1.825	0.025	0.453125	0.015625	0.105056	0.00537303	0.00722756
1.825	0.025	0.421875	0.015625	0.101378	0.00550163	0.00697452
1.825	0.025	0.390625	0.015625	0.107661	0.00630371	0.00740682
1.825	0.025	0.359375	0.015625	0.106682	0.00703092	0.00733942
1.875	0.025	0.796875	0.015625	1.22832	0.0747278	0.0850353
1.875	0.025	0.765625	0.015625	1.10636	0.0506828	0.0765919
1.875	0.025	0.734375	0.015625	0.842516	0.032774	0.0583265
1.875	0.025	0.703125	0.015625	0.704498	0.0268032	0.0487717
1.875	0.025	0.671875	0.015625	0.569587	0.0207296	0.0394319
1.875	0.025	0.640625	0.015625	0.441071	0.0156701	0.0305349
1.875	0.025	0.609375	0.015625	0.341945	0.012382	0.0236725
1.875	0.025	0.578125	0.015625	0.307456	0.0115058	0.0212849
1.875	0.025	0.546875	0.015625	0.214767	0.00899992	0.0148681
1.875	0.025	0.515625	0.015625	0.179764	0.0081121	0.0124449
1.875	0.025	0.484375	0.015625	0.137126	0.00684992	0.00949311
1.875	0.025	0.453125	0.015625	0.118385	0.00634704	0.00819565
1.875	0.025	0.421875	0.015625	0.114587	0.00655932	0.00793271
1.875	0.025	0.390625	0.015625	0.117816	0.00711576	0.00815629
1.875	0.025	0.359375	0.015625	0.130716	0.00862656	0.00904933
1.875	0.025	0.328125	0.015625	0.152072	0.0107861	0.0105278
1.925	0.025	0.796875	0.015625	1.08479	0.0582134	0.0755717
1.925	0.025	0.765625	0.015625	0.885649	0.0390141	0.0616984
1.925	0.025	0.734375	0.015625	0.743505	0.0281303	0.0517959
1.925	0.025	0.703125	0.015625	0.649186	0.0226351	0.0452253
1.925	0.025	0.671875	0.015625	0.523044	0.0184078	0.0364377
1.925	0.025	0.640625	0.015625	0.41828	0.0139169	0.0291393
1.925	0.025	0.609375	0.015625	0.325514	0.0110128	0.0226768
1.925	0.025	0.578125	0.015625	0.266572	0.00957367	0.0185706
1.925	0.025	0.546875	0.015625	0.198285	0.00784699	0.0138134

TABLE 29 – Continued

E_{beam}^{lab} [GeV]	$\pm dE_{beam}^{lab}$	$\cos \theta_{\pi^0}^{C.M.}$	$\pm d \cos \theta_{\pi^0}^{C.M.}$	$\frac{d\sigma}{d\Omega} \left[\frac{\mu b}{SR} \right]$	σ^{stat}	σ^{sys}
1.925	0.025	0.515625	0.015625	0.159563	0.00675322	0.0111159
1.925	0.025	0.484375	0.015625	0.136164	0.00599873	0.00948582
1.925	0.025	0.453125	0.015625	0.120618	0.00569356	0.00840279
1.925	0.025	0.421875	0.015625	0.119054	0.00576535	0.00829381
1.925	0.025	0.390625	0.015625	0.11006	0.00596674	0.00766731
1.925	0.025	0.359375	0.015625	0.127943	0.00741757	0.00891309
1.925	0.025	0.328125	0.015625	0.113821	0.00743841	0.00792932
1.975	0.025	0.796875	0.015625	1.05783	0.0617011	0.0741583
1.975	0.025	0.765625	0.015625	1.04006	0.0469293	0.0729124
1.975	0.025	0.734375	0.015625	0.95321	0.0359786	0.0668238
1.975	0.025	0.703125	0.015625	0.825329	0.030245	0.0578588
1.975	0.025	0.671875	0.015625	0.600463	0.0217773	0.0420948
1.975	0.025	0.640625	0.015625	0.46824	0.0163224	0.0328255
1.975	0.025	0.609375	0.015625	0.39186	0.0135775	0.0274709
1.975	0.025	0.578125	0.015625	0.323608	0.0117223	0.0226862
1.975	0.025	0.546875	0.015625	0.232215	0.00941036	0.0162792
1.975	0.025	0.515625	0.015625	0.194507	0.00831993	0.0136357
1.975	0.025	0.484375	0.015625	0.183263	0.00791206	0.0128475
1.975	0.025	0.453125	0.015625	0.179123	0.00771826	0.0125572
1.975	0.025	0.421875	0.015625	0.147556	0.00717193	0.0103443
1.975	0.025	0.390625	0.015625	0.160661	0.00783781	0.0112629
1.975	0.025	0.359375	0.015625	0.154061	0.00863208	0.0108003
1.975	0.025	0.328125	0.015625	0.173016	0.0103243	0.0121291
2.025	0.025	0.796875	0.015625	0.9509	0.0551152	0.0670833
2.025	0.025	0.765625	0.015625	0.874231	0.0412007	0.0616744
2.025	0.025	0.734375	0.015625	0.666124	0.0279365	0.0469932
2.025	0.025	0.703125	0.015625	0.593646	0.0226591	0.04188
2.025	0.025	0.671875	0.015625	0.453841	0.0169576	0.0320172
2.025	0.025	0.640625	0.015625	0.384915	0.0136651	0.0271546
2.025	0.025	0.609375	0.015625	0.328652	0.0116858	0.0231854
2.025	0.025	0.578125	0.015625	0.22036	0.00883255	0.0155458
2.025	0.025	0.546875	0.015625	0.172928	0.00741737	0.0121996
2.025	0.025	0.515625	0.015625	0.156622	0.00681856	0.0110492
2.025	0.025	0.484375	0.015625	0.150034	0.00661894	0.0105845
2.025	0.025	0.453125	0.015625	0.134518	0.00586612	0.00948984
2.025	0.025	0.421875	0.015625	0.138221	0.00620239	0.00975107
2.025	0.025	0.390625	0.015625	0.123187	0.00623476	0.00869051
2.025	0.025	0.359375	0.015625	0.141332	0.00722758	0.00997057
2.025	0.025	0.328125	0.015625	0.126326	0.00761698	0.00891195

TABLE 29 – Continued

E_{beam}^{lab} [GeV]	$\pm dE_{beam}^{lab}$	$\cos \theta_{\pi^0}^{C.M.}$	$\pm d \cos \theta_{\pi^0}^{C.M.}$	$\frac{d\sigma}{d\Omega} \left[\frac{\mu b}{SR} \right]$	σ^{stat}	σ^{sys}
2.075	0.025	0.796875	0.015625	0.824812	0.0496783	0.0585567
2.075	0.025	0.765625	0.015625	0.664876	0.0343604	0.0472022
2.075	0.025	0.734375	0.015625	0.590057	0.0256623	0.0418905
2.075	0.025	0.703125	0.015625	0.491111	0.0210266	0.0348659
2.075	0.025	0.671875	0.015625	0.405478	0.0159271	0.0287865
2.075	0.025	0.640625	0.015625	0.34524	0.0129099	0.02451
2.075	0.025	0.609375	0.015625	0.293902	0.0107793	0.0208653
2.075	0.025	0.578125	0.015625	0.219577	0.00870636	0.0155886
2.075	0.025	0.546875	0.015625	0.182721	0.00744643	0.0129721
2.075	0.025	0.515625	0.015625	0.154894	0.00660283	0.0109965
2.075	0.025	0.484375	0.015625	0.148175	0.00617657	0.0105196
2.075	0.025	0.453125	0.015625	0.147784	0.00616175	0.0104918
2.075	0.025	0.421875	0.015625	0.135314	0.00595674	0.00960648
2.075	0.025	0.390625	0.015625	0.138199	0.00635941	0.00981131
2.075	0.025	0.359375	0.015625	0.136068	0.00674357	0.00966
2.075	0.025	0.328125	0.015625	0.128444	0.00721227	0.00911878
2.075	0.025	0.296875	0.015625	0.12819	0.00814005	0.00910075
2.125	0.025	0.796875	0.015625	0.988754	0.0634836	0.070641
2.125	0.025	0.765625	0.015625	0.758339	0.0393087	0.0541792
2.125	0.025	0.734375	0.015625	0.691364	0.0315675	0.0493942
2.125	0.025	0.703125	0.015625	0.599438	0.0262569	0.0428266
2.125	0.025	0.671875	0.015625	0.492669	0.0200217	0.0351985
2.125	0.025	0.640625	0.015625	0.408179	0.0162122	0.0291621
2.125	0.025	0.609375	0.015625	0.335542	0.0131417	0.0239726
2.125	0.025	0.578125	0.015625	0.256229	0.010836	0.0183062
2.125	0.025	0.546875	0.015625	0.249584	0.0101645	0.0178314
2.125	0.025	0.515625	0.015625	0.19836	0.00850546	0.0141717
2.125	0.025	0.484375	0.015625	0.190513	0.00815848	0.0136111
2.125	0.025	0.453125	0.015625	0.175062	0.00761611	0.0125072
2.125	0.025	0.421875	0.015625	0.183841	0.00784222	0.0131344
2.125	0.025	0.390625	0.015625	0.174423	0.00791972	0.0124616
2.125	0.025	0.359375	0.015625	0.157055	0.0079486	0.0112207
2.125	0.025	0.328125	0.015625	0.147924	0.00859105	0.0105684
2.125	0.025	0.296875	0.015625	0.13154	0.00904253	0.00939778
2.175	0.025	0.796875	0.015625	0.771724	0.0515215	0.0554858
2.175	0.025	0.765625	0.015625	0.592905	0.0319427	0.042629
2.175	0.025	0.734375	0.015625	0.479139	0.0232592	0.0344494
2.175	0.025	0.703125	0.015625	0.409053	0.0189688	0.0294103
2.175	0.025	0.671875	0.015625	0.364318	0.0151571	0.0261939

TABLE 29 – Continued

E_{beam}^{lab} [GeV]	$\pm dE_{beam}^{lab}$	$\cos \theta_{\pi^0}^{C.M.}$	$\pm d \cos \theta_{\pi^0}^{C.M.}$	$\frac{d\sigma}{d\Omega} \left[\frac{\mu b}{SR} \right]$	σ^{stat}	σ^{sys}
2.175	0.025	0.640625	0.015625	0.313116	0.0124492	0.0225126
2.175	0.025	0.609375	0.015625	0.257929	0.0104735	0.0185447
2.175	0.025	0.578125	0.015625	0.190331	0.0082206	0.0136846
2.175	0.025	0.546875	0.015625	0.164988	0.00730943	0.0118624
2.175	0.025	0.515625	0.015625	0.185472	0.00739934	0.0133352
2.175	0.025	0.484375	0.015625	0.165198	0.00673677	0.0118775
2.175	0.025	0.453125	0.015625	0.165869	0.0065277	0.0119258
2.175	0.025	0.421875	0.015625	0.147777	0.00604015	0.0106249
2.175	0.025	0.390625	0.015625	0.140774	0.00609735	0.0101215
2.175	0.025	0.359375	0.015625	0.124812	0.00615429	0.00897381
2.175	0.025	0.328125	0.015625	0.107612	0.00626774	0.00773716
2.175	0.025	0.296875	0.015625	0.124333	0.00768731	0.00893938
2.225	0.025	0.796875	0.015625	0.629973	0.0428219	0.0455824
2.225	0.025	0.765625	0.015625	0.594524	0.0315391	0.0430174
2.225	0.025	0.734375	0.015625	0.433642	0.02186	0.0313767
2.225	0.025	0.703125	0.015625	0.351447	0.0169004	0.0254293
2.225	0.025	0.671875	0.015625	0.316482	0.0139447	0.0228994
2.225	0.025	0.640625	0.015625	0.285593	0.0115397	0.0206644
2.225	0.025	0.609375	0.015625	0.236587	0.00967454	0.0171185
2.225	0.025	0.578125	0.015625	0.179336	0.00786424	0.012976
2.225	0.025	0.546875	0.015625	0.169372	0.00728543	0.0122551
2.225	0.025	0.515625	0.015625	0.167602	0.00692869	0.012127
2.225	0.025	0.484375	0.015625	0.169638	0.00657002	0.0122743
2.225	0.025	0.453125	0.015625	0.172448	0.00656631	0.0124777
2.225	0.025	0.421875	0.015625	0.145337	0.00584389	0.010516
2.225	0.025	0.390625	0.015625	0.153092	0.00618386	0.0110771
2.225	0.025	0.359375	0.015625	0.133254	0.00603988	0.00964173
2.225	0.025	0.328125	0.015625	0.113851	0.00592335	0.00823783
2.225	0.025	0.296875	0.015625	0.116293	0.00695311	0.00841452
2.225	0.025	0.265625	0.015625	0.109527	0.00759495	0.00792494
2.275	0.025	0.796875	0.015625	0.668104	0.0496152	0.0486494
2.275	0.025	0.765625	0.015625	0.574595	0.0351076	0.0418403
2.275	0.025	0.734375	0.015625	0.458216	0.0259297	0.0333659
2.275	0.025	0.703125	0.015625	0.366566	0.0202809	0.0266923
2.275	0.025	0.671875	0.015625	0.333331	0.0163486	0.0242722
2.275	0.025	0.640625	0.015625	0.293659	0.0135241	0.0213834
2.275	0.025	0.609375	0.015625	0.226608	0.0108277	0.016501
2.275	0.025	0.578125	0.015625	0.212229	0.009869	0.0154539
2.275	0.025	0.546875	0.015625	0.187673	0.00873921	0.0136658

TABLE 29 – Continued

E_{beam}^{lab} [GeV]	$\pm dE_{beam}^{lab}$	$\cos \theta_{\pi^0}^{C.M.}$	$\pm d \cos \theta_{\pi^0}^{C.M.}$	$\frac{d\sigma}{d\Omega} \left[\frac{\mu b}{SR} \right]$	σ^{stat}	σ^{sys}
2.275	0.025	0.515625	0.015625	0.202167	0.00867758	0.0147212
2.275	0.025	0.484375	0.015625	0.186989	0.0079146	0.013616
2.275	0.025	0.453125	0.015625	0.194192	0.00790442	0.0141405
2.275	0.025	0.421875	0.015625	0.183112	0.00750274	0.0133337
2.275	0.025	0.390625	0.015625	0.170568	0.00752825	0.0124203
2.275	0.025	0.359375	0.015625	0.138077	0.00693248	0.0100543
2.275	0.025	0.328125	0.015625	0.125767	0.00713244	0.00915798
2.275	0.025	0.296875	0.015625	0.123027	0.00783941	0.00895846
2.275	0.025	0.265625	0.015625	0.125402	0.00884073	0.00913142
2.325	0.025	0.828125	0.015625	0.587838	0.062417	0.0430776
2.325	0.025	0.796875	0.015625	0.531353	0.0430495	0.0389383
2.325	0.025	0.765625	0.015625	0.517811	0.0319207	0.0379459
2.325	0.025	0.734375	0.015625	0.36174	0.0218805	0.0265088
2.325	0.025	0.703125	0.015625	0.331746	0.0176671	0.0243108
2.325	0.025	0.671875	0.015625	0.28304	0.0136058	0.0207416
2.325	0.025	0.640625	0.015625	0.233638	0.0114055	0.0171213
2.325	0.025	0.609375	0.015625	0.20738	0.00981019	0.0151971
2.325	0.025	0.578125	0.015625	0.189226	0.00871309	0.0138667
2.325	0.025	0.546875	0.015625	0.194462	0.00839258	0.0142504
2.325	0.025	0.515625	0.015625	0.188697	0.00783435	0.013828
2.325	0.025	0.484375	0.015625	0.2008	0.00776815	0.0147149
2.325	0.025	0.453125	0.015625	0.200909	0.00760589	0.0147229
2.325	0.025	0.421875	0.015625	0.182803	0.00708982	0.013396
2.325	0.025	0.390625	0.015625	0.156662	0.00667174	0.0114804
2.325	0.025	0.359375	0.015625	0.137011	0.00628893	0.0100404
2.325	0.025	0.328125	0.015625	0.125468	0.00637764	0.00919446
2.325	0.025	0.296875	0.015625	0.111953	0.00659538	0.00820408
2.325	0.025	0.265625	0.015625	0.099206	0.0073442	0.00726995
2.375	0.025	0.828125	0.015625	0.548163	0.060026	0.0404265
2.375	0.025	0.796875	0.015625	0.508275	0.0384805	0.0374848
2.375	0.025	0.765625	0.015625	0.421507	0.028725	0.0310857
2.375	0.025	0.734375	0.015625	0.3699	0.0227456	0.0272798
2.375	0.025	0.703125	0.015625	0.306882	0.0180125	0.0226322
2.375	0.025	0.671875	0.015625	0.287999	0.0145018	0.0212397
2.375	0.025	0.640625	0.015625	0.239131	0.0119205	0.0176357
2.375	0.025	0.609375	0.015625	0.203397	0.0101278	0.0150003
2.375	0.025	0.578125	0.015625	0.208036	0.00958022	0.0153424
2.375	0.025	0.546875	0.015625	0.189361	0.00843132	0.0139652
2.375	0.025	0.515625	0.015625	0.200896	0.00839206	0.0148159

TABLE 29 – Continued

E_{beam}^{lab} [GeV]	$\pm dE_{beam}^{lab}$	$\cos \theta_{\pi^0}^{C.M.}$	$\pm d \cos \theta_{\pi^0}^{C.M.}$	$\frac{d\sigma}{d\Omega} \left[\frac{\mu b}{SR} \right]$	σ^{stat}	σ^{sys}
2.375	0.025	0.484375	0.015625	0.21859	0.00840409	0.0161208
2.375	0.025	0.453125	0.015625	0.199353	0.00777973	0.0147021
2.375	0.025	0.421875	0.015625	0.191722	0.0075504	0.0141393
2.375	0.025	0.390625	0.015625	0.170609	0.00706075	0.0125823
2.375	0.025	0.359375	0.015625	0.144465	0.0065784	0.0106542
2.375	0.025	0.328125	0.015625	0.119632	0.00628157	0.00882278
2.375	0.025	0.296875	0.015625	0.123275	0.0070572	0.00909143
2.375	0.025	0.265625	0.015625	0.10146	0.00723587	0.00748262
2.425	0.025	0.828125	0.015625	0.521337	0.057074	0.0386936
2.425	0.025	0.796875	0.015625	0.576617	0.0456553	0.0427965
2.425	0.025	0.765625	0.015625	0.401886	0.0289284	0.029828
2.425	0.025	0.734375	0.015625	0.269773	0.0183962	0.0200225
2.425	0.025	0.703125	0.015625	0.291355	0.0178967	0.0216244
2.425	0.025	0.671875	0.015625	0.261134	0.0137204	0.0193813
2.425	0.025	0.640625	0.015625	0.239503	0.0119024	0.0177759
2.425	0.025	0.609375	0.015625	0.193335	0.00988296	0.0143493
2.425	0.025	0.578125	0.015625	0.203852	0.0097148	0.0151299
2.425	0.025	0.546875	0.015625	0.181016	0.00835338	0.013435
2.425	0.025	0.515625	0.015625	0.205761	0.0086246	0.0152716
2.425	0.025	0.484375	0.015625	0.213442	0.00828424	0.0158416
2.425	0.025	0.453125	0.015625	0.211314	0.00809701	0.0156837
2.425	0.025	0.421875	0.015625	0.198265	0.00761887	0.0147152
2.425	0.025	0.390625	0.015625	0.165371	0.00700367	0.0122738
2.425	0.025	0.359375	0.015625	0.135398	0.00627132	0.0100492
2.425	0.025	0.328125	0.015625	0.130919	0.00648269	0.00971679
2.425	0.025	0.296875	0.015625	0.121588	0.00678821	0.00902427
2.425	0.025	0.265625	0.015625	0.1144	0.00722944	0.00849079
2.475	0.025	0.234375	0.015625	0.0784686	0.00695701	0.00586114
2.475	0.025	0.265625	0.015625	0.0923377	0.00646706	0.00689707
2.475	0.025	0.296875	0.015625	0.113874	0.00659601	0.00850568
2.475	0.025	0.328125	0.015625	0.126735	0.00645756	0.00946634
2.475	0.025	0.359375	0.015625	0.137033	0.00651357	0.0102355
2.475	0.025	0.390625	0.015625	0.154976	0.00687104	0.0115758
2.475	0.025	0.421875	0.015625	0.180679	0.00754468	0.0134956
2.475	0.025	0.453125	0.015625	0.195493	0.00781907	0.0146022
2.475	0.025	0.484375	0.015625	0.18902	0.00798171	0.0141187
2.475	0.025	0.515625	0.015625	0.207071	0.0089392	0.0154669
2.475	0.025	0.546875	0.015625	0.174067	0.00854375	0.0130018
2.475	0.025	0.578125	0.015625	0.166602	0.00875828	0.0124441

TABLE 29 – Continued

E_{beam}^{lab} [GeV]	$\pm dE_{beam}^{lab}$	$\cos \theta_{\pi^0}^{C.M.}$	$\pm d \cos \theta_{\pi^0}^{C.M.}$	$\frac{d\sigma}{d\Omega}$ [$\frac{\mu b}{SR}$]	σ^{stat}	σ^{sys}
2.475	0.025	0.609375	0.015625	0.16533	0.0094689	0.0123492
2.475	0.025	0.640625	0.015625	0.199996	0.0113336	0.0149385
2.475	0.025	0.671875	0.015625	0.210999	0.0131549	0.0157603
2.475	0.025	0.703125	0.015625	0.232007	0.0155561	0.0173295
2.475	0.025	0.734375	0.015625	0.261495	0.0191808	0.0195321
2.475	0.025	0.765625	0.015625	0.311128	0.0247761	0.0232394
2.475	0.025	0.796875	0.015625	0.401083	0.0376821	0.0299585
2.475	0.025	0.828125	0.015625	0.318338	0.0486058	0.023778
2.525	0.025	0.828125	0.015625	0.53185	0.0587432	0.0399798
2.525	0.025	0.796875	0.015625	0.368561	0.0327506	0.0277052
2.525	0.025	0.765625	0.015625	0.27536	0.0226566	0.0206991
2.525	0.025	0.734375	0.015625	0.26755	0.0186544	0.0201121
2.525	0.025	0.703125	0.015625	0.203328	0.0142622	0.0152844
2.525	0.025	0.671875	0.015625	0.236053	0.0132562	0.0177444
2.525	0.025	0.640625	0.015625	0.212456	0.0112328	0.0159706
2.525	0.025	0.609375	0.015625	0.191543	0.00993106	0.0143985
2.525	0.025	0.578125	0.015625	0.159665	0.0082483	0.0120022
2.525	0.025	0.546875	0.015625	0.189257	0.00842769	0.0142267
2.525	0.025	0.515625	0.015625	0.203128	0.00843249	0.0152694
2.525	0.025	0.484375	0.015625	0.218821	0.0083287	0.016449
2.525	0.025	0.453125	0.015625	0.20334	0.00788092	0.0152853
2.525	0.025	0.421875	0.015625	0.194302	0.00759277	0.0146059
2.525	0.025	0.390625	0.015625	0.173786	0.00687563	0.0130637
2.525	0.025	0.359375	0.015625	0.138667	0.00629318	0.0104238
2.525	0.025	0.328125	0.015625	0.131741	0.00616425	0.00990314
2.525	0.025	0.296875	0.015625	0.110978	0.00606595	0.00834238
2.525	0.025	0.265625	0.015625	0.0998475	0.00622146	0.00750566
2.525	0.025	0.234375	0.015625	0.079843	0.00634883	0.0060019
2.575	0.025	0.828125	0.015625	0.38062	0.0591764	0.0287944
2.575	0.025	0.796875	0.015625	0.353018	0.0368554	0.0267064
2.575	0.025	0.765625	0.015625	0.254973	0.0254491	0.0192891
2.575	0.025	0.734375	0.015625	0.170271	0.0177321	0.0128812
2.575	0.025	0.703125	0.015625	0.201669	0.0170503	0.0152566
2.575	0.025	0.671875	0.015625	0.190125	0.0139086	0.0143833
2.575	0.025	0.640625	0.015625	0.19612	0.0132446	0.0148367
2.575	0.025	0.609375	0.015625	0.185236	0.0114433	0.0140133
2.575	0.025	0.578125	0.015625	0.166661	0.010147	0.0126081
2.575	0.025	0.546875	0.015625	0.205731	0.0108471	0.0155638
2.575	0.025	0.515625	0.015625	0.209772	0.0104455	0.0158696

TABLE 29 – Continued

E_{beam}^{lab} [GeV]	$\pm dE_{beam}^{lab}$	$\cos \theta_{\pi^0}^{C.M.}$	$\pm d \cos \theta_{\pi^0}^{C.M.}$	$\frac{d\sigma}{d\Omega}$ [$\frac{\mu b}{SR}$]	σ^{stat}	σ^{sys}
2.575	0.025	0.484375	0.015625	0.217428	0.0098697	0.0164488
2.575	0.025	0.453125	0.015625	0.203226	0.00943042	0.0153744
2.575	0.025	0.421875	0.015625	0.202188	0.00904775	0.0152958
2.575	0.025	0.390625	0.015625	0.167017	0.0081105	0.0126351
2.575	0.025	0.359375	0.015625	0.136072	0.00735185	0.010294
2.575	0.025	0.328125	0.015625	0.117428	0.00692289	0.00888356
2.575	0.025	0.296875	0.015625	0.113747	0.00705295	0.00860515
2.575	0.025	0.265625	0.015625	0.105317	0.00753987	0.00796738
2.575	0.025	0.234375	0.015625	0.079912	0.00749742	0.00604546
2.625	0.025	0.828125	0.015625	0.331328	0.0517407	0.0252256
2.625	0.025	0.796875	0.015625	0.298695	0.0362182	0.022741
2.625	0.025	0.765625	0.015625	0.171504	0.0205199	0.0130574
2.625	0.025	0.734375	0.015625	0.196149	0.0187832	0.0149337
2.625	0.025	0.703125	0.015625	0.206244	0.0169477	0.0157023
2.625	0.025	0.671875	0.015625	0.203475	0.0143047	0.0154915
2.625	0.025	0.640625	0.015625	0.165873	0.0118533	0.0126287
2.625	0.025	0.609375	0.015625	0.173829	0.0109994	0.0132344
2.625	0.025	0.578125	0.015625	0.17326	0.0101781	0.0131911
2.625	0.025	0.546875	0.015625	0.192889	0.0103292	0.0146855
2.625	0.025	0.515625	0.015625	0.213377	0.0103168	0.0162454
2.625	0.025	0.484375	0.015625	0.228334	0.0103221	0.0173841
2.625	0.025	0.453125	0.015625	0.197099	0.00906777	0.015006
2.625	0.025	0.421875	0.015625	0.190456	0.00879215	0.0145003
2.625	0.025	0.390625	0.015625	0.159611	0.0078751	0.0121519
2.625	0.025	0.359375	0.015625	0.127397	0.00697681	0.00969932
2.625	0.025	0.328125	0.015625	0.11302	0.00660273	0.00860473
2.625	0.025	0.296875	0.015625	0.0970721	0.00633241	0.00739055
2.625	0.025	0.265625	0.015625	0.0801546	0.00617686	0.00610255
2.625	0.025	0.234375	0.015625	0.0719128	0.00659729	0.00547506
2.675	0.025	0.796875	0.015625	0.314937	0.0338106	0.0241307
2.675	0.025	0.765625	0.015625	0.153004	0.0183349	0.0117233
2.675	0.025	0.734375	0.015625	0.165732	0.0167168	0.0126985
2.675	0.025	0.703125	0.015625	0.177217	0.0153539	0.0135785
2.675	0.025	0.671875	0.015625	0.167754	0.0124248	0.0128535
2.675	0.025	0.640625	0.015625	0.156321	0.0110899	0.0119775
2.675	0.025	0.609375	0.015625	0.14133	0.00931744	0.0108288
2.675	0.025	0.578125	0.015625	0.165415	0.00954058	0.0126743
2.675	0.025	0.546875	0.015625	0.206702	0.0101924	0.0158377
2.675	0.025	0.515625	0.015625	0.210035	0.00984406	0.0160931

TABLE 29 – Continued

E_{beam}^{lab} [GeV]	$\pm dE_{beam}^{lab}$	$\cos \theta_{\pi^0}^{C.M.}$	$\pm d \cos \theta_{\pi^0}^{C.M.}$	$\frac{d\sigma}{d\Omega}$ [$\frac{\mu b}{SR}$]	σ^{stat}	σ^{sys}
2.675	0.025	0.484375	0.015625	0.197629	0.00906707	0.0151425
2.675	0.025	0.453125	0.015625	0.195925	0.00875992	0.015012
2.675	0.025	0.421875	0.015625	0.187313	0.00844657	0.0143521
2.675	0.025	0.390625	0.015625	0.137559	0.00694308	0.0105399
2.675	0.025	0.359375	0.015625	0.134006	0.00686664	0.0102676
2.675	0.025	0.328125	0.015625	0.113996	0.00626382	0.00873444
2.675	0.025	0.296875	0.015625	0.101127	0.00608643	0.00774845
2.675	0.025	0.265625	0.015625	0.0829122	0.00595564	0.0063528
2.675	0.025	0.234375	0.015625	0.0665253	0.00591051	0.00509722
2.675	0.025	0.203125	0.015625	0.0388891	0.00521339	0.00297972
2.725	0.025	0.828125	0.015625	0.329393	0.0518856	0.0253995
2.725	0.025	0.796875	0.015625	0.254016	0.0295481	0.0195872
2.725	0.025	0.765625	0.015625	0.17084	0.0188833	0.0131735
2.725	0.025	0.734375	0.015625	0.184644	0.0177772	0.0142379
2.725	0.025	0.703125	0.015625	0.18057	0.0150184	0.0139237
2.725	0.025	0.671875	0.015625	0.14809	0.0117921	0.0114192
2.725	0.025	0.640625	0.015625	0.166829	0.0111659	0.0128641
2.725	0.025	0.609375	0.015625	0.156207	0.0097794	0.0120451
2.725	0.025	0.578125	0.015625	0.179439	0.0101049	0.0138365
2.725	0.025	0.546875	0.015625	0.21567	0.0103173	0.0166303
2.725	0.025	0.515625	0.015625	0.19968	0.00933654	0.0153973
2.725	0.025	0.484375	0.015625	0.226505	0.00965169	0.0174658
2.725	0.025	0.453125	0.015625	0.211763	0.00899902	0.016329
2.725	0.025	0.421875	0.015625	0.177998	0.00809613	0.0137254
2.725	0.025	0.390625	0.015625	0.165052	0.0076111	0.0127272
2.725	0.025	0.359375	0.015625	0.134786	0.00663925	0.0103934
2.725	0.025	0.328125	0.015625	0.120927	0.00637787	0.00932467
2.725	0.025	0.296875	0.015625	0.112204	0.00626791	0.00865208
2.725	0.025	0.265625	0.015625	0.0804008	0.00563038	0.0061997
2.725	0.025	0.234375	0.015625	0.0605255	0.00546047	0.00466712
2.725	0.025	0.203125	0.015625	0.0507151	0.0056114	0.00391064
2.775	0.025	0.828125	0.015625	0.393439	0.0538898	0.0305316
2.775	0.025	0.796875	0.015625	0.273904	0.0332714	0.0212554
2.775	0.025	0.765625	0.015625	0.147701	0.0172615	0.0114619
2.775	0.025	0.734375	0.015625	0.189152	0.0177726	0.0146785
2.775	0.025	0.703125	0.015625	0.191043	0.0157448	0.0148253
2.775	0.025	0.671875	0.015625	0.179129	0.0131819	0.0139008
2.775	0.025	0.640625	0.015625	0.168454	0.0120469	0.0130724
2.775	0.025	0.609375	0.015625	0.147973	0.00990459	0.0114829

TABLE 29 – Continued

E_{beam}^{lab} [GeV]	$\pm dE_{beam}^{lab}$	$\cos \theta_{\pi^0}^{C.M.}$	$\pm d \cos \theta_{\pi^0}^{C.M.}$	$\frac{d\sigma}{d\Omega} \left[\frac{\mu b}{SR} \right]$	σ^{stat}	σ^{sys}
2.775	0.025	0.578125	0.015625	0.165917	0.00984736	0.0128755
2.775	0.025	0.546875	0.015625	0.220715	0.0107054	0.0171279
2.775	0.025	0.515625	0.015625	0.215143	0.00998748	0.0166955
2.775	0.025	0.484375	0.015625	0.235101	0.0100983	0.0182443
2.775	0.025	0.453125	0.015625	0.217357	0.00953496	0.0168673
2.775	0.025	0.421875	0.015625	0.178577	0.00821856	0.0138579
2.775	0.025	0.390625	0.015625	0.165221	0.00773265	0.0128214
2.775	0.025	0.359375	0.015625	0.146908	0.00719999	0.0114003
2.775	0.025	0.328125	0.015625	0.124482	0.00668153	0.00966007
2.775	0.025	0.296875	0.015625	0.11548	0.00650545	0.00896144
2.775	0.025	0.265625	0.015625	0.0887829	0.00593414	0.00688972
2.775	0.025	0.234375	0.015625	0.0686088	0.00576351	0.00532417
2.775	0.025	0.203125	0.015625	0.0454589	0.00510179	0.00352769
2.825	0.025	0.828125	0.015625	0.326442	0.0539561	0.025494
2.825	0.025	0.796875	0.015625	0.234166	0.0282591	0.0182876
2.825	0.025	0.765625	0.015625	0.142692	0.0157981	0.0111438
2.825	0.025	0.734375	0.015625	0.141624	0.0141091	0.0110603
2.825	0.025	0.703125	0.015625	0.142912	0.0121075	0.0111609
2.825	0.025	0.671875	0.015625	0.151212	0.0112379	0.0118091
2.825	0.025	0.640625	0.015625	0.135168	0.00958015	0.0105561
2.825	0.025	0.609375	0.015625	0.134183	0.00863578	0.0104792
2.825	0.025	0.578125	0.015625	0.151178	0.00848186	0.0118065
2.825	0.025	0.546875	0.015625	0.181244	0.00910448	0.0141545
2.825	0.025	0.515625	0.015625	0.190723	0.00867091	0.0148948
2.825	0.025	0.484375	0.015625	0.187937	0.00834556	0.0146772
2.825	0.025	0.453125	0.015625	0.201656	0.00854638	0.0157487
2.825	0.025	0.421875	0.015625	0.171234	0.0075977	0.0133728
2.825	0.025	0.390625	0.015625	0.132916	0.00643782	0.0103803
2.825	0.025	0.359375	0.015625	0.125027	0.00611814	0.00976421
2.825	0.025	0.328125	0.015625	0.106059	0.00560311	0.0082828
2.825	0.025	0.296875	0.015625	0.0840789	0.00497664	0.00656627
2.825	0.025	0.265625	0.015625	0.0604825	0.00435876	0.00472347
2.825	0.025	0.234375	0.015625	0.0455578	0.00410463	0.00355791
2.825	0.025	0.203125	0.015625	0.0377567	0.00413603	0.00294866
2.875	0.025	0.828125	0.015625	0.259347	0.043061	0.0203831
2.875	0.025	0.796875	0.015625	0.275343	0.0314436	0.0216402
2.875	0.025	0.765625	0.015625	0.12666	0.0146311	0.00995471
2.875	0.025	0.734375	0.015625	0.154593	0.0151289	0.0121501
2.875	0.025	0.703125	0.015625	0.152559	0.0126851	0.0119902

TABLE 29 – Continued

E_{beam}^{lab} [GeV]	$\pm dE_{beam}^{lab}$	$\cos \theta_{\pi^0}^{C.M.}$	$\pm d \cos \theta_{\pi^0}^{C.M.}$	$\frac{d\sigma}{d\Omega}$ [$\frac{\mu b}{SR}$]	σ^{stat}	σ^{sys}
2.875	0.025	0.671875	0.015625	0.170589	0.0122462	0.0134072
2.875	0.025	0.640625	0.015625	0.118836	0.00895418	0.00933979
2.875	0.025	0.609375	0.015625	0.135775	0.00892391	0.0106711
2.875	0.025	0.578125	0.015625	0.140853	0.00853715	0.0110702
2.875	0.025	0.546875	0.015625	0.179937	0.00916386	0.014142
2.875	0.025	0.515625	0.015625	0.182827	0.00863362	0.0143691
2.875	0.025	0.484375	0.015625	0.182629	0.00831891	0.0143535
2.875	0.025	0.453125	0.015625	0.171728	0.00790903	0.0134968
2.875	0.025	0.421875	0.015625	0.150985	0.00717312	0.0118665
2.875	0.025	0.390625	0.015625	0.113608	0.00600021	0.00892893
2.875	0.025	0.359375	0.015625	0.121529	0.00618988	0.00955145
2.875	0.025	0.328125	0.015625	0.109737	0.00578549	0.00862468
2.875	0.025	0.296875	0.015625	0.0826628	0.00505585	0.00649679
2.875	0.025	0.265625	0.015625	0.055949	0.00421713	0.00439725
2.875	0.025	0.234375	0.015625	0.0495277	0.00428258	0.00389257
2.875	0.025	0.203125	0.015625	0.0291882	0.00363515	0.00229401
2.925	0.025	0.828125	0.015625	0.255257	0.0414845	0.0201893
2.925	0.025	0.796875	0.015625	0.280823	0.03206	0.0222114
2.925	0.025	0.765625	0.015625	0.166778	0.0179005	0.0131911
2.925	0.025	0.734375	0.015625	0.127694	0.0136251	0.0100998
2.925	0.025	0.703125	0.015625	0.15572	0.0130309	0.0123165
2.925	0.025	0.671875	0.015625	0.133967	0.0106605	0.010596
2.925	0.025	0.640625	0.015625	0.104845	0.00817538	0.00829259
2.925	0.025	0.609375	0.015625	0.119717	0.00863681	0.00946891
2.925	0.025	0.578125	0.015625	0.14337	0.00861475	0.0113397
2.925	0.025	0.546875	0.015625	0.16487	0.00897701	0.0130402
2.925	0.025	0.515625	0.015625	0.181416	0.00870696	0.0143489
2.925	0.025	0.484375	0.015625	0.175823	0.00841892	0.0139065
2.925	0.025	0.453125	0.015625	0.166244	0.00785605	0.0131489
2.925	0.025	0.421875	0.015625	0.141535	0.00705004	0.0111946
2.925	0.025	0.390625	0.015625	0.118947	0.00619062	0.00940799
2.925	0.025	0.359375	0.015625	0.0952219	0.00545048	0.00753148
2.925	0.025	0.328125	0.015625	0.0963326	0.00539106	0.00761933
2.925	0.025	0.296875	0.015625	0.0704442	0.00457089	0.00557171
2.925	0.025	0.265625	0.015625	0.0501592	0.00402111	0.00396729
2.925	0.025	0.234375	0.015625	0.0395638	0.00376978	0.00312926
2.925	0.025	0.203125	0.015625	0.0295314	0.00351103	0.00233576
2.975	0.025	0.828125	0.015625	0.171892	0.0359349	0.013682
2.975	0.025	0.796875	0.015625	0.207857	0.0266539	0.0165448

TABLE 29 – Continued

E_{beam}^{lab} [GeV]	$\pm dE_{beam}^{lab}$	$\cos \theta_{\pi^0}^{C.M.}$	$\pm d \cos \theta_{\pi^0}^{C.M.}$	$\frac{d\sigma}{d\Omega} \left[\frac{\mu b}{SR} \right]$	σ^{stat}	σ^{sys}
2.975	0.025	0.765625	0.015625	0.163466	0.0184487	0.0130114
2.975	0.025	0.734375	0.015625	0.144467	0.0154874	0.0114991
2.975	0.025	0.703125	0.015625	0.160643	0.0138249	0.0127866
2.975	0.025	0.671875	0.015625	0.15671	0.0124007	0.0124736
2.975	0.025	0.640625	0.015625	0.130675	0.00992733	0.0104013
2.975	0.025	0.609375	0.015625	0.133646	0.00961893	0.0106378
2.975	0.025	0.578125	0.015625	0.177111	0.0105163	0.0140974
2.975	0.025	0.546875	0.015625	0.201909	0.0105505	0.0160713
2.975	0.025	0.515625	0.015625	0.202276	0.00973613	0.0161005
2.975	0.025	0.484375	0.015625	0.200898	0.00945155	0.0159909
2.975	0.025	0.453125	0.015625	0.172985	0.00852735	0.0137691
2.975	0.025	0.421875	0.015625	0.140516	0.00746333	0.0111846
2.975	0.025	0.390625	0.015625	0.122609	0.00684314	0.00975924
2.975	0.025	0.359375	0.015625	0.116622	0.00637985	0.00928271
2.975	0.025	0.328125	0.015625	0.093257	0.00561923	0.00742295
2.975	0.025	0.296875	0.015625	0.0720537	0.0050548	0.00573524
2.975	0.025	0.265625	0.015625	0.0529957	0.00436179	0.00421828
2.975	0.025	0.234375	0.015625	0.0400204	0.0038631	0.0031855
2.975	0.025	0.203125	0.015625	0.0283842	0.00360451	0.00225929
2.975	0.025	0.171875	0.015625	0.0189268	0.00349364	0.00150651
3.175	0.025	0.828125	0.015625	0.082391	0.0295023	0.00672581
3.175	0.025	0.796875	0.015625	0.137139	0.0257647	0.0111195
3.175	0.025	0.765625	0.015625	0.168246	0.0241903	0.0137344
3.175	0.025	0.734375	0.015625	0.135699	0.0185317	0.0110775
3.175	0.025	0.703125	0.015625	0.154036	0.0168577	0.0125744
3.175	0.025	0.671875	0.015625	0.0966011	0.0109112	0.00788582
3.175	0.025	0.640625	0.015625	0.110238	0.0113617	0.00899902
3.175	0.025	0.609375	0.015625	0.149091	0.0128332	0.0121707
3.175	0.025	0.578125	0.015625	0.162193	0.0128304	0.0132402
3.175	0.025	0.546875	0.015625	0.164776	0.0117832	0.0134512
3.175	0.025	0.515625	0.015625	0.176792	0.0118159	0.014432
3.175	0.025	0.484375	0.015625	0.134277	0.00963788	0.0109614
3.175	0.025	0.453125	0.015625	0.120428	0.00888019	0.00983091
3.175	0.025	0.421875	0.015625	0.100098	0.00783108	0.00817125
3.175	0.025	0.390625	0.015625	0.0996174	0.00763063	0.00813205
3.175	0.025	0.359375	0.015625	0.0824337	0.00674036	0.0067293
3.175	0.025	0.328125	0.015625	0.0660213	0.00586821	0.0053895
3.175	0.025	0.296875	0.015625	0.050073	0.00509667	0.0040876
3.175	0.025	0.265625	0.015625	0.0331059	0.00405002	0.00270253

TABLE 29 – Continued

E_{beam}^{lab} [GeV]	$\pm dE_{beam}^{lab}$	$\cos \theta_{\pi^0}^{C.M.}$	$\pm d \cos \theta_{\pi^0}^{C.M.}$	$\frac{d\sigma}{d\Omega} \left[\frac{\mu b}{SR} \right]$	σ^{stat}	σ^{sys}
3.175	0.025	0.234375	0.015625	0.0219232	0.0033649	0.00178966
3.175	0.025	0.203125	0.015625	0.017512	0.00321971	0.00142955
3.225	0.025	0.828125	0.015625	0.125175	0.0308747	0.0102828
3.225	0.025	0.796875	0.015625	0.0984002	0.0172884	0.00808337
3.225	0.025	0.765625	0.015625	0.152511	0.0197396	0.0125285
3.225	0.025	0.734375	0.015625	0.156714	0.0174306	0.0128737
3.225	0.025	0.703125	0.015625	0.14756	0.0145413	0.0121218
3.225	0.025	0.671875	0.015625	0.108968	0.0107846	0.00895151
3.225	0.025	0.640625	0.015625	0.100061	0.00942799	0.00821977
3.225	0.025	0.609375	0.015625	0.105793	0.0094946	0.00869065
3.225	0.025	0.578125	0.015625	0.144428	0.0106877	0.0118644
3.225	0.025	0.546875	0.015625	0.148938	0.0100883	0.012235
3.225	0.025	0.515625	0.015625	0.139847	0.00926494	0.0114881
3.225	0.025	0.484375	0.015625	0.11406	0.00799618	0.00936977
3.225	0.025	0.453125	0.015625	0.103754	0.00739352	0.00852318
3.225	0.025	0.421875	0.015625	0.0703712	0.00576226	0.00578085
3.225	0.025	0.390625	0.015625	0.0777153	0.00600165	0.00638415
3.225	0.025	0.359375	0.015625	0.0645843	0.00528356	0.00530546
3.225	0.025	0.328125	0.015625	0.0382239	0.00394956	0.00314002
3.225	0.025	0.296875	0.015625	0.0325353	0.00364657	0.00267271
3.225	0.025	0.265625	0.015625	0.0237919	0.0031223	0.00195446
3.225	0.025	0.234375	0.015625	0.0160467	0.00249754	0.0013182
3.225	0.025	0.203125	0.015625	0.00929341	0.00204135	0.000763434
3.225	0.025	0.171875	0.015625	0.011982	0.00257213	0.000984297
3.275	0.025	0.828125	0.015625	0.081536	0.0250622	0.0067402
3.275	0.025	0.796875	0.015625	0.10387	0.0180742	0.00858643
3.275	0.025	0.765625	0.015625	0.140538	0.0203745	0.0116176
3.275	0.025	0.734375	0.015625	0.111433	0.0144826	0.00921162
3.275	0.025	0.703125	0.015625	0.1211	0.0124401	0.0100108
3.275	0.025	0.671875	0.015625	0.110652	0.0107134	0.00914707
3.275	0.025	0.640625	0.015625	0.0907428	0.00920738	0.00750129
3.275	0.025	0.609375	0.015625	0.11654	0.0100598	0.0096338
3.275	0.025	0.578125	0.015625	0.156079	0.0111662	0.0129023
3.275	0.025	0.546875	0.015625	0.128363	0.0093296	0.0106112
3.275	0.025	0.515625	0.015625	0.115801	0.00821845	0.00957272
3.275	0.025	0.484375	0.015625	0.106366	0.00765076	0.00879278
3.275	0.025	0.453125	0.015625	0.0891047	0.00688944	0.00736588
3.275	0.025	0.421875	0.015625	0.0794478	0.00621211	0.00656758
3.275	0.025	0.390625	0.015625	0.0659264	0.00550902	0.00544983

TABLE 29 – Continued

E_{beam}^{lab} [GeV]	$\pm dE_{beam}^{lab}$	$\cos \theta_{\pi^0}^{C.M.}$	$\pm d \cos \theta_{\pi^0}^{C.M.}$	$\frac{d\sigma}{d\Omega} \left[\frac{\mu b}{SR} \right]$	σ^{stat}	σ^{sys}
3.275	0.025	0.359375	0.015625	0.0542183	0.00483454	0.00448198
3.275	0.025	0.328125	0.015625	0.0399795	0.0041175	0.00330492
3.275	0.025	0.296875	0.015625	0.0238529	0.00312172	0.00197181
3.275	0.025	0.265625	0.015625	0.0172121	0.00258743	0.00142285
3.275	0.025	0.234375	0.015625	0.0118688	0.00218334	0.000981138
3.275	0.025	0.203125	0.015625	0.0108809	0.00218973	0.000899472
3.325	0.025	0.828125	0.015625	0.178819	0.0450287	0.014875
3.325	0.025	0.796875	0.015625	0.148778	0.0260209	0.0123761
3.325	0.025	0.765625	0.015625	0.158142	0.0229905	0.0131551
3.325	0.025	0.734375	0.015625	0.147694	0.0179627	0.012286
3.325	0.025	0.703125	0.015625	0.155215	0.0156545	0.0129115
3.325	0.025	0.671875	0.015625	0.0977589	0.0110793	0.00813209
3.325	0.025	0.640625	0.015625	0.095104	0.0102227	0.00791124
3.325	0.025	0.609375	0.015625	0.140527	0.0119607	0.0116897
3.325	0.025	0.578125	0.015625	0.155104	0.0118096	0.0129024
3.325	0.025	0.546875	0.015625	0.146787	0.010822	0.0122105
3.325	0.025	0.515625	0.015625	0.139062	0.0103929	0.0115679
3.325	0.025	0.484375	0.015625	0.117315	0.00908571	0.00975888
3.325	0.025	0.453125	0.015625	0.090374	0.00781899	0.00751777
3.325	0.025	0.421875	0.015625	0.0748855	0.00671873	0.00622936
3.325	0.025	0.390625	0.015625	0.0616267	0.0058842	0.00512642
3.325	0.025	0.359375	0.015625	0.0493178	0.00508878	0.00410251
3.325	0.025	0.328125	0.015625	0.0427136	0.00456082	0.00355314
3.325	0.025	0.296875	0.015625	0.030327	0.00376569	0.00252275
3.325	0.025	0.265625	0.015625	0.0216524	0.00322853	0.00180116
3.325	0.025	0.234375	0.015625	0.0126625	0.0024637	0.00105333
3.325	0.025	0.203125	0.015625	0.00955785	0.00221439	0.000795071
3.375	0.025	0.828125	0.015625	0.089517	0.0281836	0.00749321
3.375	0.025	0.796875	0.015625	0.129038	0.0213676	0.0108014
3.375	0.025	0.765625	0.015625	0.157131	0.0197943	0.013153
3.375	0.025	0.734375	0.015625	0.157909	0.017118	0.0132181
3.375	0.025	0.703125	0.015625	0.145245	0.0132016	0.012158
3.375	0.025	0.671875	0.015625	0.100282	0.00995758	0.00839432
3.375	0.025	0.640625	0.015625	0.111979	0.0100914	0.00937341
3.375	0.025	0.609375	0.015625	0.142806	0.0113017	0.0119539
3.375	0.025	0.578125	0.015625	0.138214	0.0106247	0.0115695
3.375	0.025	0.546875	0.015625	0.135743	0.00941298	0.0113626
3.375	0.025	0.515625	0.015625	0.106241	0.007901	0.00889315
3.375	0.025	0.484375	0.015625	0.104237	0.00750919	0.00872537

TABLE 29 – Continued

E_{beam}^{lab} [GeV]	$\pm dE_{beam}^{lab}$	$\cos \theta_{\pi^0}^{C.M.}$	$\pm d \cos \theta_{\pi^0}^{C.M.}$	$\frac{d\sigma}{d\Omega} \left[\frac{\mu b}{SR} \right]$	σ^{stat}	σ^{sys}
3.375	0.025	0.453125	0.015625	0.0743772	0.00615648	0.0062259
3.375	0.025	0.421875	0.015625	0.0637528	0.00542612	0.00533656
3.375	0.025	0.390625	0.015625	0.059033	0.00518196	0.00494148
3.375	0.025	0.359375	0.015625	0.0467286	0.00446699	0.00391152
3.375	0.025	0.328125	0.015625	0.0255833	0.00319418	0.00214151
3.375	0.025	0.296875	0.015625	0.021852	0.00295649	0.00182917
3.375	0.025	0.265625	0.015625	0.0143482	0.00232007	0.00120105
3.375	0.025	0.234375	0.015625	0.0092959	0.00187203	0.000778133
3.375	0.025	0.203125	0.015625	0.007092	0.00163888	0.000593651
3.375	0.025	0.171875	0.015625	0.00466759	0.00141745	0.00039071
3.425	0.025	0.828125	0.015625	0.0738582	0.0213812	0.00622117
3.425	0.025	0.796875	0.015625	0.0996256	0.0185161	0.0083916
3.425	0.025	0.765625	0.015625	0.104819	0.016137	0.00882905
3.425	0.025	0.734375	0.015625	0.144045	0.0156055	0.0121331
3.425	0.025	0.703125	0.015625	0.11017	0.0111905	0.00927979
3.425	0.025	0.671875	0.015625	0.0971069	0.00969817	0.00817944
3.425	0.025	0.640625	0.015625	0.0917196	0.00898747	0.00772567
3.425	0.025	0.609375	0.015625	0.127207	0.0103604	0.0107148
3.425	0.025	0.578125	0.015625	0.118156	0.00954418	0.00995246
3.425	0.025	0.546875	0.015625	0.114193	0.00871543	0.00961864
3.425	0.025	0.515625	0.015625	0.105614	0.00781728	0.00889603
3.425	0.025	0.484375	0.015625	0.0811075	0.00652225	0.0068318
3.425	0.025	0.453125	0.015625	0.0568105	0.00529443	0.00478522
3.425	0.025	0.421875	0.015625	0.0446454	0.00446516	0.00376054
3.425	0.025	0.390625	0.015625	0.0358345	0.00396247	0.00301838
3.425	0.025	0.359375	0.015625	0.0346988	0.00376203	0.00292272
3.425	0.025	0.328125	0.015625	0.0199983	0.00280097	0.00168448
3.425	0.025	0.296875	0.015625	0.0196787	0.00272618	0.00165756
3.425	0.025	0.265625	0.015625	0.0131976	0.00220018	0.00111165
3.425	0.025	0.234375	0.015625	0.00338924	0.00107789	0.00028548
3.425	0.025	0.203125	0.015625	0.00288554	0.00102441	0.000243053
3.425	0.025	0.171875	0.015625	0.00392897	0.00125413	0.000330943
3.475	0.025	0.828125	0.015625	0.140885	0.0350836	0.0119411
3.475	0.025	0.796875	0.015625	0.117097	0.0207451	0.00992486
3.475	0.025	0.765625	0.015625	0.135197	0.0186492	0.011459
3.475	0.025	0.734375	0.015625	0.160243	0.0168781	0.0135818
3.475	0.025	0.703125	0.015625	0.144014	0.0128891	0.0122063
3.475	0.025	0.671875	0.015625	0.110466	0.0104238	0.00936288
3.475	0.025	0.640625	0.015625	0.113626	0.0103441	0.0096307

TABLE 29 – Continued

E_{beam}^{lab} [GeV]	$\pm dE_{beam}^{lab}$	$\cos \theta_{\pi^0}^{C.M.}$	$\pm d \cos \theta_{\pi^0}^{C.M.}$	$\frac{d\sigma}{d\Omega}$ [$\frac{\mu b}{SR}$]	σ^{stat}	σ^{sys}
3.475	0.025	0.609375	0.015625	0.134723	0.0106518	0.0114188
3.475	0.025	0.578125	0.015625	0.1373	0.0102219	0.0116372
3.475	0.025	0.546875	0.015625	0.110817	0.00850276	0.00939261
3.475	0.025	0.515625	0.015625	0.0963913	0.00760051	0.00816991
3.475	0.025	0.484375	0.015625	0.0943933	0.00718973	0.00800056
3.475	0.025	0.453125	0.015625	0.0596837	0.00537387	0.00505865
3.475	0.025	0.421875	0.015625	0.0438251	0.00452683	0.00371452
3.475	0.025	0.390625	0.015625	0.0480156	0.00464986	0.00406969
3.475	0.025	0.359375	0.015625	0.0350717	0.0038951	0.0029726
3.475	0.025	0.328125	0.015625	0.0307723	0.00348147	0.00260819
3.475	0.025	0.296875	0.015625	0.0169101	0.00254391	0.00143327
3.475	0.025	0.265625	0.015625	0.0108499	0.00200902	0.000919612
3.475	0.025	0.234375	0.015625	0.00578645	0.00145713	0.000490447
3.475	0.025	0.203125	0.015625	0.00518669	0.00140618	0.000439612
3.575	0.025	0.765625	0.015625	0.116276	0.013403	0.00997842
3.575	0.025	0.734375	0.015625	0.0917324	0.0096779	0.00787219
3.575	0.025	0.703125	0.015625	0.0740374	0.00711545	0.00635366
3.575	0.025	0.671875	0.015625	0.0679831	0.00667601	0.0058341
3.575	0.025	0.640625	0.015625	0.0651404	0.00620084	0.00559015
3.575	0.025	0.609375	0.015625	0.0773577	0.00654087	0.00663859
3.575	0.025	0.578125	0.015625	0.076964	0.00592179	0.00660481
3.575	0.025	0.546875	0.015625	0.0734967	0.00554393	0.00630725
3.575	0.025	0.515625	0.015625	0.0557976	0.00455314	0.00478837
3.575	0.025	0.484375	0.015625	0.0388833	0.00373381	0.00333684
3.575	0.025	0.453125	0.015625	0.0323956	0.00305093	0.00278009
3.575	0.025	0.421875	0.015625	0.0209473	0.00247447	0.00179763
3.575	0.025	0.390625	0.015625	0.0234278	0.00258828	0.0020105
3.575	0.025	0.359375	0.015625	0.0131398	0.00188225	0.00112762
3.575	0.025	0.328125	0.015625	0.0133075	0.00184805	0.001142
3.575	0.025	0.296875	0.015625	0.00920698	0.00150994	0.000790115
3.575	0.025	0.265625	0.015625	0.00450495	0.0010195	0.000386601
3.575	0.025	0.234375	0.015625	0.00406441	0.000963931	0.000348795
3.575	0.025	0.203125	0.015625	0.00126721	0.000521833	0.000108748
3.575	0.025	0.171875	0.015625	0.000642807	0.000371741	5.51637e-05
3.575	0.025	0.140625	0.015625	0.000187339	0.000187339	1.60768e-05
3.625	0.025	0.859375	0.015625	0.201169	0.0869682	0.0173709
3.625	0.025	0.828125	0.015625	0.175478	0.0497967	0.0151525
3.625	0.025	0.796875	0.015625	0.132948	0.0197652	0.01148
3.625	0.025	0.765625	0.015625	0.16209	0.0178633	0.0139964

TABLE 29 – Continued

E_{beam}^{lab} [GeV]	$\pm dE_{beam}^{lab}$	$\cos \theta_{\pi^0}^{C.M.}$	$\pm d \cos \theta_{\pi^0}^{C.M.}$	$\frac{d\sigma}{d\Omega}$ [$\frac{\mu b}{SR}$]	σ^{stat}	σ^{sys}
3.625	0.025	0.734375	0.015625	0.155348	0.0141071	0.0134142
3.625	0.025	0.703125	0.015625	0.111078	0.00952975	0.0095915
3.625	0.025	0.671875	0.015625	0.0945492	0.00841697	0.00816429
3.625	0.025	0.640625	0.015625	0.134054	0.00967818	0.0115755
3.625	0.025	0.609375	0.015625	0.152541	0.0100854	0.0131719
3.625	0.025	0.578125	0.015625	0.12431	0.00835447	0.0107341
3.625	0.025	0.546875	0.015625	0.113385	0.00768037	0.00979073
3.625	0.025	0.515625	0.015625	0.0923621	0.00665032	0.00797542
3.625	0.025	0.484375	0.015625	0.0620603	0.00492125	0.00535888
3.625	0.025	0.453125	0.015625	0.041281	0.00384067	0.0035646
3.625	0.025	0.421875	0.015625	0.0419312	0.00386332	0.00362074
3.625	0.025	0.390625	0.015625	0.0293	0.00317174	0.00253004
3.625	0.025	0.359375	0.015625	0.0229943	0.00271778	0.00198555
3.625	0.025	0.328125	0.015625	0.0158606	0.00227434	0.00136956
3.625	0.025	0.296875	0.015625	0.0131584	0.00198046	0.00113622
3.625	0.025	0.265625	0.015625	0.00814096	0.00152617	0.000702969
3.625	0.025	0.234375	0.015625	0.00371388	0.000996791	0.000320692
3.625	0.025	0.203125	0.015625	0.00369933	0.000967979	0.000319435
3.625	0.025	0.171875	0.015625	0.00443712	0.00105834	0.000383143
3.625	0.025	0.140625	0.015625	0.0015978	0.000655068	0.000137969
3.625	0.025	0.109375	0.015625	0.00158352	0.000648207	0.000136736
3.625	0.025	0.078125	0.015625	0.00218094	0.000772276	0.000188324
3.625	0.025	0.046875	0.015625	0.00357323	0.000995326	0.000308547
3.625	0.025	0.015625	0.015625	0.00271688	0.000866355	0.000234602
3.625	0.025	-0.03125	0.03125	0.00355457	0.000717859	0.000306935
3.625	0.025	-0.109375	0.046875	0.00381536	0.0006031	0.000329454
3.625	0.025	-0.203125	0.046875	0.00410589	0.000670743	0.000354542
3.625	0.025	-0.296875	0.046875	0.00431874	0.000844447	0.000372922
3.625	0.025	-0.390625	0.046875	0.00460535	0.000866616	0.00039767
3.625	0.025	-0.484375	0.046875	0.0089274	0.00149173	0.000770877
3.625	0.025	-0.578125	0.046875	0.00927776	0.00194746	0.000801131
3.625	0.025	-0.671875	0.046875	0.0119556	0.00280054	0.00103236
3.675	0.025	0.890625	0.015625	0.784439	0.560023	0.0681554
3.675	0.025	0.859375	0.015625	0.339994	0.128211	0.0295402
3.675	0.025	0.828125	0.015625	0.138568	0.032547	0.0120394
3.675	0.025	0.796875	0.015625	0.144486	0.0216928	0.0125536
3.675	0.025	0.765625	0.015625	0.156598	0.0189312	0.0136059
3.675	0.025	0.734375	0.015625	0.161202	0.015162	0.014006
3.675	0.025	0.703125	0.015625	0.117451	0.0106097	0.0102046

TABLE 29 – Continued

E_{beam}^{lab} [GeV]	$\pm dE_{beam}^{lab}$	$\cos \theta_{\pi^0}^{C.M.}$	$\pm d \cos \theta_{\pi^0}^{C.M.}$	$\frac{d\sigma}{d\Omega} \left[\frac{\mu b}{SR} \right]$	σ^{stat}	σ^{sys}
3.675	0.025	0.671875	0.015625	0.106294	0.0095659	0.0092353
3.675	0.025	0.640625	0.015625	0.150251	0.0111935	0.0130544
3.675	0.025	0.609375	0.015625	0.124486	0.00957419	0.0108159
3.675	0.025	0.578125	0.015625	0.137183	0.00964416	0.0119191
3.675	0.025	0.546875	0.015625	0.117183	0.00871952	0.0101814
3.675	0.025	0.515625	0.015625	0.095636	0.00734673	0.00830926
3.675	0.025	0.484375	0.015625	0.0608082	0.00539265	0.00528327
3.675	0.025	0.453125	0.015625	0.0481197	0.00464724	0.00418085
3.675	0.025	0.421875	0.015625	0.0432767	0.00428824	0.00376006
3.675	0.025	0.390625	0.015625	0.029099	0.00343958	0.00252824
3.675	0.025	0.359375	0.015625	0.0178951	0.00259282	0.0015548
3.675	0.025	0.328125	0.015625	0.0132037	0.00221545	0.0011472
3.675	0.025	0.296875	0.015625	0.00873819	0.00172461	0.000759211
3.675	0.025	0.265625	0.015625	0.00704237	0.001509	0.000611871
3.675	0.025	0.234375	0.015625	0.00541485	0.00131974	0.000470465
3.675	0.025	0.203125	0.015625	0.00457959	0.00115251	0.000397894
3.675	0.025	0.171875	0.015625	0.00187659	0.000773679	0.000163047
3.675	0.025	0.140625	0.015625	0.0023326	0.00083418	0.000202666
3.675	0.025	0.109375	0.015625	0.000944226	0.000549509	8.20384e-05
3.675	0.025	0.078125	0.015625	0.00334262	0.00106124	0.000290421
3.675	0.025	0.046875	0.015625	0.00185019	0.000758871	0.000160752
3.675	0.025	0.015625	0.015625	0.00206999	0.000786171	0.00017985
3.675	0.025	-0.03125	0.03125	0.0043812	0.000830466	0.000380658
3.675	0.025	-0.109375	0.046875	0.00520715	0.00074876	0.000452419
3.675	0.025	-0.203125	0.046875	0.00436335	0.000741767	0.000379106
3.675	0.025	-0.296875	0.046875	0.00436157	0.000893565	0.000378952
3.675	0.025	-0.390625	0.046875	0.00427437	0.000919482	0.000371376
3.675	0.025	-0.484375	0.046875	0.00646464	0.00133654	0.000561676
3.675	0.025	-0.578125	0.046875	0.010991	0.00244673	0.000954949
3.675	0.025	-0.671875	0.046875	0.0143158	0.0042693	0.00124382
3.725	0.025	0.859375	0.015625	0.306368	0.158793	0.026783
3.725	0.025	0.828125	0.015625	0.107686	0.0294696	0.00941403
3.725	0.025	0.796875	0.015625	0.130286	0.021499	0.0113897
3.725	0.025	0.765625	0.015625	0.119466	0.0164735	0.0104439
3.725	0.025	0.734375	0.015625	0.138786	0.0135711	0.0121328
3.725	0.025	0.703125	0.015625	0.103401	0.00972562	0.00903943
3.725	0.025	0.671875	0.015625	0.0963683	0.00935744	0.00842461
3.725	0.025	0.640625	0.015625	0.131251	0.0107642	0.0114741
3.725	0.025	0.609375	0.015625	0.104825	0.00906424	0.00916393

TABLE 29 – Continued

E_{beam}^{lab} [GeV]	$\pm dE_{beam}^{lab}$	$\cos \theta_{\pi^0}^{C.M.}$	$\pm d \cos \theta_{\pi^0}^{C.M.}$	$\frac{d\sigma}{d\Omega} \left[\frac{\mu b}{SR} \right]$	σ^{stat}	σ^{sys}
3.725	0.025	0.578125	0.015625	0.110036	0.00874815	0.00961948
3.725	0.025	0.546875	0.015625	0.0835125	0.00722348	0.00730075
3.725	0.025	0.515625	0.015625	0.0609886	0.00594284	0.00533168
3.725	0.025	0.484375	0.015625	0.0460317	0.00459469	0.00402413
3.725	0.025	0.453125	0.015625	0.0317062	0.00370508	0.00277179
3.725	0.025	0.421875	0.015625	0.0289036	0.00352788	0.00252678
3.725	0.025	0.390625	0.015625	0.0223257	0.00303946	0.00195174
3.725	0.025	0.359375	0.015625	0.0158054	0.0025312	0.00138172
3.725	0.025	0.328125	0.015625	0.0139179	0.00229283	0.00121672
3.725	0.025	0.296875	0.015625	0.00517463	0.00131282	0.000452371
3.725	0.025	0.265625	0.015625	0.00453522	0.00121877	0.000396473
3.725	0.025	0.234375	0.015625	0.00233124	0.000846044	0.0002038
3.725	0.025	0.203125	0.015625	0.0016383	0.000678594	0.000143222
3.725	0.025	0.171875	0.015625	0.000604223	0.000430775	5.28218e-05
3.725	0.025	0.140625	0.015625	0.001904	0.000780969	0.00016645
3.725	0.025	0.109375	0.015625	0.00227107	0.000866211	0.000198539
3.725	0.025	0.078125	0.015625	0.000962059	0.000556981	8.41041e-05
3.725	0.025	0.046875	0.015625	0.00304724	0.000966943	0.000266393
3.725	0.025	0.015625	0.015625	0.00117316	0.000597609	0.000102559
3.725	0.025	-0.03125	0.03125	0.00401154	0.000806711	0.000350692
3.725	0.025	-0.109375	0.046875	0.00439898	0.000704775	0.000384563
3.725	0.025	-0.203125	0.046875	0.00334801	0.000664623	0.000292687
3.725	0.025	-0.296875	0.046875	0.00340897	0.000810239	0.000298015
3.725	0.025	-0.390625	0.046875	0.00312724	0.0008228	0.000273386
3.725	0.025	-0.484375	0.046875	0.00516162	0.00120418	0.000451233
3.725	0.025	-0.578125	0.046875	0.00821664	0.00189057	0.000718307
3.725	0.025	-0.671875	0.046875	0.0144184	0.00470035	0.00126047
3.725	0.025	-0.765625	0.046875	0.00939215	0.0050111	0.000821071
3.775	0.025	0.859375	0.015625	0.569584	0.292979	0.0501003
3.775	0.025	0.828125	0.015625	0.149744	0.0319912	0.0131714
3.775	0.025	0.796875	0.015625	0.107132	0.0200088	0.00942328
3.775	0.025	0.765625	0.015625	0.186541	0.0215529	0.0164081
3.775	0.025	0.734375	0.015625	0.166063	0.0154166	0.0146068
3.775	0.025	0.703125	0.015625	0.118814	0.0116172	0.0104508
3.775	0.025	0.671875	0.015625	0.113301	0.0103643	0.00996595
3.775	0.025	0.640625	0.015625	0.148814	0.0116697	0.0130896
3.775	0.025	0.609375	0.015625	0.158976	0.0118855	0.0139835
3.775	0.025	0.578125	0.015625	0.149816	0.0105492	0.0131777
3.775	0.025	0.546875	0.015625	0.115102	0.00906655	0.0101243

TABLE 29 – Continued

E_{beam}^{lab} [GeV]	$\pm dE_{beam}^{lab}$	$\cos \theta_{\pi^0}^{C.M.}$	$\pm d \cos \theta_{\pi^0}^{C.M.}$	$\frac{d\sigma}{d\Omega} \left[\frac{\mu b}{SR} \right]$	σ^{stat}	σ^{sys}
3.775	0.025	0.515625	0.015625	0.0910879	0.00760391	0.00801205
3.775	0.025	0.484375	0.015625	0.0464318	0.0049136	0.00408412
3.775	0.025	0.453125	0.015625	0.0453927	0.00465774	0.00399272
3.775	0.025	0.421875	0.015625	0.0334711	0.00402985	0.0029441
3.775	0.025	0.390625	0.015625	0.0193089	0.00295904	0.0016984
3.775	0.025	0.359375	0.015625	0.0183574	0.00285296	0.00161471
3.775	0.025	0.328125	0.015625	0.00831637	0.0018767	0.000731505
3.775	0.025	0.296875	0.015625	0.00825095	0.00177522	0.00072575
3.775	0.025	0.265625	0.015625	0.00532804	0.00140344	0.000468653
3.775	0.025	0.234375	0.015625	0.00449158	0.00122372	0.000395078
3.775	0.025	0.203125	0.015625	0.0035344	0.00108841	0.000310884
3.775	0.025	0.171875	0.015625	0.00129021	0.00064642	0.000113486
3.775	0.025	0.140625	0.015625	0.00223106	0.000916153	0.000196243
3.775	0.025	0.109375	0.015625	0.00277722	0.00099251	0.000244283
3.775	0.025	0.078125	0.015625	0.00371377	0.00112732	0.000326661
3.775	0.025	0.046875	0.015625	0.00467519	0.00125439	0.000411228
3.775	0.025	0.015625	0.015625	0.00469707	0.00130504	0.000413152
3.775	0.025	-0.03125	0.03125	0.00505564	0.000947661	0.000444692
3.775	0.025	-0.109375	0.046875	0.00415584	0.000703545	0.000365546
3.775	0.025	-0.203125	0.046875	0.00273253	0.000614994	0.000240352
3.775	0.025	-0.296875	0.046875	0.00227543	0.00067416	0.000200146
3.775	0.025	-0.390625	0.046875	0.00342792	0.000902007	0.000301518
3.775	0.025	-0.484375	0.046875	0.00473137	0.00119456	0.00041617
3.775	0.025	-0.578125	0.046875	0.0144736	0.00256072	0.00127309
3.775	0.025	-0.671875	0.046875	0.0182225	0.00509086	0.00160285
3.825	0.025	0.859375	0.015625	0.151818	0.0767167	0.0134359
3.825	0.025	0.828125	0.015625	0.0979798	0.0257357	0.00867123
3.825	0.025	0.796875	0.015625	0.107518	0.0185789	0.00951534
3.825	0.025	0.765625	0.015625	0.13314	0.0173689	0.0117829
3.825	0.025	0.734375	0.015625	0.140548	0.0135282	0.0124385
3.825	0.025	0.703125	0.015625	0.11669	0.0110413	0.0103271
3.825	0.025	0.671875	0.015625	0.120185	0.010724	0.0106363
3.825	0.025	0.640625	0.015625	0.121487	0.0104554	0.0107516
3.825	0.025	0.609375	0.015625	0.149388	0.0113435	0.0132209
3.825	0.025	0.578125	0.015625	0.113414	0.0090004	0.0100372
3.825	0.025	0.546875	0.015625	0.0938826	0.00799526	0.00830862
3.825	0.025	0.515625	0.015625	0.062862	0.00610906	0.00556329
3.825	0.025	0.484375	0.015625	0.0412509	0.00451881	0.00365071
3.825	0.025	0.453125	0.015625	0.0397857	0.00437469	0.00352103

TABLE 29 – Continued

E_{beam}^{lab} [GeV]	$\pm dE_{beam}^{lab}$	$\cos \theta_{\pi^0}^{C.M.}$	$\pm d \cos \theta_{\pi^0}^{C.M.}$	$\frac{dg}{d\Omega}$ [$\frac{\mu b}{SR}$]	σ^{stat}	σ^{sys}
3.825	0.025	0.421875	0.015625	0.0269167	0.00350843	0.00238213
3.825	0.025	0.390625	0.015625	0.0192195	0.00289641	0.00170093
3.825	0.025	0.359375	0.015625	0.00875393	0.00192678	0.000774724
3.825	0.025	0.328125	0.015625	0.00771697	0.00183551	0.000682953
3.825	0.025	0.296875	0.015625	0.0050796	0.00141396	0.000449545
3.825	0.025	0.265625	0.015625	0.0031597	0.00105856	0.000279633
3.825	0.025	0.234375	0.015625	0.00158779	0.000716952	0.00014052
3.825	0.025	0.203125	0.015625	0.000834352	0.000503639	7.38402e-05
3.825	0.025	0.171875	0.015625	0.00172486	0.000772663	0.00015265
3.825	0.025	0.140625	0.015625	0.00168606	0.000758682	0.000149217
3.825	0.025	0.109375	0.015625	0.0016574	0.000749037	0.00014668
3.825	0.025	0.078125	0.015625	0.0016166	0.000729463	0.00014307
3.825	0.025	0.046875	0.015625	0.00331947	0.00105287	0.000293773
3.825	0.025	0.015625	0.015625	0.00136981	0.000693977	0.000121228
3.825	0.025	-0.03125	0.03125	0.00199964	0.000564159	0.000176968
3.825	0.025	-0.109375	0.046875	0.00383052	0.000674544	0.000339001
3.825	0.025	-0.203125	0.046875	0.00332971	0.000673959	0.000294679
3.825	0.025	-0.296875	0.046875	0.00276179	0.000743708	0.000244419
3.825	0.025	-0.390625	0.046875	0.00394357	0.00090191	0.000349006
3.825	0.025	-0.484375	0.046875	0.00446318	0.00114559	0.000394992
3.825	0.025	-0.578125	0.046875	0.00967162	0.00207328	0.000855939
3.825	0.025	-0.671875	0.046875	0.0141962	0.00453957	0.00125636
3.875	0.025	0.859375	0.015625	0.155792	0.10114	0.0138721
3.875	0.025	0.828125	0.015625	0.105237	0.032564	0.00937057
3.875	0.025	0.796875	0.015625	0.0821387	0.0164852	0.00731383
3.875	0.025	0.765625	0.015625	0.167105	0.0204661	0.0148795
3.875	0.025	0.734375	0.015625	0.107654	0.0114425	0.0095858
3.875	0.025	0.703125	0.015625	0.109728	0.0110042	0.00977045
3.875	0.025	0.671875	0.015625	0.1188	0.0110296	0.0105782
3.875	0.025	0.640625	0.015625	0.125224	0.0105387	0.0111503
3.875	0.025	0.609375	0.015625	0.138152	0.0107962	0.0123014
3.875	0.025	0.578125	0.015625	0.101117	0.00875319	0.00900371
3.875	0.025	0.546875	0.015625	0.083911	0.00752068	0.00747165
3.875	0.025	0.515625	0.015625	0.0662482	0.00641753	0.0058989
3.875	0.025	0.484375	0.015625	0.0372092	0.00434289	0.0033132
3.875	0.025	0.453125	0.015625	0.0379445	0.00437235	0.00337868
3.875	0.025	0.421875	0.015625	0.0220942	0.00314411	0.00196732
3.875	0.025	0.390625	0.015625	0.0192957	0.00287296	0.00171814
3.875	0.025	0.359375	0.015625	0.00807967	0.00182258	0.000719434

TABLE 29 – Continued

E_{beam}^{lab} [GeV]	$\pm dE_{beam}^{lab}$	$\cos \theta_{\pi^0}^{C.M.}$	$\pm d \cos \theta_{\pi^0}^{C.M.}$	$\frac{d\sigma}{d\Omega}$ [$\frac{\mu b}{SR}$]	σ^{stat}	σ^{sys}
3.875	0.025	0.328125	0.015625	0.00786638	0.00181646	0.000700442
3.875	0.025	0.296875	0.015625	0.00467829	0.00131716	0.000416567
3.875	0.025	0.265625	0.015625	0.00226996	0.00084434	0.000202123
3.875	0.025	0.234375	0.015625	0.00116881	0.000609295	0.000104074
3.875	0.025	0.203125	0.015625	0.00128275	0.000662421	0.000114219
3.875	0.025	0.171875	0.015625	0.000957397	0.000554626	8.52491e-05
3.875	0.025	0.140625	0.015625	0.00178263	0.000802865	0.00015873
3.875	0.025	0.109375	0.015625	0.00168411	0.000756182	0.000149957
3.875	0.025	0.078125	0.015625	0.00308494	0.000993334	0.000274691
3.875	0.025	0.046875	0.015625	0.00285715	0.0010148	0.000254408
3.875	0.025	0.015625	0.015625	0.00315481	0.00100169	0.000280912
3.875	0.025	-0.03125	0.03125	0.00133385	0.000452729	0.00011877
3.875	0.025	-0.109375	0.046875	0.00298602	0.00059553	0.000265882
3.875	0.025	-0.203125	0.046875	0.00300909	0.000656053	0.000267937
3.875	0.025	-0.296875	0.046875	0.00195633	0.000627803	0.000174196
3.875	0.025	-0.390625	0.046875	0.00296308	0.000772631	0.00026384
3.875	0.025	-0.484375	0.046875	0.00584336	0.00132274	0.000520308
3.875	0.025	-0.578125	0.046875	0.00895929	0.00224897	0.000797757
3.875	0.025	-0.671875	0.046875	0.00840699	0.00290356	0.00074858
3.925	0.025	0.828125	0.015625	0.103156	0.0260962	0.00924138
3.925	0.025	0.796875	0.015625	0.122894	0.0195138	0.0110097
3.925	0.025	0.765625	0.015625	0.141015	0.0169465	0.0126331
3.925	0.025	0.734375	0.015625	0.120131	0.0115653	0.0107621
3.925	0.025	0.703125	0.015625	0.109537	0.010054	0.00981306
3.925	0.025	0.671875	0.015625	0.102499	0.00945369	0.00918251
3.925	0.025	0.640625	0.015625	0.130432	0.0102112	0.0116849
3.925	0.025	0.609375	0.015625	0.118745	0.00934831	0.010638
3.925	0.025	0.578125	0.015625	0.0983386	0.00800572	0.00880983
3.925	0.025	0.546875	0.015625	0.0792543	0.00700973	0.00710014
3.925	0.025	0.515625	0.015625	0.0464663	0.00481804	0.00416276
3.925	0.025	0.484375	0.015625	0.0325438	0.00376181	0.00291549
3.925	0.025	0.453125	0.015625	0.0328206	0.0038578	0.00294029
3.925	0.025	0.421875	0.015625	0.0178756	0.00265837	0.00160142
3.925	0.025	0.390625	0.015625	0.016265	0.00253055	0.00145713
3.925	0.025	0.359375	0.015625	0.00764831	0.00172245	0.000685187
3.925	0.025	0.328125	0.015625	0.00526846	0.0013449	0.000471985
3.925	0.025	0.296875	0.015625	0.00192667	0.000803123	0.000172604
3.925	0.025	0.265625	0.015625	0.00221874	0.000762552	0.00019877
3.925	0.025	0.234375	0.015625	0.00189496	0.000744974	0.000169764

TABLE 29 – Continued

E_{beam}^{lab} [GeV]	$\pm dE_{beam}^{lab}$	$\cos \theta_{\pi^0}^{C.M.}$	$\pm d \cos \theta_{\pi^0}^{C.M.}$	$\frac{d\sigma}{d\Omega}$ [$\frac{\mu b}{SR}$]	σ^{stat}	σ^{sys}
3.925	0.025	0.203125	0.015625	0.00120058	0.000602388	0.000107556
3.925	0.025	0.171875	0.015625	0.000688822	0.000414575	6.17094e-05
3.925	0.025	0.140625	0.015625	0.000832025	0.000482503	7.45384e-05
3.925	0.025	0.109375	0.015625	0.00114207	0.000574697	0.000102315
3.925	0.025	0.078125	0.015625	0.00145411	0.000650979	0.000130269
3.925	0.025	0.046875	0.015625	0.00388329	0.00108397	0.000347891
3.925	0.025	0.015625	0.015625	0.00149699	0.000620718	0.00013411
3.925	0.025	-0.03125	0.03125	0.00184672	0.00048186	0.000165442
3.925	0.025	-0.109375	0.046875	0.00388185	0.000628422	0.000347762
3.925	0.025	-0.203125	0.046875	0.00262963	0.000569572	0.00023558
3.925	0.025	-0.296875	0.046875	0.00225835	0.000557543	0.000202318
3.925	0.025	-0.390625	0.046875	0.00198985	0.000592446	0.000178264
3.925	0.025	-0.484375	0.046875	0.00593761	0.0011887	0.000531931
3.925	0.025	-0.578125	0.046875	0.00931196	0.00190704	0.000834228
3.925	0.025	-0.671875	0.046875	0.0120071	0.0030417	0.00107568
3.925	0.025	-0.765625	0.046875	0.00900004	0.00475426	0.000806284
3.975	0.025	0.859375	0.015625	0.178999	0.0681858	0.0161337
3.975	0.025	0.828125	0.015625	0.0594107	0.0175144	0.00535485
3.975	0.025	0.796875	0.015625	0.120877	0.0214184	0.010895
3.975	0.025	0.765625	0.015625	0.121859	0.016129	0.0109835
3.975	0.025	0.734375	0.015625	0.105441	0.0103686	0.00950366
3.975	0.025	0.703125	0.015625	0.0964305	0.00953207	0.00869155
3.975	0.025	0.671875	0.015625	0.104712	0.00940523	0.00943803
3.975	0.025	0.640625	0.015625	0.116227	0.00959372	0.0104758
3.975	0.025	0.609375	0.015625	0.108441	0.00850566	0.00977406
3.975	0.025	0.578125	0.015625	0.102593	0.00798041	0.00924699
3.975	0.025	0.546875	0.015625	0.0764188	0.0067757	0.00688784
3.975	0.025	0.515625	0.015625	0.0346272	0.00409866	0.00312105
3.975	0.025	0.484375	0.015625	0.0341369	0.0038969	0.00307685
3.975	0.025	0.453125	0.015625	0.0244856	0.00329548	0.00220695
3.975	0.025	0.421875	0.015625	0.0219144	0.00293248	0.00197521
3.975	0.025	0.390625	0.015625	0.0103559	0.00195208	0.00093341
3.975	0.025	0.359375	0.015625	0.00775568	0.00171309	0.000699041
3.975	0.025	0.328125	0.015625	0.00453695	0.00122796	0.000408928
3.975	0.025	0.296875	0.015625	0.00343096	0.00104416	0.000309242
3.975	0.025	0.265625	0.015625	0.000366597	0.000267729	3.30424e-05
3.975	0.025	0.234375	0.015625	0.00122915	0.000525864	0.000110786
3.975	0.025	0.203125	0.015625	0.00136744	0.000572883	0.000123251
3.975	0.025	0.171875	0.015625	0.00111091	0.000562432	0.00010013

TABLE 29 – Continued

E_{beam}^{lab} [GeV]	$\pm dE_{beam}^{lab}$	$\cos \theta_{\pi^0}^{C.M.}$	$\pm d \cos \theta_{\pi^0}^{C.M.}$	$\frac{d\sigma}{d\Omega} \left[\frac{\mu b}{SR} \right]$	σ^{stat}	σ^{sys}
3.975	0.025	0.140625	0.015625	0.000874984	0.000507125	7.88648e-05
3.975	0.025	0.109375	0.015625	0.00155911	0.00063974	0.000140527
3.975	0.025	0.078125	0.015625	0.00196077	0.000745528	0.00017673
3.975	0.025	0.046875	0.015625	0.00254245	0.000810245	0.000229158
3.975	0.025	0.015625	0.015625	0.000802943	0.000463714	7.23715e-05
3.975	0.025	-0.03125	0.03125	0.00299325	0.000634711	0.00026979
3.975	0.025	-0.109375	0.046875	0.00276898	0.000538379	0.000249576
3.975	0.025	-0.203125	0.046875	0.00187432	0.000458193	0.000168938
3.975	0.025	-0.296875	0.046875	0.000762916	0.000301691	6.87638e-05
3.975	0.025	-0.390625	0.046875	0.00167201	0.000552629	0.000150703
3.975	0.025	-0.484375	0.046875	0.00623332	0.00125263	0.000561827
3.975	0.025	-0.578125	0.046875	0.00762041	0.00193236	0.000686849
3.975	0.025	-0.671875	0.046875	0.0126022	0.00380008	0.00113587
3.975	0.025	-0.765625	0.046875	0.00920829	0.00575038	0.000829969
4.025	0.025	0.796875	0.015625	0.179552	0.0288219	0.0162819
4.025	0.025	0.765625	0.015625	0.185801	0.0237984	0.0168485
4.025	0.025	0.734375	0.015625	0.10672	0.0115445	0.00967745
4.025	0.025	0.703125	0.015625	0.129229	0.0125297	0.0117186
4.025	0.025	0.671875	0.015625	0.107109	0.0105312	0.00971275
4.025	0.025	0.640625	0.015625	0.119405	0.0110455	0.0108277
4.025	0.025	0.609375	0.015625	0.11361	0.0099901	0.0103022
4.025	0.025	0.578125	0.015625	0.109039	0.00923281	0.00988775
4.025	0.025	0.546875	0.015625	0.0690323	0.00710177	0.00625989
4.025	0.025	0.515625	0.015625	0.0442925	0.00499114	0.00401647
4.025	0.025	0.484375	0.015625	0.0270684	0.00400311	0.00245458
4.025	0.025	0.453125	0.015625	0.0259651	0.00373994	0.00235453
4.025	0.025	0.421875	0.015625	0.0186592	0.00309444	0.00169202
4.025	0.025	0.390625	0.015625	0.00847951	0.00191563	0.000768927
4.025	0.025	0.359375	0.015625	0.00536668	0.00156194	0.000486654
4.025	0.025	0.328125	0.015625	0.0030579	0.00116123	0.000277292
4.025	0.025	0.296875	0.015625	0.00257701	0.00101365	0.000233684
4.025	0.025	0.265625	0.015625	0.000872626	0.000440582	7.91303e-05
4.025	0.025	0.234375	0.015625	0.00113491	0.000586947	0.000102914
4.025	0.025	0.203125	0.015625	0.00111059	0.000641448	0.000100709
4.025	0.025	0.171875	0.015625	0.00233713	0.000889562	0.000211932
4.025	0.025	0.140625	0.015625	0.00153355	0.000774001	0.000139063
4.025	0.025	0.109375	0.015625	0.00243071	0.000923743	0.000220418
4.025	0.025	0.078125	0.015625	0.000993446	0.000576152	9.00863e-05
4.025	0.025	0.046875	0.015625	0.00106877	0.00059076	9.69167e-05

TABLE 29 – Continued

E_{beam}^{lab} [GeV]	$\pm dE_{beam}^{lab}$	$\cos \theta_{\pi^0}^{C.M.}$	$\pm d \cos \theta_{\pi^0}^{C.M.}$	$\frac{d\sigma}{d\Omega} \left[\frac{\mu b}{SR} \right]$	σ^{stat}	σ^{sys}
4.025	0.025	0.015625	0.015625	0.00320959	0.00104938	0.000291048
4.025	0.025	-0.03125	0.03125	0.00252541	0.000624227	0.000229006
4.025	0.025	-0.109375	0.046875	0.00318081	0.000646516	0.000288438
4.025	0.025	-0.203125	0.046875	0.00272159	0.000630497	0.000246795
4.025	0.025	-0.296875	0.046875	0.0012264	0.000435271	0.000111211
4.025	0.025	-0.390625	0.046875	0.00295911	0.000834431	0.000268334
4.025	0.025	-0.484375	0.046875	0.00546433	0.00127115	0.000495509
4.025	0.025	-0.578125	0.046875	0.00881574	0.00196032	0.000799417
4.025	0.025	-0.671875	0.046875	0.00482584	0.00234387	0.00043761
4.025	0.025	-0.765625	0.046875	0.00796982	0.00465989	0.000722708
4.075	0.025	0.828125	0.015625	0.112557	0.0313458	0.0102686
4.075	0.025	0.796875	0.015625	0.113557	0.0211855	0.0103598
4.075	0.025	0.765625	0.015625	0.128099	0.0166864	0.0116865
4.075	0.025	0.734375	0.015625	0.123744	0.0118564	0.0112892
4.075	0.025	0.703125	0.015625	0.0895964	0.00994234	0.0081739
4.075	0.025	0.671875	0.015625	0.106174	0.0100686	0.00968632
4.075	0.025	0.640625	0.015625	0.119982	0.0101831	0.010946
4.075	0.025	0.609375	0.015625	0.110708	0.00954407	0.0100999
4.075	0.025	0.578125	0.015625	0.0967122	0.00816164	0.00882307
4.075	0.025	0.546875	0.015625	0.0651656	0.00644272	0.00594507
4.075	0.025	0.515625	0.015625	0.0444416	0.00489116	0.00405442
4.075	0.025	0.484375	0.015625	0.030745	0.00413592	0.00280487
4.075	0.025	0.453125	0.015625	0.0201955	0.00318162	0.00184244
4.075	0.025	0.421875	0.015625	0.0115592	0.00224812	0.00105455
4.075	0.025	0.390625	0.015625	0.00802868	0.0019119	0.000732458
4.075	0.025	0.359375	0.015625	0.00626551	0.00163328	0.000571604
4.075	0.025	0.328125	0.015625	0.00193378	0.000878705	0.000176419
4.075	0.025	0.296875	0.015625	0.00176284	0.00080007	0.000160824
4.075	0.025	0.265625	0.015625	0.000314232	0.000314232	2.86675e-05
4.075	0.025	0.234375	0.015625	0.0010964	0.000561949	0.000100025
4.075	0.025	0.203125	0.015625	0.000511836	0.00036343	4.66949e-05
4.075	0.025	0.171875	0.015625	0.000972801	0.000566241	8.87488e-05
4.075	0.025	0.140625	0.015625	0.00297815	0.000993311	0.000271697
4.075	0.025	0.109375	0.015625	0.0010134	0.000586073	9.24527e-05
4.075	0.025	0.078125	0.015625	0.00197372	0.000811656	0.000180063
4.075	0.025	0.046875	0.015625	0.00168554	0.000699649	0.000153772
4.075	0.025	0.015625	0.015625	0.00239847	0.000814365	0.000218813
4.075	0.025	-0.03125	0.03125	0.00268277	0.000656639	0.00024475
4.075	0.025	-0.109375	0.046875	0.00176057	0.000457511	0.000160618

TABLE 29 – Continued

E_{beam}^{lab} [GeV]	$\pm dE_{beam}^{lab}$	$\cos \theta_{\pi^0}^{C.M.}$	$\pm d \cos \theta_{\pi^0}^{C.M.}$	$\frac{d\sigma}{d\Omega} \left[\frac{\mu b}{SR} \right]$	σ^{stat}	σ^{sys}
4.075	0.025	-0.203125	0.046875	0.00232348	0.000560034	0.000211971
4.075	0.025	-0.296875	0.046875	0.00178933	0.000546316	0.00016324
4.075	0.025	-0.390625	0.046875	0.00229404	0.000713604	0.000209286
4.075	0.025	-0.484375	0.046875	0.00382524	0.000999199	0.000348977
4.075	0.025	-0.578125	0.046875	0.00628689	0.00155248	0.000573554
4.075	0.025	-0.671875	0.046875	0.029913	0.0166793	0.00272897
4.125	0.025	0.828125	0.015625	0.108518	0.0308889	0.00995997
4.125	0.025	0.796875	0.015625	0.135004	0.0255722	0.0123909
4.125	0.025	0.765625	0.015625	0.106765	0.0158661	0.00979904
4.125	0.025	0.734375	0.015625	0.107271	0.0117011	0.0098455
4.125	0.025	0.703125	0.015625	0.117317	0.012201	0.0107676
4.125	0.025	0.671875	0.015625	0.122339	0.0116452	0.0112285
4.125	0.025	0.640625	0.015625	0.144445	0.011827	0.0132574
4.125	0.025	0.609375	0.015625	0.0965259	0.00905144	0.00885929
4.125	0.025	0.578125	0.015625	0.079606	0.00784046	0.00730635
4.125	0.025	0.546875	0.015625	0.0499008	0.00578828	0.00457996
4.125	0.025	0.515625	0.015625	0.0348351	0.00449352	0.00319722
4.125	0.025	0.484375	0.015625	0.0245501	0.00374456	0.00225324
4.125	0.025	0.453125	0.015625	0.0246465	0.00365304	0.00226209
4.125	0.025	0.421875	0.015625	0.0133091	0.00263886	0.00122153
4.125	0.025	0.390625	0.015625	0.00706667	0.00188234	0.00064859
4.125	0.025	0.359375	0.015625	0.00535118	0.00158261	0.000491139
4.125	0.025	0.328125	0.015625	0.00388065	0.0012987	0.000356171
4.125	0.025	0.296875	0.015625	0.000994919	0.00050831	9.13152e-05
4.125	0.025	0.265625	0.015625	0.000709097	0.000430385	6.5082e-05
4.125	0.025	0.234375	0.015625	0.00195188	0.000873455	0.000179146
4.125	0.025	0.203125	0.015625	0.00118348	0.000689868	0.000108622
4.125	0.025	0.171875	0.015625	0.000336716	0.000336716	3.09043e-05
4.125	0.025	0.140625	0.015625	0.00168043	0.000755436	0.000154232
4.125	0.025	0.109375	0.015625	0.00194617	0.000803836	0.000178622
4.125	0.025	0.078125	0.015625	0.00226562	0.00092689	0.000207942
4.125	0.025	0.046875	0.015625	0.00308881	0.00103666	0.000283495
4.125	0.025	0.015625	0.015625	0.00255662	0.000860263	0.00023465
4.125	0.025	-0.03125	0.03125	0.00207655	0.000568609	0.000190589
4.125	0.025	-0.109375	0.046875	0.00193545	0.000487014	0.000177638
4.125	0.025	-0.203125	0.046875	0.00232096	0.000570411	0.000213021
4.125	0.025	-0.296875	0.046875	0.00168435	0.000606527	0.000154592
4.125	0.025	-0.390625	0.046875	0.00203144	0.000676006	0.000186449
4.125	0.025	-0.484375	0.046875	0.00558002	0.00129889	0.000512143

TABLE 29 – Continued

E_{beam}^{lab} [GeV]	$\pm dE_{beam}^{lab}$	$\cos \theta_{\pi^0}^{C.M.}$	$\pm d \cos \theta_{\pi^0}^{C.M.}$	$\frac{d\sigma}{d\Omega} \left[\frac{\mu b}{SR} \right]$	σ^{stat}	σ^{sys}
4.125	0.025	-0.578125	0.046875	0.00686487	0.00175411	0.000630068
4.125	0.025	-0.671875	0.046875	0.00530206	0.00213083	0.000486631
4.125	0.025	-0.765625	0.046875	0.00996731	0.00543239	0.000914814
4.175	0.025	0.828125	0.015625	0.159843	0.0393864	0.014759
4.175	0.025	0.796875	0.015625	0.0802805	0.0184046	0.00741266
4.175	0.025	0.765625	0.015625	0.105307	0.0145943	0.0097235
4.175	0.025	0.734375	0.015625	0.143456	0.0131045	0.013246
4.175	0.025	0.703125	0.015625	0.0850762	0.00905132	0.00785546
4.175	0.025	0.671875	0.015625	0.112797	0.0103435	0.010415
4.175	0.025	0.640625	0.015625	0.115796	0.0099595	0.0106919
4.175	0.025	0.609375	0.015625	0.08309	0.00778288	0.00767207
4.175	0.025	0.578125	0.015625	0.084664	0.00753167	0.0078174
4.175	0.025	0.546875	0.015625	0.0430448	0.0049603	0.00397452
4.175	0.025	0.515625	0.015625	0.0300052	0.00381837	0.00277051
4.175	0.025	0.484375	0.015625	0.0191593	0.00298484	0.00176906
4.175	0.025	0.453125	0.015625	0.0156163	0.00270691	0.00144192
4.175	0.025	0.421875	0.015625	0.0113572	0.00221047	0.00104866
4.175	0.025	0.390625	0.015625	0.00425516	0.00130439	0.000392898
4.175	0.025	0.359375	0.015625	0.00410255	0.00124985	0.000378807
4.175	0.025	0.328125	0.015625	0.00088158	0.000567719	8.14002e-05
4.175	0.025	0.296875	0.015625	0.000979684	0.000570474	9.04585e-05
4.175	0.025	0.265625	0.015625	0.000513441	0.000371439	4.74083e-05
4.175	0.025	0.234375	0.015625	0.00111116	0.000559186	0.000102598
4.175	0.025	0.203125	0.015625	0.00133755	0.000672467	0.000123502
4.175	0.025	0.171875	0.015625	0.0014902	0.000679428	0.000137597
4.175	0.025	0.140625	0.015625	0.000292233	0.000292233	2.69832e-05
4.175	0.025	0.109375	0.015625	0.0012791	0.000641037	0.000118105
4.175	0.025	0.078125	0.015625	0.0016244	0.000702452	0.000149988
4.175	0.025	0.046875	0.015625	0.00144444	0.000597164	0.000133372
4.175	0.025	0.015625	0.015625	0.00115415	0.000522324	0.000106568
4.175	0.025	-0.03125	0.03125	0.00173481	0.000494416	0.000160182
4.175	0.025	-0.109375	0.046875	0.00234806	0.000514147	0.000216806
4.175	0.025	-0.203125	0.046875	0.00143223	0.00039887	0.000132244
4.175	0.025	-0.296875	0.046875	0.00115284	0.000448895	0.000106447
4.175	0.025	-0.390625	0.046875	0.00318105	0.000763163	0.00029372
4.175	0.025	-0.484375	0.046875	0.00199501	0.000672285	0.000184208
4.175	0.025	-0.578125	0.046875	0.00626358	0.00156449	0.000578344
4.175	0.025	-0.671875	0.046875	0.01102	0.00311369	0.00101753
4.225	0.025	0.859375	0.015625	0.413673	0.293604	0.0384257

TABLE 29 – Continued

$E_{\text{beam}}^{\text{lab}}$ [GeV]	$\pm dE_{\text{beam}}^{\text{lab}}$	$\cos \theta_{\pi^0}^{C.M.}$	$\pm d \cos \theta_{\pi^0}^{C.M.}$	$\frac{d\sigma}{d\Omega}$ [$\frac{\mu\text{b}}{\text{SR}}$]	σ^{stat}	σ^{sys}
4.225	0.025	0.828125	0.015625	0.186254	0.057041	0.017301
4.225	0.025	0.796875	0.015625	0.121091	0.023133	0.011248
4.225	0.025	0.765625	0.015625	0.136322	0.0169137	0.0126628
4.225	0.025	0.734375	0.015625	0.100738	0.011043	0.00935749
4.225	0.025	0.703125	0.015625	0.113746	0.0114739	0.0105658
4.225	0.025	0.671875	0.015625	0.121138	0.0114055	0.0112524
4.225	0.025	0.640625	0.015625	0.118583	0.0104563	0.0110151
4.225	0.025	0.609375	0.015625	0.097972	0.00875764	0.00910052
4.225	0.025	0.578125	0.015625	0.068189	0.0070067	0.00633401
4.225	0.025	0.546875	0.015625	0.03838	0.00463737	0.00356508
4.225	0.025	0.515625	0.015625	0.0245027	0.00357492	0.00227603
4.225	0.025	0.484375	0.015625	0.0180799	0.00304401	0.00167942
4.225	0.025	0.453125	0.015625	0.0172839	0.00308181	0.00160548
4.225	0.025	0.421875	0.015625	0.00532104	0.00154837	0.000494266
4.225	0.025	0.390625	0.015625	0.0109805	0.00223423	0.00101997
4.225	0.025	0.359375	0.015625	0.00293902	0.00100885	0.000273003
4.225	0.025	0.296875	0.015625	0.000685277	0.000487303	6.36547e-05
4.225	0.025	0.265625	0.015625	0.00041824	0.000295747	3.88499e-05
4.225	0.025	0.234375	0.015625	0.000321278	0.000321278	2.98432e-05
4.225	0.025	0.203125	0.015625	0.000637812	0.000464213	5.92457e-05
4.225	0.025	0.171875	0.015625	0.00109767	0.000639862	0.000101962
4.225	0.025	0.140625	0.015625	0.00183765	0.000772497	0.000170698
4.225	0.025	0.109375	0.015625	0.00135423	0.000677494	0.000125793
4.225	0.025	0.078125	0.015625	0.00206493	0.000801302	0.000191809
4.225	0.025	0.046875	0.015625	0.000857181	0.000501991	7.96227e-05
4.225	0.025	0.015625	0.015625	0.0014249	0.000659902	0.000132358
4.225	0.025	-0.03125	0.03125	0.00272239	0.000650144	0.00025288
4.225	0.025	-0.109375	0.046875	0.000880132	0.000313117	8.17546e-05
4.225	0.025	-0.203125	0.046875	0.000889964	0.000338441	8.26678e-05
4.225	0.025	-0.296875	0.046875	0.00109354	0.000435745	0.000101578
4.225	0.025	-0.390625	0.046875	0.00152007	0.000585922	0.000141198
4.225	0.025	-0.484375	0.046875	0.00318901	0.00092872	0.000296224
4.225	0.025	-0.578125	0.046875	0.0049833	0.00149497	0.000462894
4.225	0.025	-0.671875	0.046875	0.00352309	0.00135559	0.000327257
4.225	0.025	-0.765625	0.046875	0.00845758	0.00673751	0.000785616
4.275	0.025	0.859375	0.015625	0.108775	0.0626854	0.0101645
4.275	0.025	0.828125	0.015625	0.148464	0.041969	0.0138733
4.275	0.025	0.796875	0.015625	0.133051	0.02475	0.012433
4.275	0.025	0.765625	0.015625	0.103307	0.0150091	0.00965359

TABLE 29 – Continued

E_{beam}^{lab} [GeV]	$\pm dE_{beam}^{lab}$	$\cos \theta_{\pi^0}^{C.M.}$	$\pm d \cos \theta_{\pi^0}^{C.M.}$	$\frac{d\sigma}{d\Omega}$ [$\frac{\mu b}{SR}$]	σ^{stat}	σ^{sys}
4.275	0.025	0.734375	0.015625	0.092442	0.0111701	0.00863826
4.275	0.025	0.703125	0.015625	0.0942768	0.0102024	0.00880972
4.275	0.025	0.671875	0.015625	0.103133	0.00988119	0.0096373
4.275	0.025	0.640625	0.015625	0.0981521	0.00909411	0.00917184
4.275	0.025	0.609375	0.015625	0.0877918	0.00833437	0.00820372
4.275	0.025	0.578125	0.015625	0.059107	0.00648506	0.00552327
4.275	0.025	0.546875	0.015625	0.0358319	0.00435644	0.00334832
4.275	0.025	0.515625	0.015625	0.0264568	0.00388726	0.00247226
4.275	0.025	0.484375	0.015625	0.0153472	0.00273898	0.00143412
4.275	0.025	0.453125	0.015625	0.0152219	0.00271848	0.00142242
4.275	0.025	0.421875	0.015625	0.00551327	0.001602	0.000515189
4.275	0.025	0.390625	0.015625	0.0100199	0.00216799	0.000936315
4.275	0.025	0.359375	0.015625	0.00391292	0.0013259	0.000365644
4.275	0.025	0.328125	0.015625	0.00101513	0.000591993	9.48593e-05
4.275	0.025	0.265625	0.015625	0.000377997	0.000377997	3.53221e-05
4.275	0.025	0.234375	0.015625	0.00179193	0.000743831	0.000167448
4.275	0.025	0.203125	0.015625	0.00106606	0.000617235	9.96179e-05
4.275	0.025	0.171875	0.015625	0.00130225	0.000653869	0.000121689
4.275	0.025	0.140625	0.015625	0.00156363	0.00070276	0.000146114
4.275	0.025	0.109375	0.015625	0.000958126	0.000561606	8.95323e-05
4.275	0.025	0.078125	0.015625	0.00137393	0.000585645	0.000128387
4.275	0.025	0.046875	0.015625	0.000941149	0.00051525	8.79459e-05
4.275	0.025	0.015625	0.015625	0.00140721	0.000580676	0.000131497
4.275	0.025	-0.03125	0.03125	0.00151611	0.000468442	0.000141673
4.275	0.025	-0.109375	0.046875	0.00188233	0.000461323	0.000175895
4.275	0.025	-0.203125	0.046875	0.00102215	0.000361112	9.55149e-05
4.275	0.025	-0.296875	0.046875	0.0019926	0.000595448	0.000186199
4.275	0.025	-0.390625	0.046875	0.00262576	0.000738816	0.000245365
4.275	0.025	-0.484375	0.046875	0.0017583	0.000676421	0.000164304
4.275	0.025	-0.578125	0.046875	0.0056173	0.00147088	0.00052491
4.275	0.025	-0.671875	0.046875	0.00457392	0.002195	0.000427411
4.275	0.025	-0.765625	0.046875	0.00381885	0.00227725	0.000356853
4.325	0.025	0.859375	0.015625	0.0998969	0.0829986	0.00939062
4.325	0.025	0.828125	0.015625	0.0886967	0.0331026	0.00833776
4.325	0.025	0.796875	0.015625	0.143223	0.0311464	0.0134634
4.325	0.025	0.765625	0.015625	0.123176	0.0187237	0.0115789
4.325	0.025	0.734375	0.015625	0.125422	0.0146265	0.0117901
4.325	0.025	0.703125	0.015625	0.122725	0.0130661	0.0115365
4.325	0.025	0.671875	0.015625	0.101414	0.0113066	0.00953326

TABLE 29 – Continued

E_{beam}^{lab} [GeV]	$\pm dE_{beam}^{lab}$	$\cos \theta_{\pi^0}^{C.M.}$	$\pm d \cos \theta_{\pi^0}^{C.M.}$	$\frac{d\sigma}{d\Omega} \left[\frac{\mu b}{SR} \right]$	σ^{stat}	σ^{sys}
4.325	0.025	0.640625	0.015625	0.113008	0.0110662	0.0106231
4.325	0.025	0.609375	0.015625	0.0943864	0.00958557	0.00887261
4.325	0.025	0.578125	0.015625	0.0700971	0.00780328	0.00658935
4.325	0.025	0.546875	0.015625	0.0305548	0.00445386	0.00287225
4.325	0.025	0.515625	0.015625	0.0274508	0.00435442	0.00258046
4.325	0.025	0.484375	0.015625	0.014483	0.0028975	0.00136144
4.325	0.025	0.453125	0.015625	0.00607691	0.00193961	0.000571248
4.325	0.025	0.421875	0.015625	0.0111568	0.00247417	0.00104877
4.325	0.025	0.390625	0.015625	0.00145244	0.00085499	0.000136533
4.325	0.025	0.359375	0.015625	0.000992341	0.000701933	9.32831e-05
4.325	0.025	0.328125	0.015625	0.000551009	0.000484366	5.17966e-05
4.325	0.025	0.265625	0.015625	0.000569118	0.000569118	5.34989e-05
4.325	0.025	0.234375	0.015625	0.00157521	0.000797858	0.000148075
4.325	0.025	0.203125	0.015625	0.00168565	0.000845076	0.000158456
4.325	0.025	0.171875	0.015625	0.000436842	0.000436842	4.10645e-05
4.325	0.025	0.140625	0.015625	0.00078312	0.00056018	7.36157e-05
4.325	0.025	0.109375	0.015625	0.00110515	0.000559355	0.000103887
4.325	0.025	0.078125	0.015625	0.00049505	0.000358602	4.65362e-05
4.325	0.025	0.046875	0.015625	0.00244068	0.000942353	0.000229431
4.325	0.025	0.015625	0.015625	0.00153168	0.000695479	0.000143983
4.325	0.025	-0.03125	0.03125	0.00183382	0.00058622	0.000172384
4.325	0.025	-0.109375	0.046875	0.00120321	0.000387444	0.000113105
4.325	0.025	-0.203125	0.046875	0.000764219	0.000353075	7.18389e-05
4.325	0.025	-0.296875	0.046875	0.00152047	0.000587512	0.000142929
4.325	0.025	-0.390625	0.046875	0.00298188	0.000872489	0.000280305
4.325	0.025	-0.484375	0.046875	0.00350449	0.00107858	0.000329432
4.325	0.025	-0.578125	0.046875	0.00687412	0.00203598	0.000646188
4.325	0.025	-0.671875	0.046875	0.00709608	0.00230759	0.000667053
4.375	0.025	0.796875	0.015625	0.181013	0.0368367	0.017117
4.375	0.025	0.765625	0.015625	0.128923	0.0186633	0.0121913
4.375	0.025	0.734375	0.015625	0.107173	0.013497	0.0101346
4.375	0.025	0.703125	0.015625	0.098919	0.0116991	0.00935402
4.375	0.025	0.671875	0.015625	0.0902651	0.0106374	0.00853569
4.375	0.025	0.640625	0.015625	0.0919821	0.0101982	0.00869805
4.375	0.025	0.609375	0.015625	0.0920906	0.00944236	0.00870831
4.375	0.025	0.578125	0.015625	0.0450461	0.00597958	0.00425967
4.375	0.025	0.546875	0.015625	0.0317021	0.00471016	0.00299783
4.375	0.025	0.515625	0.015625	0.0285135	0.00451426	0.00269631
4.375	0.025	0.484375	0.015625	0.0233621	0.0040793	0.00220918

TABLE 29 – Continued

E_{beam}^{lab} [GeV]	$\pm dE_{beam}^{lab}$	$\cos \theta_{\pi^0}^{C.M.}$	$\pm d \cos \theta_{\pi^0}^{C.M.}$	$\frac{d\sigma}{d\Omega}$ [$\frac{\mu b}{SR}$]	σ^{stat}	σ^{sys}
4.375	0.025	0.453125	0.015625	0.0114018	0.00268166	0.00107818
4.375	0.025	0.421875	0.015625	0.00663759	0.0020216	0.000627667
4.375	0.025	0.390625	0.015625	0.00546304	0.00171434	0.000516598
4.375	0.025	0.359375	0.015625	0.00118441	0.000715933	0.000112
4.375	0.025	0.296875	0.015625	0.00191316	0.000961537	0.000180913
4.375	0.025	0.265625	0.015625	0.000566112	0.000566112	5.35329e-05
4.375	0.025	0.234375	0.015625	0.00117972	0.000692646	0.000111558
4.375	0.025	0.203125	0.015625	0.00110487	0.000649958	0.000104479
4.375	0.025	0.171875	0.015625	0.00102767	0.000727611	9.71792e-05
4.375	0.025	0.140625	0.015625	0.00145582	0.000841306	0.000137666
4.375	0.025	0.109375	0.015625	0.00154576	0.00077704	0.000146171
4.375	0.025	0.078125	0.015625	0.00101349	0.000586776	9.58377e-05
4.375	0.025	0.046875	0.015625	0.000872753	0.000620931	8.25297e-05
4.375	0.025	-0.03125	0.03125	0.00133298	0.00051103	0.00012605
4.375	0.025	-0.109375	0.046875	0.0018132	0.000508905	0.000171461
4.375	0.025	-0.203125	0.046875	0.00165162	0.000534951	0.000156181
4.375	0.025	-0.296875	0.046875	0.000652268	0.000390127	6.16801e-05
4.375	0.025	-0.390625	0.046875	0.0017719	0.000740998	0.000167555
4.375	0.025	-0.484375	0.046875	0.00136593	0.000684397	0.000129166
4.375	0.025	-0.578125	0.046875	0.00490632	0.0016963	0.000463953
4.375	0.025	-0.671875	0.046875	0.00541771	0.00240692	0.000512312
4.425	0.025	0.828125	0.015625	0.0678822	0.028766	0.00645718
4.425	0.025	0.796875	0.015625	0.0950102	0.026926	0.00903769
4.425	0.025	0.765625	0.015625	0.126966	0.0209723	0.0120775
4.425	0.025	0.734375	0.015625	0.0889445	0.0141291	0.0084607
4.425	0.025	0.703125	0.015625	0.0786856	0.0122166	0.00748484
4.425	0.025	0.671875	0.015625	0.100466	0.0135771	0.00955664
4.425	0.025	0.640625	0.015625	0.120527	0.0138124	0.0114649
4.425	0.025	0.609375	0.015625	0.0815412	0.0105497	0.00775647
4.425	0.025	0.578125	0.015625	0.0309641	0.00586398	0.00294541
4.425	0.025	0.546875	0.015625	0.0302845	0.0055983	0.00288076
4.425	0.025	0.515625	0.015625	0.0326497	0.00591147	0.00310575
4.425	0.025	0.484375	0.015625	0.0229457	0.00463001	0.00218267
4.425	0.025	0.453125	0.015625	0.0107976	0.00313324	0.00102711
4.425	0.025	0.421875	0.015625	0.00951475	0.00289593	0.000905075
4.425	0.025	0.390625	0.015625	0.00234372	0.00135514	0.000222942
4.425	0.025	0.359375	0.015625	5.62375e-05	5.62375e-05	5.3495e-06
4.425	0.025	0.328125	0.015625	0.00126045	0.000913204	0.000119898
4.425	0.025	0.296875	0.015625	0.000770074	0.000770074	7.32521e-05

TABLE 29 – Continued

E_{beam}^{lab} [GeV]	$\pm dE_{beam}^{lab}$	$\cos \theta_{\pi^0}^{C.M.}$	$\pm d \cos \theta_{\pi^0}^{C.M.}$	$\frac{d\sigma}{d\Omega}$ [$\frac{\mu b}{SR}$]	σ^{stat}	σ^{sys}
4.425	0.025	0.265625	0.015625	0.000760338	0.000760338	7.23259e-05
4.425	0.025	0.234375	0.015625	0.00119086	0.000842069	0.000113279
4.425	0.025	0.203125	0.015625	0.00138778	0.000981643	0.00013201
4.425	0.025	0.171875	0.015625	0.000671095	0.000671095	6.38368e-05
4.425	0.025	0.140625	0.015625	0.000501406	0.000501406	4.76954e-05
4.425	0.025	0.109375	0.015625	0.000983545	0.000697644	9.35581e-05
4.425	0.025	0.078125	0.015625	0.0013506	0.000792608	0.000128474
4.425	0.025	0.046875	0.015625	0.00171105	0.00099773	0.00016276
4.425	0.025	0.015625	0.015625	0.00220995	0.00101508	0.000210218
4.425	0.025	-0.03125	0.03125	0.000764343	0.000462672	7.27069e-05
4.425	0.025	-0.109375	0.046875	0.00152663	0.000548018	0.000145218
4.425	0.025	-0.203125	0.046875	0.00111232	0.000436312	0.000105808
4.425	0.025	-0.296875	0.046875	0.00162231	0.000669356	0.00015432
4.425	0.025	-0.390625	0.046875	0.00320106	0.00107841	0.000304496
4.425	0.025	-0.484375	0.046875	0.00485727	0.00156025	0.000462039
4.425	0.025	-0.578125	0.046875	0.00453189	0.00166267	0.000431088
4.425	0.025	-0.671875	0.046875	0.0111263	0.00468865	0.00105837
4.475	0.025	0.859375	0.015625	0.12399	0.0757557	0.0118641
4.475	0.025	0.828125	0.015625	0.0576143	0.0231691	0.00551287
4.475	0.025	0.796875	0.015625	0.125161	0.0275767	0.0119761
4.475	0.025	0.765625	0.015625	0.101325	0.0136847	0.00969539
4.475	0.025	0.734375	0.015625	0.115034	0.0129898	0.0110072
4.475	0.025	0.703125	0.015625	0.0888287	0.0101074	0.00849964
4.475	0.025	0.671875	0.015625	0.110716	0.010846	0.010594
4.475	0.025	0.640625	0.015625	0.080486	0.0082435	0.00770137
4.475	0.025	0.609375	0.015625	0.0662117	0.00729689	0.00633552
4.475	0.025	0.578125	0.015625	0.0421482	0.00511011	0.00403299
4.475	0.025	0.546875	0.015625	0.0265427	0.00387175	0.00253976
4.475	0.025	0.515625	0.015625	0.0220254	0.00355168	0.00210752
4.475	0.025	0.484375	0.015625	0.0179155	0.00316585	0.00171426
4.475	0.025	0.453125	0.015625	0.00972425	0.00229109	0.000930473
4.475	0.025	0.421875	0.015625	0.00187996	0.000946686	0.000179885
4.475	0.025	0.390625	0.015625	0.00264912	0.00108734	0.000253483
4.475	0.025	0.359375	0.015625	0.00102234	0.000638954	9.78237e-05
4.475	0.025	0.328125	0.015625	0.000255183	0.000255183	2.44174e-05
4.475	0.025	0.296875	0.015625	0.000605304	0.000453564	5.7919e-05
4.475	0.025	0.265625	0.015625	0.00123665	0.000716987	0.00011833
4.475	0.025	0.234375	0.015625	0.00117741	0.000683187	0.000112661
4.475	0.025	0.203125	0.015625	0.000690032	0.000487933	6.60262e-05

TABLE 29 – Continued

E_{beam}^{lab} [GeV]	$\pm dE_{beam}^{lab}$	$\cos \theta_{\pi^0}^{C.M.}$	$\pm d \cos \theta_{\pi^0}^{C.M.}$	$\frac{d\sigma}{d\Omega}$ [$\frac{\mu b}{SR}$]	σ^{stat}	σ^{sys}
4.475	0.025	0.171875	0.015625	0.000326998	0.000326998	3.12891e-05
4.475	0.025	0.140625	0.015625	0.000961033	0.000562252	9.19572e-05
4.475	0.025	0.109375	0.015625	0.000357087	0.000254438	3.41681e-05
4.475	0.025	0.078125	0.015625	0.00190611	0.000755857	0.000182388
4.475	0.025	0.046875	0.015625	0.000792197	0.000481576	7.5802e-05
4.475	0.025	0.015625	0.015625	0.00153432	0.000630029	0.000146813
4.475	0.025	-0.03125	0.03125	0.00165942	0.00052934	0.000158783
4.475	0.025	-0.109375	0.046875	0.00100029	0.000315612	9.57136e-05
4.475	0.025	-0.203125	0.046875	0.000817753	0.000329914	7.82473e-05
4.475	0.025	-0.296875	0.046875	0.000786411	0.000357961	7.52483e-05
4.475	0.025	-0.390625	0.046875	0.00191499	0.000653111	0.000183238
4.475	0.025	-0.484375	0.046875	0.00414817	0.00108299	0.000396921
4.475	0.025	-0.578125	0.046875	0.00648562	0.00156766	0.000620581
4.475	0.025	-0.671875	0.046875	0.00332368	0.00152462	0.000318029
4.475	0.025	-0.765625	0.046875	0.00730035	0.00588252	0.00069854
4.525	0.025	0.828125	0.015625	0.169151	0.0464839	0.0162808
4.525	0.025	0.796875	0.015625	0.196622	0.0363831	0.0189248
4.525	0.025	0.765625	0.015625	0.107109	0.0146014	0.0103092
4.525	0.025	0.734375	0.015625	0.0940024	0.0116591	0.00904771
4.525	0.025	0.703125	0.015625	0.0933639	0.0105311	0.00898624
4.525	0.025	0.671875	0.015625	0.104338	0.0101461	0.0100425
4.525	0.025	0.640625	0.015625	0.0806453	0.00813974	0.00776209
4.525	0.025	0.609375	0.015625	0.0711438	0.00753167	0.00684757
4.525	0.025	0.578125	0.015625	0.029585	0.00397487	0.00284754
4.525	0.025	0.546875	0.015625	0.0253842	0.00373621	0.00244322
4.525	0.025	0.515625	0.015625	0.0204201	0.00336744	0.00196543
4.525	0.025	0.484375	0.015625	0.0169026	0.00301552	0.00162687
4.525	0.025	0.453125	0.015625	0.00563449	0.00170921	0.000542318
4.525	0.025	0.421875	0.015625	0.00826941	0.00203379	0.000795928
4.525	0.025	0.390625	0.015625	0.00556476	0.00155277	0.000535606
4.525	0.025	0.359375	0.015625	0.00101043	0.000533871	9.7254e-05
4.525	0.025	0.328125	0.015625	0.000245308	0.000245308	2.36108e-05
4.525	0.025	0.265625	0.015625	0.000671953	0.000475737	6.46753e-05
4.525	0.025	0.234375	0.015625	0.00224034	0.000918141	0.000215632
4.525	0.025	0.203125	0.015625	0.00130527	0.00065763	0.000125632
4.525	0.025	0.171875	0.015625	0.000976669	0.000567424	9.40041e-05
4.525	0.025	0.140625	0.015625	0.000329118	0.000250006	3.16775e-05
4.525	0.025	0.109375	0.015625	0.000924543	0.000485126	8.8987e-05
4.525	0.025	0.078125	0.015625	0.000569098	0.000338812	5.47755e-05

TABLE 29 – Continued

E_{beam}^{lab} [GeV]	$\pm dE_{beam}^{lab}$	$\cos \theta_{\pi_0}^{C.M.}$	$\pm d \cos \theta_{\pi_0}^{C.M.}$	$\frac{d\sigma}{d\Omega}$ [$\frac{\mu b}{SR}$]	σ^{stat}	σ^{sys}
4.525	0.025	0.046875	0.015625	0.00155448	0.000643267	0.000149618
4.525	0.025	0.015625	0.015625	0.000787219	0.000468381	7.57696e-05
4.525	0.025	-0.03125	0.03125	0.000974724	0.000404841	9.38168e-05
4.525	0.025	-0.109375	0.046875	0.00178781	0.00043517	0.000172076
4.525	0.025	-0.203125	0.046875	0.00079307	0.000310387	7.63327e-05
4.525	0.025	-0.296875	0.046875	0.000938122	0.0004293	9.02939e-05
4.525	0.025	-0.390625	0.046875	0.00201774	0.000644603	0.000194207
4.525	0.025	-0.484375	0.046875	0.00216944	0.000744364	0.000208808
4.525	0.025	-0.578125	0.046875	0.00471074	0.00127495	0.000453407
4.525	0.025	-0.671875	0.046875	0.00657534	0.00231631	0.000632875
4.525	0.025	-0.765625	0.046875	0.0048861	0.00325906	0.000470286
4.575	0.025	0.828125	0.015625	0.0805331	0.0310533	0.00779682
4.575	0.025	0.796875	0.015625	0.141824	0.037159	0.0137307
4.575	0.025	0.765625	0.015625	0.122847	0.0184752	0.0118934
4.575	0.025	0.734375	0.015625	0.105063	0.0136266	0.0101716
4.575	0.025	0.703125	0.015625	0.0775617	0.00967583	0.00750914
4.575	0.025	0.671875	0.015625	0.106368	0.0113646	0.010298
4.575	0.025	0.640625	0.015625	0.0723819	0.00878613	0.00700766
4.575	0.025	0.609375	0.015625	0.065293	0.00761659	0.00632135
4.575	0.025	0.578125	0.015625	0.029692	0.00429648	0.00287463
4.575	0.025	0.546875	0.015625	0.0228688	0.00378367	0.00221405
4.575	0.025	0.515625	0.015625	0.0182582	0.00347948	0.00176767
4.575	0.025	0.484375	0.015625	0.0113493	0.00279006	0.00109878
4.575	0.025	0.453125	0.015625	0.00778591	0.00217818	0.000753793
4.575	0.025	0.421875	0.015625	0.00530707	0.00174285	0.000513804
4.575	0.025	0.390625	0.015625	0.00138725	0.000822063	0.000134307
4.575	0.025	0.359375	0.015625	0.00104538	0.000657098	0.000101208
4.575	0.025	0.296875	0.015625	0.000660639	0.000471386	6.39598e-05
4.575	0.025	0.265625	0.015625	0.00110682	0.000652065	0.000107157
4.575	0.025	0.234375	0.015625	0.00130239	0.000759102	0.000126091
4.575	0.025	0.203125	0.015625	0.00038269	0.00038269	3.70502e-05
4.575	0.025	0.171875	0.015625	0.000350445	0.000350445	3.39284e-05
4.575	0.025	0.140625	0.015625	0.00075249	0.000435855	7.28524e-05
4.575	0.025	0.109375	0.015625	0.00107811	0.000565292	0.000104377
4.575	0.025	0.078125	0.015625	0.000520139	0.000372525	5.03573e-05
4.575	0.025	0.046875	0.015625	0.00160788	0.000735274	0.000155667
4.575	0.025	0.015625	0.015625	0.00102057	0.000593038	9.88064e-05
4.575	0.025	-0.03125	0.03125	0.00224396	0.000656444	0.000217249
4.575	0.025	-0.109375	0.046875	0.000577244	0.000290044	5.58859e-05

TABLE 29 – Continued

E_{beam}^{lab} [GeV]	$\pm dE_{beam}^{lab}$	$\cos \theta_{\pi^0}^{C.M.}$	$\pm d \cos \theta_{\pi^0}^{C.M.}$	$\frac{d\sigma}{d\Omega}$ [$\frac{\mu b}{SR}$]	σ^{stat}	σ^{sys}
4.575	0.025	-0.203125	0.046875	0.00052955	0.000266192	5.12684e-05
4.575	0.025	-0.296875	0.046875	0.00100314	0.000471674	9.71194e-05
4.575	0.025	-0.390625	0.046875	0.00211765	0.000713635	0.000205021
4.575	0.025	-0.484375	0.046875	0.00293443	0.000945179	0.000284097
4.575	0.025	-0.578125	0.046875	0.00354045	0.00120453	0.000342769
4.575	0.025	-0.671875	0.046875	0.00967392	0.00360382	0.000936581
4.625	0.025	0.859375	0.015625	0.129423	0.0759737	0.0126035
4.625	0.025	0.828125	0.015625	0.144812	0.0431363	0.014102
4.625	0.025	0.796875	0.015625	0.147914	0.0325833	0.0144042
4.625	0.025	0.765625	0.015625	0.119344	0.0181586	0.0116219
4.625	0.025	0.734375	0.015625	0.0893049	0.0120864	0.00869668
4.625	0.025	0.703125	0.015625	0.0896334	0.0111881	0.00872867
4.625	0.025	0.671875	0.015625	0.116599	0.0119193	0.0113547
4.625	0.025	0.640625	0.015625	0.0758536	0.00872422	0.00738676
4.625	0.025	0.609375	0.015625	0.0539528	0.006802	0.00525402
4.625	0.025	0.578125	0.015625	0.0312243	0.00448686	0.00304068
4.625	0.025	0.546875	0.015625	0.0182389	0.0032215	0.00177614
4.625	0.025	0.515625	0.015625	0.0219396	0.00395083	0.00213652
4.625	0.025	0.484375	0.015625	0.0128134	0.00296881	0.00124779
4.625	0.025	0.453125	0.015625	0.00535321	0.00179849	0.000521306
4.625	0.025	0.421875	0.015625	0.00359108	0.00148649	0.000349706
4.625	0.025	0.390625	0.015625	0.00307197	0.00120016	0.000299154
4.625	0.025	0.359375	0.015625	0.00048291	0.00048291	4.70266e-05
4.625	0.025	0.296875	0.015625	0.000926795	0.000657303	9.02531e-05
4.625	0.025	0.265625	0.015625	0.000389546	0.000389546	3.79347e-05
4.625	0.025	0.234375	0.015625	0.00135678	0.000785645	0.000132125
4.625	0.025	0.203125	0.015625	0.00239459	0.000999983	0.00023319
4.625	0.025	0.171875	0.015625	0.000673206	0.000508289	6.55581e-05
4.625	0.025	0.140625	0.015625	0.000247525	0.000247525	2.41044e-05
4.625	0.025	0.109375	0.015625	0.000728411	0.000520889	7.0934e-05
4.625	0.025	0.078125	0.015625	0.00103495	0.000520543	0.000100786
4.625	0.025	0.046875	0.015625	0.00122972	0.000630703	0.000119753
4.625	0.025	0.015625	0.015625	0.000936617	0.00056464	9.12095e-05
4.625	0.025	-0.03125	0.03125	0.00172112	0.00056613	0.000167606
4.625	0.025	-0.109375	0.046875	0.000735522	0.000307538	7.16265e-05
4.625	0.025	-0.203125	0.046875	0.00101502	0.000410546	9.88444e-05
4.625	0.025	-0.296875	0.046875	0.00133431	0.000519088	0.000129938
4.625	0.025	-0.390625	0.046875	0.00192009	0.00068327	0.000186982
4.625	0.025	-0.484375	0.046875	0.000861039	0.000497424	8.38495e-05

TABLE 29 – Continued

E_{beam}^{lab} [GeV]	$\pm dE_{beam}^{lab}$	$\cos \theta_{\pi^0}^{C.M.}$	$\pm d \cos \theta_{\pi^0}^{C.M.}$	$\frac{d\sigma}{d\Omega} \left[\frac{\mu b}{SR} \right]$	σ^{stat}	σ^{sys}
4.625	0.025	-0.578125	0.046875	0.00526232	0.00153198	0.000512454
4.625	0.025	-0.671875	0.046875	0.00340146	0.0019433	0.000331241
4.625	0.025	-0.765625	0.046875	0.00784709	0.00493501	0.000764164
4.675	0.025	0.796875	0.015625	0.125099	0.0294113	0.0122534
4.675	0.025	0.765625	0.015625	0.100952	0.0159501	0.00988829
4.675	0.025	0.734375	0.015625	0.141461	0.0164596	0.0138561
4.675	0.025	0.703125	0.015625	0.0828885	0.0105476	0.00811893
4.675	0.025	0.671875	0.015625	0.103998	0.0110373	0.0101866
4.675	0.025	0.640625	0.015625	0.0805088	0.00907947	0.00788584
4.675	0.025	0.609375	0.015625	0.0436178	0.00602343	0.00427237
4.675	0.025	0.578125	0.015625	0.0270709	0.00424306	0.00265159
4.675	0.025	0.546875	0.015625	0.0160469	0.0030108	0.00157179
4.675	0.025	0.515625	0.015625	0.0150398	0.00328741	0.00147315
4.675	0.025	0.484375	0.015625	0.0111164	0.00276478	0.00108885
4.675	0.025	0.453125	0.015625	0.0054829	0.00174828	0.000537051
4.675	0.025	0.421875	0.015625	0.00191136	0.0011071	0.000187218
4.675	0.025	0.390625	0.015625	0.000388092	0.00036261	3.80137e-05
4.675	0.025	0.296875	0.015625	0.00102763	0.000739239	0.000100656
4.675	0.025	0.234375	0.015625	0.00081417	0.000577214	7.9748e-05
4.675	0.025	0.203125	0.015625	0.00042824	0.00042824	4.19462e-05
4.675	0.025	0.171875	0.015625	0.000829178	0.000489582	8.1218e-05
4.675	0.025	0.140625	0.015625	0.00171704	0.000787143	0.000168184
4.675	0.025	0.109375	0.015625	0.000911701	0.000593285	8.93012e-05
4.675	0.025	0.078125	0.015625	0.000366104	0.000366104	3.58599e-05
4.675	0.025	0.046875	0.015625	0.00112088	0.000579073	0.00010979
4.675	0.025	0.015625	0.015625	0.00054378	0.000384688	5.32633e-05
4.675	0.025	-0.03125	0.03125	0.000403107	0.000285058	3.94843e-05
4.675	0.025	-0.109375	0.046875	0.000729296	0.000286308	7.14346e-05
4.675	0.025	-0.203125	0.046875	0.00104548	0.000431481	0.000102405
4.675	0.025	-0.296875	0.046875	0.00140183	0.000507386	0.00013731
4.675	0.025	-0.390625	0.046875	0.0018463	0.000624725	0.000180845
4.675	0.025	-0.484375	0.046875	0.00142428	0.00064881	0.000139509
4.675	0.025	-0.578125	0.046875	0.00171104	0.000802161	0.000167596
4.675	0.025	-0.671875	0.046875	0.00548408	0.00204619	0.000537166
4.675	0.025	-0.765625	0.046875	0.00265184	0.0020809	0.000259748
4.725	0.025	0.859375	0.015625	0.17598	0.117755	0.0173375
4.725	0.025	0.796875	0.015625	0.135768	0.0301987	0.0133758
4.725	0.025	0.765625	0.015625	0.114589	0.0176329	0.0112893
4.725	0.025	0.734375	0.015625	0.124911	0.0153866	0.0123062

TABLE 29 – Continued

E_{beam}^{lab} [GeV]	$\pm dE_{beam}^{lab}$	$\cos \theta_{\pi^0}^{C.M.}$	$\pm d \cos \theta_{\pi^0}^{C.M.}$	$\frac{d\sigma}{d\Omega} \left[\frac{\mu b}{SR} \right]$	σ^{stat}	σ^{sys}
4.725	0.025	0.703125	0.015625	0.0894225	0.0110989	0.00880987
4.725	0.025	0.671875	0.015625	0.0897915	0.0100697	0.00884622
4.725	0.025	0.640625	0.015625	0.0660607	0.00806146	0.00650827
4.725	0.025	0.609375	0.015625	0.0346958	0.00515908	0.00341821
4.725	0.025	0.578125	0.015625	0.0227967	0.0038065	0.00224592
4.725	0.025	0.546875	0.015625	0.0180919	0.00337449	0.00178241
4.725	0.025	0.515625	0.015625	0.0155423	0.00320838	0.00153122
4.725	0.025	0.484375	0.015625	0.00869109	0.00242632	0.000856243
4.725	0.025	0.453125	0.015625	0.00648322	0.00205733	0.000638725
4.725	0.025	0.421875	0.015625	0.00347612	0.00142993	0.000342466
4.725	0.025	0.390625	0.015625	0.000720131	0.000455304	7.09471e-05
4.725	0.025	0.359375	0.015625	0.00117674	0.000722575	0.000115932
4.725	0.025	0.328125	0.015625	0.00102655	0.000635047	0.000101136
4.725	0.025	0.296875	0.015625	0.000319107	0.000319107	3.14383e-05
4.725	0.025	0.265625	0.015625	0.000810707	0.000577223	7.98705e-05
4.725	0.025	0.203125	0.015625	0.00100269	0.000709556	9.87849e-05
4.725	0.025	0.171875	0.015625	0.00153053	0.000772462	0.000150787
4.725	0.025	0.140625	0.015625	0.00161696	0.000682704	0.000159302
4.725	0.025	0.109375	0.015625	0.000727766	0.000515006	7.16993e-05
4.725	0.025	0.046875	0.015625	0.000917925	0.000536324	9.04337e-05
4.725	0.025	0.015625	0.015625	0.000645094	0.000459353	6.35544e-05
4.725	0.025	-0.03125	0.03125	0.000836699	0.000379202	8.24313e-05
4.725	0.025	-0.109375	0.046875	0.000228681	0.000142	2.25296e-05
4.725	0.025	-0.203125	0.046875	0.00106993	0.000409118	0.000105409
4.725	0.025	-0.296875	0.046875	0.00114197	0.000468369	0.000112507
4.725	0.025	-0.390625	0.046875	0.00246396	0.00078951	0.000242749
4.725	0.025	-0.484375	0.046875	0.00256441	0.000973814	0.000252645
4.725	0.025	-0.578125	0.046875	0.00601269	0.00161551	0.000592368
4.725	0.025	-0.671875	0.046875	0.0042911	0.0019829	0.000422757
4.775	0.025	0.859375	0.015625	0.506723	0.411792	0.0502115
4.775	0.025	0.828125	0.015625	0.103947	0.0486197	0.0103002
4.775	0.025	0.796875	0.015625	0.114793	0.0338232	0.0113749
4.775	0.025	0.765625	0.015625	0.137988	0.0221303	0.0136733
4.775	0.025	0.734375	0.015625	0.0916904	0.0144558	0.00908566
4.775	0.025	0.703125	0.015625	0.0871364	0.0134627	0.0086344
4.775	0.025	0.671875	0.015625	0.0986284	0.0121865	0.00977315
4.775	0.025	0.640625	0.015625	0.0670485	0.00958751	0.00664388
4.775	0.025	0.609375	0.015625	0.0279098	0.00533634	0.0027656
4.775	0.025	0.578125	0.015625	0.0257539	0.00488865	0.00255197

TABLE 29 – Continued

E_{beam}^{lab} [GeV]	$\pm dE_{beam}^{lab}$	$\cos \theta_{\pi_0}^{C.M.}$	$\pm d \cos \theta_{\pi_0}^{C.M.}$	$\frac{d\sigma}{d\Omega} \left[\frac{\mu b}{SR} \right]$	σ^{stat}	σ^{sys}
4.775	0.025	0.546875	0.015625	0.022081	0.00452066	0.00218802
4.775	0.025	0.515625	0.015625	0.0141162	0.00357578	0.00139878
4.775	0.025	0.484375	0.015625	0.00963612	0.00301835	0.000954849
4.775	0.025	0.453125	0.015625	0.00718002	0.00242527	0.000711472
4.775	0.025	0.421875	0.015625	0.00180835	0.00127871	0.000179191
4.775	0.025	0.390625	0.015625	0.00102209	0.000684537	0.00010128
4.775	0.025	0.328125	0.015625	0.000318673	0.000318673	3.15775e-05
4.775	0.025	0.296875	0.015625	0.00151553	0.000902883	0.000150175
4.775	0.025	0.234375	0.015625	0.000456488	0.000456488	4.52336e-05
4.775	0.025	0.203125	0.015625	0.000602803	0.000602803	5.97321e-05
4.775	0.025	0.171875	0.015625	0.00127327	0.000739247	0.000126169
4.775	0.025	0.140625	0.015625	0.000832409	0.00050403	8.24839e-05
4.775	0.025	0.109375	0.015625	0.00102078	0.000728921	0.00010115
4.775	0.025	0.078125	0.015625	0.000288859	0.000288859	2.86232e-05
4.775	0.025	0.046875	0.015625	0.00160834	0.00082851	0.000159371
4.775	0.025	-0.03125	0.03125	0.000843706	0.000389527	8.36034e-05
4.775	0.025	-0.109375	0.046875	0.00118826	0.000439429	0.000117745
4.775	0.025	-0.203125	0.046875	0.000998542	0.000463963	9.89461e-05
4.775	0.025	-0.296875	0.046875	0.00110807	0.000516351	0.000109799
4.775	0.025	-0.390625	0.046875	0.00157959	0.000803938	0.000156522
4.775	0.025	-0.484375	0.046875	0.00200367	0.000909214	0.000198544
4.775	0.025	-0.578125	0.046875	0.00446643	0.00158845	0.000442581
4.775	0.025	-0.671875	0.046875	0.00342294	0.00176179	0.000339181
4.775	0.025	-0.765625	0.046875	0.00336739	0.00336739	0.000333677
4.825	0.025	0.828125	0.015625	0.163197	0.0570993	0.0162647
4.825	0.025	0.796875	0.015625	0.129839	0.0283573	0.0129401
4.825	0.025	0.765625	0.015625	0.1225	0.0202109	0.0122087
4.825	0.025	0.734375	0.015625	0.0843346	0.0132045	0.00840503
4.825	0.025	0.703125	0.015625	0.122429	0.0141927	0.0122016
4.825	0.025	0.671875	0.015625	0.090083	0.0108923	0.00897793
4.825	0.025	0.640625	0.015625	0.0810514	0.00949449	0.00807782
4.825	0.025	0.609375	0.015625	0.034545	0.00515728	0.00344286
4.825	0.025	0.578125	0.015625	0.0303909	0.00489469	0.00302884
4.825	0.025	0.546875	0.015625	0.0289755	0.00456247	0.00288778
4.825	0.025	0.515625	0.015625	0.0145471	0.0033907	0.00144981
4.825	0.025	0.484375	0.015625	0.00720397	0.00229965	0.000717968
4.825	0.025	0.453125	0.015625	0.00350448	0.00157898	0.000349266
4.825	0.025	0.421875	0.015625	0.0013752	0.000940563	0.000137057
4.825	0.025	0.390625	0.015625	0.000180093	0.000180093	1.79486e-05

TABLE 29 – Continued

E_{beam}^{lab} [GeV]	$\pm dE_{beam}^{lab}$	$\cos \theta_{\pi^0}^{C.M.}$	$\pm d \cos \theta_{\pi^0}^{C.M.}$	$\frac{d\sigma}{d\Omega} \left[\frac{\mu b}{SR} \right]$	σ^{stat}	σ^{sys}
4.825	0.025	0.359375	0.015625	0.00122539	0.000729265	0.000122125
4.825	0.025	0.328125	0.015625	0.000794462	0.000582482	7.91783e-05
4.825	0.025	0.265625	0.015625	0.00111276	0.000789573	0.000110901
4.825	0.025	0.234375	0.015625	0.000393732	0.000393732	3.92405e-05
4.825	0.025	0.203125	0.015625	0.000789088	0.000567247	7.86427e-05
4.825	0.025	0.171875	0.015625	0.00126119	0.000738417	0.000125694
4.825	0.025	0.140625	0.015625	0.00106216	0.000592439	0.000105858
4.825	0.025	0.109375	0.015625	0.00208318	0.000856797	0.000207616
4.825	0.025	0.046875	0.015625	0.000463402	0.000327679	4.6184e-05
4.825	0.025	-0.03125	0.03125	0.00116297	0.00044431	0.000115905
4.825	0.025	-0.109375	0.046875	0.000506022	0.000254296	5.04316e-05
4.825	0.025	-0.203125	0.046875	0.000525052	0.00028215	5.23282e-05
4.825	0.025	-0.296875	0.046875	0.00181616	0.000587387	0.000181004
4.825	0.025	-0.390625	0.046875	0.000836525	0.000488687	8.33705e-05
4.825	0.025	-0.484375	0.046875	0.0010432	0.000618703	0.000103969
4.825	0.025	-0.578125	0.046875	0.00674014	0.00186154	0.000671741
4.825	0.025	-0.671875	0.046875	0.00170321	0.0012782	0.000169746
4.825	0.025	-0.859375	0.046875	0.00458963	0.00458963	0.000457415
4.875	0.025	0.828125	0.015625	0.136626	0.0517902	0.0136949
4.875	0.025	0.796875	0.015625	0.131021	0.0267694	0.0131331
4.875	0.025	0.765625	0.015625	0.0960303	0.0160951	0.00962574
4.875	0.025	0.734375	0.015625	0.0851225	0.0119686	0.00853238
4.875	0.025	0.703125	0.015625	0.109202	0.0132644	0.010946
4.875	0.025	0.671875	0.015625	0.0678509	0.00889449	0.00680114
4.875	0.025	0.640625	0.015625	0.0544038	0.00718895	0.00545325
4.875	0.025	0.609375	0.015625	0.0241525	0.00425137	0.00242096
4.875	0.025	0.578125	0.015625	0.021749	0.00368879	0.00218004
4.875	0.025	0.546875	0.015625	0.0149952	0.00312313	0.00150306
4.875	0.025	0.515625	0.015625	0.00785231	0.00231318	0.000787088
4.875	0.025	0.484375	0.015625	0.00671898	0.00221545	0.000673486
4.875	0.025	0.453125	0.015625	0.00293421	0.0014092	0.000294115
4.875	0.025	0.421875	0.015625	0.00111144	0.000655067	0.000111406
4.875	0.025	0.359375	0.015625	0.000365117	0.000365117	3.65981e-05
4.875	0.025	0.328125	0.015625	0.00122103	0.000708031	0.000122391
4.875	0.025	0.296875	0.015625	0.000378853	0.000378853	3.79749e-05
4.875	0.025	0.265625	0.015625	0.000733345	0.000523814	7.35079e-05
4.875	0.025	0.234375	0.015625	0.000794581	0.000569099	7.9646e-05
4.875	0.025	0.203125	0.015625	0.000445692	0.000445692	4.46746e-05
4.875	0.025	0.171875	0.015625	0.000567232	0.000401237	5.68573e-05

TABLE 29 – Continued

E_{beam}^{lab} [GeV]	$\pm dE_{beam}^{lab}$	$\cos \theta_{\pi^0}^{C.M.}$	$\pm d \cos \theta_{\pi^0}^{C.M.}$	$\frac{d\sigma}{d\Omega} \left[\frac{\mu b}{SR} \right]$	σ^{stat}	σ^{sys}
4.875	0.025	0.140625	0.015625	0.000521284	0.000373308	5.22517e-05
4.875	0.025	0.109375	0.015625	0.000748707	0.000549715	7.50477e-05
4.875	0.025	0.078125	0.015625	0.00189909	0.000792281	0.000190358
4.875	0.025	0.046875	0.015625	0.00153968	0.000717651	0.000154332
4.875	0.025	0.015625	0.015625	0.000425426	0.000323645	4.26432e-05
4.875	0.025	-0.03125	0.03125	0.000262332	0.00019127	2.62952e-05
4.875	0.025	-0.109375	0.046875	0.00103166	0.000371293	0.00010341
4.875	0.025	-0.203125	0.046875	0.000970676	0.000401071	9.72971e-05
4.875	0.025	-0.296875	0.046875	0.00076472	0.000382803	7.66528e-05
4.875	0.025	-0.390625	0.046875	0.00206973	0.000699766	0.000207463
4.875	0.025	-0.484375	0.046875	0.00160325	0.000659751	0.000160704
4.875	0.025	-0.578125	0.046875	0.00254561	0.000947474	0.000255163
4.875	0.025	-0.671875	0.046875	0.00263358	0.00133898	0.000263981
4.875	0.025	-0.765625	0.046875	0.00868432	0.00504866	0.000870486
4.925	0.025	0.828125	0.015625	0.196786	0.0754285	0.0198383
4.925	0.025	0.796875	0.015625	0.0955964	0.0313006	0.0096372
4.925	0.025	0.765625	0.015625	0.0868923	0.0143031	0.00875973
4.925	0.025	0.734375	0.015625	0.101527	0.0128765	0.0102351
4.925	0.025	0.703125	0.015625	0.0822143	0.0104196	0.00828813
4.925	0.025	0.671875	0.015625	0.0867744	0.00985449	0.00874784
4.925	0.025	0.640625	0.015625	0.0523457	0.00675547	0.00527704
4.925	0.025	0.609375	0.015625	0.0192464	0.00327896	0.00194026
4.925	0.025	0.578125	0.015625	0.0220155	0.00353909	0.00221941
4.925	0.025	0.546875	0.015625	0.0100395	0.00243654	0.0010121
4.925	0.025	0.515625	0.015625	0.00883319	0.00223342	0.000890486
4.925	0.025	0.484375	0.015625	0.00554771	0.00185792	0.000559272
4.925	0.025	0.453125	0.015625	0.0021674	0.00110292	0.000218498
4.925	0.025	0.421875	0.015625	0.000498972	0.000475539	5.0302e-05
4.925	0.025	0.390625	0.015625	0.00094828	0.000621511	9.55974e-05
4.925	0.025	0.328125	0.015625	0.000391624	0.000391624	3.94801e-05
4.925	0.025	0.296875	0.015625	0.000806926	0.000571058	8.13473e-05
4.925	0.025	0.234375	0.015625	0.000368414	0.000284101	3.71403e-05
4.925	0.025	0.171875	0.015625	0.000917094	0.000532869	9.24535e-05
4.925	0.025	0.140625	0.015625	0.00075903	0.000445354	7.65188e-05
4.925	0.025	0.109375	0.015625	0.000155716	0.000155716	1.56979e-05
4.925	0.025	0.046875	0.015625	0.000538505	0.000381225	5.42874e-05
4.925	0.025	0.015625	0.015625	0.000474968	0.000395967	4.78821e-05
4.925	0.025	-0.03125	0.03125	0.0004514	0.000262504	4.55062e-05
4.925	0.025	-0.109375	0.046875	0.000328085	0.000189708	3.30747e-05

TABLE 29 – Continued

E_{beam}^{lab} [GeV]	$\pm dE_{beam}^{lab}$	$\cos \theta_{\pi^0}^{C.M.}$	$\pm d \cos \theta_{\pi^0}^{C.M.}$	$\frac{d\sigma}{d\Omega} \left[\frac{\mu b}{SR} \right]$	σ^{stat}	σ^{sys}
4.925	0.025	-0.203125	0.046875	0.00047142	0.000277583	4.75244e-05
4.925	0.025	-0.296875	0.046875	0.00105855	0.000405166	0.000106713
4.925	0.025	-0.390625	0.046875	0.00117929	0.000490027	0.000118885
4.925	0.025	-0.484375	0.046875	0.00192879	0.000687113	0.000194443
4.925	0.025	-0.578125	0.046875	0.00318801	0.00102179	0.000321387
4.925	0.025	-0.671875	0.046875	0.00182015	0.00105909	0.000183491
4.975	0.025	0.828125	0.015625	0.192892	0.0653746	0.0195568
4.975	0.025	0.796875	0.015625	0.0811066	0.0209492	0.0082232
4.975	0.025	0.765625	0.015625	0.0828601	0.0167764	0.00840097
4.975	0.025	0.734375	0.015625	0.075571	0.0132424	0.00766196
4.975	0.025	0.703125	0.015625	0.0902356	0.0126834	0.00914876
4.975	0.025	0.671875	0.015625	0.0589496	0.0087835	0.00597675
4.975	0.025	0.640625	0.015625	0.0497839	0.00716927	0.00504747
4.975	0.025	0.609375	0.015625	0.0261306	0.00463315	0.00264932
4.975	0.025	0.578125	0.015625	0.0189319	0.00377605	0.00191946
4.975	0.025	0.546875	0.015625	0.0140526	0.00335925	0.00142476
4.975	0.025	0.515625	0.015625	0.00877436	0.0026883	0.00088961
4.975	0.025	0.484375	0.015625	0.00398093	0.00165031	0.000403617
4.975	0.025	0.453125	0.015625	0.0028519	0.00145254	0.000289147
4.975	0.025	0.421875	0.015625	0.00165451	0.000955422	0.000167747
4.975	0.025	0.328125	0.015625	0.000390136	0.000390136	3.95549e-05
4.975	0.025	0.296875	0.015625	0.000876853	0.000621897	8.89019e-05
4.975	0.025	0.265625	0.015625	0.0019461	0.00099819	0.00019731
4.975	0.025	0.234375	0.015625	0.000579965	0.000579965	5.88012e-05
4.975	0.025	0.203125	0.015625	0.000911099	0.00064445	9.2374e-05
4.975	0.025	0.171875	0.015625	0.00131731	0.000761836	0.000133559
4.975	0.025	0.140625	0.015625	0.000294007	0.000294007	2.98086e-05
4.975	0.025	0.109375	0.015625	0.000659755	0.000466617	6.68909e-05
4.975	0.025	0.078125	0.015625	0.00025523	0.00025523	2.58771e-05
4.975	0.025	0.046875	0.015625	0.000757255	0.000540606	7.67762e-05
4.975	0.025	-0.03125	0.03125	0.000402417	0.000289574	4.08e-05
4.975	0.025	-0.109375	0.046875	0.000336121	0.00020855	3.40785e-05
4.975	0.025	-0.203125	0.046875	0.00101115	0.000459873	0.000102518
4.975	0.025	-0.296875	0.046875	0.00115327	0.000528419	0.000116927
4.975	0.025	-0.390625	0.046875	0.000783302	0.000455365	7.9417e-05
4.975	0.025	-0.484375	0.046875	0.000897034	0.000519308	9.09481e-05
4.975	0.025	-0.578125	0.046875	0.00484686	0.00159271	0.000491411
4.975	0.025	-0.671875	0.046875	0.00471218	0.00184603	0.000477756
4.975	0.025	-0.765625	0.046875	0.00600622	0.0045426	0.000608956

TABLE 29 – Continued

E_{beam}^{lab} [GeV]	$\pm dE_{beam}^{lab}$	$\cos \theta_{\pi^0}^{C.M.}$	$\pm d \cos \theta_{\pi^0}^{C.M.}$	$\frac{d\sigma}{d\Omega} \left[\frac{\mu b}{SR} \right]$	σ^{stat}	σ^{sys}
5.025	0.025	0.859375	0.015625	0.268524	0.164823	0.02738
5.025	0.025	0.796875	0.015625	0.108065	0.0295186	0.0110189
5.025	0.025	0.765625	0.015625	0.0998779	0.019394	0.010184
5.025	0.025	0.734375	0.015625	0.10113	0.0161977	0.0103117
5.025	0.025	0.703125	0.015625	0.0845319	0.011926	0.00861929
5.025	0.025	0.671875	0.015625	0.0963317	0.0121934	0.00982245
5.025	0.025	0.640625	0.015625	0.0476093	0.00722189	0.00485448
5.025	0.025	0.609375	0.015625	0.0278016	0.00451821	0.00283479
5.025	0.025	0.578125	0.015625	0.0231696	0.00436779	0.00236248
5.025	0.025	0.546875	0.015625	0.0116915	0.00319742	0.00119213
5.025	0.025	0.515625	0.015625	0.0205068	0.0042584	0.00209097
5.025	0.025	0.484375	0.015625	0.00653164	0.00218915	0.000665997
5.025	0.025	0.453125	0.015625	0.00273548	0.00139402	0.000278923
5.025	0.025	0.421875	0.015625	0.000391916	0.000391916	3.99617e-05
5.025	0.025	0.390625	0.015625	0.000117343	0.000117343	1.19649e-05
5.025	0.025	0.359375	0.015625	0.000435814	0.000435814	4.44377e-05
5.025	0.025	0.328125	0.015625	0.000224998	0.000224998	2.29419e-05
5.025	0.025	0.296875	0.015625	0.00121982	0.000863148	0.000124378
5.025	0.025	0.234375	0.015625	0.000978354	0.000600492	9.97577e-05
5.025	0.025	0.203125	0.015625	0.000374345	0.000328573	3.81701e-05
5.025	0.025	0.171875	0.015625	0.00229679	0.00095668	0.000234192
5.025	0.025	0.140625	0.015625	0.000363242	0.000363242	3.70379e-05
5.025	0.025	0.109375	0.015625	0.000483801	0.000483801	4.93307e-05
5.025	0.025	0.078125	0.015625	0.000325887	0.000325887	3.32291e-05
5.025	0.025	0.046875	0.015625	0.000328847	0.000328847	3.35309e-05
5.025	0.025	0.015625	0.015625	0.000653228	0.000403834	6.66064e-05
5.025	0.025	-0.03125	0.03125	0.000428713	0.000250671	4.37137e-05
5.025	0.025	-0.109375	0.046875	0.000329077	0.00017298	3.35543e-05
5.025	0.025	-0.203125	0.046875	0.000264086	0.000264086	2.69275e-05
5.025	0.025	-0.296875	0.046875	0.000409884	0.000290217	4.17938e-05
5.025	0.025	-0.390625	0.046875	0.002395	0.000851342	0.000244206
5.025	0.025	-0.484375	0.046875	0.000386038	0.000386038	3.93624e-05
5.025	0.025	-0.578125	0.046875	0.00340708	0.00122254	0.000347402
5.025	0.025	-0.765625	0.046875	0.00370088	0.00370088	0.00037736
5.075	0.025	0.828125	0.015625	0.0542755	0.0273167	0.0055656
5.075	0.025	0.796875	0.015625	0.112873	0.0268587	0.0115744
5.075	0.025	0.765625	0.015625	0.0653682	0.0130142	0.00670309
5.075	0.025	0.734375	0.015625	0.0877203	0.0139034	0.00899514
5.075	0.025	0.703125	0.015625	0.0810284	0.0110177	0.00830894

TABLE 29 – Continued

E_{beam}^{lab} [GeV]	$\pm dE_{beam}^{lab}$	$\cos \theta_{\pi^0}^{C.M.}$	$\pm d \cos \theta_{\pi^0}^{C.M.}$	$\frac{d\sigma}{d\Omega}$ [$\frac{\mu b}{SR}$]	σ^{stat}	σ^{sys}
5.075	0.025	0.671875	0.015625	0.0750858	0.00919214	0.00769956
5.075	0.025	0.640625	0.015625	0.0257608	0.00460368	0.00264161
5.075	0.025	0.609375	0.015625	0.0159423	0.00315213	0.00163478
5.075	0.025	0.578125	0.015625	0.0165377	0.00337163	0.00169584
5.075	0.025	0.546875	0.015625	0.0130008	0.00297577	0.00133315
5.075	0.025	0.515625	0.015625	0.00730841	0.0022306	0.00074943
5.075	0.025	0.484375	0.015625	0.00629569	0.00213658	0.000645582
5.075	0.025	0.421875	0.015625	0.00014366	0.00014366	1.47314e-05
5.075	0.025	0.390625	0.015625	0.00105265	0.000751611	0.000107943
5.075	0.025	0.359375	0.015625	0.000403813	0.000403813	4.14084e-05
5.075	0.025	0.328125	0.015625	0.000317542	0.000317542	3.25618e-05
5.075	0.025	0.296875	0.015625	0.000934842	0.000548507	9.58619e-05
5.075	0.025	0.265625	0.015625	0.00139739	0.000809682	0.000143293
5.075	0.025	0.234375	0.015625	0.000940128	0.000553237	9.64041e-05
5.075	0.025	0.171875	0.015625	0.000357759	0.000357759	3.66858e-05
5.075	0.025	0.140625	0.015625	0.000526269	0.00037309	5.39655e-05
5.075	0.025	0.078125	0.015625	0.0010669	0.00053742	0.000109404
5.075	0.025	0.046875	0.015625	0.000387521	0.000387521	3.97378e-05
5.075	0.025	0.015625	0.015625	5.19472e-05	5.19472e-05	5.32685e-06
5.075	0.025	-0.03125	0.03125	0.000186983	0.000149042	1.91739e-05
5.075	0.025	-0.109375	0.046875	0.000352445	0.000186402	3.6141e-05
5.075	0.025	-0.203125	0.046875	0.000286475	0.000202992	2.93762e-05
5.075	0.025	-0.296875	0.046875	0.00101812	0.000470025	0.000104402
5.075	0.025	-0.390625	0.046875	0.00128095	0.000524561	0.000131353
5.075	0.025	-0.484375	0.046875	0.00108034	0.0005465	0.000110782
5.075	0.025	-0.578125	0.046875	0.00136074	0.000698705	0.000139535
5.075	0.025	-0.671875	0.046875	0.00441104	0.00184902	0.000452324
5.075	0.025	-0.765625	0.046875	0.00242697	0.00242697	0.00024887
5.125	0.025	0.859375	0.015625	0.385914	0.334807	0.0397967
5.125	0.025	0.828125	0.015625	0.111856	0.0551269	0.011535
5.125	0.025	0.796875	0.015625	0.0826278	0.0264607	0.00852085
5.125	0.025	0.765625	0.015625	0.105948	0.0189759	0.0109257
5.125	0.025	0.734375	0.015625	0.103678	0.0147297	0.0106916
5.125	0.025	0.703125	0.015625	0.0762847	0.0112357	0.00786673
5.125	0.025	0.671875	0.015625	0.0850605	0.0100638	0.00877172
5.125	0.025	0.640625	0.015625	0.0271737	0.00512253	0.00280224
5.125	0.025	0.609375	0.015625	0.0214144	0.00370528	0.00220832
5.125	0.025	0.578125	0.015625	0.0087812	0.00235123	0.000905546
5.125	0.025	0.546875	0.015625	0.0113775	0.00289355	0.00117329

TABLE 29 – Continued

E_{beam}^{lab} [GeV]	$\pm dE_{beam}^{lab}$	$\cos \theta_{\pi^0}^{C.M.}$	$\pm d \cos \theta_{\pi^0}^{C.M.}$	$\frac{d\sigma}{d\Omega} \left[\frac{\mu b}{SR} \right]$	σ^{stat}	σ^{sys}
5.125	0.025	0.515625	0.015625	0.00602349	0.00214025	0.000621162
5.125	0.025	0.484375	0.015625	0.00442525	0.00180949	0.000456346
5.125	0.025	0.453125	0.015625	0.00122662	0.000885686	0.000126493
5.125	0.025	0.421875	0.015625	0.000435346	0.000435346	4.48943e-05
5.125	0.025	0.359375	0.015625	0.000457013	0.000457013	4.71287e-05
5.125	0.025	0.328125	0.015625	0.00140502	0.000854195	0.00014489
5.125	0.025	0.296875	0.015625	0.000797619	0.000569861	8.22531e-05
5.125	0.025	0.234375	0.015625	0.00127291	0.000670119	0.000131266
5.125	0.025	0.203125	0.015625	0.000222648	0.000222648	2.29602e-05
5.125	0.025	0.171875	0.015625	0.000666836	0.000474225	6.87663e-05
5.125	0.025	0.140625	0.015625	0.000359493	0.000359493	3.70721e-05
5.125	0.025	0.078125	0.015625	0.000370749	0.000370749	3.82329e-05
5.125	0.025	0.015625	0.015625	0.000295376	0.000295376	3.04602e-05
5.125	0.025	-0.03125	0.03125	0.000276409	0.000201294	2.85042e-05
5.125	0.025	-0.109375	0.046875	0.000384186	0.000213955	3.96185e-05
5.125	0.025	-0.203125	0.046875	0.000802087	0.000378175	8.27139e-05
5.125	0.025	-0.296875	0.046875	0.000967106	0.000439995	9.97312e-05
5.125	0.025	-0.390625	0.046875	0.00094064	0.000474275	9.7002e-05
5.125	0.025	-0.484375	0.046875	0.000388649	0.000388649	4.00788e-05
5.125	0.025	-0.578125	0.046875	0.00284178	0.00109249	0.000293054
5.125	0.025	-0.671875	0.046875	0.00395639	0.00248707	0.000407996
5.125	0.025	-0.765625	0.046875	0.00323969	0.00323969	0.000334088
5.175	0.025	0.828125	0.015625	0.115455	0.0776587	0.0119732
5.175	0.025	0.796875	0.015625	0.140331	0.0330353	0.014553
5.175	0.025	0.765625	0.015625	0.116847	0.0211249	0.0121175
5.175	0.025	0.734375	0.015625	0.0890882	0.0136304	0.00923883
5.175	0.025	0.703125	0.015625	0.0799125	0.0117068	0.00828727
5.175	0.025	0.671875	0.015625	0.0801567	0.0104628	0.0083126
5.175	0.025	0.640625	0.015625	0.0304072	0.00532887	0.00315336
5.175	0.025	0.609375	0.015625	0.0232621	0.00437536	0.00241238
5.175	0.025	0.578125	0.015625	0.0178125	0.00370948	0.00184723
5.175	0.025	0.546875	0.015625	0.0110726	0.00284898	0.00114828
5.175	0.025	0.515625	0.015625	0.00989978	0.00279314	0.00102665
5.175	0.025	0.484375	0.015625	0.00348639	0.00156376	0.000361554
5.175	0.025	0.453125	0.015625	0.000654581	0.000654581	6.78829e-05
5.175	0.025	0.421875	0.015625	0.00129471	0.000924898	0.000134267
5.175	0.025	0.390625	0.015625	0.000357598	0.000357598	3.70845e-05
5.175	0.025	0.328125	0.015625	0.000562774	0.000562774	5.83621e-05
5.175	0.025	0.296875	0.015625	0.00109047	0.000771788	0.000113087

TABLE 29 – Continued

E_{beam}^{lab} [GeV]	$\pm dE_{beam}^{lab}$	$\cos \theta_{\pi^0}^{C.M.}$	$\pm d \cos \theta_{\pi^0}^{C.M.}$	$\frac{d\sigma}{d\Omega} \left[\frac{\mu b}{SR} \right]$	σ^{stat}	σ^{sys}
5.175	0.025	0.234375	0.015625	0.000826489	0.0004782	8.57104e-05
5.175	0.025	0.203125	0.015625	0.000783232	0.000536785	8.12245e-05
5.175	0.025	0.171875	0.015625	0.000690261	0.000484058	7.15831e-05
5.175	0.025	0.046875	0.015625	0.000323306	0.000307946	3.35282e-05
5.175	0.025	0.015625	0.015625	0.00010251	0.00010251	1.06307e-05
5.175	0.025	-0.03125	0.03125	0.000353776	0.000251607	3.66881e-05
5.175	0.025	-0.109375	0.046875	0.000597693	0.000317943	6.19833e-05
5.175	0.025	-0.203125	0.046875	0.000883852	0.000450752	9.16593e-05
5.175	0.025	-0.296875	0.046875	0.000710787	0.000415277	7.37117e-05
5.175	0.025	-0.390625	0.046875	0.00118125	0.000599047	0.0001225
5.175	0.025	-0.484375	0.046875	0.000991642	0.000579238	0.000102838
5.175	0.025	-0.578125	0.046875	0.00172492	0.000881743	0.000178882
5.175	0.025	-0.671875	0.046875	0.00543353	0.0024321	0.000563481
5.175	0.025	-0.765625	0.046875	0.00182601	0.00129308	0.000189365
5.225	0.025	0.828125	0.015625	0.229013	0.0898058	0.023883
5.225	0.025	0.796875	0.015625	0.0809243	0.0238777	0.00843931
5.225	0.025	0.765625	0.015625	0.0871602	0.0180723	0.00908963
5.225	0.025	0.734375	0.015625	0.0947268	0.0157159	0.00987873
5.225	0.025	0.703125	0.015625	0.0723301	0.0112775	0.00754305
5.225	0.025	0.671875	0.015625	0.0715238	0.00989086	0.00745897
5.225	0.025	0.640625	0.015625	0.0293395	0.00537495	0.00305972
5.225	0.025	0.609375	0.015625	0.0249705	0.00482709	0.00260408
5.225	0.025	0.578125	0.015625	0.0106752	0.00264472	0.00111328
5.225	0.025	0.546875	0.015625	0.0109068	0.00296501	0.00113743
5.225	0.025	0.515625	0.015625	0.00627247	0.00223961	0.000654134
5.225	0.025	0.484375	0.015625	0.00186311	0.00131743	0.000194298
5.225	0.025	0.453125	0.015625	0.000622359	0.000622359	6.49036e-05
5.225	0.025	0.390625	0.015625	4.89247e-05	4.89247e-05	5.10218e-06
5.225	0.025	0.328125	0.015625	0.00172682	0.000997302	0.000180084
5.225	0.025	0.296875	0.015625	0.000979334	0.000698094	0.000102131
5.225	0.025	0.265625	0.015625	0.000756045	0.00048325	7.88453e-05
5.225	0.025	0.234375	0.015625	0.0005311	0.0005311	5.53865e-05
5.225	0.025	0.203125	0.015625	0.000352625	0.000352625	3.6774e-05
5.225	0.025	0.171875	0.015625	0.00057294	0.000448595	5.97499e-05
5.225	0.025	0.140625	0.015625	0.000592191	0.000425818	6.17575e-05
5.225	0.025	0.078125	0.015625	0.000214041	0.000214041	2.23216e-05
5.225	0.025	0.046875	0.015625	0.00069224	0.000460649	7.21913e-05
5.225	0.025	-0.03125	0.03125	0.00053518	0.000316917	5.58121e-05
5.225	0.025	-0.109375	0.046875	0.000426902	0.000247509	4.45201e-05

TABLE 29 – Continued

E_{beam}^{lab} [GeV]	$\pm dE_{beam}^{lab}$	$\cos \theta_{\pi^0}^{C.M.}$	$\pm d \cos \theta_{\pi^0}^{C.M.}$	$\frac{d\sigma}{d\Omega} \left[\frac{\mu b}{SR} \right]$	σ^{stat}	σ^{sys}
5.225	0.025	-0.203125	0.046875	0.000512052	0.000324747	5.34001e-05
5.225	0.025	-0.296875	0.046875	0.00122507	0.000519339	0.000127758
5.225	0.025	-0.390625	0.046875	0.000793285	0.000459844	8.27289e-05
5.225	0.025	-0.484375	0.046875	0.00142763	0.000720865	0.000148883
5.225	0.025	-0.578125	0.046875	0.00305781	0.00110133	0.000318889
5.225	0.025	-0.671875	0.046875	0.0048724	0.00223714	0.000508125
5.225	0.025	-0.765625	0.046875	0.000788241	0.000788241	8.22029e-05
5.275	0.025	0.828125	0.015625	0.0937248	0.0553342	0.00982891
5.275	0.025	0.796875	0.015625	0.102486	0.0299585	0.0107477
5.275	0.025	0.765625	0.015625	0.10515	0.0220995	0.011027
5.275	0.025	0.734375	0.015625	0.0938525	0.0170683	0.00984229
5.275	0.025	0.703125	0.015625	0.0736443	0.0136848	0.00772306
5.275	0.025	0.671875	0.015625	0.0514804	0.0101791	0.00539874
5.275	0.025	0.640625	0.015625	0.0158588	0.00450742	0.00166311
5.275	0.025	0.609375	0.015625	0.0227212	0.00508701	0.00238276
5.275	0.025	0.578125	0.015625	0.012008	0.00351015	0.00125928
5.275	0.025	0.546875	0.015625	0.0113113	0.0036615	0.00118621
5.275	0.025	0.515625	0.015625	0.00665581	0.00273078	0.000697994
5.275	0.025	0.484375	0.015625	0.00325884	0.00188785	0.000341754
5.275	0.025	0.453125	0.015625	0.00228274	0.00134118	0.00023939
5.275	0.025	0.421875	0.015625	0.000505506	0.000505506	5.30123e-05
5.275	0.025	0.328125	0.015625	0.00145288	0.0010276	0.000152363
5.275	0.025	0.296875	0.015625	0.00144754	0.00104157	0.000151804
5.275	0.025	0.203125	0.015625	0.00177212	0.0010397	0.000185842
5.275	0.025	0.171875	0.015625	0.00127728	0.000934142	0.000133948
5.275	0.025	0.140625	0.015625	0.000734469	0.000519441	7.70236e-05
5.275	0.025	0.078125	0.015625	0.000385773	0.000385773	4.0456e-05
5.275	0.025	-0.03125	0.03125	0.00056497	0.000332276	5.92483e-05
5.275	0.025	-0.109375	0.046875	0.000211257	0.000172202	2.21545e-05
5.275	0.025	-0.203125	0.046875	0.000362432	0.000257428	3.80082e-05
5.275	0.025	-0.390625	0.046875	0.00034278	0.00034278	3.59473e-05
5.275	0.025	-0.484375	0.046875	0.000803272	0.000568839	8.4239e-05
5.275	0.025	-0.578125	0.046875	0.0015275	0.000883421	0.000160188
5.275	0.025	-0.671875	0.046875	0.00120035	0.00120035	0.00012588
5.275	0.025	-0.765625	0.046875	0.00118528	0.00118528	0.0001243
5.325	0.025	0.828125	0.015625	0.146898	0.0857378	0.015491
5.325	0.025	0.796875	0.015625	0.0780917	0.0227346	0.00823511
5.325	0.025	0.765625	0.015625	0.107273	0.0220867	0.0113124
5.325	0.025	0.734375	0.015625	0.0556513	0.0104659	0.00586867

TABLE 29 – Continued

E_{beam}^{lab} [GeV]	$\pm dE_{beam}^{lab}$	$\cos \theta_{\pi^0}^{C.M.}$	$\pm d \cos \theta_{\pi^0}^{C.M.}$	$\frac{d\sigma}{d\Omega} \left[\frac{\mu b}{SR} \right]$	σ^{stat}	σ^{sys}
5.325	0.025	0.703125	0.015625	0.0911749	0.012481	0.00961478
5.325	0.025	0.671875	0.015625	0.0625382	0.00914147	0.00659492
5.325	0.025	0.640625	0.015625	0.0153297	0.00314701	0.00161658
5.325	0.025	0.609375	0.015625	0.0194802	0.00369279	0.00205427
5.325	0.025	0.578125	0.015625	0.00934426	0.00251572	0.000985392
5.325	0.025	0.546875	0.015625	0.00535512	0.00192375	0.00056472
5.325	0.025	0.515625	0.015625	0.00586862	0.00211656	0.000618871
5.325	0.025	0.484375	0.015625	0.00330394	0.00147935	0.000348414
5.325	0.025	0.453125	0.015625	0.000578403	0.000578403	6.09951e-05
5.325	0.025	0.328125	0.015625	0.000947244	0.000672732	9.98909e-05
5.325	0.025	0.296875	0.015625	0.000957418	0.000677106	0.000100964
5.325	0.025	0.265625	0.015625	0.000779066	0.000779066	8.21558e-05
5.325	0.025	0.234375	0.015625	0.000584169	0.000507131	6.16031e-05
5.325	0.025	0.203125	0.015625	0.0012138	0.000607285	0.000128001
5.325	0.025	0.109375	0.015625	0.000311117	0.000311117	3.28086e-05
5.325	0.025	0.078125	0.015625	0.000236049	0.000221711	2.48924e-05
5.325	0.025	0.046875	0.015625	0.000177653	0.000147011	1.87343e-05
5.325	0.025	0.015625	0.015625	0.000103756	0.000103756	1.09415e-05
5.325	0.025	-0.03125	0.03125	9.59198e-05	9.59198e-05	1.01152e-05
5.325	0.025	-0.109375	0.046875	0.000102521	0.000102521	1.08113e-05
5.325	0.025	-0.296875	0.046875	0.00127187	0.000596403	0.000134124
5.325	0.025	-0.390625	0.046875	0.000220037	0.000220037	2.32038e-05
5.325	0.025	-0.484375	0.046875	0.000519287	0.000369409	5.47611e-05
5.325	0.025	-0.578125	0.046875	0.00152526	0.000765933	0.000160845
5.325	0.025	-0.671875	0.046875	0.00393186	0.00209204	0.000414631
5.325	0.025	-0.765625	0.046875	0.0010151	0.0010151	0.000107046
5.375	0.025	0.828125	0.015625	0.171107	0.12617	0.0181442
5.375	0.025	0.796875	0.015625	0.097751	0.0236442	0.0103655
5.375	0.025	0.765625	0.015625	0.137659	0.0252309	0.0145973
5.375	0.025	0.734375	0.015625	0.0849872	0.0146105	0.00901203
5.375	0.025	0.703125	0.015625	0.078504	0.0122291	0.00832455
5.375	0.025	0.671875	0.015625	0.0436942	0.00834236	0.00463333
5.375	0.025	0.640625	0.015625	0.0192435	0.00416032	0.00204057
5.375	0.025	0.609375	0.015625	0.0139762	0.00315204	0.00148203
5.375	0.025	0.578125	0.015625	0.00813544	0.00250496	0.000862681
5.375	0.025	0.546875	0.015625	0.00779456	0.00249655	0.000826534
5.375	0.025	0.515625	0.015625	0.0116622	0.00314497	0.00123666
5.375	0.025	0.484375	0.015625	0.000997105	0.000711657	0.000105733
5.375	0.025	0.453125	0.015625	0.000986691	0.000700649	0.000104629

TABLE 29 – Continued

E_{beam}^{lab} [GeV]	$\pm dE_{beam}^{lab}$	$\cos \theta_{\pi^0}^{C.M.}$	$\pm d \cos \theta_{\pi^0}^{C.M.}$	$\frac{d\sigma}{d\Omega} \left[\frac{\mu b}{SR} \right]$	σ^{stat}	σ^{sys}
5.375	0.025	0.328125	0.015625	0.000569499	0.000569499	6.03896e-05
5.375	0.025	0.296875	0.015625	0.000657469	0.000541642	6.97178e-05
5.375	0.025	0.234375	0.015625	0.000783289	0.000556224	8.30598e-05
5.375	0.025	0.203125	0.015625	0.00024842	0.00024842	2.63425e-05
5.375	0.025	0.171875	0.015625	0.000777093	0.000550523	8.24028e-05
5.375	0.025	0.140625	0.015625	0.00032583	0.00032583	3.45509e-05
5.375	0.025	0.109375	0.015625	0.000513814	0.000513814	5.44848e-05
5.375	0.025	0.078125	0.015625	0.000542873	0.000439014	5.75662e-05
5.375	0.025	0.046875	0.015625	0.000709591	0.000418591	7.52449e-05
5.375	0.025	0.015625	0.015625	0.000522075	0.00039017	5.53607e-05
5.375	0.025	-0.03125	0.03125	0.000352938	0.000251562	3.74255e-05
5.375	0.025	-0.203125	0.046875	0.00047842	0.000349584	5.07316e-05
5.375	0.025	-0.296875	0.046875	0.000934006	0.000470237	9.90418e-05
5.375	0.025	-0.390625	0.046875	0.000641769	0.00045762	6.8053e-05
5.375	0.025	-0.484375	0.046875	0.000665733	0.000471444	7.05942e-05
5.375	0.025	-0.578125	0.046875	0.000797977	0.000574208	8.46174e-05
5.375	0.025	-0.671875	0.046875	0.000717934	0.000717934	7.61296e-05
5.375	0.025	-0.765625	0.046875	0.00560995	0.00293369	0.000594878
5.425	0.025	0.828125	0.015625	0.131953	0.0636497	0.0140697
5.425	0.025	0.796875	0.015625	0.0689777	0.022336	0.00735485
5.425	0.025	0.765625	0.015625	0.0935719	0.0189818	0.00997724
5.425	0.025	0.734375	0.015625	0.0804354	0.0139956	0.00857654
5.425	0.025	0.703125	0.015625	0.0898376	0.0129289	0.00957907
5.425	0.025	0.671875	0.015625	0.0350783	0.00679906	0.00374028
5.425	0.025	0.640625	0.015625	0.0165506	0.00341867	0.00176474
5.425	0.025	0.609375	0.015625	0.0165584	0.00396433	0.00176556
5.425	0.025	0.578125	0.015625	0.0107861	0.00290016	0.00115008
5.425	0.025	0.546875	0.015625	0.0107626	0.00283846	0.00114758
5.425	0.025	0.515625	0.015625	0.00178035	0.00126186	0.000189833
5.425	0.025	0.453125	0.015625	0.000483783	0.000483783	5.15841e-05
5.425	0.025	0.390625	0.015625	0.000841008	0.000841008	8.96737e-05
5.425	0.025	0.359375	0.015625	0.000135645	0.000135645	1.44633e-05
5.425	0.025	0.265625	0.015625	0.000386602	0.000386602	4.1222e-05
5.425	0.025	0.234375	0.015625	0.000442188	0.000442188	4.71489e-05
5.425	0.025	0.203125	0.015625	0.000536931	0.000536931	5.7251e-05
5.425	0.025	0.171875	0.015625	0.000608925	0.000431996	6.49275e-05
5.425	0.025	0.109375	0.015625	0.00125401	0.000738381	0.000133711
5.425	0.025	0.078125	0.015625	0.000122317	0.000122317	1.30422e-05
5.425	0.025	0.046875	0.015625	0.000301484	0.000252513	3.21462e-05

TABLE 29 – Continued

E_{beam}^{lab} [GeV]	$\pm dE_{beam}^{lab}$	$\cos \theta_{\pi^0}^{C.M.}$	$\pm d \cos \theta_{\pi^0}^{C.M.}$	$\frac{d\sigma}{d\Omega} \left[\frac{\mu b}{SR} \right]$	σ^{stat}	σ^{sys}
5.425	0.025	0.015625	0.015625	0.000181339	0.000181339	1.93355e-05
5.425	0.025	-0.03125	0.03125	0.00032588	0.000238601	3.47475e-05
5.425	0.025	-0.109375	0.046875	0.000447455	0.00026555	4.77105e-05
5.425	0.025	-0.203125	0.046875	0.000401066	0.000292447	4.27643e-05
5.425	0.025	-0.296875	0.046875	0.000162337	0.000162337	1.73095e-05
5.425	0.025	-0.390625	0.046875	0.000871647	0.000447755	9.29406e-05
5.425	0.025	-0.484375	0.046875	0.00133562	0.000670899	0.000142412
5.425	0.025	-0.578125	0.046875	0.00116206	0.000673168	0.000123906
5.425	0.025	-0.671875	0.046875	0.000728213	0.000728213	7.76468e-05
5.425	0.025	-0.765625	0.046875	0.00252326	0.00252326	0.000269046

VITA

PERSONAL DATA

Name: Michael C. Kunkel

Address: Department of Physics 4600 Elkhorn Ave
Norfolk, VA 23529

EDUCATION

August, 2007-August, 2014: Ph.D. in Physics- Old Dominion University,
Norfolk, VA

August, 2007- August, 2008: MS in Physics- Old Dominion University,
Norfolk, VA

August, 2003-August, 2007: BS in Space Physics- Embry-Riddle Aeronautical University,
Prescott, AZ

August, 2003-August, 2007: BS in Aeronautics- Embry-Riddle Aeronautical University,
Prescott, AZ

August, 2001-August, 2003: Type 65 Certification Airframes and Powerplants -
Embry-Riddle Aeronautical University, Camp Pendleton, CA